July 31, 1973

To the Graduate Council:

I am submitting herewith a dissertation written by Gann Ting entitled "Thermodynamic and Electrochemical Studies of Niobium in Molten Fluorides and Chloroaluminates." I recommend that it be accepted in partial fulfillment of the requirements for the degree of Doctor of Philosophy, with a major in Chemistry.

Major Professor

We have read this dissertation
and recommend its acceptance:

Charles F. Baes Jr.

George T. Condo

G. P. Smith

J. O. Chambers

Accepted for the Council:

Vice Chancellor for
Graduate Studies and Research

THERMODYNAMIC AND ELECTROCHEMICAL STUDIES OF NIOBIUM IN MOLTEN FLUORIDES AND CHLOROALUMINATES

A Dissertation

Presented to

the Graduate Council of

The University of Tennessee

In Partial Fulfillment

of the Requirements for the Degree

Doctor of Philosophy

---

by

Gann Ting

August 1973

ACKNOWLEDGMENT

The author wishes to express his appreciation to Drs. G. Mamantov and C. F. Baes, Jr. for their guidance and encouragement throughout this investigation. Appreciation is expressed to Drs. C. E. Bamberger and K. W. Fung for their valuable assistance and suggestions in the laboratory, to D. L. Manning for making his instruments available for this work and for helpful discussions, to G. M. Begun for assistance with the Raman experiments, and to J. P. Young for performing the UV spectrometric analysis.

Thanks are also expressed to the Oak Ridge National Laboratory operated for the United States Atomic Energy Commission by Union Carbide Corporation, especially to its Reactor Chemistry Division, for allowing the author to do this research, for providing equipment, materials, and facilities, and to the members of the Analytical Chemistry Division for sample analysis. Support of the National Science Foundation, Grant GP-32433X, for work carried out at the Department of Chemistry, University of Tennessee, is gratefully acknowledged. I would also like to thank Mrs. J. Wallace for typing this manuscript, and to S. C. Lin for drawing the figures.

Financial support from the Institute of Nuclear Energy Research, Chinese Atomic Energy Council, Republic of China, is gratefully acknowledged.

1119019

ABSTRACT

The oxide chemistry of niobium(V) has been studied in molten $LiF-BeF_2$ mixtures. The stoichiometry of an oxygen-containing niobium(V) species (NbO_2F) has been established in molten Li_2BeF_4 from the heterogeneous equilibrations of $NiNb_2O_6$ and NiO with the melt containing NiF_2, the equilibrium quotient for the reaction was determined. The equilibrium quotient for the heterogeneous reaction of Nb_2O_5 and BeO with molten $LiF-BeF_2$ mixtures (67-33 and 52-48 mole %) was also determined, and the effect of the melt composition on the solubility of Nb_2O_5(c) and on the activity coefficient of NbO_2F(d) have been examined. The free energies of formation of NbO_2F(d) and $NiNb_2O_6$(c) has been estimated from the experimental results. A Pourbaix diagram for niobium in molten Li_2BeF_4 at 500° and a phases diagram at 600° involving NbO_2F and NiF_2 and the equilibrium oxide phases (Nb_2O_5, $NiNb_2O_6$, NiO, and BeO) in molten Li_2BeF_4 were constructed.

The electrochemical reduction of Nb(V) in molten $LiF-BeF_2-ZrF_4$ (65.6-29.4-5.0 mole %) has been studied by linear sweep voltammetry with pyrolytic graphite and platinum electrodes. Potentials were measured with respect to a Ni(II) (saturated)/Ni reference electrode. Nb(V) was found to form NbO_2F. The results at the pyrolytic graphite electrode were reproducible; three reduction steps were observed at low scan rates (< 0.5 V/sec) and one reduction step was observed at high scan rates (> 5 V/sec). Mechanisms are proposed for the reduction of niobium(V). The results with platinum electrode were complicated and irreproducible.

The electrochemical reduction of Nb(V) chloride and Nb(V) oxychloride in molten $AlCl_3-NaCl$ mixtures (63-37 to 50-50 mole %) has

been examined by means of chronoamperometry, differential pulse polarography, chronopotentiometry and linear sweep voltammetry using platinum and tungsten electrodes. Potentials were measured with respect to an Al(III) ($AlCl_3$-NaCl, 63-37 mole %)/Al reference electrode. The effect of the melt composition, temperature and Nb(V) concentration on the reduction steps was studied. The results show that the stability of the niobium species and the electrode reduction mechanisms of Nb(V) chloride and oxychloride are very sensitive to the melt composition and to the temperature. The number of reduction steps, the redox potentials, and the stability of the various niobium species at different melt compositions and temperatures are reported. Reduction mechanisms of niobium(V) chloride and oxychloride are proposed.

Some vibrational spectroscopic studies of solid Nb_2O_5 and $NiNb_2O_5$ were performed; the results indicate that the symmetric stretching frequencies of Nb-O in Nb_2O_5 and $NiNb_2O_6$ are 992 and 882 cm^{-1}, respectively.

TABLE OF CONTENTS

CHAPTER		PAGE
I.	INTRODUCTION	1
	A. Review of the Literature	2
	1. Oxide chemistry in molten Li_2BeF_4 and $LiF-BeF_2-ThF_4$	2
	2. Chemistry of niobium oxides, fluorides, oxyfluorides and oxo-fluoro complexes	5
	3. Chemistry of niobium chlorides and oxychlorides .	10
	4. Electrochemistry of niobium in molten chlorides and fluorides	14
	B. Review of Basic Principles	19
	1. Acid-base concepts in molten chlorides and fluorides	19
	2. EMF measurements	21
	3. Representation of equilibria by Pourbaix diagrams.	23
	4. Linear sweep voltammetry	26
	5. Chronopotentiometry	30
	6. Chronoamperometry and construction of stationary electrode polarograms	43
	7. Pulse polarography	43
	8. Studies of adsorption by linear sweep voltammetry and chronopotentiometry	46
	C. Proposed Research	49
II.	EXPERIMENTAL	51

CHAPTER PAGE

A. Materials 51

1. Materials for equilibria and electrochemical studies in molten fluorides 51

2. Materials for electrochemical studies in molten chloroaluminates 52

B. Apparatus 53

1. Apparatus for equilibria studies in molten fluorides 53

2. Apparatus for electrochemical studies in molten chloroaluminates 58

3. Apparatus for electrochemical studies in molten fluorides 61

C. Procedures 64

1. Procedure for equilibria studies 64

2. Procedure for electrochemical studies in molten chloroaluminates 66

3. Procedure for electrochemical studies in molten fluorides 68

III. RESULTS AND DISCUSSION 69

A. The Oxide Chemistry of Niobium in Molten $LiF-BeF_2$ Mixtures 69

1. Equilibrations of Nb_2O_5 and BeO with molten $LiF-BeF_2$ mixtures 70

2. Equilibrations involving nickel niobates in molten Li_2BeF_4 80

CHAPTER PAGE

3. Equilibrations of $NiNb_2O_6$ and NiO with molten Li_2BeF_4 and determination of the stoichiometry of an oxygen-containing niobium species in the melt. 87

4. Estimation of the heat of formation and the lattice energy of $NiNb_2O_6$ 97

B. Studies of Nb(V) in Molten $LiF-BeF_2-ZrF_4$ (65.6-29.4-5.0 Mole %) 102

C. Electrochemistry of Niobium Pentachloride in Molten $AlCl_3$-NaCl Mixtures 114

1. Electrochemistry of Nb(V) in molten $AlCl_3$-NaCl (63-37 mole %) 114

2. Electrochemistry of Nb(V) in molten $AlCl_3$-NaCl (61-39 mole %) 127

3. Electrochemistry of Nb(V) in molten $AlCl_3$-NaCl (55-45 mole %) 130

4. Electrochemistry of Nb(V) in molten $AlCl_3$-NaCl (50-50 mole %) 141

5. Effect of melt composition and temperature on the reduction of Nb(V) in molten $AlCl_3$-NaCl mixtures 176

D. Electrochemistry of Niobium Oxychloride in Molten $AlCl_3$-NaCl Mixtures 180

1. Electrochemistry of niobium oxychloride in molten $AlCl_3$-NaCl (63-37 and 56-44 mole %) . . 181

2. Electrochemistry of niobium oxychloride in molten $AlCl_3$-NaCl (50-50 mole %) 187

CHAPTER PAGE

3. Effect of melt composition and temperature on the electrochemical reduction of niobium oxychloride in molten chloroaluminates 205

E. Vibrational Spectroscopic Studies of Solid Nb_2O_5 and $NiNb_2O_6$ 206

IV. SUMMARY 214

LIST OF REFERENCES 219

VITA 231

LIST OF TABLES

TABLE		PAGE
I.	Oxide Chemistry in Molten Li_2BeF_4 and $LiF-BeF_2-ThF_4$	3
II.	Niobium Chlorides, Fluorides, Oxides and Complexes Involving These Elements	6
III.	Solid State Reactions of Niobium Oxide and Oxyfluoride	8
IV.	Thermodynamic Properties of Some Niobium Compounds	11
V.	Electrochemical Studies of Niobium in Molten Chlorides and Fluorides	17
VI.	Summary of Some Equations and of Diagnostic Criteria of Linear Sweep Voltammetry	31
VII.	Summary of Some Diagnostic Criteria of Chronopotentiometry	41
VIII.	Summary of Equations for Analysis of the Current-Potential Curves	44
IX.	Analysis of Solid Phases by Various Methods	81
X.	Reactions of Various Equilibrium Solid Phases in Molten Li_2BeF_4	84
XI.	Equilibrium Reactions and Data for Constructing the Phase Diagram at 600°	86
XII.	Equilibrium Reactions and Data for Construction of Pourbaix Diagram at 500°	95
XIII.	Cation and Anion Parameters and Calculated ΔH_R for Some Binary Oxides	99

TABLE PAGE

XIV. Voltammetric Results for the Reduction of Nb(V) in Molten LiF-BeF_2-ZrF_4 (65.6-29.4-5.0 mole %) at Pyrolytic Graphite Electrode at 500°. (Ni(II) (Saturated)/Ni Reference Electrode 110

XV. Voltammetric Results for the Reduction of Nb(V). Melt Composition: $AlCl_3$-NaCl (63-37 Mole %) 125

XVI. Voltammetric Results for the Reduction of Nb(V) at Platinum Electrode, Melt Composition: $AlCl_3$-NaCl (55-45 mole %); Nb(V) Concentration: 1.42×10^{-2} M; Al(III)/Al Reference Electrode 138

XVII. Voltammetric Results for the Reduction of Nb(V). Melt Composition: $AlCl_3$-NaCl (55-45 mole %); Nb(V) Concentration 1.42×10^{-2} M; Temperature 150° . 139

XVIII. Concentration Dependence of the Diffusion Current . . . 144

XIX. Polarographic Results for the Reduction of Nb(V) at Platinum and Tungsten Electrodes. Melt Composition: $AlCl_3$-NaCl (50-50 mole %) 147

XX. Chronopotentiometric Results for the Reduction of Nb(V) at Platinum and Tungsten Electrodes. Melt Composition: $AlCl_3$-NaCl (50-50 mole %) 153

XXI. Voltammetric Results for the Reduction of Nb^{5+} to Nb^{4+} at the Platinum Electrode. Melt Composition: $AlCl_3$-NaCl (50-50 mole %) 161

TABLE PAGE

XXII. Voltammetric Results for the Four Reduction Steps at Platinum Electrode. Melt Composition: $AlCl_3$-NaCl (50-50 mole %) 163

XXIII. Voltammetric Results for the Adsorption Process at the Platinum Electrode 173

XXIV. Effect on Melt Composition of the Reduction of Nb(V) in Molten $AlCl_3$-NaCl Mixtures at the Platinum Electrode 177

XXV. Voltammetric Results for the Reduction of Nb(V) (Added as $NbOCL_3$) at the Platinum Electrode. Melt Composition: $AlCl_3$-NaCl (63-37 mole %) . . . 184

XXVI. Voltammetric Results for the Reduction of Nb(V) (Added as $NbOCl_3$) at the Platinum Electrode. Melt Composition: $AlCl_3$-NaCl (56-44 mole %) . . . 186

XXVII. Voltammetric Results for the Reduction of NbO(III). Melt Composition: $AlCl_3$-NaCl (50-50 mole %) . . . 196

XXVIII. Voltammetric Results for the Reduction of NbO(III) at Higher Temperatures 200

XXIX. Vibrational Frequencies (cm^{-1}) of Solid Nb_2O_5 and $NiNb_2O_6$ at 25° 212

LIST OF FIGURES

FIGURE		PAGE
1.	A Typical Cyclic Voltammogram	27
2.	Schematic Diagram of the Experimental Apparatus for Equilibrium Studies	54
3.	Reaction Vessel for Equilibrium Studies	55
4.	Devices for Sampling Molten Fluorides and for Adding Reagents to the Reaction Vessel	56
5.	Electrochemical Cell for Studies in Chloroaluminates . . .	60
6.	Apparatus for Electrochemical Studies in Molten Fluorides and Ni(II)/Ni Reference Electrode	62
7.	An SEM Photograph of a Typical Particle of Solid Phase Obtained from Equilibrating BeO and Nb_2O_5 in Molten Li_2BeF_4 at 728° and the Corresponding X-ray Fluorescence Spectrum	72
8.	Concentration of Nb(V) in LiF-BeF_2 Mixtures at Equilibrium with BeO and Nb_2O_5 Under Circulating CO_2-CO Mixtures	73
9.	Effect of Melt Composition on the Concentration of Niobium(V) in LiF-BeF_2 Mixtures at Equilibrium with BeO and Nb_2O_5 at 606°	76
10.	Effect of Free Fluoride Concentration, $(X_{LiF} - 2X_{BeF_2}) \times 100$, on the Concentration of Nb(V) in LiF-BeF_2 Mixtures at 606°	78

FIGURE PAGE

11. Activity Coefficients of Assumed Components NbF_5, $NbOF_3$, NbO_2F and BeF_2 in LiF-BeF_2 Mixtures at 606° 79

12. Concentrations of (a) Niobium(V) and (b) Nickel(II) in Molten Li_2BeF_4 Equilibrated with NiO-Nb_2O_5 Phases and BeO 83

13. Phase Diagram Representing the NbO_2F and NiF_2 Concentrations in Molten Li_2BeF_4 at 600° as a Function of the Oxide Phases Present at Equilibrium . . 85

14. The Effect of NiF_2 Concentration on the Concentration of Niobium in Molten Li_2BeF_4 in the Presence of NiO and $NiNb_2O_6$ 90

15. Calculated Nb(V) Concentrations as a Function of NiF_2 Concentration for Various Assumed Nb(V)-Soluble Species. 91

16. The Temperature Dependence of the Equilibrium Quotient for the Reaction 93

17. Pourbaix Diagram for Niobium in Molten Li_2BeF_4 at 500° . . 94

18. Correlation Diagram of Heats of Reaction of Some Binary Oxides with Group Number and Period 100

19. Cyclic Voltammograms of Molten LiF-BeF_2-ZrF_4 (65.6-29.4-5.0 Mole %) at a Platinum Electrode at 500°, Electrode Area: 0.08 cm^2; Scan Rate: 0.1 V/sec; Ni(II)/Ni Reference Electrode 103

FIGURE PAGE

20. Cyclic Voltammogram for the Reduction of Nb(V) in Molten LiF-BeF_2-ZrF_4 at Pyrolytic Graphite Electrode at 500°; Electrode Area: 0.16 cm^2; Nb(V) Concentration: 5.17 x 10^{-2} M; Scan Rate: 0.1 V/sec 104

21. Two Cycle Voltammograms for the Reduction of Nb^{5+} in Molten LiF-BeF_2-ZrF_4 at Pyrolytic Graphite Electrode at 500°. Plot of $Log(i_p - i)/i$ vs Potential for the First Reduction Step at Second Cycle 107

22. Cyclic Voltammograms at Fast Scan Rates for the Reduction of Nb(V) at Pyrolytic Graphite Electrode at 500°; Electrode Area: 0.16 cm^2; Nb(V) Concentration: 5.17 x 10^{-2} M 109

23. Polarogram Constructed from Current-Time Curves for the Reduction of Nb(V) at Platinum Electrode at 180° . . . 115

24. Chronopotentiograms for the Reduction of Nb(V) at Platinum Electrode at 180° and the Plot of $i_o\tau^{1/2}$ vs i_o 117

25. Tests of the AR-SR, SAR, and SR-AR Models for the Reduction of Nb(V) at Platinum Electrode at 180°. Melt Composition: $AlCl_3$-NaCl (63-37 Mole %); Electrode Area: 0.10 cm^2; Nb(V) Concentration: 1.50 x 10^{-2} M . . 119

26. Cyclic Voltammograms in the Absence and Presence of Nb(V). 120

FIGURE PAGE

27. Variation of i_p with Nb(V) Concentration at Platinum Electrode at 180° 122

28. Plot of $i_p/v^{1/2}$ vs v for the First Wave 123

29. Cyclic Voltammograms for the Reduction of Nb(V) at Tungsten Electrode at 180° 129

30. Polarograms Constructed from Current-Time Curves for the Reduction of Nb(V) at Platinum Electrode at 180° . 131

31. Polarogram Constructed from Current-Time Curves for the Reduction of Nb(V) at Platinum Electrode at 140° . . . 133

32. Chronopotentiograms for the Reduction of Nb(V) at Platinum Electrode 134

33. Cyclic Voltammograms for the Reduction of Nb(V) at Platinum Electrode 136

34. Polarogram Constructed from Current-Time Curves for the Reduction of Nb(V) at Platinum Electrode at 180°; Plot of E vs Log $(i_d - i)/i$ for the First Wave 143

35. Polarogram Constructed from Current-Time Curves at Tungsten Electrode at 180°. Plot of E vs Log $(i_d - i)/i$ for the Two Waves Shown 145

36. Differential Pulse Polarogram for the Reduction of Nb(V) at Platinum Electrode at 160° 148

37. Chronopotentiogram for the First Reduction Step of Nb(V) at Platinum Electrode at 160° 150

FIGURE PAGE

38. Plot of $i_o\tau^{1/2}$ vs i_o for the First Reduction Step of Nb(V) at Platinum Electrode at 180° 151

39. Chronopotentiogram for the Reduction of Nb(V) at Tungsten Electrode at 160° 152

40. Cyclic Voltammogram (First Scan) for the Reduction of Nb(V) at Platinum Electrode at 160° 156

41. Cyclic Voltammograms for the Reduction of Nb(V) at Platinum Electrode at Fast Scan Rates 157

42. Cyclic Voltammogram for the Reduction of Nb(V) at Tungsten Electrode at 180° 158

43. Variation of i_p of the First Reduction Step with Nb(V) Concentration at Platinum Electrode at 180° 159

44. Plot of $i_p/v^{1/2}$ vs v for the First Reduction Step at Platinum Electrode 160

45. Plot of $E^c_{p(1)}$ vs Log C for the Reduction of Nb^{5+} to Nb^{4+} at Platinum Electrode at 180° 166

46. Cyclic Voltammogram for the Reduction of Nb(V) at Platinum Electrode at 300° 171

47. Cyclic Voltammogram for the Reduction of Nb(V) at Platinum Electrode at 220° 172

48. Variation if i_p with Nb(V) (Added as $NbOCl_3$) Concentration at Platinum Electrode 183

49. Polarogram Constructed from Current-Time Curves for the Reduction of NbO(III) at Tungsten Electrode at 245° . . 188

FIGURE PAGE

50. Polarogram Constructed from Current-Time Curves for the Reduction of NbO(III) at Platinum Electrode at 190° . . 190

51. Differential Pulse Polarograms for the Reduction of NbO(III) at Tungsten Electrode at 280° 191

52. Differential Pulse Polarograms for the Reduction of NbO(III) at Tungsten Electrode at 180° 192

53. Linear Sweep Voltammograms for the Reduction of NbO(III) at the Platinum Electrode at 175° 195

54. Cyclic Voltammogram for the Reduction of NbO(III) at the Platinum Electrode at 150° 197

55. Cyclic Voltammograms for the Reduction of NbO(III) at the Platinum Electrode at 190° 198

56. Cyclic Voltammograms for the Reduction of NbO(III) at the Platinum Electrode at 340° 201

57. Cyclic Voltammogram for the Reduction of NbO(III) at the Platinum Electrode at 340° 202

58. Raman Spectrum of Solid Nb_2O_5; 4880 Å Laser Excitation . . 208

59. Infrared Spectrum of Solid Nb_2O_5 at 25° 209

60. Raman Spectrum of Solid $NiNb_2O_6$ at 25°; 4880 Å Laser Excitation 210

61. Infrared Spectrum of Solid $NiNb_2O_6$ at 25° 211

CHAPTER I

INTRODUCTION

The research activity on molten salt systems has increased rapidly in recent years and produced many important advances in the understanding of these systems. Fundamental aspects as well as practical applications have benefitted from such research. In fundamental studies the molten salt systems provide an important testing ground for theories of liquids and solutions. These systems also represent a large class of nonaqueous solvents in which interesting coordination, redox and acid-base reactions may be explored by spectroscopic, electrochemical and thermodynamic techniques. Molten salts have been applied to process metallurgy, nuclear technology, fuel cells and batteries and also used as catalysts or as reaction media.

Because of the importance of this new fascinating area of research, molten salt chemistry and its various aspects have been extensively reviewed and discussed in recent years. The reviews include theoretical investigations of the structure of molten salts,[1-3] thermodynamic studies,[1-12] transport properties,[1,2,4,5,8,9,13,14] electronic spectroscopic studies,[1,2,4,5,8,15,16] vibrational spectroscopic studies,[1,5,6,8,15] electrochemical studies,[1,2,5,9,13,17-25] reaction kinetics,[2] diffraction studies of molten salt structures,[1,9] phase diagrams,[1,5,8] experimental techniques,[6,8,26-28] molten salt batteries and fuel cells,[6,8] stabilities of complex ions in molten salts,[29] complexes of actinides in molten salts,[30] and nuclear applications of molten salts.[31,32]

Niobium is an important fission product and structural material. The understanding of the chemistry of niobium in molten salts is useful both in nuclear technology and in process metallurgy. The purpose of this dissertation is to study the heterogeneous equilibrium and redox reactions of niobium in molten fluorides and in chloroaluminates by using solubility measurements and electrochemical techniques. In this chapter we will first review some chemistry of niobium which is of interest, and then summarize some of the basic principles which will be used in the discussion that follows.

A. Review of the Literature

1. Oxide Chemistry in Molten Li_2BeF_4 and $LiF-BeF_2-ThF_4$

The oxide chemistry in molten fluorides has been studied by a transpiration method[33] and by solubility measurements.[34-39] The work has been done at the Oak Ridge National Laboratory in connection with the development of a molten salt reactor experiment (MSRE) and a molten salt breeder reactor (MSBR).[35,38] Most of the work was concerned with the oxide chemistry of actinide elements (such as ThO_2, PaO_2, Pa_2O_5, UO_2, PuO_2). The purposes of these studies were either to examine the tolerance limits for oxide contamination of an MSBR fuel or to find separation or recycling conditions based on oxide precipitation.[36-38] Table I gives a summary of reactions that have been studied in these melts.

The heterogeneous equilibrium studies of the oxide chemistry in molten fluorides indicate that the stable solid phases in the molten fluorides are either pure solids or solid solutions. The soluble species

TABLE I

OXIDE CHEMISTRY IN MOLTEN Li_2BeF_4 AND $LiF-BeF_2-ThF_4$

Molten Fluoride Mixture	Reaction[a]	Q[b]	Log Q = a + b $(10^3/T)^c$ a	b	Reference
$LiF-BeF_2$ (67-33 mole %)	$BeO(c) \rightleftarrows Be^{2+}(d) + O^{2-}(d)$	X_O^{2-}	-0.39	-2.63	33,34
	$ZrO_2(c) \rightleftarrows Zr^{4+}(d) + 2O^{2-}(d)$	$X_{Zr^{4+}} \cdot X_{O^{2-}}^2$	-3.66	-5.74	34
	$FeO(c) \rightleftarrows Fe^{2+}(d) + O^{2-}(d)$	$X_{Fe^{2+}} \cdot X_{O^{2-}}$	-0.73	-3.91	34
	$NiO(c) \rightleftarrows Ni^{2+}(d) + O^{2-}(d)$	$X_{Ni^{2+}} \cdot X_{O_2^{2-}}$	-2.76	-4.20	34
	$ThO_2(c) \rightleftarrows Th^{4+}(d) + 2O^{2-}(d)$	$X_{Th^{4+}} \cdot X_{O^{2-}}^2$	-2.46	-4.57	34
	$UO_2(c) \rightleftarrows U^{4+}(d) + 2O^{2-}(d)$	$X_{U^{4+}} \cdot X_{O^{2-}}^2$	-2.46	-6.95	34
	$1/2\ Pu_2O_3(c) + 3/2\ BeF_2(d) \rightleftarrows PuF_3(d) + 3/2\ BeO(c)$	X_{PuF_3}	-2.83	-1.11	34
	$2HF(g) + BeO(c) \rightleftarrows BeF_2(d) + H_2O(g)$	$P_{H_2O}/(P_{HF})^2$	-4.40	5.80	33
$LiF-BeF_2-ThF_4$ (72-16-12 mole %)	$1/2\ NiO(c) + 3/4\ ThO_2(ss) + PuF_3(d) \rightleftarrows PuO_2(ss) + 3/4\ ThF_4(d) + 1/2\ Ni^\circ$	$\frac{X_{PuO_2}}{X_{PuF_3}} \left(\frac{X_{ThF_4}}{ThO_2}\right)^{3/4}$	0.926		35
	$ThO_2(ss) + UF_4(d) \rightleftarrows UO_2(ss) + ThF_4(d)$	$\left(\frac{X_{UO_2}\gamma_{UO_2}}{X_{ThO_2}\gamma_{ThO_2}}\right)\left(\frac{X_{ThF_4}}{X_{UF_4}}\right)$	0.00	2.38	37

TABLE I (Continued)

Molten Fluoride Mixture	Reaction[a]	Q[b]	log Q = a + b(10³/T)[c] a	b	Reference
	$PaF_4(d) + ThO_2(ss) \rightleftarrows PaO_2(ss) + ThF_4(d)$	$\frac{X_{PuO_2}\gamma_{PuO_2}}{X_{ThO_2}\gamma_{ThO_2}} \frac{X_{ThF_4}}{X_{PaF_4}}$	0.00	1.64	38
	$PaO_{2.5} \cdot nLiF(c) + 5/4\ ThF_4(d) \rightleftarrows PaF_5(d) + nLiF(d) + 5/4\ ThO_2(c)$	$\frac{X_{PaF_5}}{(X_{ThF_4})^{5/4}}$	4.49	-8.66	38
	$PaO_{2.5} \cdot nLiF(c) + 5/4\ UF_4(d) \rightleftarrows PaF_5(d) + nLiF(d) + 5/4\ UO_2(ss)$	$[(X_{UO_2}\gamma_{UO_2})^{5/4} (X_{PaF_5})]/(X_{UF_4})^{5/4}$	4.49	-5.69	38
	$PaO_{2.5} \cdot nLiF(c) + 5F^-(d) \rightleftarrows PaF_5(d) + nLiF(d) + 2.5O^{2-}(d)$	$(X_{PaF_5})(X_{O^{2-}})^{2.5}$	0.91	-12.76	38

[a](c), (ss), (d) and (g) indicate the crystalline, solid solution, dissolved and gaseous states, respectively.

[b]P_i is in atmospheres; X_i is the mole fraction.

[c]Temperature range: 700–1000°K.

in the melts are fluoride complexes. Except for the suggested presence of the Zr_2O^{6+} complex,[34] no other system has revealed, so far, the existence of oxo-fluoro complexes in these fluoride melts.

2. Chemistry of Niobium Oxides, Fluorides, Oxyfluorides and Oxo-fluoro Complexes

The chemistry of niobium oxides, fluorides, oxyfluorides and oxo-fluoro complexes has been extensively studied. Table II summarizes most of such reported compounds.[40-54] The complicated chemistry of the oxides and fluorides of niobium can be observed from this table.

Various oxyfluorides of niobium(V) have been prepared by fusing appropriate mixtures of niobium pentoxide and niobium dioxide fluoride (NbO_2F) or by the thermal decomposition of other oxyfluorides.[55-66] Some of the typical solid state reactions are shown in Table III. The binary compounds of niobium pentoxide with oxides of transition elements and with common niobium alloying elements have been studied by Goldschmidt[67,68] and Felten[69] for the purpose of improving the strength requirements and the oxidation resistance of niobium in high temperature applications. Goldschmidt found that Nb_2O_5 reacted with NiO. A rutile (tetragonal) structure of $NiNb_2O_6$ is formed at high temperature, and columbite (orthorhombic) $NiNb_2O_6$ is formed at low temperatures. Blasse[70] has suggested that the formation of metal oxides containing Nb^{5+} ($LiNbO_3$, Li_3NbO_4, $NiNb_2O_6$, $Ni_4Nb_2O_9$) can be qualitatively explained by introducing a metal-metal bond between pentavalent niobium ions. Tkachenko[71] and Abbattista[72] have investigated the equilibrium and phase relationships in the system Ni-Nb-O; they found that under equilibrium conditions at 1250° two niobates, $NiNb_2O_6$ and $Ni_4Nb_2O_9$, were present. Novin and Rappinger[52] have

TABLE II

NIOBIUM CHLORIDES, FLUORIDES, OXIDES AND COMPLEXES INVOLVING THESE ELEMENTS

Oxidation State	Chlorides and Fluorides	Oxides	Oxychlorides and Oxyfluorides	Chloro, Fluoro, Oxo-chloro and Oxo-fluoro Complexes	Complex Oxides (Niobates)
V	$NbCl_5$ or (Nb_2Cl_{10})	Nb_2O_5(α,β,γ,δ,ε form)	$NbOCl_3$, NbO_2Cl, Nb_3O_7Cl	$NaNbCl_6$, $NaNbOCl_4$, K_2NbOCl_5	$LiNbO_3$, Li_3NbO_4
	NbF_5		$NbOF_3$, NbO_2F, Nb_3O_7F	$LiNbF_6$, K_2NbF_7, K_3NbF_8	$LiNb_3O_8$, $NiNb_2O_6$
			$Nb_5O_{12}F$, $Nb_{17}O_{42}F$, $Nb_{31}O_{77}F$	K_2NbOF_5, K_3NbOF_6, K_2NbO_3F	$Ni_4Nb_2O_9$, Fe_3NbO_7
			$Nb_{59}O_{147}F$, $Nb_{34}O_{84}F_2$	$K_3NbO_2F_4$, $K_2NaNbO_2F_4$	$FeNb_3O_9$, $Fe_8Nb_{10}O_{37}$
			$Nb_{65}O_{161}F_3$	KNb_2O_5F, $LiNb_6O_{15}F$, $NaSrNb_2O_6F$	$AlNbO_4$, $AlNb_{11}O_{29}$
				$MgNb_{14}O_{35}F_2$	
IV	$NbCl_4$ or Nb_2Cl_8	NbO_2	$NbOCl_2$	Na_2NbCl_6, $CaNbCl_5$	$CaNbO_3$, $CuNbO_3$
	NbF_4			$MNbO_2F$(M:Li,Na,K)	Na_2NbO_3, Na_4NbO_4
III	$NbCl_3$		NbOCl	$M_3Nb_2Cl_9$(M:Na,K,Rb,Cs)	
	NbF_3				
II	$NbCl_2$	NbO		M_2NbCl_4(M:K,Rb,Cs)	

TABLE II (Continued)

Oxidation State	Chlorides and Fluorides	Oxides	Oxychlorides and Oxyfluorides	Chloro, Fluoro, Oxo-chloro and Oxo-fluoro Complexes	Complex Oxides (Niobates)
					$CuNbO_{3.12}$
Non-stoichiometric Compounds	Nb_3Cl_8 ($NbCl_{2.67}$)	$NbO_{2.49}$ ($Nb_{53}O_{132}$)			
	Nb_4Cl_{11} ($NbCl_{2.5}$)	$NbO_{2.48}$	$NbO_{0.99}F_{2.25}$	$CsNb_4Cl_{11}$	
	Nb_6Cl_{15} ($NbCl_{2.5}$)	$NbO_{2.473}$ ($Nb_{25}O_{62}$)	$NbO_{1.65}F_{1.39}$	$K_4Nb_6Cl_{18}$	$Ni_{2/3}Nb_{11}\ 1/3O_{29}$
	Nb_6Cl_{14} ($NbCl_{2.33}$)	$NbO_{2.46}$ ($Nb_{47}O_{116}$)		$Na_4Nb_6Cl_{18}$	$Ni_{1/3}Nb_{24}\ 2/3O_{62}$
		$NbO_{2.45}$ ($Nb_{22}O_{54}$)	$NbO_{1.25}F_{1.75}$		
	Nb_6Cl_{11}($NbCl_{1.83}$)	$NbO_{2.42}$ ($Nb_{12}O_{29}$)			
	Nb_6F_{15} ($NbF_{2.5}$)	$NbO_{2.40}$			

TABLE III

SOLID STATE REACTIONS OF NIOBIUM OXIDE AND OXYFLUORIDE

Reaction	Experimental Temperature (°C)	Compound Formed	Reference
$4NbO_2F(s) \rightarrow Nb_3O_7F(s) + NbOF_3(g)$	700-760	Nb_3O_7F (orthorhombic)	55,56,57
$Nb_2O_5(s) + NbO_2F(s) \rightarrow Nb_3O_7F(s)$	1000-1270	Nb_3O_7F (orthorhombic)	57,58,60
$Nb_2O_5(s) + NbO_2F(s) \rightarrow Nb_5O_{12}F(s)$	500-800	$Nb_5O_{12}F$ (orthorhombic)	55
$8Nb_2O_5(s) + NbO_2F(s) \rightarrow Nb_{17}O_{42}F(s)$		$Nb_{17}O_{42}F$ (monoclinic)	56
$15Nb_2O_5(s) + NbO_2F(s) \rightarrow Nb_{31}O_{77}F(s)$	1100	$Nb_{31}O_{77}F$ (monoclinic)	56
$2KF(s) + NaF(s) + NbO_2F(s) \rightarrow K_2NaNbO_2F_4(s)$	400-900	$K_2NaNbO_2F_4$ (cubic)	61
$KF + Nb_2O_5(s) \rightarrow KNb_2O_5F(s)$	900	KNb_2O_5 (tetragonal)	63
$LiF + 3Nb_2O_5(s) \rightarrow LiNb_6O_{15}F(s)$	800-1200	$LiNb_6O_{15}F$ (orthorhombic)	64,65
$3LiNb_3O_8(s) + 4Nb_2O_5(s) + NbOF_3(g) \rightarrow 3LiNb_6O_{15}F$	940-1190	$LiNb_6O_{15}F$ (orthorhombic)	59
$LiF + NbO_2(s) \rightarrow LiNbO_2F$	800	$LiNbO_2F$ (hexagonal)	66

performed a phase analysis on the niobium rich side of the $NiO-Nb_2O_5$ at temperatures between 1200-1500°, and observed that $Ni_{2/3}Nb_{11\ 1/3}O_{29}$ (orthorhombic), $Ni_{2/3}Nb_{11\ 1/3}O_{29}$ (monoclinic), and $Ni_{1/3}Nb_{24\ 2/3}O_{62}$ were present. Recently, Senegas and Galy[73] studied the solid reactions of the system $NiNb_2O_6-NiF_2$ and reported that solid solutions $Ni_{3-2x}Nb_{2x}O_{6x}F_{6(1-x)}$ ($0 \leq x \leq 0.65$ at 800°) with rutile structure were formed, where the x-value increases with increasing temperature.

Weaver et al.,[74] have studied the disproportionation reaction $2NbF_4(s) \rightleftharpoons NbF_3(s) + NbF_5(g)$, the polymerization of NbF_5,[75] and the decomposition reaction $4NbO_2F(s) \rightleftharpoons Nb_3O_7F(s) + NbOF_3(g)$, the latter two by means of time of flight mass spectrometry. For the last reaction, an enthalpy of $\Delta H° = 30 \pm 1.5$ (Kcal/mole) was obtained. Toth and Smith[76] have studied the UV and visible spectra of NbF_5 and NbF_4 both in the molten state and in Li_2BeF_4 solution, but the results were not reproducible.

Budova and Voskresenskaya[77] have examined the dissolution of the acidic oxide Nb_2O_5 in various fluorides (LiF, NaF, KF, Na_3AlF_6, and binary mixtures of these fluorides) by a visual method. The X-ray diffraction patterns of the solid phases obtained from the system containing lithium and sodium indicated the formation of lithium and sodium metaniobate ($LiNbO_3$ and $NaNbO_3$). The solubility of Nb_2O_5 in the individual fluorides at 1000° increases in the order of $LiF < NaF < Na_3AlF_6 < KF < K_3AlF_6$, which is opposite to the solubility order of basic oxides (those of Be, Mg, Ca, Ba, Cu, and Zn). They suggested that the difference was possibly due to the formation of oxo and oxo-fluoro complexes. Fordyce and Baum have studied the infrared-reflection spectra of Nb(V) in molten LiF-KF.[78] From their observed spectra, they suggested that the NbF_7^{2-} complex ion

was the predominant species in the melts, and that the $NbOF_6^{3-}$ anion was the predominant species in the melts containing hydrolyzed Nb(V). Pausewang and Rüdorff[61] studied the following reaction,

$$2KF(s) + NaF(s) + NbO_2F(s) \rightarrow K_2NaNbO_2F_4(s)$$

in the temperature range 400-900°. Based on infrared investigations they reported that $NbO_2F_4^{3-}$ belongs to C_{2v} symmetry. The Nb-O stretching frequencies were observed between 810-950 cm^{-1}.

Weaver et al.[79] have equilibrated niobium metal and a lower valent niobium fluoride in molten Li_2BeF_4 with hydrogen and hydrogen fluoride. Their results suggested that the lowest oxidation state of niobium was four..

3. Chemistry of Niobium Chlorides and Oxychlorides

The various aspects, such as thermodynamic and physical properties,[40,46] synthesis and reactions,[40-42,44,45,51,80,81] bonding and structure,[40-47,50] of the chemistry of niobium chlorides and oxychlorides have been reviewed. These compounds are listed in Table II, p 6. Thermodynamic properties are listed in Table IV.[35,46,83-86]

Niobium pentachloride is dimeric in the solid state.[87] This compound behaves as a Lewis acid in solution, forming $NbCl_6^-$ and adducts such as $NbCl_5 \cdot L$, where L = R_2O, R_2S, $POCl_3$, etc.[43] The preparation and properties of $MNbCl_6$ (M: Na, K, Rb, Cs) have been reviewed by Canterford and Colton.[40] The formation of M_2NbCl_6 (M: Na, K, Rb, Cs), M_2NbCl_5 (M: Na, K, Rb, Cs) and M_2NbCl_4 (M: K, Rb, Cs) was reported by Safonov et al.[88-94]

The metal-metal bonding, metal atom clusters and nonstoichiometry are characteristic features of the lower oxidation states of niobium

TABLE IV

THERMODYNAMIC PROPERTIES OF SOME NIOBIUM COMPOUNDS

Compound	ΔH°_{298} (Kcal/mole)	S°_{298}(e.u.)	ΔG°_T (Kcal/mole)	Temperature Range (°K)	Reference
Nb_2O_5(c)	-453.5 ± 0.4	32.8 ± 0.2	-451.85 + 102.55 ($T/10^3$)		46,82
			-440.2 + 94.1 ($T/10^3$)	1050-1300	83
			-455.5 + 152.6 ($T/10^3$) - 15.2 ($T/10^3$) log T	298-1700	46
NbO_2(c)	-189.7 ± 1	(13.0)	-189.24 + 41.93 ($T/10^3$)		46,84
			-184.5 + 38.7 ($T/10^3$)	1177-1361	95
			-190.9 + 71.0 ($T/10^3$) - 9.0 ($T/10^3$) log T	298-1040	46
NbO(c)	-97.2 ± 1	(11.5)	-99.5 + 20.7 ($T/10^3$)	1177-1388	46,83
			-97.6 + 28.0 ($T/10^3$) - 2.8 ($T/10^3$) log T		46
$NbCl_5$(c)	-190.5 ± 0.5	54.0 ± 2	-196.2 + 90.9 ($T/10^3$)	298-477	85
			-197.9 + 136.3 ($T/10^3$) - 15.9 ($T/10^3$) log T		46,85
NbF_5(g)	-433.5 ± 1.5	38.3 ± 0.1	-416.7 + 54.5 ($T/10^3$)		35

TABLE IV (Continued)

Compound	ΔH°_{298} (Kcal/mole)	S°_{298} (e.u.)	ΔG°_T (Kcal/mole)	Temperature Range (°K)	Reference
$NbCl_4(c)$	-166.0 ± 1	44.0 ± 2	$-169.1 + 72.9\ (T/10^3)$	298-600	85
			$-169.5 + 111.2\ (T/10^3) - 13.3\ (T/10^3)\ \log T$		46,85
$NbCl_{2.67}(c)$	-128.6 ± 1	32.8 ± 2	$-130.5 + 54.8\ (T/10^3)$	298-700	46,85
$NbCl_{2.33}(c)$	-113.5 ± 1	31.2 ± 2	$-114.61 + 61.83\ (T/10^3) - 7.65\ (T/10^3)\ \log T$		46,83
$NbCl_3(c)$	-139 ± 3	$(35) \pm 2.5$	$-134.7 + 49.9\ (T/10^3)$		46,85,86
			$-135.5 + 126.5\ (T/10^3) - 26.6\ (T/10^3)\ \log T$		85,86
$NbOCl_3(c)$	-210.5 ± 1.5	(38)	$-210.5 + 75.0\ (T/10^3)$		46
$NbOCl_2(c)$	-185.0 ± 1	(29)	$-185.0 + 57.4\ (T/10^3)$		46

chlorides. The degree of metal condensation increases with decreasing oxidation state — a consequence of lowering the halogen-metal ratio.[40] The increasing condensation may be summarized as follows:

$$NbCl_5(Nb_2Cl_{10}) \rightarrow NbCl_4(Nb_2Cl_8) \longrightarrow Nb_3Cl_8(NbCl_{2.67}) \xrightarrow{Nb/MX} MNb_4Cl_{11}(M{:}Cs,Rb)$$

$$\text{Nb or Nb + KCl} \rightarrow (Nb_6Cl_{12})Cl_{n/2} \leftarrow \text{Nb or Nb + KCl}$$

$$n = 4, 6 \text{ or}$$

$$K_4Nb_6Cl_{18}$$

Niobium oxychloride ($NbOCl_3$) has the appearance of white long fibrous needles. According to Ozin and Reynolds[95] the highest niobium/-oxygen vibration mode in the solid is 769 cm^{-1}; this frequency was assigned to Nb-O-Nb vibration. The spectra of $NbOCl_3$ indicate the existence of infinite Nb-O-Nb chains.[95] Morozov and Krokhin[96] studied the reaction between $NbOCl_3$ and alkali chlorides by thermal analysis. Niobium oxychloride reacts with alkali chlorides to form $MNbOCl_4$ and M_2NbOCl_5 (M:K, Rb, Cs). The stability of the compounds decreases with decreasing ionic radius of the alkali metal (Cs_2NbOCl_5 > Rb_2NbOCl_5 > K_2NbOCl_5). Canterford and Cotton[40] have reviewed some of the thermodynamic and spectroscopic properties of M_2NbOCl_5 and $MNbOCl_4$ (M:Na, K, Rb, Cs).

Schäfer *et al.*[97] reported the formation of $NbCl_5(g)$ and AlOCl by the reaction of $NbOCl_3(s)$ with $Al_2Cl_6(g)$.

$$2NbOCl_3 + Al_2Cl_6(g) \rightleftarrows 2AlOCl(s) + 2NbCl_5(g).$$

Korshunov and Rokhlenko[98] studied the reactions between Nb_2O_5 and $Na(K)AlCl_4$ and $NbOCl_3$ and $Na(K)AlCl_4$ by vapor pressure measurements.

They reported that Nb_2O_5 is converted to $NbOCl_3$, but no interaction was observed between $Na(K)AlCl_4$ and $NbOCl_3$.

4. Electrochemistry of Niobium in Molten Chlorides and Fluorides

The electrochemistry of niobium in aqueous solutions is complicated by the tendency of niobium(V) to hydrolyze and by the instability of the lower oxidation states of the element.[99] The complications due to the hydrolysis of Nb(V) were also observed in the electrochemical studies of Nb(V) in nonaqueous solvents, such as DMF.[100] The electrochemistry of niobium in molten chlorides has been studied mostly in alkali chloride mixtures, and the investigated species of niobium in the melts were normally produced by anodic dissolution of the niobium metal. Several techniques have been applied to the investigation of the electrochemistry of niobium in molten salts, such as voltammetry,[101-104] potentiometry,[105-109] and chronopotentiometry.[110-112]

Gut[101] reported that niobium(V) gave two polarographic reduction waves at -0.78V and -1.28V vs a Pt(II)/Pt reference electrode in the melt composition $AlCl_3$-NaCl-KCl (50-25-25 mole %) at 200°. In the more acidic melt, $AlCl_3$-NaCl-KCl (60-26-14 mole %) at 120°, the two steps almost overlap. Gut interpreted the overlapping as being due to a one step 2-electron reduction. However, the E vs log $(i_d - i)/i$ plot was not linear. Caton and Freund[102] carried out polarographic studies on niobium in molten LiCl-KCl eutectic. Niobium ions were generated by controlled potential electrolysis with an average n value of 3.64. They suggested that the solution contained Nb^{4+} and Nb^{3+} in a ratio of 3:1. Two polarographic waves were observed. The first wave corresponded to Nb^{4+}/Nb^{3+}, but the second wave was not reproducible and the deposition of a black

solid was observed. Sakawa and Kuroda[104] studied the voltammetric reduction of NbF_7^{2-} in molten NaCl-KCl (50-50 mole %) at a molybdenum electrode. They concluded that the reduction proceeded in two steps. The first step was a two electron reversible process forming a soluble reduced species and the second step was an irreversible process with metallic niobium as a product.

Yang and coworkers[105] studied the following cell $Nb/NbCl_3$, LiCl-KCl (eutectic)||LiCl-KCl (eutectic), AgCl/Ag in the temperature range 760-830°. Niobium was generated in the melt by anodic dissolution of the metal. They claimed that Nb^{3+} was the predominant species in dilute melts, but that mixed valence states (possibly Nb^{3+} and Nb^{4+}) prevailed in more concentrated melts. The relative amounts of the coexisting species in equilibrium melts varied with the temperature and niobium concentration. Suzuki[106,107] investigated the equilibrium between niobium and its subchloride in LiCl-KCl eutectic melt at temperatures of 500 and 650°. He concluded that the equilibrium composition of the subchloride in the melt was Nb_3^{8+}. Pimenov[108] in the same melt also found the average valence for niobium ions in equilibrium with the metal to be less than 3. However, he assumed that these results were due to the presence of Nb^{2+} and Nb^{3+} ions in equilibrium. Based on this assumption, he obtained the standard potentials for Nb^{2+}/Nb, Nb^{3+}/Nb, and Nb^{3+}/Nb^{2+} couples and the equilibrium constant for the disproportionation reaction $3Nb^{2+} \rightleftarrows 2Nb^{3+} + Nb$. Ivanovski and Krasilnikov[109] studied the interaction of $NbCl_2$ and $NbCl_3$ in molten NaCl-KCl mixtures with fluoride ions by potentiometric techniques. They concluded that the interaction led

to the formation of insoluble tri- and divalent niobium fluoride compounds (Na_2NbF_4, Na_3NbF_6, K_2NbF_4 and K_3NbF_6).

Pimenov and Baimakov[110] determined the diffusion coefficients for Nb^{3+} and Nb^{2+} in molten NaCl-KCl and LiCl-KCl mixtures by using chronopotentiometry. Nb^{3+} was produced by anodization and Nb^{2+} was formed by reaction of Nb^{3+} with niobium metal. Recently Inman[111] investigated the niobium system in molten alkali chloride mixtures by chronopotentiometry. No reduction wave could be detected for Nb^{3+} which was formed at low current densities (< 5 mA/cm^2). Nb^{4+}, produced at high current densities (> 50 mA/cm^2), was reduced reversibly to Nb^{3+}.

Very few electrochemical studies of niobium in molten fluorides have been made. Senderoff and Mellors[112] have investigated by chronopotentiometry the electrode reduction of Nb(V) from K_2NbF_7 added to LiF-NaF-KF (46.5-11.5-42.0 mole %) at 750°. They concluded that the reduction of Nb^{5+} in solution involved three steps: Nb^{5+}/Nb^{4+}, Nb^{4+}/Nb^{+}, and Nb^{+}/Nb at the potentials -0.11V, -0.76V, and -1.02V, respectively, with respect to Ni/Ni(II) (1 mole %) reference electrode. The first two steps were reversible and diffusion controlled; the last step was irreversible. Voltammetric studies of niobium in molten LiF-BeF_2-ZrF_4 (65.6-27.4-5.0 mole %) at 500° were initiated by Clayton,[113] but the results were not reproducible and no conclusions could be reached. Table V gives a summary of the reported electrochemical studies of niobium in molten chlorides and fluorides.

It is apparent that more work is needed to resolve the contradictory results, to examine the effect of melt composition on reduction mechanisms, and to distinguish the differences in the mechanism of reduction of Nb(V)

TABLE V

ELECTROCHEMICAL STUDIES OF NIOBIUM IN MOLTEN CHLORIDES AND FLUORIDES

Experimental Technique	Melt Composition	Temperature °C	Electrodes	Solutes Investigated	Reference
Voltammetry	$AlCl_3$-NaCl-KCl (60-26-14 mole %) $AlCl_3$-NaCl-KCl (50-25-25 mole %)	120 200	Working electrode: Pt Reference electrode Pt(II)/Pt	Nb^{5+} (by adding $NbCl_5$)	101
Voltammetry	LiCl-KCl (eutectic)	450	Working electrode: Pt Reference electrode: Pt(II)/Pt	Nb^{4+} and Nb^{3+} (by anodic dissolution of the Nb metal)	102
Voltammetry	NaCl-KCl (50-50 mole %) LiCl-KCl (eutectic)	650 450	Working electrode: graphite	Nb^{4+} and Nb^{3+} (by anodic dissolution of Nb)	103
Voltammetry	NaCl-KCl (50-50 mole %)	750	Working electrode: Mo	Nb^{5+} (by adding K_2NbF_7)	104
Potentiometry	LiCl-KCl (eutectic)	760-830	Working electrode: Nb Reference electrode: Ag(I)/Ag	Nb^{3+} and Nb^{4+} ($3<n<4$) (by anodic dissolution of Nb metal)	105
Potentiometry	LiCl-KCl (eutectic)	500 650	Working electrode: Nb Reference electrode: Ag(I)/Ag	Nb_3^{8+} (by anodic dissolution of Nb metal and by adding Nb_3Cl_8)	106,107
Potentiometry	LiCl-KCl (eutectic)	400-700	Working electrode: Nb Reference electrode: Ag(I)/Ag	Nb^{3+} and Nb^{2+} (by anodic dissolution of Nb metal)	108

TABLE V (Continued)

Experimental Technique	Melt Composition	Temperature °C	Electrodes	Solutes Investigated	Reference
Potentiometric	NaCl-KCl (50-50 mole %)	700-900	Working electrode: Nb Reference electrode: $Cl_2(g)/Cl^-$	Nb^{3+} and Nb^{2+} (by anodic dissolution of Nb metal)	109
Chronopotentiometry	NaCl-KCl (50-50 mole %) LiCl-KCl (eutectic)	800 400-600	Working electrode: Mo	Nb^{2+} and Nb^{3+} (by anodic dissolution of Nb metal)	110
Chronopotentiometry	NaCl-KCl (50-50 mole %) LiCl-KCl (eutectic) KCl-CsCl (70-30 and 50-50 mole %)	760 720 760 750	Working electrode: Pt	Nb^{4+} and Nb^{3+} (by anodic dissolution of Nb metal)	111
Chronopotentiometry	LiF-NaF-KF (46.5-11.5-42.0 mole %)	650-800	Working electrode: Pt Reference electrode: Ni(II)/Ni	Nb^{5+} (by adding K_2NbF_7)	112

chloride and oxychloride by means of better electrochemical techniques.

B. Review of Basic Principles

1. Acid-Base Concepts in Molten Chlorides and Fluorides

The acid-base concept, which has been employed in molten oxide containing systems, was introduced by Lux and Flood.[114,115]

$$\text{Acid} + O^{2-} \rightleftarrows \text{Base or Donor (complex)} \rightleftarrows \text{Acceptor} + O^{2-} \qquad (1)$$

$$K = \frac{(\text{Base})}{(\text{Acid})(O^{2-})} \qquad (1a)$$

$$pO^{2-} = -pK - \log \frac{(\text{Base})}{(\text{Acid})} \qquad (1b)$$

This concept, which is related to the Lewis acid-base concept, can be extended to molten halide systems, namely

$$\text{Acid} + X^{-} \rightleftarrows \text{Base} \quad ,$$

e.g.,

$$BeF_2 + 2F^{-} \rightleftarrows BeF_4^{2-} \quad .$$

Tremillon and Letisse[116] have applied these ideas to $AlCl_3$-NaCl melts. The structure of $AlCl_3$-NaCl melts can be summarized as follows:[117-120]

X_{AlCl_3}	0.00	0.50	0.67	1.00
X_{NaCl}	1.00	0.50	0.33	0.00
Major species in the melt	Na^+, Cl^-; $AlCl_4^-$	Na^+, $AlCl_4^-$; $Al_2Cl_7^-$, Al_2Cl_6	Na^+, $Al_2Cl_7^-$; $AlCl_4^-$, Al_2Cl_6	
Stoichiometry	NaCl	$NaAlCl_4$	$Na_2Al_2Cl_7$	Al_2Cl_6

$AlCl_3$-NaCl melts can be described by the following three equilibrium reactions[116,118,121-123]

$$2AlCl_3(l) \rightleftarrows Al_2Cl_6(l) \qquad K_2 \qquad (2)$$

$$AlCl_4^- + AlCl_3 \rightleftarrows Al_2Cl_7^- \qquad K_3 \qquad (3)$$

$$2AlCl_4^- \rightleftarrows Al_2Cl_7^- + Cl^- \qquad K_4 \qquad (4)$$

The equilibrium constant for reaction (4) is

$$K_4 = \frac{(X_{Al_2Cl_7^-})(X_{Cl^-})}{(X_{AlCl_4^-})^2} \qquad (4a)$$

where

$$pCl^- = pK_4 - \log \frac{(X_{AlCl_4^-})^2}{(X_{Al_2Cl_7^-})} \qquad (4b)$$

At 175°, the pCl^- values are 7.1, 6.5, 3.8 at the melt compositions $AlCl_3$-NaCl: 63-37, 55-45, 50-50 mole %, respectively.[118]

Thus, in the modified Lewis (or Lux-Flood) acid-base concept, pure alkali halides have the highest degree of basicity; as the solvent composition changes from alkali halide rich to alkali halide deficient melts, the solvent becomes acidic (pCl^- values increase).

Acid-base characteristics of the melts are very important in determining solute chemistry in molten salts, such as the stabilization of the lower oxidation state in acidic media (Cd_2^{2+},[124] Bi^+, Bi_5^{3+},[125,126] Hg_3^{2+},[127] Te_2^{2+},[128] Te_4^{2+},[129] coordination equilibria[119,130] and catalytic properties.[131]

The increasing stability of the higher oxidation states or the decreasing stability of the lower oxidation states in basic media can be seen from the following reaction:

$$Nb + 3NbCl_4(d) \rightleftarrows 4NbCl_3(d) \qquad (5)$$

$$\Delta G^\circ = - RT\ln \frac{(X_{NbCl_3}\gamma_{NbCl_3})^4}{(X_{NbCl_4}\gamma_{NbCl_4})^3} \quad (5a)$$

or

$$\log \frac{(X_{NbCl_3})^4}{(X_{NbCl_4})^3} = - \frac{\Delta G^\circ}{2.3\ RT} - \log \frac{(\gamma_{NbCl_3})^4}{(\gamma_{NbCl_4})^3} \quad (5b)$$

Ions of the higher valence state, owing to their higher charges and smaller sizes, have a greater tendency for forming complex ions, i.e., γ_{NbCl_4} is smaller than γ_{NbCl_3}, which indicates that

$$\log \frac{(X_{NbCl_3})^4}{(X_{NbCl_4})^3}$$

is likely to be smaller in the more basic melt. The higher valence state is thus favored in the more basic melt.

2. EMF Measurements

EMF measurements are capable of providing directly the free energy of the electrochemical reaction of the cell process, which gives a direct measure of the relative thermodynamic stability and determines the redox equilibrium and complex stability of electroactive species in a given solvent. For a redox reaction $O + ne \rightleftharpoons R$, the equilibrium potential, E_{eq}, is given by the Nernst equation:[132]

$$E_{eq} = E^\circ + \frac{RT}{nF} \ln \frac{a_O}{a_R} \quad (6)$$

where E° is the standard electrode potential of the redox couple (V), a_O and a_R are the activities of O and R, and the other symbols have their usual significance. In dilute solutions, the activity coefficients approach unity at infinite dilution and, therefore in the above equation

activities can be approximated by concentrations:

$$E_{eq} = E^\circ + \frac{RT}{nF} \ln \frac{\gamma_O X_O}{\gamma_R X_R} \approx E^\circ + \frac{RT}{nF} \ln \frac{X_O}{X_R} \qquad (7)$$

where γ's and X's are the activity coefficients and mole fractions of the oxidized and reduced forms. The standard electrode potential of the redox couple can be determined experimentally by measuring the potential with respect to a reference electrode as in the following cell:

$$M_1 | M_1^{m+}(a_1) || a_O, a_R | M_2 \text{ (inert electrode)},$$

where the left-hand cell represents a reference electrode. The cell voltage for a dilute solution is given by:

$$E_{cell} = E^o_{O/R} + \frac{RT}{nF} \ln \frac{C_O}{C_R} - (E^o_{M_1^{m+}/M_1} + \frac{RT}{mF} \ln C_{M_1^{m+}}) + E_j \qquad (8)$$

where C's are the molar concentrations and E_j is the liquid-liquid junction potential which arises from differences in concentration and mobility of ions diffusing across the interface;[20] its value is frequently negligible. Since $E_{M_1^{m+}/M_1} = 0$ for a reference electrode in a particular melt system, the cell voltage becomes

$$E_{cell} = E^o_{O/R} + \frac{RT}{nF} \ln \frac{C_O}{C_R} - \frac{RT}{mF} \ln C_{M_1^{m+}} \quad . \qquad (9)$$

Since the last term of this equation is known and constant for a reference electrode, a Nernst plot of E_{cell} vs log C_O/C_R should be linear with a slope of 2.3 RT/nF, from which n can be determined. Extrapolation of the plot to $C_O/C_R = 1$ will give the standard electrode potential, $E^o_{O/R}$. Such measurements have been proven useful for the determination of standard electrode potentials in molten salts and for the establishment of EMF

series. Various EMF series in different molten salt systems have been reported, such as LiF-BeF_2 (67-33 mole %),[35] LiF-BeF_2-ZrF_4 (65.6-29.4-5.0 mole %), LiF-NaF-KF (46.5-11.5-42.0 mole %),[133] $MgCl_2$-KCl (32.5-67.5 mole %),[134] LiCl-KCl eutectic, NaCl-KCl (50-50 mole %), NaF-KF eutectic, $MgCl_2$-NaCl-KCl, eutectic, $AlCl_3$-NaCl-KCl eutectic, and Li_2SO_4-Na_2SO_4-K_2SO_4 eutectic.[135] EMF measurements in molten salts[17,20-22] have been reviewed several times, most extensively by Laity[20] and Braunstein and Braunstein.[136]

EMF measurements may provide free energies of formation of pure molten salts, free energy of mixing in binary molten salt mixtures, excess chemical potentials of selected components in multicomponent molten salt mixtures, equilibrium constants for homogeneous and heterogeneous reactions, and EMF series of dissolved species in molten salts.[136,137] When interpreting EMF measurements, some sources of error should be noted, such as the junction potential, mixed potentials, thermal EMF, metal solubility in the solvent and electronic conduction.[136]

3. Representation of Equilibria by Pourbaix Diagrams

The Pourbaix diagram[138] is a convenient and useful way to illustrate the equilibria data in the form of E/pH, E/pO^{2-} and $\log(p_{HF}/p_{H_2}^{1/2})$/-(log X_O2-)[36,139-144] by a graphical method. The Pourbaix diagrams can be used to represent various complicated equilibria of inorganic chemistry, analytical chemistry, corrosion, electrodeposition, and metal extracting. In the case of an electrochemical reaction in aqueous solution for two soluble species

$$O + aH_2O + ne^- \rightleftarrows R + bH^+ \tag{10}$$

$$K_{10} = \frac{(R)(H^+)^b}{(O)} \tag{10a}$$

in which O is the oxidized form and R the reduced form. The Nernst equation corresponding to the above reaction is:

$$E = E^\circ + \frac{bRT}{nF} pH + \frac{RT}{nF} \log \frac{(O)}{(R)} \quad . \tag{10b}$$

It is noted that the equilibrium potential increases when the percentage of the oxidized form increases. From a E vs pH diagram, one can easily choose the conditions of potential and pH for which the oxidized form (O) and the reduced form (R) can be simultaneously stable.

In the case of the equilibria reactions in molten fluorides the stability of the ions and solids which participate in the hetereogeneous or homogeneous reactions can be represented in a Pourbaix diagram by using the following general equations:

(a) The stability boundary between a metal (M) and a soluble species (M^{x+}):

$$\frac{1}{x} M^{x+}(d) + 1/2\ H_2(g) + F^-(d) \rightleftarrows \frac{1}{x} M^\circ + HF(g) \tag{11}$$

$$K_{11} = \frac{p_{HF}}{p_{H_2}^{1/2}} \quad \frac{1}{(M^{x+})^{1/x}} \tag{11a}$$

$$\log\left(\frac{p_{HF}}{p_{H_2}^{1/2}}\right) = \log K_{11} + \frac{1}{x} \log (M^{x+}) \tag{11b}$$

in which the redox potential ($\log p_{HF}/p_{H_2}^{1/2}$) is a function of the metallic ion concentration.

(b) The stability boundary between a metal (M) and its oxide ($MO_{x/2}$)

$$\frac{1}{x} MO_{x/2}(s) + 1/2\ H_2(g) + F^-(d) \rightleftarrows \frac{1}{x} M^\circ + HF(g) + 1/2\ O^{2-}(d) \tag{12}$$

$$K_{12} = \left(\frac{p_{HF}}{p_{H_2}^{1/2}}\right)(O^{2-})^{1/2} \tag{12a}$$

$$\log \frac{p_{HF}}{p_{H_2}^{1/2}} = \log K_{12} - 1/2 \log (O^{2-}) \qquad (12b)$$

in which the stability (or the redox potential) of the oxide is a function of the oxide concentration.

(c) The stability boundary between two solid oxide phases $MO_{x/2}$ and $MO_{y/2}$:

$$MO_{y/2}(s) + \frac{y-x}{2} H_2(g) + (y-x)F^-(d) \rightleftarrows MO_{x/2}(s) + (y-x)HF(g) + (\frac{y-x}{2})O^{2-}(d) \qquad (13)$$

$$K_{13} = \left(\frac{p_{HF}}{p_{H_2}^{1/2}} \right)^{(y-x)} (O^{2-})^{(y-x)/2} \qquad (13a)$$

$$\log \frac{p_{HF}}{p_{H_2}^{1/2}} = \frac{1}{y-x} \log K_{13} - 1/2 \log (O^{2-}) \qquad (13b)$$

in which the stability (or redox potential) of the two oxides is a function of the oxide concentration.

(d) The stability boundary between two soluble species M^{x+} and M^{y+}:

$$M^{y+}(d) + (\frac{y-x}{2})H_2(g) + (y-x)F^-(d) \rightleftarrows M^{x+}(d) + (y-x)HF(g) \qquad (14)$$

$$K_{14} = \left(\frac{p_{HF}}{p_{H_2}^{1/2}} \right)^{(y-x)} \frac{(M^{x+})}{(M^{y+})} \qquad (14a)$$

$$\log \frac{p_{HF}}{p_{H_2}^{1/2}} = \frac{1}{y-x} \log K_{14} - \frac{1}{y-x} \log \frac{(M^{x+})}{(M^{y+})} \qquad (14b)$$

in which the stability (or redox potential) of the two soluble species is a function of their concentration ratio.

(e) The stability boundary between one soluble species (M^{x+}) and an insoluble oxide ($MO_{y/2}$):

$$MO_{y/2}(s) + (\frac{y-x}{2}) H_2(g) + (y-x)F^-(d) \rightleftarrows M^{x+} + (y-x) HF(g) + \frac{y}{2} O^{2-}(d) \qquad (15)$$

$$K_{15} = \left(\frac{p_{HF}}{p_{H_2}^{1/2}}\right)^{(y-x)} (M^{x+})(O^{2-})^{y/2} \qquad (15a)$$

$$\log \left(\frac{p_{HF}}{p_{H_2}^{1/2}}\right) = \frac{1}{y-x} \log K_{15} - \frac{1}{y-x} \log (M^{x+}) - \frac{y}{2(y-x)} \log (O^{2-}) \qquad (15b)$$

in which the relative stability of M^{x+} with respect to $MO_{y/2}$ is a function of M^{x+} ion concentration and oxide ion concentration The same principles can be applied to any equilibrium boundary if we have the required equilibrium data. We will apply these principles to illustrate the relative stabilities of niobium species in molten Li_2BeF_4 in Chapter III.

4. Linear Sweep Voltammetry

Linear sweep voltammetry (cyclic voltammetry, linear sweep chronoamperometry, stationary electrode polarography) is an electrochemical technique, in which the potential of the stationary working electrode is varied linearly with time (in an unstirred solution containing an electroactive species). The resulting current-potential curve (voltammogram) for a simple reversible reduction process has the shape shown in Figure 1. Assuming that the solution contains only the oxidized form, the potential sweep is begun at a potential anodic with respect to the standard potential (E°) of the redox couple (at which there is no current flow), and the potential is swept in a cathodic (negative) direction. As the standard potential is approached, the current increases rapidly until a maximum is reached and then the current decreases. Species O diffuses toward the electrode surface because a concentration gradient is established. Eventually, the rate of the electron transfer becomes more rapid than the rate of diffusion of O to the electrode surface; the peak current is

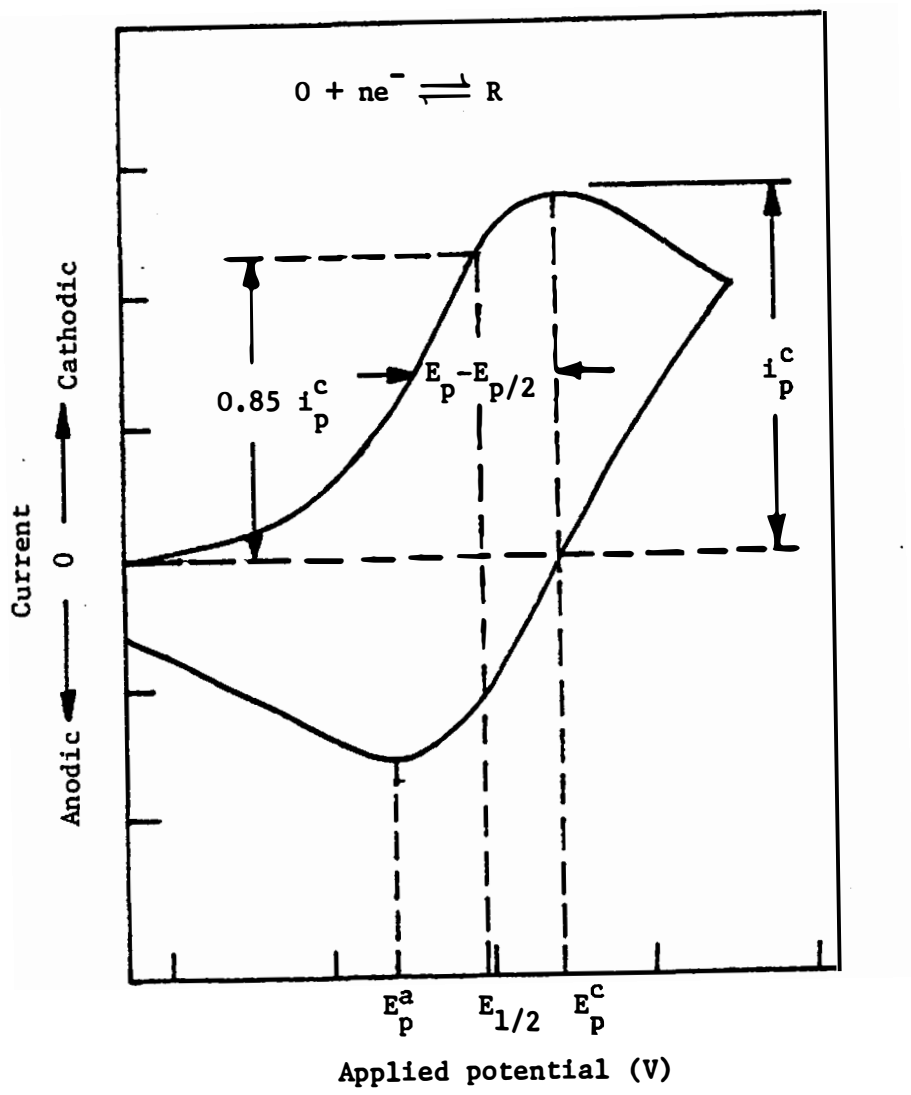


Figure 1. A typical cyclic voltammogram.

then observed. Beyond the peak the current decays because the concentration gradient decreases as the diffusion layer becomes larger. Upon reversal of the direction of the potential sweep, the reoxidation of the reduced species will commence to occur, resulting in an anodic peak. The composite current-potential curve is known as the cyclic voltammogram. The peak current i_p for a simple reversible (fast charge transfer) process is given by the Randles-Sevick equation:[132]

$$i_p = 0.452 \frac{(nF)^{3/2}}{(RT)^{1/2}} AD^{1/2}Cv^{1/2} \quad . \tag{16}$$

The peak potential E_p in this case is independent of the concentration of the reactant and is related to the polarographic half-wave potential $E_{1/2}$ by the following equation:[132]

$$E_p = E_{1/2} - 1.11 \frac{RT}{nF} \quad . \tag{17}$$

The value of $E_{1/2}$ may be estimated from a voltammogram of a simple reversible process from the fact that it occurs at a point corresponding to 0.85 i_p on the wave.[145] The half peak potential $E_{p/2}$ is sometimes a convenient reference point;[145] it is related to $E_{1/2}$ and E_p by the following equations:

$$E_{p/2} = E_{1/2} + 1.09 \frac{RT}{nF} \tag{18}$$

$$\Delta E = E_{p/2} - E_p = 2.20 \frac{RT}{nF} \quad . \tag{19}$$

The above equations are valid only for a reversible electrode reaction where the product is soluble in the electrode or in the solution. If the electrode reaction is a reversible deposition of an insoluble product under diffusion-controlled conditions, the peak current is given by:[132]

$$i_p = 0.61 \frac{(nF)^{3/2}}{(RT)^{1/2}} AD^{1/2}Cv^{1/2} \quad . \tag{20}$$

The peak potential in this case depends on the concentration of the reactants. For a reduction process it shifts in the anodic direction with increasing concentration as shown by:[132]

$$E_p = E^\circ + \frac{RT}{nF} \ln \gamma \cdot C - 0.849 \frac{RT}{nF} \tag{21}$$

where γ is the activity coefficient of the reactant. The half-peak potential is similarly dependent on the concentration of the reactant and, in fact, it differs from E_p by a constant value at all concentrations and sweep rates, as shown by the relationship:[146]

$$E_{p/2} - E_p = 0.77 \frac{RT}{nF} \quad . \tag{22}$$

Mamantov *et al.*[146] have concluded that, in linear sweep voltammetry for reversible processes where both the reactants and products are soluble, the plot of log $(i_p - i)/i$ vs potential should be linear in the range 0.35-0.70 i_p with a slope of 0.58 (nF/RT). For the reversible deposition of an insoluble substance, the plot of log $(i_p - i)$ vs E should result in a straight line in the range 0.5-0.9 i_p with a slope of 2.2 (nF/RT). These relationships were applied to a number of systems by Clayton.[113]

The theory of linear sweep voltammetry has been extended to irreversible electrode processes,[132,145,147,148] to chemical reactions coupled to reversible or irreversible charge transfers[145,149-158] to chemical reactions (irreversible,[149] reversible,[150,151] disproportionation[150]) coupled between two charge transfers (ECE mechanism), to multicharge transfers,[159] to multicharge transfer with catalytic (cyclic) regeneration of the reactions,[160] to adsorption of reactants or products, and

to rate controlled adsorption of products. In these theoretical treatments, convenient diagnostic criteria, such as the variation of $i_p/v^{1/2}$, E_p, and i_p^c/i_p^a with scan rate have been developed for the qualitative and quantitative characterization of unknown systems. Two reviews on linear sweep voltammetry have appeared recently.[161] Table VI shows an extensive summary of all the electrode reaction mechanisms that can be presently characterized by linear sweep voltammetry.

Comparing to other electrochemical techniques, the major advantages of linear sweep voltammetry are as follows: (1) this method is more sensitive, faster than conventional polarography[145] and the voltammograms are usually better defined; (2) the time scale of the experiment is wider; it can be varied from that of conventional polarography (a few mV per sec) to several thousand V/sec (where charging current and adsorption become important); (3) since the rate of voltage scan can be related to the kinetic parameters of the electrode reaction, the linear sweep voltammetry is one of the most effective tools for studying the mechanisms of the electrode reactions,[145,149] and to detect the electroactive intermediates.

Because of the extensively available theory and the short time of polarization, which can minimize the interference of the convective transport, linear sweep voltammetry has become a powerful tool for the investigation of molten salt systems. This method was originally applied to molten salt systems by Hills et al.[162] Extensive studies by this method have been made by Mamantov, Manning and coworkers.[137]

5. Chronopotentiometry

Chronopotentiometry is an electrochemical technique characterized by the application of a constant current and the subsequent measurement

TABLE VI

SUMMARY OF SOME EQUATIONS AND OF DIAGNOSTIC CRITERIA
OF LINEAR SWEEP VOLTAMMETRY

Mechanism	Peak Current and Peak Potential	Diagnostic Criteria	Reference
Reversible charge transfer $O + ne \rightleftarrows R$	Both reactants and products are soluble. $i_p = 0.452\ (nF)^{3/2}\ (D_o v)^{1/2}\ AC/(RT)^{1/2}$ $E_p - E_{p/2} = -2.20\ RT/nF$, $E_p - E_{1/2} = -1.09\ RT/nF$ Reversible deposition of an insoluble product $i_p = 0.61\ (nF)^{3/2}(D_o v)^{1/2}AC/(RT)^{1/2}$ $E_p = E^\circ + RT/nF \cdot \ln C_\gamma - 0.849\ RT/nF$ $E_p - E_{p/2} = -0.77\ RT/nF$	1. E_p is independent of v 2. $E_p^c - E_p^a = -(59/n)(T/298)$ mV and is independent of v 3. $i_p/v^{1/2}$ is independent of v. 4. i_p^a/i_p^c is unity and independent of v.	145 132
$mO + ne^- \rightleftarrows qR$	m = 2, q = 1 $i_p = 0.353(nF)^{3/2}(D_o v)^{1/2}AC/RT)^{1/2}$ $E_p - E_{p/2} = -(81.4/n)(T/298)$mV, $E_p - E_{1/2} = -(36.0/n)(T/298)$mV	1. $i_p^a/i_p^c = 1.09$ 2. $i_p/v^{1/2}$ is independent of v.	156
	m = 3, q = 1 $i_p = 0.303(nF)^{3/2}(D_o v)^{1/2}AC/(RT)^{1/2}$ $E_p - E_{p/2} = -(104.5/n)(T/298)$mV $E_p - E_{1/2} = -(49.8/n)(T/298)$mV	1. $i_p^a/i_p^c = 1.16$ 2. $i_p/v^{1/2}$ is independent of v The second and third order curves appear lower and broader than the first order voltammogram	

TABLE VI (Continued)

Mechanism	Peak Current and Peak Potential	Diagnostic Criteria	Reference
Quasi-reversible Charge transfer $O + ne^- \rightleftarrows R$		1. E_p shifts with v. 2. $E_p^c - E_p^a = -(60/n)(T/298)$mV at low v but increases as v increases. 3. $i_p/v^{1/2}$ is independent of v. 4. $i_p^a/i_p^c = 1$ only for $\alpha = 0.5$	147 148
Irreversible charge transfer $O + ne^- \xrightarrow{k_s} R$	$i_p = 0.227\ nFACk_s \exp[-\alpha n_a F\cdot(E_p - E^\circ)/RT]$ $E_p = E^\circ - RT\cdot[0.780 + \ln (D_o\ a)^{1/2} - \ln k_s]/\alpha n_a F$ $E_p - E_{p/2} = -1.857\ (RT/\alpha n_a F)$ $(E_p)_2 - (E_p)_1 = RT/\alpha n_a F \ln (v_1/v_2)^{1/2}$	1. E_p shifts cathodically by $(30/\alpha n)(T/298)$ mV for 10-fold increase in v. 2. $i_p/v^{1/2}$ is independent of v 3. $i_p^a = 0$	145
Reversible charge transfer followed by a reversible chemical reaction $O + ne^- \rightleftarrows R$ $R \underset{k_b}{\overset{k_f}{\rightleftharpoons}} Z$ $(K = k_b/k_f)(1 = k_f + k_b)$	If the chemical reaction is very slow, normal reversible behavior will be observed. If l/a is large and $K(a/l)^{1/2}$ is also large, irreversible case will be observed. $E_p = E_{1/2} - RT[(0.780 + \ln K(a/l)^{1/2} - \ln (1+K)]/nF$ Cathodic shift of potential will be observed.	1. For small values of $K(a/l)^{1/2}$, the curves approach reversible behavior, for large values of $K(a/l)^{1/2}$ the curves approach irreversible behavior, E_p shifts cathodically (60/n)(T/298) for ten-fold increase in $K(a/l)^{1/2}$. 2. $i_p/v^{1/2}$ virtually constant with v. 3. i_p^a/i_p^c decreases from unity as v increases.	145

TABLE VI (Continued)

Mechanism	Peak Current and Peak Potential	Diagnostic Criteria	Reference
$O + ne^- \rightleftarrows R$	If K is small (pure kinetic current) $i_p = 0.527\ (nF)^{3/2}(D_O v)^{1/2} AC/(RT)^{1/2}$	1. $i_p/v^{1/2}$ is independent for v.	153
$2R \underset{k_b}{\overset{k_f}{\rightleftharpoons}} Z$	$E_p = E_{1/2} - 0.902\ RT/nF + RT/3NF$	2. E_p depends on lnv and lnC.	154
$(K = k_b/k_f)$	$\ln 2RT/3nF + RT/3nF \ln k_b - RT/3nF \ln v + RT/3nF \ln C$		155
	If K is large (pure diffusion current) $i_p = 0.500\ (nF)^{3/2}(D_O v)^{1/2} AC/(RT)^{1/2}$	1. $i_p/v^{1/2}$ is independent of v. 2. E_p is independent of v but depends on lnC.	
	$E_p = E^\circ - 0.70\ RT/nF - RT/4nF$ $\ln D_O/D_z - RT/2nF \ln K + RT/2nF \ln C$		
$O + ne^- \rightleftarrows R$	$i_p = k(nF)^{3/2}(D_O v)^{1/2} AC/(RT)^{1/2}$	m = 3, m = 2, m = 2, m = 1, m = 1 q = 1, q = 1, q = 3, q = 2, q = 3	152
$mR \underset{k_b}{\overset{k_f}{\rightleftharpoons}} qZ$	where m = 3, m = 2, m = 2, m = 1, m = 1 q = 1, q = 1, q = 3, q = 2, q = 3 k = 0.525, k = 0.499, k = 0.411, k = 0.384, k = 0.346	i_p^a/i_p^c = 1.143, 1.086, 0.952, 0.917, 0.869.	
	$E_{1/2} = E^\circ - RT\,[q\ln (D_O/D_R)^{1/2}\ q/m + (q - m)\ \ln C + q\ln K/m]/nF$	$E_p - E_{p/2} = -(35/n)(T/298), -(40.2/n)(T/298), -(70.3/n)(T/298) - (83.9/n)(T/298), -(108.6/n)(T/298)$ mV. A general trend, as q/m decreases, peak current increases, peak width $(E_p - E_{p/2})$ decreases.	

TABLE VI (Continued)

Mechanism	Peak Current and Peak Potential	Diagnostic Criteria	Reference
Reversible charge transfer followed by an irreversible chemical reaction $O + ne^- \rightleftarrows R$ $R \xrightarrow{k_f} Z$	If k_f/a is small Reversible voltammogram is obtained. If k_f/a is large $E_p = E_{1/2} - RT\,[0.780 - \ln (k_f/a)^{1/2}]/nF$ $E_p - E_{p/2} = -(48/n)(T/298)(mV)$	1. k_f/a is small, reversible voltammogram is observed. k_f/a is very large, no anodic current is observed. 2. E_p^c shifts cathodically by $(30/n)(T/298)$mV at low v, lesser shift at higher v. 3. $i_p/v^{1/2}$ is independent of v. 4. i_p^a/i_p^c increases toward unity as v increases.	145
$O + ne^- \rightleftarrows R$ $2R \xrightarrow{k_f} Z$	$i_p = 0.526(nF)^{3/2}(D_o v)^{1/2}AC/(RT)^{1/2}$ $E_p = E^\circ + RT(\ln 4.78\pi 3D_o/2D_R)/3nF$ $- RT(\ln a/k_f C)/3nF$ $E_p - E_{p/2} = -(39/n)(T/298)(mV)$	1. $i_p/v^{1/2}$ is independent of v. 2. E_p^c anodically shifts with increasing initial concentration. 3. The current potential curve is sharper.	157,158
Reversible chemical reaction preceding a reversible charge transfer $Z \underset{k_b}{\overset{k_f}{\rightleftharpoons}} O$ $O + ne^- \rightleftarrows R$ $(K = k_f/k_b \; 1 = k_f + k_b)$	$i_p = 4.64 \times 10^6 n^{3/2} (D_o v)^{1/2} AC(K/1+K)/T^{1/2}$ If $(k_f + k_b)/a < 0.025$ and $K < 0.5$	1. E_p shifts anodically with increasing v. 2. $i_p/v^{1/2}$ decreases as v increases. 3. i_p^a/i_p^c is generally greater than unity with a value of unity at lower v and increases as v increases. 4. The cathodic voltammogram is very flat as v increases.	145

TABLE VI (Continued)

Mechanism	Peak Current and Peak Potential	Diagnostic Criteria	Reference
$Z \underset{k_b}{\overset{k_f}{\rightleftharpoons}} 2O$ $O + ne^- \rightleftarrows R$ $(K = k_f/k_b)$	If K is large (pure diffusion currents) $i_p = 1.087(nF)^{3/2}(D_z v)^{1/2} AC_o/(RT)^{1/2}$ $E_{p/2} = E + 0.40\ RT/nF + RT[\ln (D_R/D_z)]/2nF + RT/2nF \cdot \ln K/2nF - RT(\ln C_o)/2nF$ If K is small (pure kinetic currents) $i_p = 1.155\ nFD_o^{1/2} k_b^{1/2} K^{3/4} C_o^{3/4}$ $E_{p/2} = E_{1/2} - 0.13\ RT/nF - RT/2nF \cdot \ln 4/3 \cdot RT/nF - RT/2nF \cdot \ln k_b - RT/4nF \ln K + RT/2nF \cdot \ln v - RT/4nF \cdot \ln C_o$	1. $E_{p/2}$ is independent of v but depends on ln C_o. 2. $i_p/v^{1/2}$ is independent of v. 1. Wave shape current is observed. The plateau current is independent of v, but depends on $C_o^{3/4}$. 2. The half-plateau potential anodically shifts with ln v but cathodically shifts with ln C_o.	155
Reversible chemical reaction preceding an irreversible charge transfer $Z \underset{k_b}{\overset{k_f}{\rightleftharpoons}} O$ $O + ne^- \xrightarrow{k_a} R$	The empirical equation for obtaining kinetic parameter is $i_k/i_d = 1/[1.02 + 0.53(b)^{1/2}/K(1)^{1/2}]$ $b = \alpha n_a F/RT$ i_k = observed peak current with kinetic complication i_d = pure diffusion controlled peak current	1. For large values of $(b)^{1/2}/K(1)^{1/2}$ the potential shifts anodic by about $(60/\alpha n_a)(298/T)$(mV) for 10-fold increase. The potential does not depend on $(b)^{1/2}/K(1)^{1/2}$ for small value of the kinetic parameter. 2. $i_p/v^{1/2}$ decreases with increasing v. 3. Lack of anodic response.	145

TABLE VI (Continued)

Mechanism	Peak Current and Peak Potential	Diagnostic Criteria	Reference
Catalytic reaction with reversible charge transfer $O + ne^- \rightleftharpoons R + Z$ k_c	If k_c/a is small Reversible voltammogram is obtained, $E_p - E_{1/2} = -(28.5/n)(T/298)$ mV If k_c/a is large $i = nFA(Dk_c)^{1/2} C_o/\{1 + \exp[nF/RT(E - E_{1/2})]\}$ $i = nFAC_o (Dk_c)^{1/2}$ (for very cathodic potentials)	1. Low k_c/a, E_p is independent of k_c/a. Intermediate k_c/a, the peak potential shifts cathodically by about (60/n)(T/298) mV for 10-fold increase in k_f/a. 2. Small k_c/a, $i_p^a/i_p^c = 1$. $k_c/a > 1.0$, no cathodic peak is observed. $k_c/a > 10$, $E_{1/2}$ is independent on k_f/a. 3. $i_p/v^{1/2}$ decreases with scan rate at low v, but independent of v at high v.	145
Catalytic reaction with irreversible charge transfer $O + ne^- \xrightarrow{k_s} R + Z$ k_c	If k_c/b is small, irreversible voltammogram is obtained. If k_c/b is large $i = nFAC_o(k_cD)^{1/2}/\{1 + \exp[(\alpha n_a F/RT\cdot(E - E^\circ + RT/\alpha NaF\cdot\ln(\pi Db)^{1/2}/k_s + RT/\alpha NaF\cdot\ln(k_s/\pi a)]\}$	1. E_p or $E_{p/2}$ shifts cathodically with increasing k_c/b. $k_c/b > 0.6$. Cathodic peaks are not observed. 2. $i_p/v^{1/2}$ decrease with increasing v at low v but $i_p/v^{1/2}$ is independent of v at high v. 3. No anodic current would be observed.	145
Multicharge transfer $A + n_1e \rightarrow B$ $B + n_2e \rightarrow C$	The total current for the two step reaction is given by $i_t = n_1Faf_A(t) + n_2FA[(f_A(t) + f_B(t)]$ where $f_A(t) = C_A(\pi Da_1)^{1/2} \psi(a_1,t)$ $f_B(t) = C_A(\pi Da_1)^{1/2} \chi(a_1,t)$	1. $i_p/v^{1/2}$ is independent of scan rate, which indicate that the total current function is made up charge transfers not coupled to chemical reactions. 2. The nature of the voltammogram is dependent on several factors: the nature of the charge transfer steps (R-R, R-I, I-R, or I-I). The potential separation between the individual charge transfers, the number of electrons in the specific step. For detailed discussion see Reference 152.	159

TABLE VI (Continued)

Mechanism	Peak Current and Peak Potential	Diagnostic Criteria	Reference
Chemical reaction coupled between two charge transfer (ECE mechanism) $A + n_1e \rightleftarrows B$ $B \xrightarrow{k_f} C$ $C + n_2e^- \cdots\!\!\rightarrow D$	R-R (reversible - reversible) $i_t = n_1FAC_A(\pi Da)^{1/2}\chi(at) + n_2FAC_A \cdot(\pi Da)^{1/2}\phi(at)$ R-I (reversible-irreversible) $i_t = n_1FAC_A(\pi Da)^{1/2}\chi(at) + n_2FA(\pi Db)^{1/2}\,\phi(bt)$	1. $i_p/v^{1/2}$ is dependent on v, which can be used to distinguish from multicharge transfer. 2. The detailed behavior of the voltammogram depends upon many factors; the nature of the charge transfer (R-R, R-I, I-R or I-I), the reversibility of the chemical reaction (or the kinetic parameters k_f/a), the relative values of $E_1^\bullet$ and E_2° and the ratio of n_2/n_1. For detailed discussion see Reference 149.	149
$A + n_1e \rightleftarrows B$ $B \underset{k_b}{\overset{k_f}{\rightleftharpoons}} C$ $C + n_2e^- \rightleftarrows D$ $(K = k_b/k_f)$ $A + n_1e^- \rightleftarrows B$ $2B \xrightarrow{k_d} A + Z$	For detailed discussion see References 150.	1. The tendency to reach the ECE behavior is favored by an increase of either acidity or mass transfer rate and by a decrease of initial concentration. For disproportionation the influence of these factors is in the opposite direction. 2. The variation of peak current with the initial concentration can be used to distinguish between ECE and disproportionation reaction. For ECE $i_p \propto C$, but for disproportionation, the peak current variation is markedly larger than a direct proportionality to the concentration.	150 150

TABLE VI (Continued)

Mechanism	Peak Current and Peak Potential	Diagnostic Criteria	Reference
Multicharge transfer with catalytic (cyclic) regeneration of the reactant $A + n_1e \rightarrow B + Z$ $\uparrow$ k_c $\downarrow$ $B + n_2e \rightarrow C$	For detailed discussion, see Reference 160.	Qualitatively the effect of a catalytic chemical reaction coupled to two charge transfers will enhance the maximum current for the first charge transfer because of the chemical regeneration of A.	160

of the electrode potential as a function of time. As the electrolysis proceeds, the concentration of the electroactive species near the electrode decreases until it is too small to sustain the imposed current; at this point the potential changes to some other value corresponding to another electrode reaction (i.e., second charge transfer or the decomposition of the solvent). The time elasping between the sudden changes of potential is called the transition time τ.

The solution is unstirred and an excess of supporting electrolyte is provided to prevent convection and migration, respectively. For a simple electrode process and under the conditions of linear diffusion, the transition time τ (in seconds) is related to the concentration by Sand's equation.[132]

$$\tau^{1/2} = \frac{\pi^{1/2} nFAD^{1/2} C}{2i} \tag{23}$$

For a reversible process, $O + ne^- \rightleftarrows R$, where both O and R are soluble, the potential-time relationship is given by the Karaoglanoff equation:[132]

$$E = E_{\tau/4} + \frac{RT}{nF} \ln \frac{(\tau^{1/2} - t^{1/2})}{t^{1/2}} \tag{24}$$

where $E_{\tau/4} = E^\circ - \frac{RT}{nF} \ln \frac{\gamma_R}{\gamma_O} \left(\frac{D_O}{D_R}\right)^{1/2}$, $E_{\tau/4}$ is equal to the polarographic half-wave potential $E_{1/2}$.[132] The theoretical basis of this technique has been extended to irreversible processes, consecutive and stepwise processes, kinetic processes, coupled chemical reactions and adsorption processes.

The theory and applications of this method have been reviewed by Paunovic,[163] Davis,[164] Lingane,[165] and Adams.[166] Diagnostic criteria for different cases have been discussed and summarized by Reinmuth[167-169]

and Adams.[166] In Table VII a brief summary of some typical diagnostic criteria for use in the studies is given.

There are several side processes which can cause complications that should be considered. These processes are: (1) charging of the double layer, (2) formation or reduction of oxide (or other) films, (3) oxidation or reduction of species adsorbed on the electrode surface, (4) surface roughness of solid electrodes. Bard[170] has derived a generalized equation to account for such side processes. The equation is:

$$\frac{i_o\tau^{1/2}}{C} = \begin{pmatrix}\text{Sand equation}\\ \text{component}\end{pmatrix} + \begin{pmatrix}\text{Double-layer}\\ \text{charging}\end{pmatrix} + \begin{pmatrix}\text{oxide}\\ \text{effects}\end{pmatrix} + \begin{pmatrix}\text{adsorption}\\ \text{effects}\end{pmatrix}$$

$$= \frac{10^{-3}\pi^{1/2}nFD^{1/2}}{2} + \frac{10^{-3}(C_d)_{av}\Delta E}{C\tau^{1/2}} + \frac{Q_{ox}}{C\tau^{1/2}} + \frac{10^{3}nF\Gamma}{C\tau^{1/2}}$$

where $(C_d)_{av}$ is the average value of the double layer capacity (mF/cm^2) in potential interval ΔE over which the chronopotentiogram spans, Q_{ox} represents the millicoulombs required for the formation or dissolution of oxide films, and Γ is the amount ($mole/cm^2$) of electroactive material adsorbed on the electrode surface.

A simplified version in terms of the Sand component and a summed correction can be expressed by[170]

$$\frac{i_o\tau^{1/2}}{C} = \frac{10\text{-}3\ \pi^{1/2}nFD^{1/2}}{2} + \frac{B}{C\tau^{1/2}} \quad . \tag{26}$$

The above equation shows the deviation caused by the double layer, oxide and adsorption corrections (B factors) which will lead to positive deviations in the plot of $i_o\tau^{1/2}$ vs i_o.

Chronopotentiometry was first applied to molten salt studies by Laitinen and coworkers.[171,172]

TABLE VII

SUMMARY OF SOME DIAGNOSTIC CRITERIA OF CHRONOPOTENTIOMETRY

Kinetic Scheme	Potential-Time, Current-Time Relationships	Diagnostic Criteria	Reference
Reversible charge transfer $O + ne^- \rightleftarrows R$	$E = E_{\tau/4} + \frac{RT}{nF} \ln \frac{\tau^{1/2}-t^{1/2}}{t^{1/2}}$ $i_o\tau^{1/2} = \frac{nF(\pi D)^{1/2}C}{2}$	$i_o\tau^{1/2}$ is independent of i_o. $i_o t^{1/2}$ is independent of i_o. E vs log $(\tau^{1/2}-t^{1/2})/t^{1/2}$ is linear with slope = 2.3RT/nF. $\tau_r/\tau_f = 1/3$.	167
Irreversible charge transfer $O + ne^- \xrightarrow{k_f} R$	$E = \frac{RT}{\alpha n_a F} \ln \frac{2k_f}{(\pi D)^{1/2}} + \frac{RT}{\alpha n_a F} \ln (\tau^{1/2}-t^{1/2})$ $i_o\tau^{1/2} = \frac{nF(\pi D)^{1/2}C}{2}$	$i_o\tau^{1/2}$ is independent of i_o. $i_o t^{1/2}$ decreases with increasing i_o. E vs log $(\tau^{1/2}-t^{1/2})$ plot is linear with slope = $2.3RT/\alpha n_a F$.	167
Preceding chemical reaction $Z \underset{k_b}{\overset{k_f}{\rightleftharpoons}} O + ne^- \rightleftarrows R$	$i_o\tau^{1/2} = \frac{nFC(\pi D)^{1/2}}{2} - \frac{\pi^{1/2} i_o}{2K(k_f + k_b)^{1/2}}$	$i_o\tau^{1/2}$ is a linear function of i_o, decreasing with increasing i_o.	168

TABLE VII (Continued)

Kinetic Scheme	Potential-Time, Current-Time Relationships	Diagnostic Criteria	Reference
Adsorption of the reactant	AR-SR model[a] $i\tau = nFA\Gamma + D\pi(nFAC)^2/4i$ SAR model[b] $i\tau = nFA\Gamma + 1/2\ nFAC(\pi Dt)^{1/2}$ SR-AR model[c] $(i\tau)^{1/2} = (nFA\Gamma)^{1/2} + \frac{nFAc(D\pi)^{1/2}}{2(i)^{1/2}}$	$i\ \tau^{1/2}$ increases with increasing i. SR-AR: $i\tau$ vs $1/i$ plot is linear. SAR: $i\tau$ vs $(t)^{1/2}$ plot is linear. SR-AR: $(i\tau)^{1/2}$ vs $1/(i)^{1/2}$ plot is linear.	163 164

[a]AR-SR model assumes that the depletion of the adsorbed reactant precedes the reduction of the solute reactant at the electrode surface.

[b]SAR model assumes the parallel depletion of adsorbed and solution reactants at the electrode surface.

[c]SR-AR model is the reverse of the AR-SR model.

6. Chronoamperometry and Construction of Stationary Electrode Polarograms

Chronoamperometry is an electrochemical technique involving the application of a potential step to an electrochemical cell containing an unstirred solution of an electroactive species and a large excess of supporting electrolyte, and the measurement of the current decay as a function of time. The resulting current is governed by the rate of diffusion for rapid electron transfer processes. The relationship between current and time for a linear diffusion process is given by the Cottrell equation:[132]

$$it^{1/2} = \frac{nFAD^{1/2}C}{\pi^{1/2}} \quad . \tag{27}$$

The application of this technique to electrochemical studies of various transfer processes has been reviewed by Adams.[166]

This technique has been used for the construction of polarograms from current-time curves.[127,173] The potential is stepped from a value at which no electrochemical reaction is taking place to some chosen value. The current is subsequently measured during intervals ranging from a few msec to a few sec. The polarogram is constructed by plotting current values corresponding to a given time vs the applied potential steps. The analysis of these polarograms is analogous to that of conventional polarograms.[17,137,174] Table VIII summarizes three common uses.

7. Pulse Polarography

Pulse polarography was first introduced by Barker and Gardner[175] as an extension of square wave polarography. With pulses of constant amplitude, superimposed on a slowly changing polarizing voltage, a derivative polarogram (differential pulse polarography) is obtained. If,

TABLE VIII

SUMMARY OF EQUATIONS FOR ANALYSIS OF THE CURRENT-POTENTIAL CURVES

Mechanism	Current-Voltage Function	Remarks	Reference
$O + ne^- \rightleftarrows R$	$E = E_{1/2} + \frac{2.3RT}{nF} \log \frac{i_d - i}{i}$	Reversible process involving two soluble species (either in the solution or the electrode)	17
	$E_{1/2} = E^\circ - \frac{2.3RT}{nF} \log \frac{\gamma_R}{\gamma_O} \left(\frac{D_O}{D_R}\right)^{1/2}$		174
	(Heyrovsky-Ilkovic equation)		
$O + ne^- \rightleftarrows R$	$E = E_{1/2} + \frac{2.3RT}{nF} \log (i_d - i)$	Reversible deposition of an insoluble product	17
	$E_{1/2} = E^\circ + \frac{2.3RT}{nF} \log \gamma_O + \frac{2.3RT}{nF} \log \frac{C}{2}$		174
	(Kolthoff-Lingane equation)		
	$\Delta E_{1/2} = \frac{2.3RT}{nF}$ (log C)		
$O + ne^- \rightarrow R$	$E = E_{1/2} + \frac{2.3RT}{\alpha n_a F} \log \frac{i_d - i^a}{i}$	Irreversible charge transfer	17 174

[a] α is the transfer coefficient for the electrode process. n_a is the number of electrons involved in the rate determining step.

however, the polarizing voltage is kept constant and the amplitude of the pulse is gradually increased, a normal polarogram is obtained (integral or normal pulse polarography).[175,176]

In differential pulse polarography for a reversible electrode reaction, $O + ne \rightleftarrows R$, where the product is soluble in either the solution or in the electrode, the change in current produced by a small potential pulse ΔE is given by:[175]

$$\Delta i = \frac{n^2F^2}{RT} AC\Delta E \, (D/\pi t)^{1/2} \frac{P}{(1 + P)^2} \tag{28}$$

where $P = \exp (E - E_{1/2}) \frac{nF}{RT}$, R, T, F, $E_{1/2}$ and D have their usual significance; t represents the elapsed time after the potential change and E is the potential of the electrode just before the potential change. This equation is valid only for $\Delta E << \frac{RT}{nF}$. Maximizing Δi with E by differentiating and equating to zero, it is found that P = 1 when Δi is maximum. Thus the equation representing the maximum current is given by:[176]

$$\Delta i_{max} = \frac{n^2F^2}{4RT} AC\Delta E \, (\frac{D}{\pi t})^{1/2} . \tag{29}$$

From Equations 28 and 29, it can be shown that a reversible wave is symmetrical at a potential close to $E_{1/2}$, and the maximum height of the wave is proportional to n^2. Equations 28 and 29 give peak half-widths of $(\frac{90.4}{n})(\frac{T}{298})$ mV.[176] The relationship between peak potential and polarographic half-wave potential is given by

$$E_{peak} = E_{1/2} - \frac{\Delta E}{2} . \tag{30}$$

For infinitely small pulses the peak potential will occur at the polarographic half-wave potential.

In normal pulse polarography, for a reversible electrode reaction, the current-potential relationship is given by:[175,176]

$$i = nFCA \left(\frac{D}{\pi t}\right)^{1/2} \left(\frac{1}{1 + P}\right) \tag{31}$$

where $P = \exp (nF/RT)(E - E_{1/2})$. As the pulse potential becomes more negative than $E_{1/2}$, P approaches zero, thus the limiting current obtained in this method is the Cottrell current:

$$i_{\ell} = nFCA \left(\frac{D}{\pi t}\right)^{1/2} \tag{32}$$

Since the concentration of the product formed is very low because the charge passed is quite small, pulse polarography is a superior method to study systems which give erratic and ill-defined waves by conventional polarography or linear sweep voltammetry. The charging current problem is also minimized by this technique.[176]

8. Studies of Adsorption by Linear Sweep Voltammetry and Chronopotentiometry

The theory of linear sweep voltammetry (cyclic voltammetry) of adsorption behavior has been discussed by Shain *et al.*[177-180] One can use the diagnostic criteria of the variation of peak shape, peak current, and peak potential as a function of scan rate, bulk concentration and temperature to correlate the theoretical and experimental parameters. Shain *et al.* have reported the theoretical treatment of the following systems: (1) weak and strong adsorption (desorption) of reactant and product:[177,180]

$$O_{soln} \rightleftarrows O_{ads} \qquad O + ne^- \rightleftarrows R \qquad R_{soln} \rightleftarrows R_{ads}$$

(2) reversible charge transfer followed by an irreversible chemical reaction with weak adsorption of the reactant (Langmuir isotherm):[179]

$$O_{soln} \rightleftharpoons O_{ads} \qquad O + ne^- \rightleftharpoons R \qquad R \xrightarrow{k} Z$$

and (3) rate-controlled adsorption of product:[178]

$$O + ne^- \rightleftharpoons R \underset{k_d}{\overset{k_a}{\rightleftharpoons}} R_{ads} \ .$$

For system (3), Hulbert and Shain[178] have considered three limiting cases: rapid adsorption and desorption, slow desorption, and slow adsorption. If the scan rate is slow with respect to the adsorption and desorption rate constants (equilibrium adsorption), the peak potential and peak width can be characterized by Equations 33 and 34:

$$E_p - E_{1/2} = \frac{RT}{nF(\sigma + 1)} \ln (C_o/K') \tag{33}$$

$$n\Delta E_w = 3.526\ RT/[(1 + \sigma)F] \tag{34}$$

where σ is the potential-dependent parameter, and K' is the potential-independent adsorption equilibrium constant. The potential of this equilibrium adsorption-desorption system shifts toward cathodic values as σ or K' increase, the prepeaks are symmetrical with respect to the zero current function axis, and the peak potential. If the desorption rate constant is small with respect to the adsorption rate constant and the scan rate, the equations of the adsorption peak potential and peak width at half-height are as follows:

$$E_{p(a)} - E_{1/2} = \frac{RT}{nF(1 + \sigma/2)} \ln \left[\frac{C_o k'_a}{a(1 + \sigma/2)}\right] \tag{35}$$

$$n\Delta E_w = \frac{2.446\ RT}{F(1 + \sigma/2)} \tag{36}$$

where k_a' is the potential independent adsorption rate constant. The potential of the rate controlled adsorption peak moves toward cathodic values as the scan rate or σ increases and the bulk concentration or k_a' decreases. The peak width is a function of n and σ as in the equilibrium adsorption case. If the adsorption rate constant is small with respect to the desorption rate constant and the scan rate, the desorption peak potential and peak width can be described by the following:

$$E_{p(d)} - E_{1/2} = \frac{2RT}{nF\sigma} \ln \left(\frac{a\sigma}{2k_d'}\right) \tag{37}$$

$$n\Delta E_w = \frac{4.892\ RT}{\sigma F} \quad . \tag{38}$$

The desorption peak moves toward anodic potentials as the scan rate increases and as k_d' or σ decrease. The kinetic desorption peak potential is independent of the bulk concentration. The peak width is also a function of n and σ.

The theory of chronopotentiometry of adsorption has been discussed by several authors.[181,182] The limited utility of chronopotentiometry for the study of adsorption has been pointed out by Lingane.[183] The three most used theoretical models are described as follows: (1) according to the AR and SR model the depletion of the adsorbed reactant precedes the reduction of solute reactant at the electrode surface. The appropriate equation is:

$$i\tau = nFA\Gamma + D\pi(nFAC)^2/4i \tag{39}$$

where Γ is the surface excess. A plot of $i\tau$ vs 1/i should be linear with an intercept $nFA\Gamma$.

(2) The SR-AR model is the reverse of AR-SR model; the appropriate equation is:

$$(i\tau)^{1/2} = (nFA\Gamma)^{1/2} + nFAC(D\pi)^{1/2}/2i^{1/2} \quad . \tag{40}$$

A plot of $(i\tau)^{1/2}$ vs $i^{-1/2}$ should be linear, with an intercept of $(nFA\Gamma)^{1/2}$.

(3) The SAR model, in which paralled depletion of adsorbed and solution reactants, according to a fixed ratio, take place is described by the equation:

$$i\tau = nFA\Gamma + 1/2\ nFAC\ (\pi D\tau)^{1/2} \quad . \tag{41}$$

A plot of $i\tau$ vs $\tau^{1/2}$ should be linear with an intercept $nFA\Gamma$.

C. Proposed Research

Niobium is an important structural element and fission product. The chemistry of niobium in molten fluorides and chlorides is of interest to both nuclear applications and to process metallurgy. There are two primary goals in this study: (1) to investigate the heterogeneous equilibria between soluble niobium species and Nb(V) oxide and niobate in molten fluorides by using a solubility measurement technique, (2) to study the stability and electrode reduction-oxidation mechanisms of Nb(V) in molten fluorides and chloroaluminates and to examine the effect of acid-base properties of solvents, temperature and Nb(V) concentration on the Nb(V) reduction mechanisms by using electrochemical techniques. The specific purposes of this dissertation are as follows:

(1) To study the heterogeneous equilibria between solid Nb_2O_5 and soluble Nb(V) species in molten LiF-BeF_2 mixtures;

(2) To study the heterogeneous equilibria between $NiNb_2O_6$(s) and soluble Nb(V) species in molten Li_2BeF_4;

(3) To study the stability and electrode reduction-oxidation mechanisms of Nb(V) in molten LiF-BeF_2-ZrF_4.

(4) To study the electrochemistry of $NbCl_5$ in molten $AlCl_3$-NaCl mixtures by means of linear sweep voltammetry, chronopotentiometry, chronoamperometry and pulse polarography;

(5) To study the electrochemistry of $NbOCl_3$ in molten $AlCl_3$-NaCl mixtures by means of the above electrochemical techniques.

CHAPTER II

EXPERIMENTAL

A. Materials

1. Materials for Equilibria and Electrochemical Studies in Molten Fluorides

Lithium fluoride (99.5%) was obtained from American Potash and Chemical Corp. Commercial BeF_2 was purified by distillation, and LiF-BeF_2-ZrF_4 (65.6-29.4-5.0 mole %, liquidus temperature 434°) was prepared by members of the Reactor Chemistry Division at Oak Ridge National Laboratory.

Commercial H_2 was purified by passage through a Deoxo unit (Fisher Scientific Co.), a magnesium perchlorate drying tube, and finally a liquid nitrogen trap. Commercial helium was purified by passage through an Ascarite trap, a magnesium perchlorate trap, and a liquid nitrogen trap. Commercial argon was purified by passage through a molecular sieve (Linde 13X), and a magnesium perchlorate trap. High purity CO_2 was purified by passage through a magnesium perchlorate trap. Anhydrous HF (99.9%) was used without further purification. A small cylinder (6 lb) of anhydrous liquid HF was kept at the desired temperature (16-35°) $\pm$ 0.1° to obtain the required pressures.

High purity BeO and NiO were obtained from the Reactor Chemistry Division. Nb_2O_5 (99.97%) was obtained from Apache Chemicals. K_2NbF_7 was obtained from Kawecki Chemical Co. and purified by recrystallization.[184]

Carrier free Nb^{95} (99.5% radioactivity purity) was obtained from the Isotope Division, ORNL.

The single crystals of lanthanum(III) fluoride used to fabricate reference electrode compartments were obtained from Optovac, Inc. Boron nitride (grade HP) used in the construction of reference electrodes was obtained from the Carborundum Company. Two platinum containers (2 in diameter, 6 in high and 3-13/16 in diameter, 6 in high) were fabricated from platinum sheet which was supplied by Engelhard Industries.

2. Materials for Electrochemical Studies in Molten Chloroaluminates

$AlCl_3$ (anhydrous, iron-free) obtained from Fluka AG was purified by heating with aluminum metal (M6N grade from Alfa Inorganics) at 230° for 2-3 days. The melt was then sublimed through a glass frit, cooled and stored in a dry box (moisture level $\leq$ 2 ppm). NaCl (reagent grade) was twice recrystallized from water and then dried under vacuum at 400° for 10 hours prior to its use. The preparation of $AlCl_3$-NaCl melts has been described previously.[127,185] The desired quantities of NaCl-$AlCl_3$ were weighed in the dry box (typical moisture level $\leq$ 2 ppm), sealed in a Pyrex tube under vacuum with a piece of aluminum metal, and digested for several days at 200°. After the impurities had settled, the melt was cooled slowly, frozen and stored. The purity of the melts employed in each experiment was checked voltammetrically.

$NbCl_5$ from Alfa Inorganics was purified by sublimation through a frit at 220° in a Pyrex tube. The yellow granular crystals were identified by Raman spectra of the solid and the melt; the spectra agreed with data reported in the literature.[87] $NbOCl_3$ was obtained as a by product of the purification of $NbCl_5$. It was collected at 350° (middle part of

of the Pyrex tube subjected to a temperature gradient). This is based on the same principle as the chemical transport method to prepare $NbOCl_3$ from the $Nb_2O_5/NbCl_5$ reaction.[81] The deposited white fibrous needle crystals of $NbOCl_3$ were also identified by their Raman spectra. The results agreed with Ozin's report.[95] No extra lines corresponding to $NbCl_5$ were observed.

Platinum wire and foil were used as pure metals, obtained from Engelhard Industries.

B. Apparatus

1. Apparatus for Equilibria Studies in Molten Fluorides

The experiments were carried out in the apparatus shown in Figure 2. The whole system included various gas supplies, a reaction vessel, and a gas circulation system. The circulation system included a copper filter, a copper cold-trap, a titration line, an IR cell and a finger pump or a diaphragm pump for agitating by gas recirculation.

a. Reaction vessel. A sketch of the nickel reaction vessel to contain the $LiF-BeF_2$ mixtures is shown in Figure 3. Devices for sampling the molten fluorides and for adding reagents to the reaction vessel are shown in Figure 4. The reaction vessel used was a welded cylindrical grade A nickel container (Schedule 40 pipe) (2.5 in dia., 12 in length). A 4 in section of 0.5 in ID nickel pipe was welded to the sampling port. The top of the sampling port was closed with a stainless steel or monel ball valve having an internal clearance of 0.5 in. A side arm of 0.25 in ID tubing with filter served as gas-outlet line. The thermocouple well made of 3/8 in nickel tubing extended to within 0.125 in of the

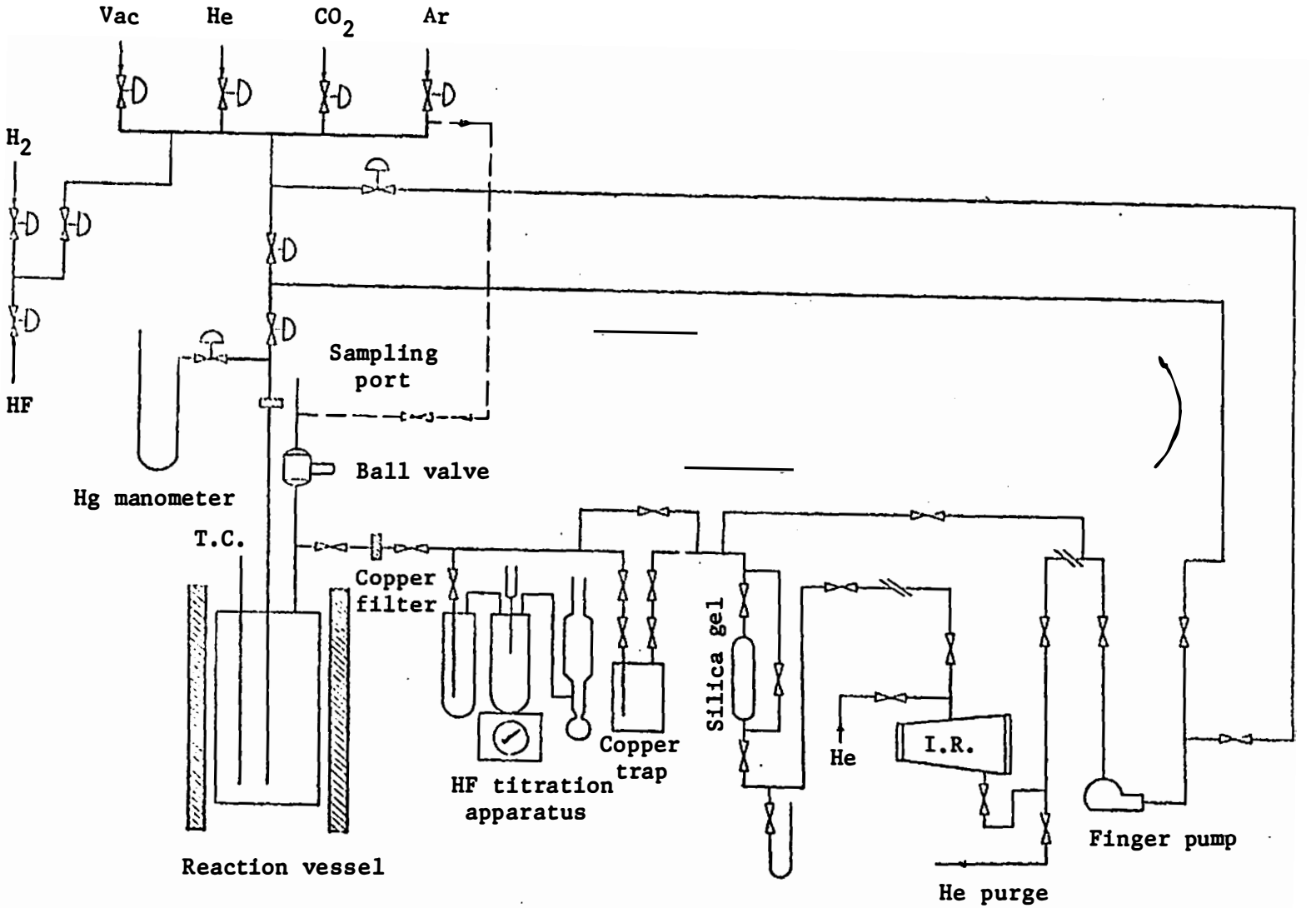


Figure 2. Schematic diagram of the experimental apparatus for equilibrium studies.

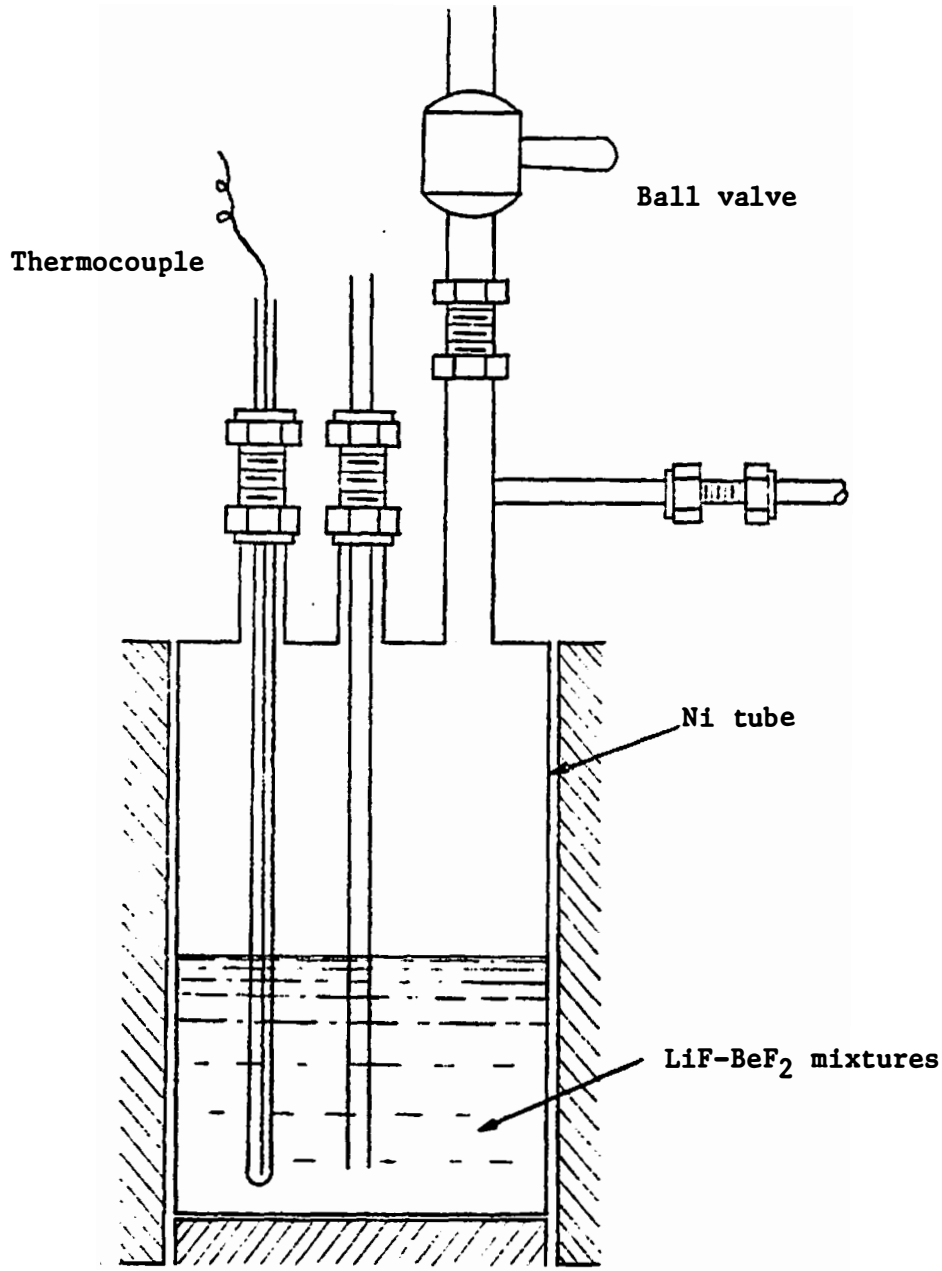


Figure 3. Reaction vessel for equilibrium studies.

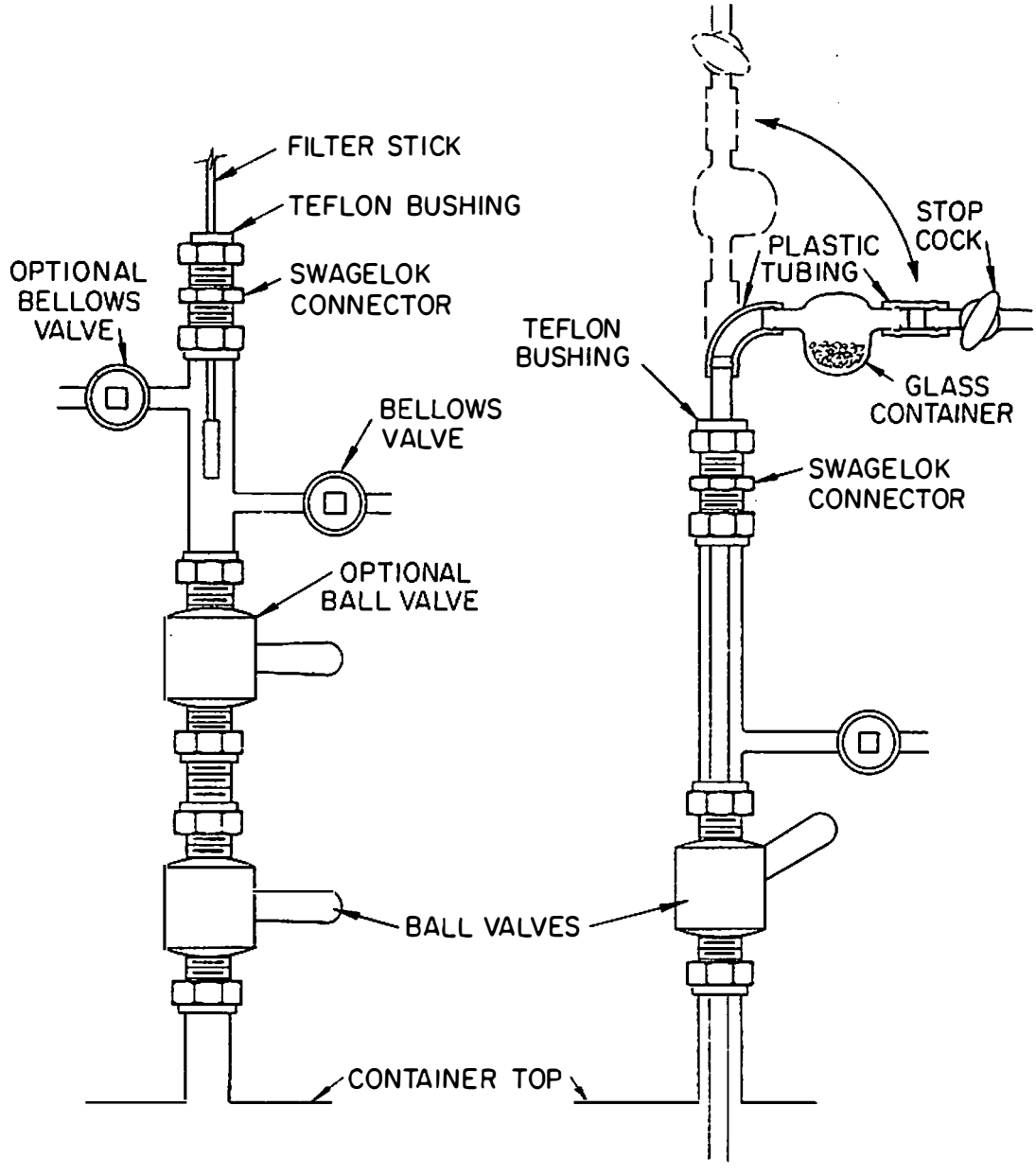


Figure 4. Devices for sampling molten fluorides and for adding reagents to the reaction vessel.

bottom. The gas inlet tube, 3/8 in ID, extended 3/8 in to within 0.25 in of the vessel bottom for agitation and purification of the melt by admitting gases beneath the melt surface. The vessel was equipped with Swagelok fittings through which the gas sparge tube, the thermocouple well and the gas outlet tube were connected. A similar apparatus has been used satisfactorily before.[186] When CO_2/CO mixture was used as the circulation gases in one series of experiments, the nickel reaction vessel was also equipped with a graphite liner.

b. Furnace. The reaction vessel was mounted vertically in a 3 in ID tube furnace. The temperature of the equilibrating mixture was controlled to $\pm$ 2° by an L&N series 60 DAT control unit and was continually recorded on a Honeywell recorder. Sometimes, the temperature of the reaction vessel was checked with a calibrated chromel-alumel thermocouple and a Leeds-Northrup K-3 potentiometer.

c. Filter sticks. H_2-fired copper filter sticks were used to take filtered samples of the molten fluoride mixtures. The sintered copper filter material had an average pore size of 0.0004 in. The 0.125 in copper tubing filter sticks could be slipped through a Teflon plug and the ball valve without contamination of the melt by air. Samples of the melt were drawn by reducing the gas pressure in the filter sticks. Figure 4 (p 56) shows the sampling device with the filter stick; a detailed description is given elsewhere.[187]

d. Flow control of gases. The HF manifold pressure was controlled by regulating the temperature of the HF supply cylinder. The flow of HF was controlled by a mass spectrometer leak valve (diaphragm type adjustable

leak valve obtained from Oak Ridge Gaseous Diffusion Plant). The gas flowed to a monel tee where it was mixed with H_2. The mixed gases were passed through the gas inlet tube. A pressure relief valve (Moore Products Co.) was used to reduce the hydrogen manifold pressure to a constant value of 3.0 psi (gauge). The flow was then controlled by a brass needle valve obtained from Nuclear Products Co. The H_2 was then mixed with the HF as described above. The helium, argon, and CO_2 were controlled with the same type needle valve used for H_2. The gas was circulated in the gas system with a flow rate of 100 ml/sec by the action of the finger pump or the diaphragm pump which was calibrated before the experiment. This leak-tight system was maintained at a positive gas pressure of 200 torr. When CO_2 was used as the recirculation gas, the CO_2, and CO spectra were obtained with a Perkin-Elmer Model 21 Spectrometer with a cell (10 cm path length) containing KBr or NaCl windows. The CO_2/CO ratio was determined by measuring the band intensity ratio of CO_2 and CO at 2349 cm^{-1} and 2143 cm^{-1}, respectively.

e. Radioactivity counting apparatus. The concentration of ^{95}Nb in filtered fluoride samples was determined by measuring the γ-peak height at 0.77 MeV with a TMC Model-403 Pulse Height Analyzer coupled with a 3 in x 3 in NaI detector. Sometimes the activity was also checked by using a lithium-drifted germanium crystal detector coupled to a Nuclear Systems 50/50 radiospectrometer for eliminating possible errors due to contamination by a small amount of ^{95}Zr.

2. Apparatus for Electrochemical Studies in Chloroaluminates

a. Electrochemical cell. Sealed evacuated Pyrex cells (4 cm

diameter, 6 cm length) were employed for electrochemical studies in chloroaluminates (see Figure 5). This cell has been described previously;[127] it is used for volatile melts. The electrode connections were made with tungsten wire sealed with uranium glass to pyrex. The reference electrode was an aluminum wire immersed in the melt, $AlCl_3$-NaCl (63-37 mole %), which was separated from the main compartment by a thin Pyrex membrane. This arrangement is advantageous in a long duration experiment because it avoids possible reactions between aluminum in the reference compartment and oxidizing solutes in the main compartment. Because of the relatively high resistance of the Pyrex membrane, a platinum quasi-reference electrode[188] was used for the measurements; the potential was frequently checked vs the Al(III)/Al reference electrode. The working (indicator) electrodes were platinum and tungsten wires (0.1 cm^2). A large area platinum foil was used as the counter electrode.

b. Furnace. A 4 in ID aluminum tube furnace was used. The temperature was controlled to $\pm$ 1° by a temperature controller. This controller was a Null detector model 155 Microvoltmeter (Keithley-Instruments). The temperature was measured using a chromel/alumel thermocouple; a N.L.S. X-13 digital voltmeter was used to measure the thermocouple EMF's.

c. Instrumentation for voltammetric, chronopotentiometric, chronoamperometric, EMF and pulse polarographic measurements. Voltammograms, chronopotentiograms and current-time curves were obtained with the controlled-potential, controlled-current cyclic voltammeter.[189]

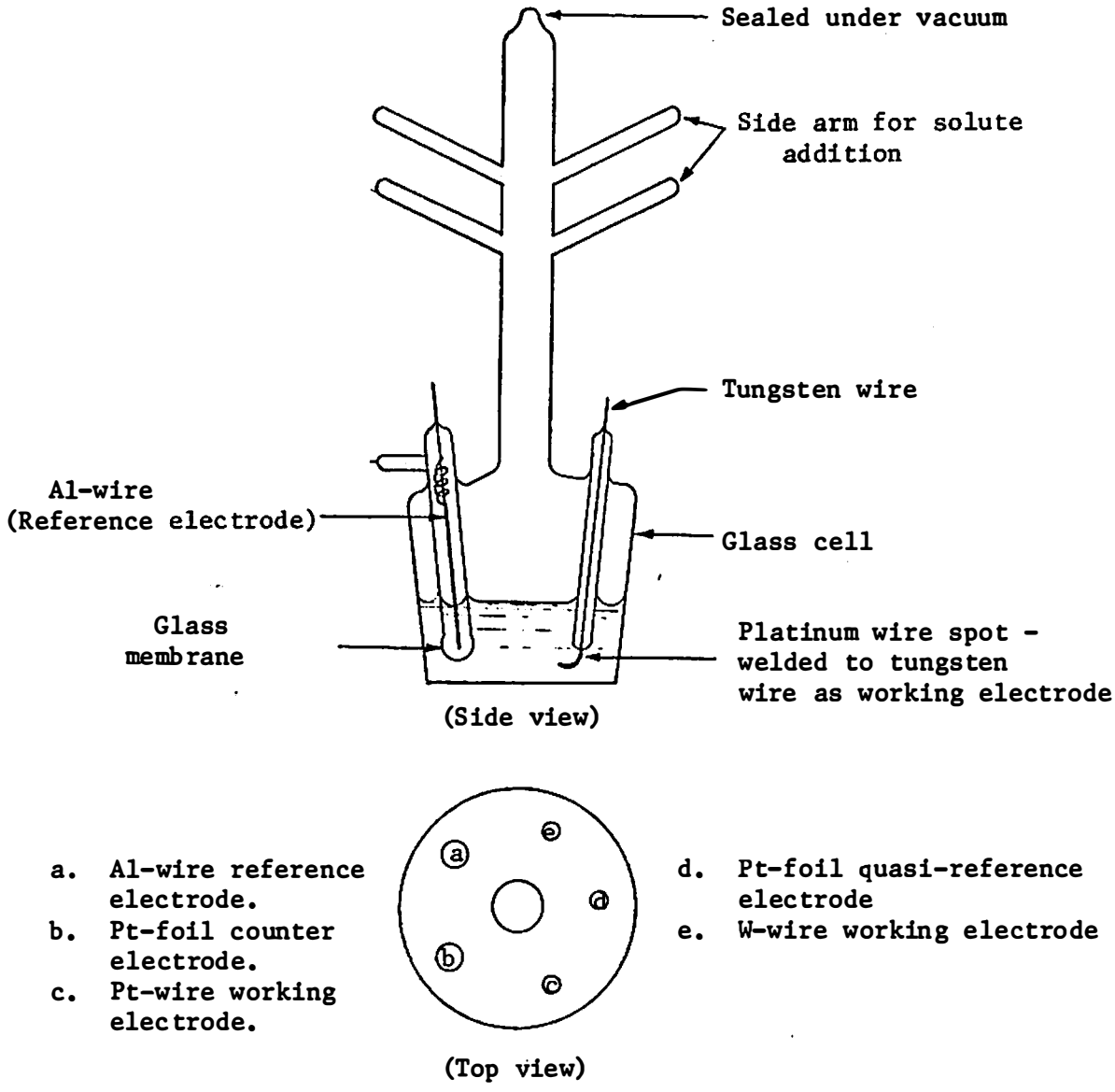


Figure 5. Electrochemical cell for studies in chloroaluminates.

The curves were recorded either with a Moseley 2D-2A X-Y recorder or a type 549 Tektronix storage oscilloscope with a Tektronix Model C-12 camera. The potentials were measured with a Model 895 A d.c. Differential Voltmeter (John Fluke) or a Keithley Model 601 electrometer.

Differential pulse polarograms were obtained with the Princeton Applied Research (PAR) Model 174 polarographic analyzer used in conjunction with a Model 172 Drop Timer. The pulse polarograms were recorded on a Moseley 2D-2A X-Y recorder.

3. Apparatus for Electrochemical Studies in Molten Fluorides

a. Electrochemical cell assembly. The experimental apparatus employed for these studies is shown in Figure 6. The containers used in this study were flanged nickel containers (2 1/2 in diameter, 10 in length, and 4 in diameter and 10 in length) with Teflon O-rings. They were equipped with seven nickel risers ending in Teflon-sealed Swagelok fittings. These contained one platinum tube for gas sparging, one sealed platinum tube for chromel-alumel thermocouple, one sampling port with ball valve, and four electrode ports. The melt was contained in a platinum cell (2 in diameter and 6 in long or 3-13/16 in diameter and 6 in long).

A three-electrode system was used for all measurements; platinum rods (1/8 in diameter) were used as counter and quasi-reference electrodes. The potential of the quasi-reference electrode was measured with respect to a Ni(II)/Ni reference electrode. The platinum working electrode (0.5 mm diameter) was immersed to depths of 4-5 mm (typical electrode area 0.078-0.1 cm^2). The pyrolytic graphite working electrode (1 mm diameter)

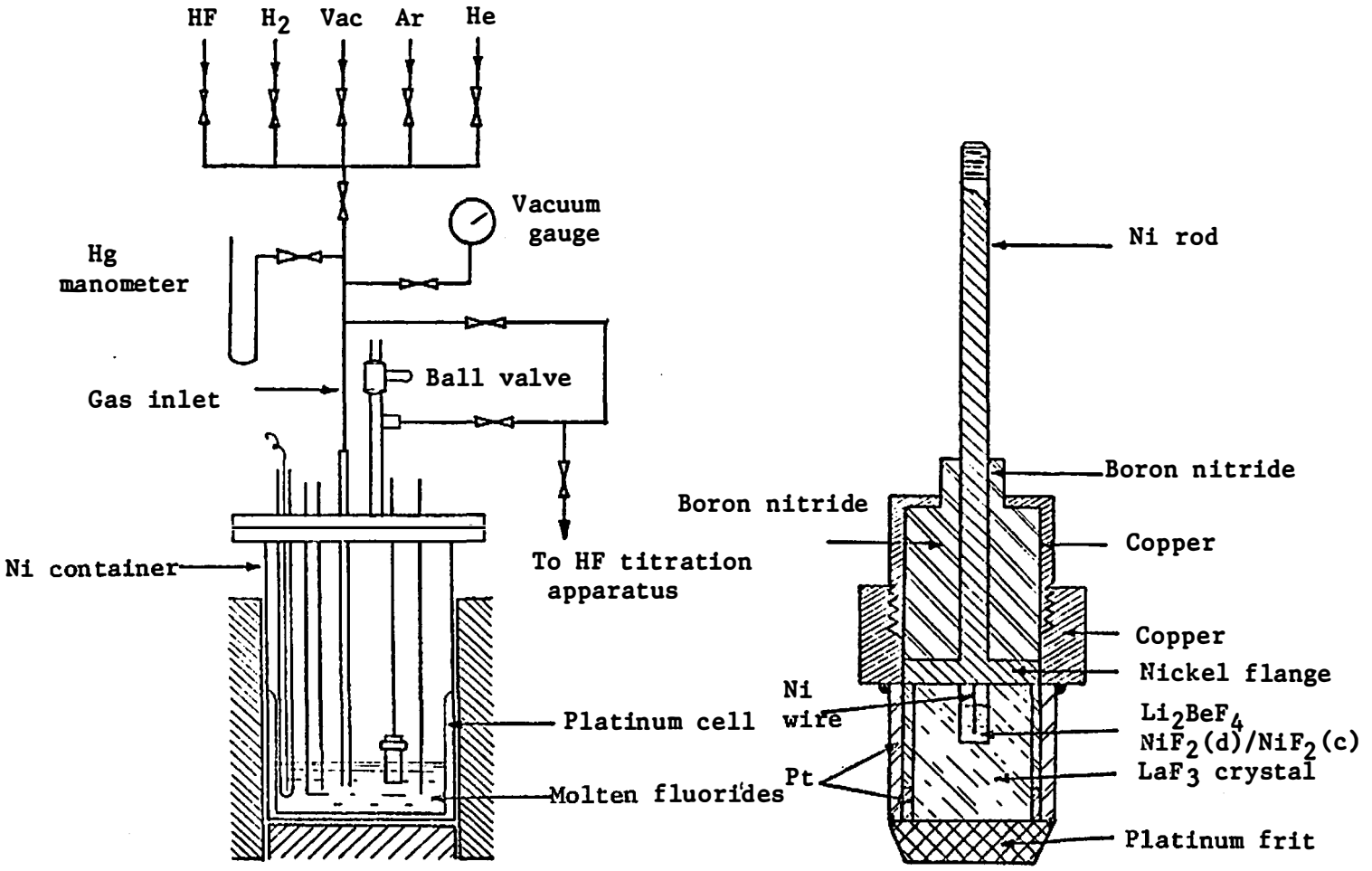


Figure 6. Apparatus for electrochemical studies in molten fluorides and Ni(II)/Ni reference electrode.

consisted of an unsheathed pyrolytic graphite rod (prepared by the Metals and Ceramics Division of ORNL) which was attached to a 1/8 in nickel rod by means of a threaded connection. The reference electrode employed in this study was a NiF_2 (saturated Li_2BeF_4)/Ni reference electrode, which has been described previously.[190] Because of the interaction of copper and nickel with Nb(V) in the melt,[113] we used a platinum sheath and frit for constructing the reference electrode (see Figure 6). This electrode included a LaF_3 single crystal (1/4 in diameter, 1 in long with a hole 1/8 in diameter, 3/8 in deep) as a membrane for separating the reference electrode couple from the bulk of the melt. The platinum sheath, BN inserts, and platinum frit simply served as a means of suspending the LaF_3 cup in the melt while minimizing direct contact of LaF_3 with the fluoride melts.

b. Furnace. The electrolytic cell was mounted vertically in a 3 in or 4 in ID tube furnace. The temperature controller was the same as described previously under equilibria studies (p 57).

c. Instrumentation. The cyclic voltammeter used in this study was the same as described previously.[189] Cyclic voltammograms were recorded either on a Hewlett-Packard 7005B X-Y recorder or on a Tektronix type 549 storage oscilloscope equipped with a Tektronix type C-12 camera attachment. Photographs were taken using type 42 Polaroid film. The potentials were measured with a Keithley 600A electrometer.

C. Procedures

1. Procedure for Equilibria Studies

a. Preparation of labelled Nb_2O_5 and $NiNb_2O_6$. Labelled Nb_2O_5 was prepared by dissolving Nb_2O_5 (5-6 g) in 10 ml of 27.5 M HF containing a few drops of concentrated HNO_3 in a platinum crucible. The resulting solution was transferred to a 500 ml polyethylene beaker, where carrier free ^{95}Nb-oxalate (2-5 mc) was added, the solution was diluted to 100 ml, and concentrated NH_4OH added to adjust pH to 8-10. Nb_2O_5 was thus precipitated, and then filtered with suction, washed with water, and finally ignited at 1000° overnight. The prepared $Nb^*_2O_5$ was identified by x-ray powder diffraction as high temperature form of Nb_2O_5, H-Nb_2O_5 (Bruner). (other notations used for this form have been α- Nb_2O_5, Holtzberg, β -Nb_2O_5 Goldschmidt).[54]

An equal mole ratio of labelled Nb_2O_5 (5.52 g) and NiO (1.55 g) were mixed, blended in a crucible and pressed into pellets under a pressure of approximately 5000 psi. The pellets, in a platinum crucible, were heated in a furnace at 1150°, for 2-3 days. The labelled $NiNb_2O_6$ was identified by x-ray powder diffraction.

b. Purification of fluoride melts. The molten fluorides were purified by sparging with an H_2-HF mixture (0.9-0.1 atm) at 600° for 6-8 hr to convert the impurity oxides (e.g. NiO, BeO, FeO, Cr_2O_3, etc.) to fluorides. This was followed by passing H_2 (6-8 hr) alone to reduce the impurity fluorides to the metals, and finally by bubbling argon to remove the H_2 and HF.[191] The concentration of HF in the H_2-HF mixtures was calculated by using the following gas law equation:

$$P_{HF} = \frac{(\text{mmoles, HF})(0.08205)(\text{abs. temp. of Bubble-O-Meter})}{\text{ml of } H_2 \text{ passed}} \qquad (42)$$

$$= n_{HF}\, RT/V$$

c. Equilibrations of the solid oxide phases with molten $LiF-BeF_2$ mixtures. Three series of experiments have been carried out in these studies. In the first series, the experiments were performed in a welded cylindrical nickel vessel containing initially 500 g of $LiF-BeF_2$ (67-33 mole %) which was purified by the $HF-H_2$ treatment. Excess BeO (1.76 g) was added along with 2.76 g labelled $H-Nb_2O_5$. Later NiO was added. Agitation was provided by means of a vigorous flow of argon which was bubbled through the melt and then recirculated by means of a finger pump acting on a length of flexible tygon tubing in the circuit (see Figure 2, p 54). In the second series of experiments, the equilibrations were carried out in a welded cylindrical nickel vessel with a graphite liner. Initially 500 g of $LiF-BeF_2$ (67-33 mole %) which had been purified by the $HF-H_2$ treatment were placed in the vessel. BeO (2.41 g) was added along with 3.59 g labelled $H-Nb_2O_5$. Agitation of the molten mixture was provided by means of a vigorous flow of $CO-CO_2$ or $CO-CO_2-Ar$ gas mixtures through the melt by means of a finger pump. Changes of the melt composition were made by adding known amounts of BeF_2 through the ball valve. In the third series of experiments the equilibrations were carried out in a nickel container and stirring was provided by recirculating argon by means of a diaphragm pump. Initially 500 g of $LiF-BeF_2$ (67-33 mole %), which had been purified, were placed in the vessel. BeO (0.148 g) and NiO (4.06 g) were added along with 4.63 g of labelled $NiNb_2O_6$. NiF_2 was added stepwise through the ball valve.

Filtered samples of the melt were taken with copper filter sticks (pore size 25-50μ) as a function of time in order to follow the approach to equilibrium. The time required for equilibrium varied from 20 to 100 hr. The concentration of niobium in filtered samples was determined by the usual radioactivity counting technique (sodium iodide detector and lithium drifted germanium detector). The uncertainty was ± 1 ppm or 10% error for concentrations below 100 ppm; the error was 5% for >100 ppm. The results were also checked with wet analysis. The concentration of nickel was determined by members of the Analytical Chemistry Division by using a colorimetric method.

Samples of the equilibrated solid phases were collected for each equilibrium point at the tips of the filter sticks. After washing with hot water to remove the solvent salts, the solids were examined by members of the Analytical Chemistry Division by x-ray powder diffraction, emission spectroscopy, and scanning electron microscopy (SEM) with x-ray fluorescence analysis.

2. Procedure for Electrochemical Studies in Molten Chloroaluminates

a. Electrochemical cell operation. The electrochemical cells were cleaned with chromic acid solution and washed with distilled water. The tungsten microelectrode was cleaned by anodization[192] in a solution of 5 M NaOH containg 1% by wt of $NaNO_2$. The aluminum wire in the reference electrode was cleaned with a mixture of concentrated H_2SO_4, H_3PO_4, and HNO_3. Finally the cell was rinsed with distilled water, evacuated to a reduced pressure, loaded in a drybox, closed with vacuum-tight fittings, evacuated to 10^{-2} torr for about 2 hr, gently heated and sealed.

Additions were made in the drybox. After each addition, the cell was evacuated and resealed under vacuum. The same procedure has been used previously.[192] Data for the density of the melt were taken from the work of Boston.[193]

b. Voltammetric and chronopotentiometric measurements. The general procedure for recording voltammograms involved the following steps: (1) examination of the background (residual) current and the cathodic and anodic limits of the solvent melt for each new batch of melt, (2) examination of the current-potential characteristics after additions of solute material. Scans were started at initial potentials at which essentially no current was observed to flow. Curves were recorded at a variety of scan rates and in different potential regions. Good reproducibility was obtained with a waiting period 5-10 min after each voltammogram, thus relying on natural convection to eliminate the concentration gradients produced by the previous run. A similar procedure was followed for chronopotentiometric measurements.

c. Construction of polarograms from chronoamperometric measurements. The polarograms were obtained from a series of chronoamperograms in which the potential of the working electrode was stepped from an initial potential at which no current flowed to some chosen potential. The potentials were increased by 20 mV or 50 mV for each step. The currents were measured at a given time (usually 0.02 sec to 5 sec) after the initiation of each step. Measurements at each step were corrected for residual currents at the same potential in the solvent melt. Current vs potential plots resulted in polarographic

S-shaped waves. As before, it was necessary to wait 5-10 minutes between each chronoamperogram.

3. Procedure for Electrochemical Studies in Molten Fluorides

a. Electrochemical cell operation. The platinum cell was cleaned with cleaning solution, rinsed with distilled water, and then dried in the oven. The empty platinum cell was placed in a drybox for loading with 100-200 grams of the solvent salt. The platinum cell with the salt was sealed in a plastic bag, removed from the drybox, opened in air and placed into the nickel container immediately. This container was then evacuated and flushed with helium several times. The salt was heated to about 200° under vacuum overnight. With an overpressure of about 5 psi of helium or argon on the system, the temperature was then raised to 500°, and the electrodes were immersed to the desired depths. Solute additions were carried out in the drybox using a similar procedure as described above. Sometimes, additions were also made through the ball valve without atmospheric contamination.

b. Voltammetric measurements. The same procedure was followed as described before for studying the electrochemistry of niobium in chloroaluminates.

CHAPTER III

RESULTS AND DISCUSSION

A. The Oxide Chemistry of Niobium in Molten LiF-BeF_2 Mixtures

The chemistry of niobium in molten fluorides is of interest for several reasons. It was observed in the molten salt reactor that the appearance of fission product ^{95}Nb in the fuel seemed to be a sensitive function of the state of oxidation (the U^{4+}/U^{3+} ratio) of the fuel.[194] This effect, which presumably involves the oxidation of the metal to a lower valence state in solution, might be a useful indicator of the state of oxidation of the fuel. Niobium pentoxide (Nb_2O_5), like protactinium pentoxide (Pa_2O_5), is expected to be sparingly soluble in molten fluorides and it has been proposed that Nb(V)* might be used as a stand-in for Pa(V) in studies of fuel reprocessing methods involving oxide precipitation. Protactinium is difficult to work with since it is a highly radioactive element. There may be some important differences, however, between the chemistry of Nb(V) and that of Pa(V). It seems likely that Nb(V), unlike Pa(V),[38] forms oxyions such as $NbO_xF_y^{(2x+y-5)-}$ in molten fluorides. In the system $NiO-Nb_2O_5$,[67,68,71,72] at least two intermediate compounds, $NiNb_2O_6$ and $Ni_4Nb_2O_9$, are known, and since NiO is also a sparingly soluble oxide, precipitation of these nickel niobates may be expected to complicate the chemistry of Nb(V) in the presence of O^{2-} and Ni^{2+} ions.

---

*This commonly used notation for the oxidation state of an element will be used interchangeably with that used previously in Chapter I (Nb^{5+}).

Weaver et al.[79] equilibrated niobium metal and a lower valent niobium fluoride in Li_2BeF_4 with hydrogen. Their results suggested the reaction

$$4HF(g) + Nb^\circ \rightleftarrows NbF_4(d) + 2H_2(g) \qquad (43)$$

$$Q_{43} = X_{NbF_4} P^2_{H_2}/P^4_{HF} \sim 10^{12} \quad (500°) \quad .$$

Senderoff and Mellors[112] report potentials, obtained chronopotentiometrically, for the formation of Nb(I), Nb(IV), and Nb(V) in molten LiF-NaF-KF (46.5-11.5-42 mole %) at 750°. The results indicate, in agreement with the results of Weaver and Friedman, that: Nb(IV) should be stable in the presence of nickel or nickel-base alloys; Nb(I) should disproportionate to the metal and Nb(IV); and Nb(V) should oxidize nickel to form appreciable concentrations of NiF_2 in solution.

The purpose of the present study has been to explore further the chemistry of niobium in molten fluorides by studying heterogeneous equilibria involving oxide phases of niobium(V). Three series of equilibrations have been made using the apparatus described in Chapter II, Section B, p 53. In the first series, performed in a nickel vessel, $NiNb_2O_6$ and $Ni_4Nb_2O_9$ were formed. In the second, performed in a graphite-lined vessel under circulating mixtures of CO and CO_2, the equilibrium solid phase was Nb_2O_5. In the third, performed in a nickel vessel, the equilibrium solid phases were $NiNb_2O_6$ and NiO. The second series of experiments will be described first.

1. Equilibrations of Nb_2O_5 and BeO with Molten $LiF-BeF_2$ Mixtures

In this series of experiments, the equilibrations were carried out in a nickel container with a graphite liner. Agitation of the

molten mixture was provided by means of a vigorous flow of $CO-CO_2$-Ar gas mixtures. CO was formed by the reaction of CO_2 with graphite. The equilibrium solid oxides in this study were examined by various methods. Emission spectroscopy revealed beryllium and niobium to be the only metallic elements present in appreciable amounts. X-ray powder diffraction showed BeO to be present in all samples, β-Nb_2O_5 in two early samples and γ-Nb_2O_5[54] in samples taken near the end of the series; the other samples gave an unidentified pattern, perhaps that of an unreported polymorph of Nb_2O_5.[54] The scanning electron microscopy (SEM) showed well-formed crystals containing major amounts of niobium (see Figure 7). From this evidence it may be concluded that BeO and Nb_2O_5 were the equilibrium phases.

The gas phase analysis showed that only traces of niobium were found deposited in the cold trap or on the KBr windows of the infrared cell. This is consistent with the calculated[35] equilibrium constant for the reaction

$$1/2\ Nb_2O_5(c) + 5/2\ BeF_2(d) \rightleftarrows NbF_5(g) + 5/2\ BeO(c) \qquad (44)$$

$$\log (P_{NbF_5}) = 2.05 - 11.76\ (10^3/T)$$

which predicts that the partial pressures of NbF_5 generated in these equilibrations will be in the range 10^{-13} to $10^{-9.4}$ atm.

From the niobium content of filtered samples (Figure 8) it appears that there was no effect of the CO_2/CO ratio, which was varied from 0.1 to 1.8. Since variation of this ratio should have caused changes in the NbF_4 content of the melt because of changes in the oxidation potential of the system (cf. reaction 45 below) the amount of NbF_4 present evidently was small. Since, moreover, no visible or UV absorption spectrum

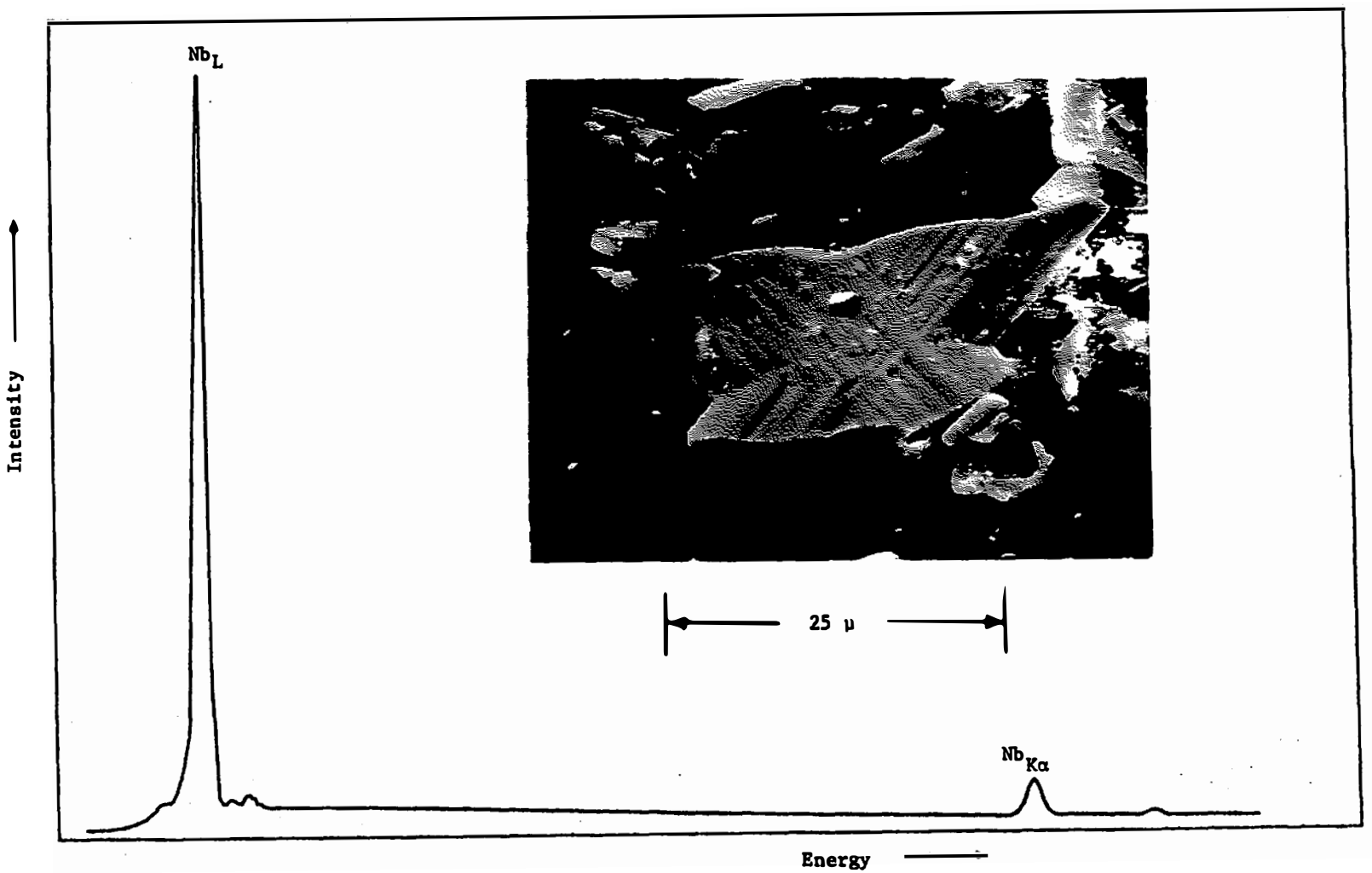


Figure 7. An SEM photograph of a typical particle of solid phase obtained from equilibrating BeO and Nb_2O_5 in molten Li_2BeF_4 at 728° and the corresponding x-ray fluorescence spectrum.

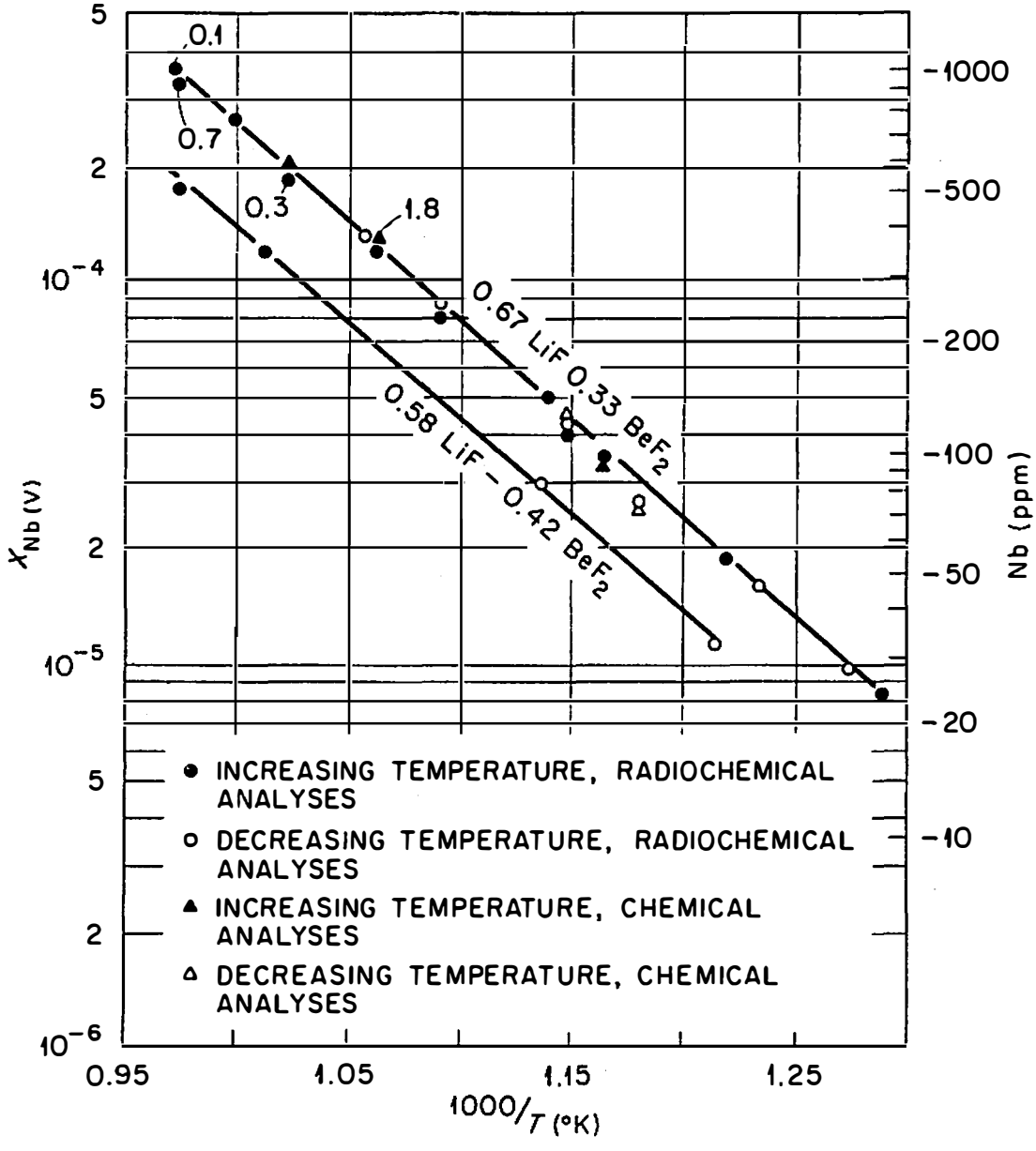


Figure 8. Concentration of Nb(V) in LiF-BeF_2 mixtures at equilibrium with BeO and Nb_2O_5 under circulating CO_2-CO mixtures.

The numbers in the graph show the P_{CO_2}/P_{CO} ratio.

corresponding to niobium(IV) was detected in filtered samples (spectroscopic analysis was performed by J. P. Young, Analytical Chemistry Divison, ORNL), it is concluded that only niobium(V) was present in appreciable amounts in solution. The CO_2/CO ratio was always higher than the values at which Nb_2O_5 is expected to be reduced to NbO_2.[82,84]

The conclusion that Nb(IV) was not present in solution is confirmed by the following calculation. From the estimate of Weaver and Friedman[79] of the equilibrium constant for the reduction of NbF_4 in Li_2BeF_4 by hydrogen, one can calculate

$$\Delta G^f_{773°K}(NbF_4(d)) = -306.4 \text{ (kcal/mole)} \quad .$$

This combined with ΔG^f values for Nb_2O_5, BeO, BeF_2, CO, and CO_2[35,82] gives for the reaction

$$1/2\ Nb_2O_5(c) + 1/2\ CO\ (g) + 2BeF_2(d) \rightleftharpoons NbF_4(d) + 2BeO(c) + 1/2\ CO_2(g) \quad (45)$$

the very small equilibrium constant

$$X_{NbF_4}\ (P_{CO_2}/P_{CO})^{1/2} \sim 1 \times 10^{-27} \quad .$$

Hence, the amount of NbF_4 in the solutions is expected to be quite negligible.

With only Nb(V) present in solution in equilibrium with $Nb_2O_5(c)$ and BeO(c), Nb(V) concentration (Figure 8, p 73) is found to be far greater than would have been predicted from the reported stabilities in molten fluorides of NbF_4,[79,112] NbF_5[112] and the available free energy data for $Nb_2O_5(c)$, BeO(c), and $BeF_2(d)$.[35] In particular, if NbF_5 were the component in the present solutions, then $NbF_4(d)$ should be unstable under all conditions, disproportionating completely to the metal and $NbF_5(d)$. This, however, is not consistent with the observed stability of NbF_4 in oxide-free melts.[79,112]

The evident stability of Nb(V) in the present system is most plausibly explained by the formation of one or more oxygen containing species, such as NbO_xF_{5-2x}. Then the equilibrium reaction is:

$$1/2\ Nb_2O_5(c) + \frac{5-2x}{2}\ BeF_2(d) \rightleftarrows NbO_xF_{5-2x}(d) + \frac{5-2x}{2}\ BeO(c) \qquad (46)$$

where, as usual, the species in solution are represented as neutral components. The equilibrium quotient for the reaction (46) is defined

$$Q_{46} = X_{NbO_xF_{5-2x}}$$

where

$$X_{NbO_xF_{5-2x}} \sim \frac{n_{NbO_xF_{5-2x}}}{n_{LiF} + n_{BeF_2}} .$$

From Figure 8 (p 73) the results in LiF-BeF_2 (67-33 mole %) give

$$\log Q_{46} = 1.70 - 5.27\ (10^3/T) \qquad (46a)$$

and

$$\Delta G(\text{reaction 46}) = -RT\ln Q_{46} = 24.12 - 7.78\ (T/10^3)(\text{Kcal/mole}) . \qquad (46b)$$

In LiF-BeF_2 (52-48 mole %)

$$\log Q_{46} = 0.90 - 4.81\ (10^3/T) \qquad (46c)$$

$$\Delta G(\text{reaction 46}) = 22.01 - 4.11\ (T/10^3)(\text{Kcal/mole}). \qquad (46d)$$

The variation of $X_{Nb(V)}$ with melt composition at 606° is shown in Figure 9. The temperature dependence of the solubility of Nb_2O_5 at melt composition LiF-BeF_2 (52-48 mole %) is plotted in Figure 8 (p 73). These results indicate that the Nb(V) concentration or the solubility decreases with increasing BeF_2 concentration (also see Figure 8). This phenomenon may be explained by the fact that Nb_2O_5 is an acidic oxide. Increasing the acidity of the melt (increasing the BeF_2 concentration) will decrease the Nb_2O_5 solubility. Also, increasing the basicity of the melt (increasing the free fluoride concentrations) will stabilize

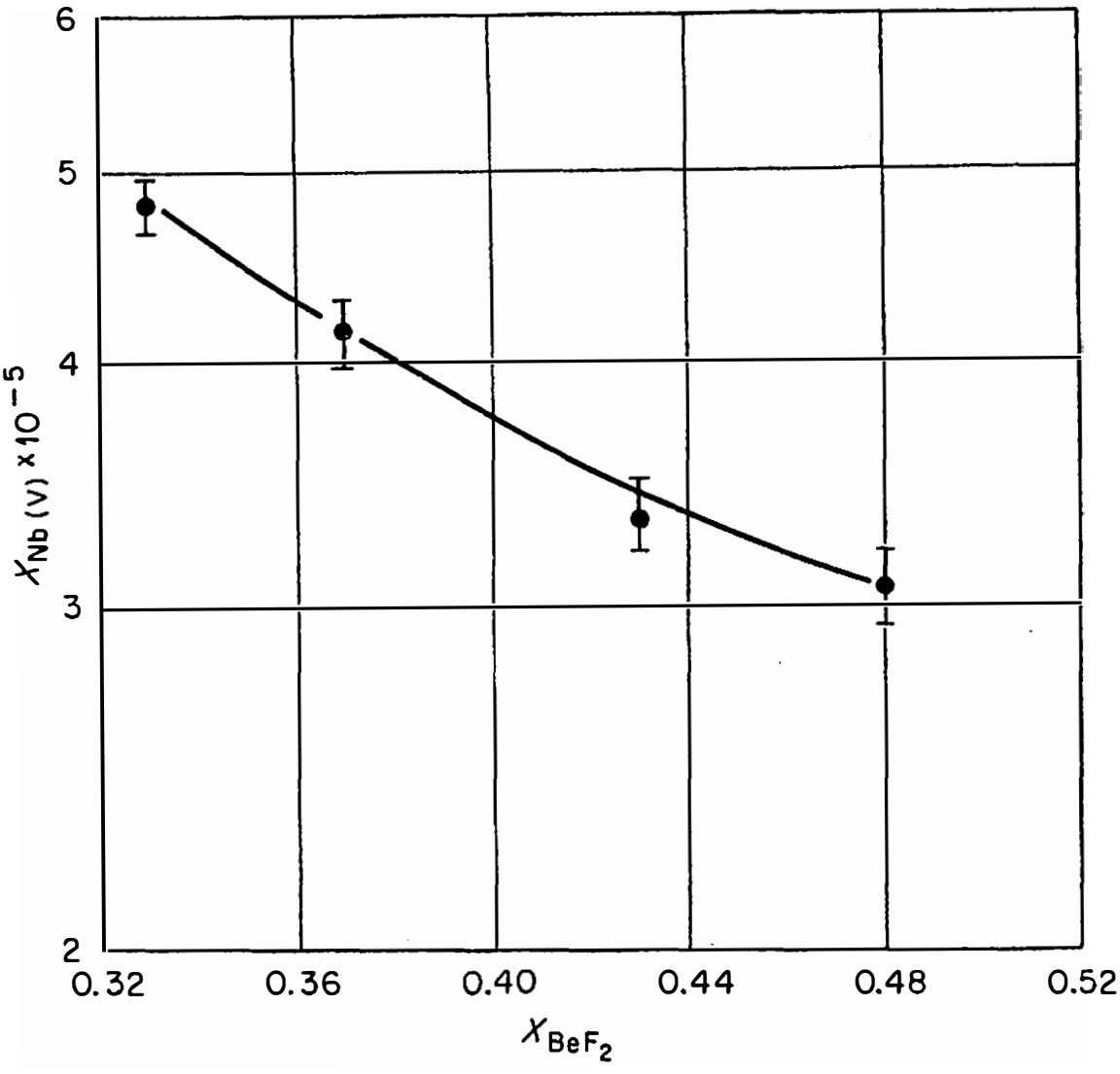


Figure 9. Effect of melt composition on the concentration of niobium(V) in LiF-BeF_2 mixtures at equilibrium with BeO and Nb_2O_5 at 606°.

the Nb(V) complex and give higher Nb(V) concentrations in the melt. Figure 10 shows that indeed Nb(V) concentration increases with increasing free fluoride concentration. The free fluoride concentration is given approximately by $(X_{LiF} - 2X_{BeF_2}) \times 100$.

The variation of $X_{NbO_xF_{5-2x}}$ (i.e., Q_{46}) with melt composition, shown in Figure 9 (p 76), may be used to estimate the activity coefficient γ of the NbO_xF_{5-2x} as follows. For Reaction 46

$$K_{46} = X_{NbO_xF_{5-2x}} \cdot \gamma_{NbO_xF_{5-2x}} / (a_{BeF_2})^{\frac{5-2x}{2}} \qquad (46e)$$

where a_{BeF_2} is the activity of BeF_2 in the solution. Hence

$$\gamma_{NbO_xF_{5-2x}} = \frac{K_{46}}{Q_{46}} (a_{BeF_2})^{\frac{5-2x}{2}} \quad . \qquad (46f)$$

As has been customary in previous studies,[35] one defines standard states such that $\gamma_{NbO_xF_{5-2x}} = 1$ and $a_{BeF_2} = 1$ in Li_2BeF_4 (33 mole % BeF_2). Hence

$$K_{46} = (Q_{46})_{X_{BeF_2}} = 0.33 \qquad (46g)$$

Introducing values for a_{BeF_2}, available from previous measurements,[195] we obtain the activity coefficients for NbO_xF_{5-2x} (where x = 0, 1, 2), shown in Figure 11. Figure 11 shows the changes of the activity coefficient for various assumed Nb(V) species with the melt composition. The variation found for γ_{NbF_5} with melt composition is so large that NbF_5 is unlikely to be the predominant Nb(V) species in solution. The smaller changes found for the activity coefficient of the assumed components $NbOF_3$ and NbO_2F are more reasonable, suggesting that an oxy-ion of Nb(V) is indeed present. The similar increase of γ_{NbO_2F} and γ_{BeF_2} with X_{BeF_2} indicates that if the species is NbO_2F it competes with

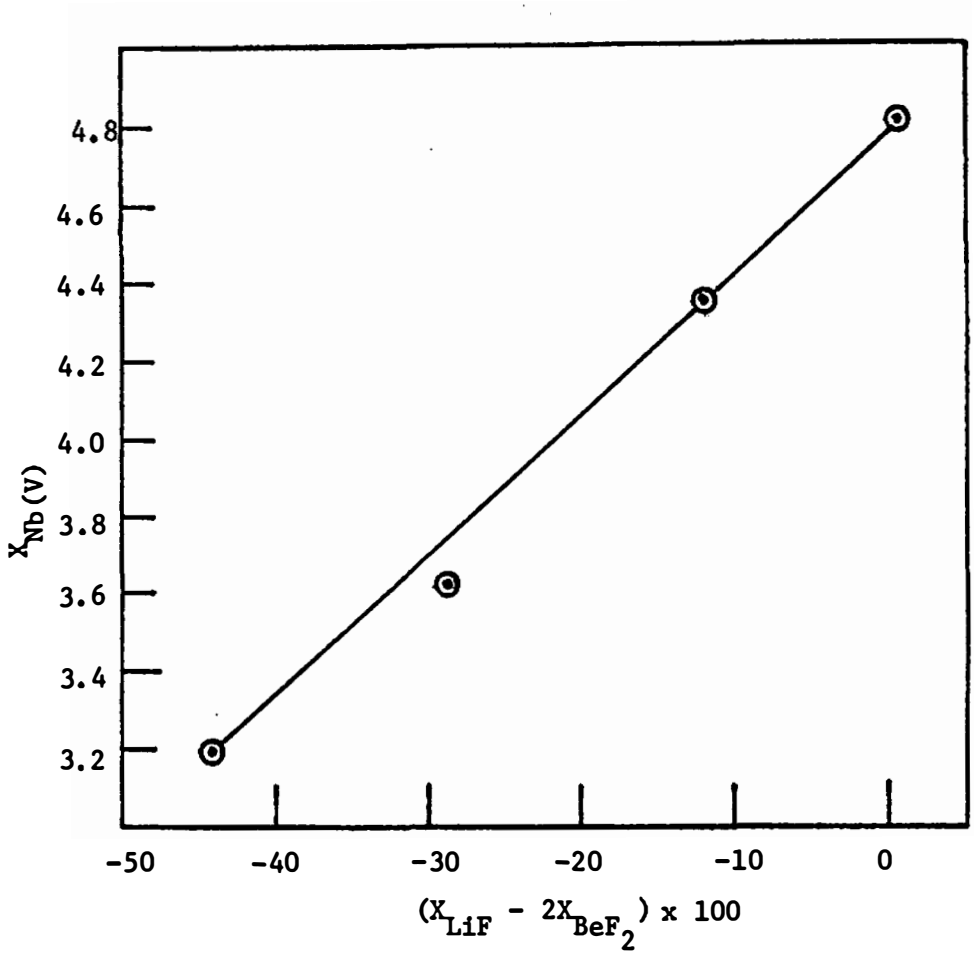


Figure 10. Effect of free fluoride concentration, $(X_{LiF} - 2X_{BeF_2}) \times 100$, on the concentration of Nb(V) in $LiF-BeF_2$ mixtures at 606°.

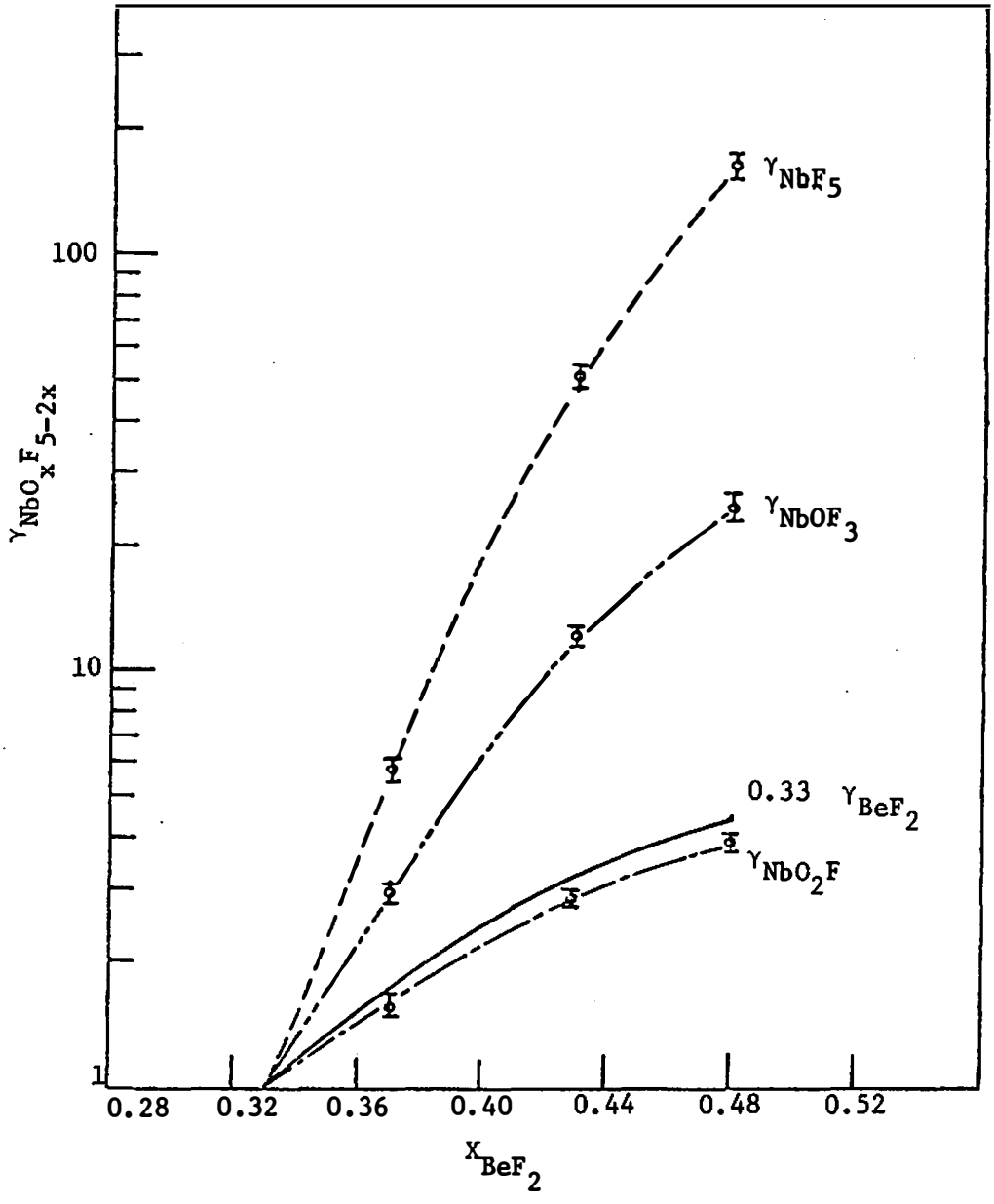


Figure 11. Activity coefficients of assumed components NbF_5, $NbOF_3$, NbO_2F and BeF_2 in $LiF-BeF_2$ mixtures at 606°.

BeF_2 for the fluoride ions, possibly forming an anion with -2 or -3 charge, that is $NbO_2F_3^{2-}$ or $NbO_2F_4^{3-}$. Pausewang and Rüdorff[61] reported the presence $NbO_2F_3^{2-}$ in $K_2NbO_2F_3$. Luzhnaya et al.[196] reported the existence of $TaO_2F_3^{2-}$ in a K, Ta||F, O system. These results are quite consistent with the formation of $NbO_2F_3^{2-}$ or $NbO_2F_4^{3-}$. The IR spectrum of the solidified equilibrated salt sampled at 754° (Nb(V) concentration 1050 ppm) was also obtained using the KBr pellet technique. Besides the absorption bands corresponding to Li_2BeF_4:[197] 340(m), 375(w), 415(m), 475(w), and 810(s) cm^{-1}, two bands at 710(s) cm^{-1} and 910(s) cm^{-1} were observed. These two bands were possibly due to the Nb-F,[198] and Nb-O[61] stretching vibration of the equilibrium oxy-ions of niobium(V).

2. Equilibrations Involving Nickel Niobates in Molten Li_2BeF_4

In this series of measurements, Nb_2O_5, BeO, and NiO were equilibrated in Li_2BeF_4 in a nickel container under circulating argon. Some difficulty was encountered in obtaining filtered samples free of solids. As judged by the reproducibility of the ^{95}Nb and nickel content of successive samples, this was corrected by use of finer porosity filters (maximum pore size 10 microns).

At the outset of these experiments, only Nb_2O_5 and BeO were introduced; however, the nickel content of filtered samples quickly rose to values expected for NiO saturation, and, as will become clear below, Nb_2O_5 was also being converted to $NiNb_2O_6$. The oxygen for the NiO presumably was supplied by in-leakage of air early in the run. Table IX shows the results of analyses of the solid phase by various methods. The phase $Ni_4Nb_2O_9$ was tentatively identified on the basis of the Ni/Nb

TABLE IX

ANALYSIS OF SOLID PHASES BY VARIOUS METHODS

Temperature °C	SEM[a] Photo No.	Minor Phase Size and Characteristics	Minor Phase $A_{Nbk_\alpha}/A_{Nik_\alpha}$	Minor Phase Stoichiometry	Major Phase Photo No.	Major Phase Size	Major Phase $A_{Nbk_\alpha}/A_{Nik_\alpha}$	Major Phase Stoichiometry	Average Composition $A_{Nbk_\alpha}/A_{Nik_\alpha}$	Average Composition Stoichiometry	X-ray Diffraction	Chemical Analysis (mole ratio)
705°	1	25μ, well defined	0.233	$NiNb_2O_6$	7	≤ 6μ	0.243	$NiNb_2O_6$		$NiNb_2O_6$ major phase	BeO $NiNb_2O_6$ major phase	n_{Nb}/n_{Ni} = 1.70/1
	2	shape with		$NiNb_2O_6$								
	3	sharp edges.	0.204	$NiNb_2O_6$	8		0.204	$NiNb_2O_6$	0.174	$Ni_4Nb_2O_9$ minor phase		
	4	25μ, round edges	0.0675	$Ni_4Nb_2O_9$	9		0.211	$NiNb_2O_6$				
	5	25μ, round edges	0.0740	$Ni_4Nb_2O_9$								
	6	25μ, round edges	0.0710	$Ni_4Nb_2O_9$								
755°	10	25-80μ	0.0815	$Ni_4Nb_2O_9$	16	≤ 6 μ	0.106	$Ni_4Nb_2O_9$	0.0446	$Ni_4Nb_2O_9$	BeO $NiNb_2O_6$	n_{Nb}/n_{Ni} = 1/1.8
	11	25-80μ	0.0715	$Ni_4Nb_2O_9$								
	12	25-80μ	0.0851	$Ni_4Nb_2O_9$								
	13	25-80μ	0.0662	$Ni_4Nb_2O_9$	17		0.0858	$Ni_4Nb_2O_9$			$Ni_4Nb_2O_9$[c]	
	14	25-80μ	0.0666	$Ni_4Nb_2O_9$								
	15	25-80μ	0.0640	$Ni_4Nb_2O_9$								

[a]Standardization for quantitative analyses of Nb and Ni by X-ray fluorescence:
Standard (1) Ni-Nb (33-67 mole %) alloy corresponding to $NiNb_2O_6$ composition, the X-ray fluorescence intensity ratio between niobium and nickel is $A_{Nbk_\alpha}/A_{Nik_\alpha}$ = 0.170 to 0.209.

Standard (2) Ni-Nb (67-33 mole %) alloy corresponding to $Ni_4Nb_2O_9$ composition, the X-ray fluorescence intensity ratio between niobium and nickel is $A_{Nbk_\alpha}/A_{Nik_\alpha}$ = 0.058 to 0.080.

Ni-Nb alloys were prepared by Metals and Ceramics Division at Oak Ridge National Laboratory.

[b]Photograph numbers 1-9 were taken on the same sample; photograph numbers 10-17 were taken on another sample.

[c]X-ray diffraction patterns showed that extra lines other than BeO and $NiNb_2O_6$ were present, but no positive identification could be made for $Ni_4Nb_2O_9$.

mole ratio in single crystals, determined by SEM using a Ni-Nb alloy of known composition as the standard. The uncertainty in this analysis is ± 30%, and the existence of $Ni_4Nb_2O_9$ is not conclusive.

In discussing the results (points numbered in chronological order in Figure 12), it will be convenient to refer to Table X and Figure 13. Figure 13 is constructed using data in Table XI which will be discussed later. Here the reaction between the BeO and Nb_2O_5 (Reaction I, Table X) is the same as Reaction 46 (p 75). The reaction between BeO and NiO (Reaction 3, Table X) is derived from available thermodynamic data.[35] The other reactions were generated as follows from the data in Figure 12.

(a) Points 1-3. Since the nickel content in solution indicated NiO saturation in these initial samples and the X-ray patterns of an oxide sample taken at point 5 indicated the presence of $NiNb_2O_6$ and BeO as well, it was presumed that the dissolved Nb(V) concentration corresponds to a point at which all three oxide phases (NiO, $NiNb_2O_6$ and BeO) were present (see Figure 13), and which was possibly metastable with respect to the precipitation of $Ni_4Nb_2O_9$. With the position of this point presumably established (Point A, Figure 13), the reaction between BeO and $NiNb_2O_6$ (Reaction 2, Table X), would give a slope of - 1/2, in the plot of log $X_{NbO_xF_{5-2x}}$ vs log X_{NiF_2}.

After Point 3, the apparatus was cooled to room temperature and NiO was added.

(b) Points 4 and 5. The nickel content of the melt appears somewhat lower and the niobium content somewhat higher than previously.

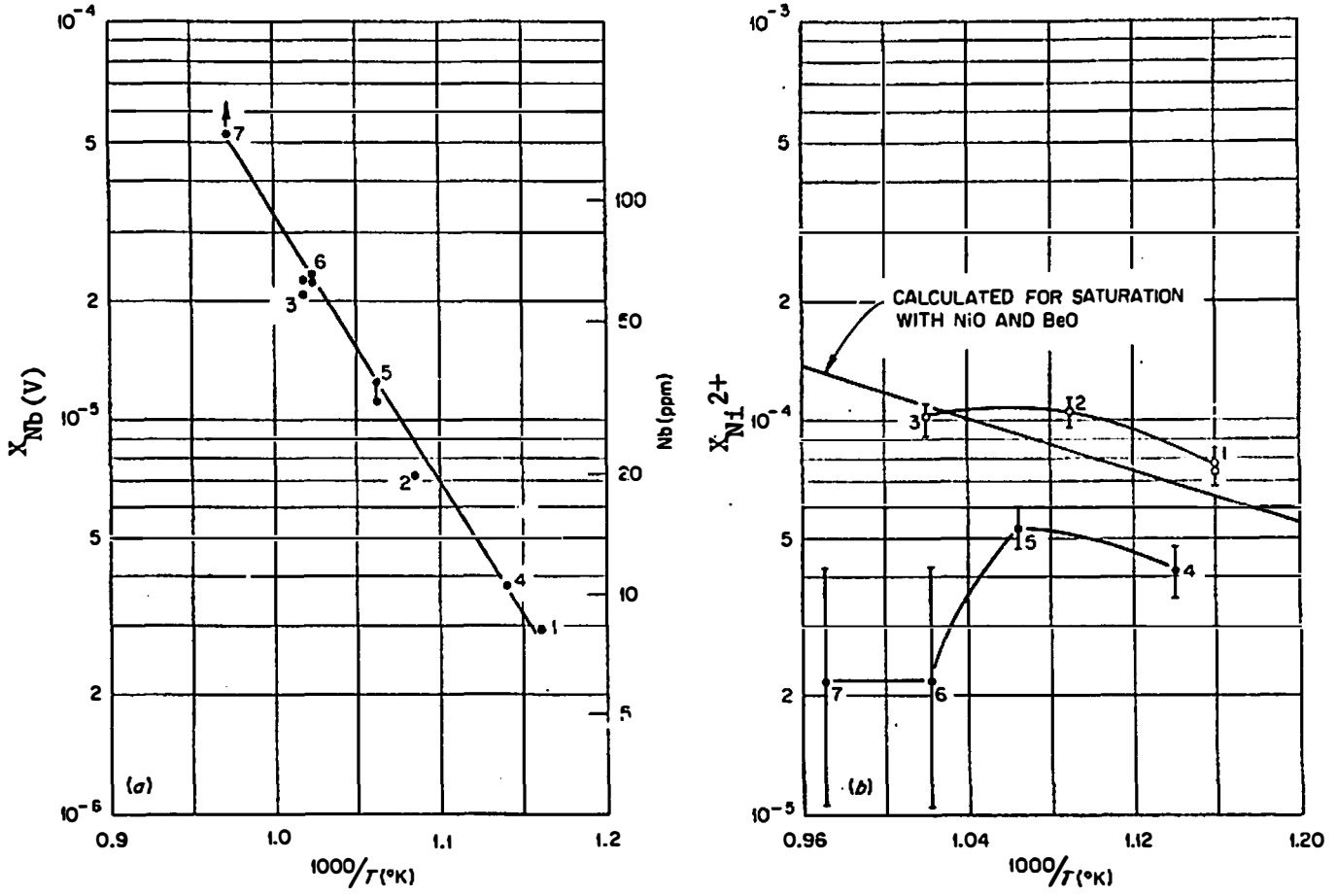


Figure 12. Concentrations of (a) niobium(V) and (b) nickel(II) in molten Li_2BeF_4 equilibrated with $NiO-Nb_2O_5$ phases and BeO.

The numbers indicate the order in which points were determined. The straight line in (b) represents calculated values corresponding to saturation with NiO and BeO

TABLE X

REACTIONS OF VARIOUS EQUILIBRIUM SOLID PHASES IN MOLTEN Li_2BeF_4

Saturating Oxide Phase	Reaction	Equilibrium Constant Expression
(1) Nb_2O_5 + BeO	$1/2\ Nb_2O_5(c) + \frac{5-2x}{2}\ BeF_2(d) \rightleftarrows NbO_xF_{5-2x}(d) + \frac{5-2x}{2}\ BeO(c)$	$X_{NbO_xF_{5-2x}}$
(2) $NiNb_2O_6$ + BeO	$1/2\ NiNb_2O_6(c) + (3-x)BeF_2(d) \rightleftarrows NbO_xF_{5-2x}(d) + (3-x)BeO(c) + 1/2\ NiF_2(d)$	$(X_{NbO_xF_{5-2x}})(X_{NiF_2})^{1/2}$
(3) NiO + BeO	$NiO(c) + BeF_2(d) \rightleftarrows NiF_2(d) + BeO(c)$	X_{NiF_2}
(4) Nb_2O_5 + $NiNb_2O_6$	$(3-x)Nb_2O_5(c) + \frac{5-2x}{2}\ NiF_2(d) \rightleftarrows NbO_xF_{5-2x} + \frac{5-2x}{2}\ NiNb_2O_6(c)$	$(X_{NbO_xF_{5-2x}})/(X_{NiF_2})^{\frac{5-2x}{2}}$
(5) $NiNb_2O_6$ + $Ni_4Nb_2O_9$	$\frac{9-2x}{6}\ NiNb_2O_6(c) + \frac{5-2x}{2}\ NiF_2(d) \rightleftarrows NbO_xF_{5-2x} + \frac{3-x}{3}\ Ni_4Nb_2O_9(c)$	$(X_{NbO_xF_{5-2x}})/(X_{NiF_2})^{\frac{5-2x}{2}}$

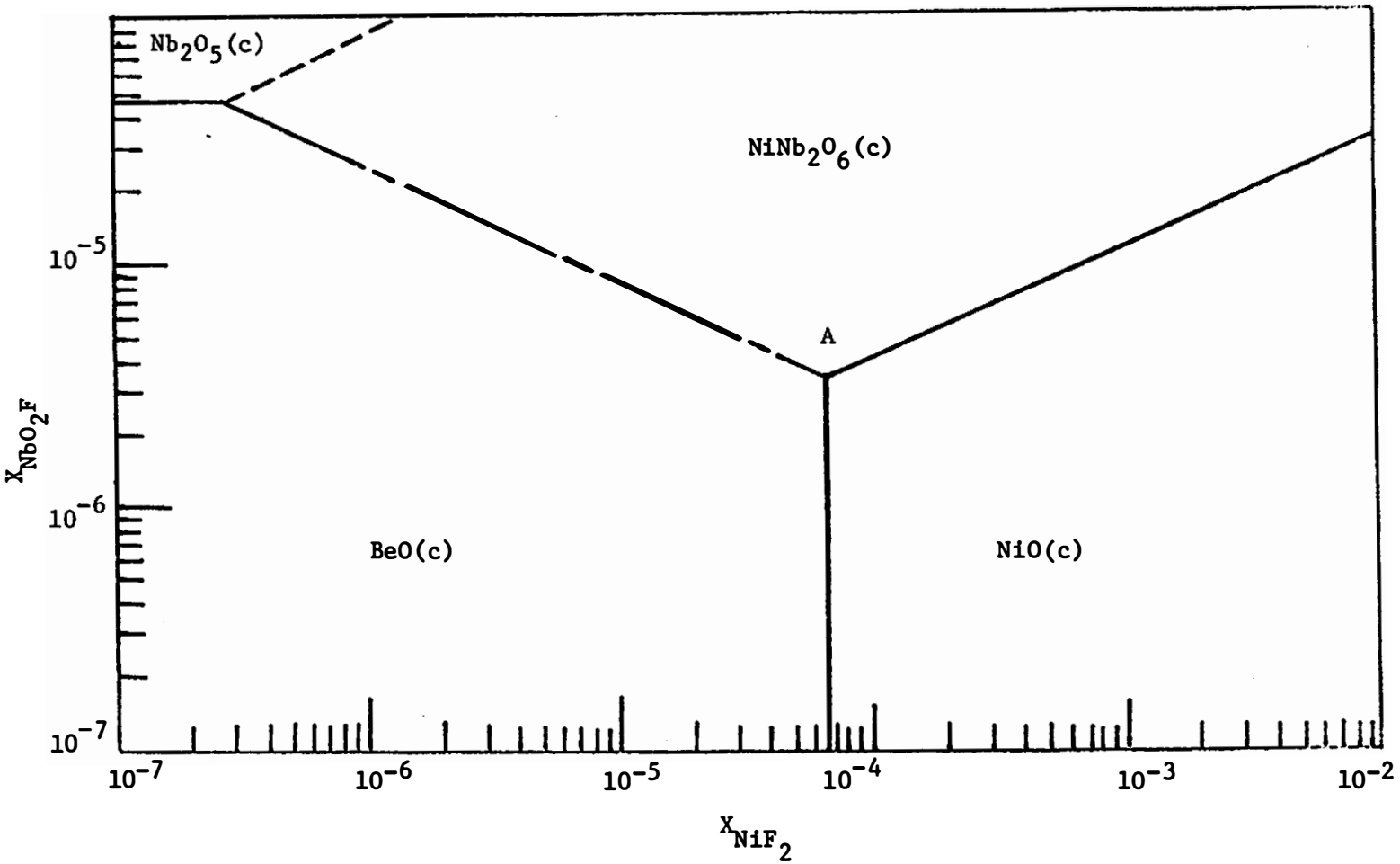


Figure 13. Phase diagram representing the NbO_2F and NiF_2 concentrations in molten Li_2BeF_4 at 600° as a function of the oxide phases present at equilibrium.

TABLE XI

EQUILIBRIUM REACTIONS AND DATA FOR CONSTRUCTING THE PHASE DIAGRAM AT 600°

Boundary	Equilibrium Reaction	Q	Data[a]
(1) $Nb_2O_5(c)/BeO(c)$	$1/2\ Nb_2O_5(c) + 1/2\ BeF_2(d) \rightleftarrows NbO_2F(d) + 1/2\ BeO(c)$	X_{NbO_2F}	$\log X_{NbO_2F} = -4.34$
(2) $Nb_2O_5(c)/NiNb_2O_6(c)$	$Nb_2O_5(c) + 1/2\ NiF_2(d) \rightleftarrows NbO_2F(d) + 1/2\ NiNb_2O_6(c)$	$X_{NbO_2F}/X_{NiF_2}^{1/2}$	$\log X_{NbO_2F} = -1.06 + 1/2 \cdot \log X_{NiF_2}$
(3) $NiNb_2O_6(c)/BeO(c)$	$1/2\ NiNb_2O_6(c) + BeF_2(d) \rightleftarrows NbO_2F(d) + 1/2\ NiF_2(d) + BeO(c)$	$X_{NbO_2F} \cdot X_{NiF_2}^{1/2}$	$\log X_{NbO_2F} = -6.50 - 1/2 \cdot \log X_{NiF_2}$
(4) $NiO(c)/BeO(c)$	$NiO(c) + BeF_2(d) \rightleftarrows NiF_2(d) + BeO(c)$	X_{NiF_2}	$\log X_{NiF_2} = -4.18$
(5) $NiNb_2O_6(c)/NiO(c)$	$1/2\ NiNb_2O_6(c) + 1/2\ NiF_2(d) \rightleftarrows NbO_2F(d) + NiO(c)$	$X_{NbO_2F} \cdot X_{NiF_2}^{-1/2}$	$\log X_{NbO_2F} = -3.44 + 1/2 \cdot \log X_{NiF_2}$

[a]The data for reactions (1) and (5) were obtained from the experimental results; the data for reactions (2) and (3) were estimated from the experimental results; the data for reaction (4) were obtained from Reference 35.

This may reflect the conversion of small amounts of $NiNb_2O_6$ to $Ni_4Nb_2O_9$ according to Reaction 5, Table X (p 84).

(c) Point 6. Here the nickel content of the melt has fallen well below the value corresponding to NiO saturation; however, the niobium content has not risen appreciably. Hence, even though $Ni_4Nb_2O_9$ was apparently detected in minor amounts with the SEM, it is thought that the system was still at Point A, Figure 13 (p 85), where NiO, $NiNb_2O_6$ and BeO were present.

(d) Point 7. Here the SEM suggested major amounts of $Ni_4Nb_2O_9$, the nickel content of the melt remained low, and the niobium content began to rise with time. However, final equilibrium with respect to $NiNb_2O_6$, $Ni_4Nb_2O_9$, and BeO was not established. The existence of $Ni_4Nb_2O_9$ was also not conclusive.

On the basis of these results it is clear that the solubility of niobium can be quite low ($\sim$ 10 ppm, $X = 5.68 \times 10^{-6}$) in melts containing appreciable amounts of O^{2-} and Ni^{2+} ions.

Based on the reactions in Table X (p 84), it was decided to equilibrate molten Li_2BeF_4 with nickel niobates ($NiNb_2O_6$ or $Ni_4Nb_2O_9$) and NiO, expecting that this would not only define more precisely the solubility of Nb(V) in the presence of O^{2-} and Ni^{2+} ions, but would also indicate the stoichiometry of NbO_xF_{5-2x} in solution.

3. Equilibrations of $NiNb_2O_6$ and NiO with Molten Li_2BeF_4 and Determination of the Stoichiometry of an Oxygen-Containing Niobium Species in the Melt

From the previous experiments involving equilibration of Nb_2O_5

and BeO with molten LiF-BeF_2 mixtures, the higher than expected solubility of Nb(V), the changes of $\gamma_{Nb(V)}$ with X_{BeF_2}, and the infrared spectrum of the solidified equilibrium salt suggested the existence of a soluble niobium oxyfluoride of unknown stoichiometry NbO_xF_{5-2x}. In the equilibrations performed in a nickel container, $NiNb_2O_6$ and possibly $Ni_4Nb_2O_9$ were formed. As mentioned before, these compounds seemed useful for determining the stoichiometry of NbO_xF_{5-2x} by means of heterogeneous equilibria reactions involving nickel niobates. Attempts to synthesize $Ni_4Nb_2O_9$ using various ratios of Nb_2O_5/NiO (1:1, 1:3, 1:4, 1:5) were not fruitful; the only compound formed was $NiNb_2O_6$, which was identified by X-ray powder diffraction analysis. Thus, the following equilibrium was studied by adding NiF_2 to molten Li_2BeF_4 saturated with BeO, NiO, and $NiNb_2O_6$ (labelled with ^{95}Nb.)

$$1/2\ NiNb_2O_6(c) + \frac{5-2x}{2}\ NiF_2(d) \rightleftharpoons NbO_xF_{5-2x}(d) + (3-x)NiO(c) \qquad (47)$$

where

$$Q_{47} = X_{NbO_xF_{5-2x}} \Big/ (X_{NiF_2})^{\frac{(5-2x)}{2}} \qquad (47a)$$

and

$$\log X_{NbO_xF_{5-2x}} = \log Q_{47} + \frac{5-2x}{2} \log X_{NiF_2} . \qquad (47b)$$

Equation (47b) would then result, by a graphical method, in the determination of the stoichiometry of the soluble niobium species.

The equilibration was performed in a nickel container and stirring was provided by recirculating argon. Filtered samples of the melt were obtained at various intervals at the beginning of the equilibration and following each addition of NiF_2. The concentration of Nb(V) was determined radiometrically. Occasionally wet analytical methods were also

employed and the concentration of nickel was always determined colorimetrically. Samples of the solid phases were examined by X-ray powder diffraction; the analyses showed that BeO, NiO and $NiNb_2O_6$ were present at the first equilibrium point, but later only NiO and $NiNb_2O_6$ were present as expected (Figure 13, p 85). No significant amount of niobium was found deposited in the cold trap of the gas outlet line. This is consistent with the calculated equilibrium constant for the reaction

$$1/2\ NiNb_2O_6(c) + 5/2\ NiF_2(d) \rightleftarrows NbF_5(g) + 3\ NiO(c) \qquad (48)$$

which on rearrangement gives

$$\log P_{NbF_5} = 7.98 - 10.27\ (10^3/T) + 5/2 \log X_{NiF_2} \qquad (48a)$$

and predicts that the partial pressure of NbF_5 generated in these equilibrations at 600° will be in the range 10^{-14} to 10^{-9} atm, when X_{NiF_2} changes from 6.3×10^{-5} to 8.5×10^{-3}. The ΔG^f of $NiNb_2O_6$ used in this calculation is obtained from estimates below.

The results obtained are shown in Figure 14, in which the Ni^{2+} concentration was varied between those corresponding to NiO and NiF_2[35] saturations. The values of the slopes of the lines are 1/2 at the two temperatures studied, indicating that x = 2 in NbO_xF_{5-2x}. Thus, the stoichiometry of the Nb oxyfluoride is now established and Equation 47 (p 88) can be written as:

$$1/2\ NiNb_2O_6(c) + 1/2\ NiF_2(d) \rightleftharpoons NbO_2F(d) + NiO(c) \qquad (47c)$$

$$Q_{48} = X_{NbO_2F} \Big/ X_{NiF_2}^{1/2}$$

where, at 600°

$$\log X_{NbO_2F} = \log Q_{48} + 1/2 \log X_{NiF_2} = -3.40 + 1/2 \log X_{NiF_2} . \qquad (47d)$$

The good agreement of the data with x = 2 is compared in Figure 15 with lines drawn for other values of x (x = 0, NbF_5; x = 1, $NbOF_3$) at

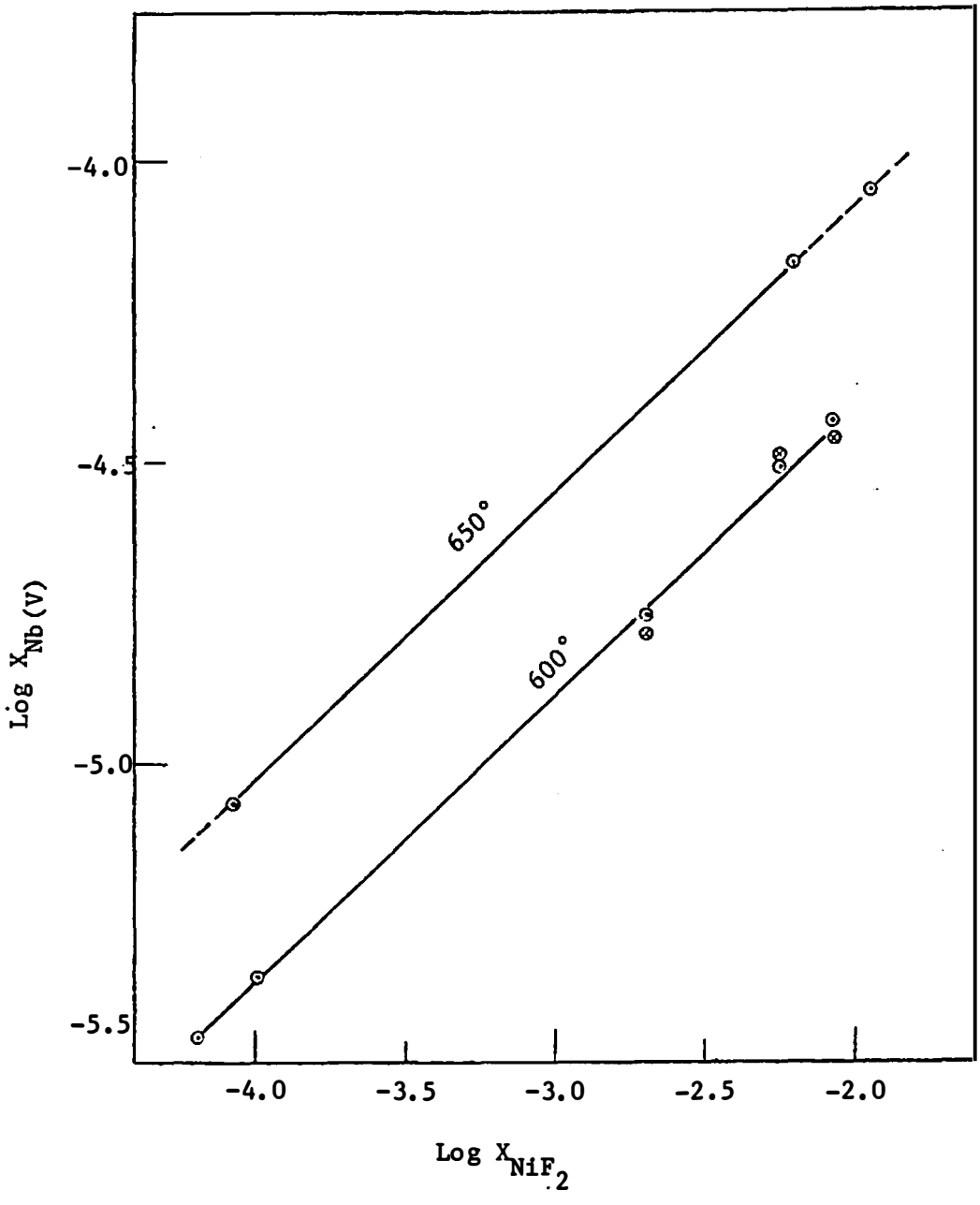


Figure 14. The effect of NiF_2 concentration on the concentration of niobium in molten Li_2BeF_4 in the presence of NiO and $NiNb_2O_6$.

radiochemical analyses chemical analyses

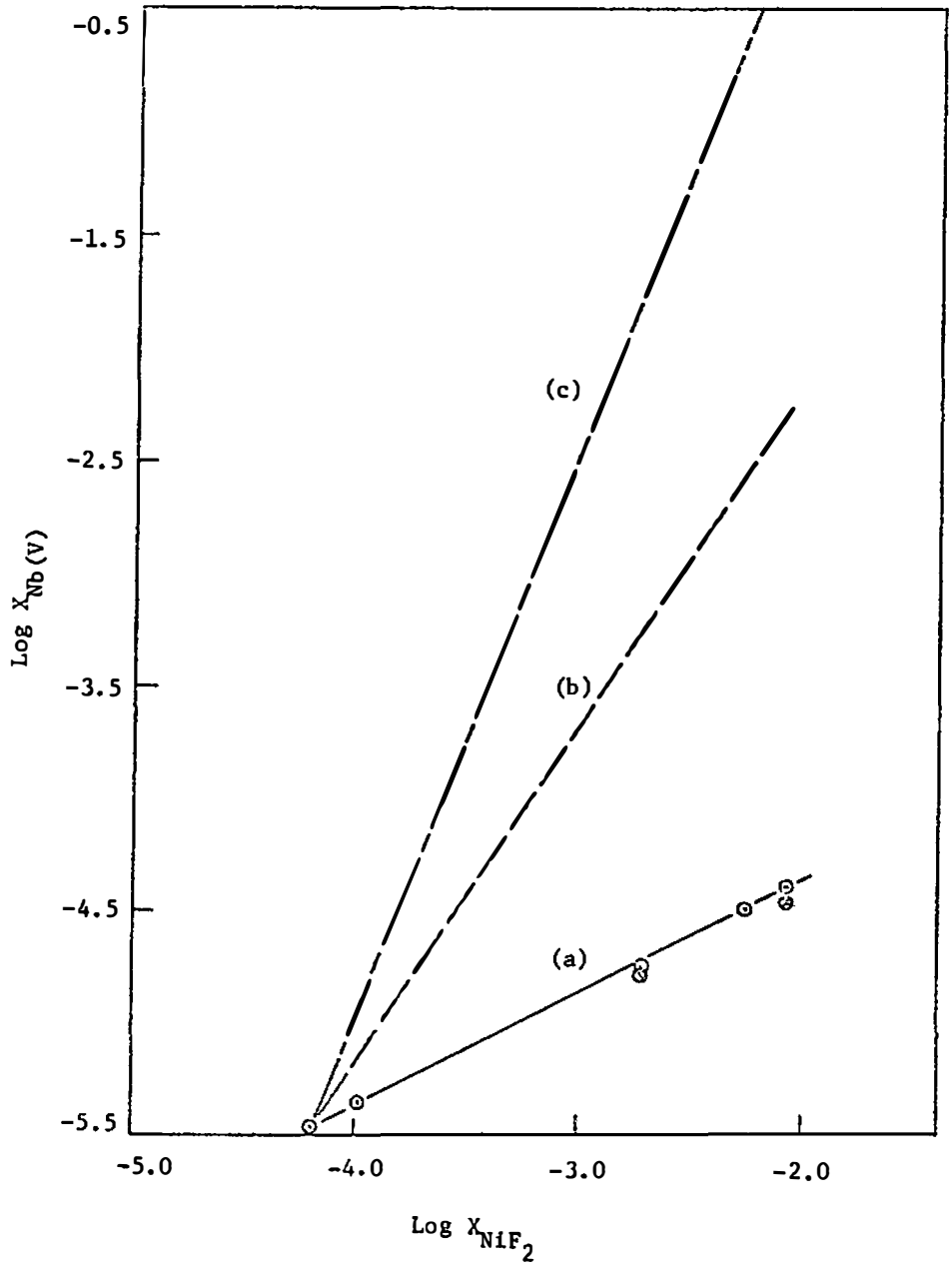


Figure 15. Calculated Nb(V) concentrations as a function of NiF_2 concentration for various assumed Nb(V)-soluble species.

The points are experimentally determined.
⊙ radiochemical analyses, ⊗ chemical analyses

(a) 1/2 $NiNb_2O_6(c)$ + 1/2 $NiF_2(d)$ $\rightleftharpoons$ $NbO_2F(d)$ + $NiO(c)$

(b) 1/2 $NiNb_2O_6(c)$ + 3/2 $NiF_2(d)$ $\rightleftharpoons$ $NbOF_3(d)$ + $2NiO(c)$

(3) 1/2 $NiNb_2O_6(c)$ + 5/2 $NiF_2(d)$ $\rightleftharpoons$ $NbF_5(d)$ + $3NiO(c)$

600°. These results give strong evidence for the formation of NbO_2F in molten Li_2BeF_4 in equilibrium with $NiNb_2O_6$ and NiO. This stoichiometry is also in agreement with that of $NbO_2F_3^{2-}$ and $TaO_2F_3^{2-}$, reported by other authors,[61,196] respectively.

The temperature effect on Q_{47c} is plotted in Figure 16 which gives

$$\log Q_{47c} = 1.81 - 4.58\ (10^3/T) \tag{47e}$$

and

$$\Delta G \text{ (reaction 47c)} = 20.96 - 8.28\ (T/10^3) \text{ (kcal/mole)} . \tag{47f}$$

The existence of NbO_2F(d) in the $NiNb_2O_6$(c), NiO(c)/Li_2BeF_4 system suggests that the equilibrium reaction in the Nb_2O_5(c), BeO(c)/Li_2BeF_4 system (see page 75) is

$$1/2\ Nb_2O_5(c) + 1/2\ BeF_2(d) \rightleftarrows NbO_2F(d) + 1/2\ BeO(c) . \tag{49}$$

The equilibrium quotient for reaction 49 is given by

$$Q_{49} = X_{NbO_2F} . \tag{49a}$$

Using the available free energies of formation[35] of Nb_2O_5(c), BeF_2(d), BeO(c) and the free energy of reaction (46b, p 75), we can estimate the free energy of formation of NbO_2F(d) in molten Li_2BeF_4.

$$\Delta G^f_{NbO_2F} = -250.7 + 45.9\ (T/10^3) \text{(kcal/mole)} \tag{49b}$$

Combining $\Delta G^f_{NbO_2F}$ with ΔG^f values[35,79,82] for NbF_5(g), Nb_2O_5(c), NbO_2(c), NbF_4(d), BeO(c), BeO(d), and BeF_2(d), one can generate the Pourbaix diagram, at 500°, shown in Figure 17. The equilibria reactions and data for constructing this diagram are listed in Table XII. This diagram shows the stability (or redox potential) of different known niobium compounds and and species as a function of oxide concentration (log $X_{O^{2-}}$). The vertical line (BeO(c) saturation) corresponds to the experimental result from the equilibrium of Nb_2O_5 and BeO in molten Li_2BeF_4 at 500°.

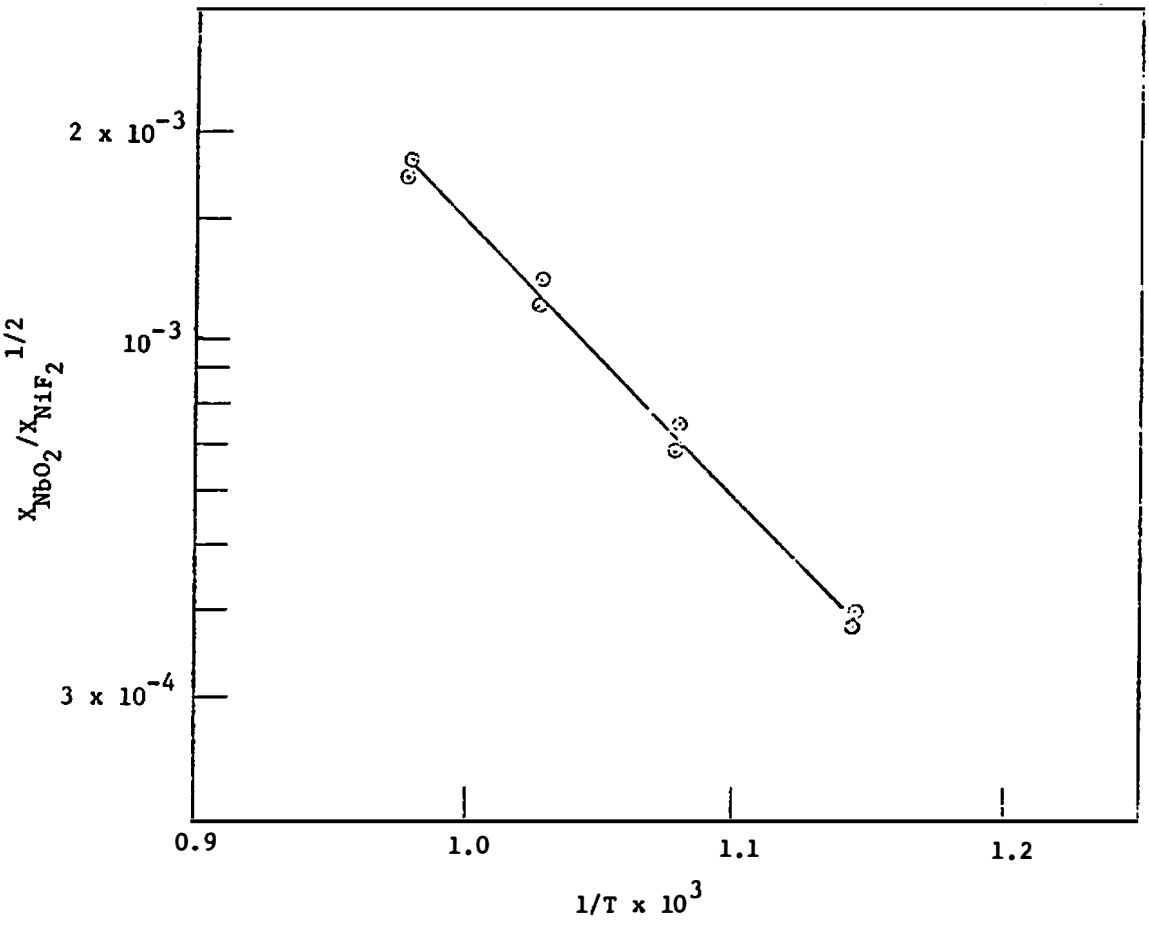


Figure 16. The temperature dependence of the equilibrium quotient for the reaction.

$$1/2\ NiNb_2O_6(c) + 1/2\ NiF_2(d) \rightleftharpoons NbO_2F(d) + NiO(c)$$

⊙ radiochemical analyses ⊗ chemical analyses

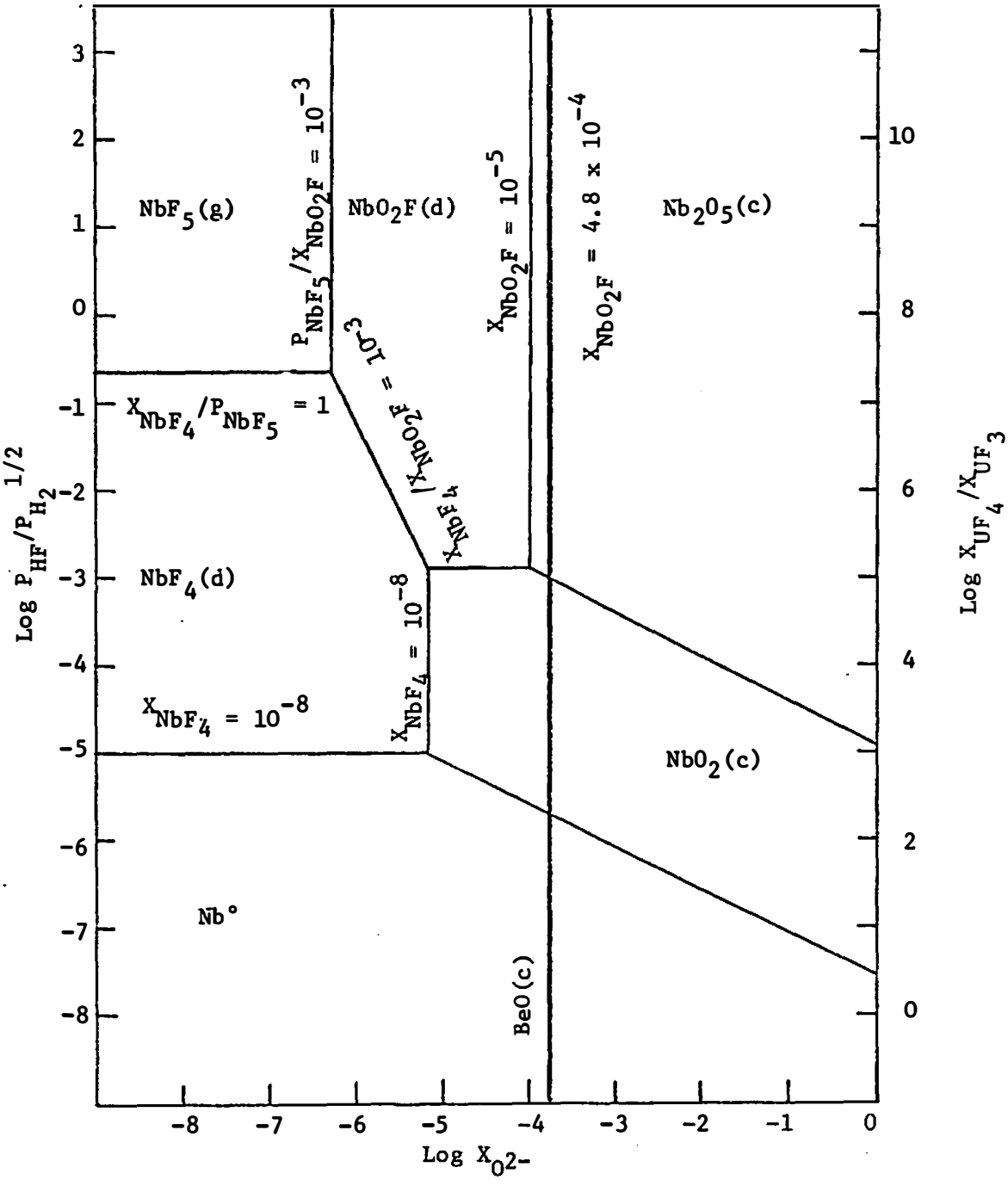


Figure 17. Pourbaix diagram for niobium in molten Li_2BeF_4 at 500°.

TABLE XII

EQUILIBRIUM REACTIONS AND DATA FOR CONSTRUCTION OF POURBAIX DIAGRAM AT 500°

Boundary	Equilibrium Reaction	Q	Equation
$Nb^{\circ}/NbO_2(c)$	$1/4\ NbO_2(c) + 1/2\ H_2(g) + 1/2\ BeF_2(d) \rightleftharpoons 1/4\ Nb^{\circ} + HF(g) + 1/2\ BeO(d)$	$\frac{P_{HF}}{P_{H_2}^{1/2}} \cdot X_{O-2}^{1/2}$	$\log \frac{P_{HF}}{P_{H_2}^{1/2}} = -7.55 - 1/2 \cdot \log X_{O-2}$
$NbO_2(c)/Nb_2O_5(c)$	$1/2\ Nb_2O_5(c) + 1/2\ H_2(g) + 1/2\ BeF_2(d) \rightleftharpoons NbO_2(c) + HF(g) + 1/2\ BeO(d)$	$\frac{P_{HF}}{P_{H_2}^{1/2}} \cdot X_{O-2}^{1/2}$	$\log \frac{P_{HF}}{P_{H_2}^{1/2}} = -4.89 - 1/2 \cdot \log X_{O-2}$
$Nb^{\circ}/NbF_4(d)$	$1/4\ NbF_4(d) + 1/2\ H_2(g) \rightleftharpoons 1/4\ Nb^{\circ} + HF(g)$	$\frac{P_{HF}}{P_{H_2}^{1/2}} \cdot \frac{1}{X_{NbF_4}^{1/4}}$	$\log \frac{P_{HF}}{P_{H_2}^{1/2}} = -3.01 + 1/4 \cdot \log X_{NbF_4} = -5.0$
$NbF_4(d)/NbF_5(g)$	$NbF_5(g) + 1/2\ H_2(g) \rightleftharpoons NbF_4(d) + HF(g)$	$\frac{P_{HF}}{P_{H_2}^{1/2}} \cdot \frac{X_{NbF_4}}{P_{NbF_5}}$	$\log \frac{P_{HF}}{P_{H_2}^{1/2}} = -0.065 - \log \frac{X_{NbF_4}}{P_{NbF_5}} = -0.065$
$NbF_5(g)/NbO_2F(d)$	$1/2\ NbO_2F(d) + BeF_2(d) \rightleftharpoons 1/2\ NbF_5(g) + BeO(d)$	$X_{O-2} \left(\frac{P_{NbF_5}}{X_{NbO_2F}} \right)^{1/2}$	$\log X_{O-2} = -7.81 - 1/2 \cdot \log \frac{P_{NbF_5}}{X_{NbO_2F}} = -6.31$
$NbO_2F(d)/Nb_2O_5(c)$	$Nb_2O_5(c) + BeF_2(d) \rightleftharpoons 2NbO_2F(d) + BeO(d)$	$X_{O-2} \cdot X_{NbO_2F}^2$	$\log X_{O-2} = -14.02 - 2 \cdot \log X_{NbO_2F} = -4.02$

TABLE XII (Continued)

Boundary	Equilibrium Reaction	Q	Equation
$NbF_4(d)/NbO_2F(d)$	$NbO_2F(d) + 1/2\ H_2(g) + 2BeF_2(d) \rightleftharpoons NbF_4(d) + HF(g) + 2BeO(d)$	$\frac{P_{HF}}{P_{H_2}^{1/2}}\ \frac{X_{NbF_4} X_{O^{-2}}^2}{X_{NbO_2F}}$	$\log \frac{P_{HF}}{P_{H_2}^{1/2}} = -16.25 - 2\cdot\log X_{O^{-2}} - \log \frac{X_{NbF_4}}{X_{NbO_2F}} = -13.25 - 2\cdot\log X_{O^{-2}}$
$NbF_4(d)/NbO_2(c)$	$1/2\ NbO_2(c) + BeF_2(d) \rightleftarrows 1/2\ NbF_4(d) + BeO(d)$	$X_{O^{-2}}\ X_{NbF_4}^{1/2}$	$\log X_{O^{-2}} = -9.19 - 1/2\cdot\log X_{NbF_4} = -5.19$
$NbO_2F(d)/NbO_2(c)$	$NbO_2F(d) + 1/2\ H_2(g) \rightleftarrows NbO_2(c) + HF(g)$	$\frac{P_{HF}}{P_{H_2}^{1/2}}\ \frac{1}{X_{NbO_2F}}$	$\log \frac{P_{HF}}{P_{H_2}^{1/2}} = 2.13 + \log X_{NbO_2F} = -2.87$
$BeO(c)/BeO(d)$	$BeO(c) \rightleftarrows Be^{+2}(d) + O^{-2}(d)$	$X_{O^{-2}}$	$\log X_{O^{-2}} = -3.79$
$UF_4(d)/UF_3(d)$	$1/2\ H_2(g) + UF_4(d) \rightleftarrows UF_3(d) + HF(g)$	$\frac{P_{HF}}{P_{H_2}^{1/2}} \cdot \frac{X_{UF_3}}{X_{UF_4}}$	$\log \frac{P_{HF}}{P_{H_2}^{1/2}} = -8.0 + \log \frac{X_{UF_4}}{X_{UF_3}}$

$X_{NbO_2F} = 10^{-5}$; $X_{NbF_4} = 10^{-8}$; $P_{NbF_5} = 10^{-8}$ atm; these are the data corresponding to the experimental conditions.

Furthermore, combining $\Delta G^f_{NbO_2F}$ with available ΔG^f for NiF_2(d) and NiO(c),[35] we can estimate the free energy of formation of $NiNb_2O_6$(c) from reaction (47c).

$$\Delta G^f_{NiNb_2O_6(c)} = - 509.0 + 112.7\ (T/10^3)\ (kcal/mole) \qquad (50)$$

Combining the experimental results of Reactions 47c (p 89) and 49 (p 92) with available ΔG^f of BeO(c), NiO(c), BeF_2(d) and NiF_2(d)[35] we can generate the whole phase diagram shown in Figure 13 (p 85), which represents the NbO_2F and NiF_2 concentrations in molten Li_2BeF_4 at 600° as a function of the oxide phases present at equilibrium. The corresponding equilibrium reactions and data for constructing this figure are summarized in Table XI (p 86)

The equilibrium point involving Nb_2O_5, BeO, and $NiNb_2O_6$ is obtained from Figure 12 (p 83). The equilibrium point involving $NiNb_2O_6$, BeO and NiO is obtained from Figure 14 (p 90), the first equilibrium point in that series of experiments. The dashed boundaries between $Nb_2O_5/NiNb_2O_6$ and $BeO/NiNb_2O_6$ were drawn with slopes +1/2 and -1/2 based on Reactions 2 and 3 in Table XI..

4. Estimation of the Heat of Formation and the Lattice Energy of $NiNb_2O_6$

Schwitzgebel et al.[199] have reported that the standard heat of reaction between a_{ij} moles of oxide i, e.g., (NiO) with b_{ij} moles of oxide j e.g. (Nb_2O_5) is given by

$$\Delta H^\circ_{R_{ij}} = - b_{ij}(K_i - A_j)^{n_j} \qquad (51)$$

where

K_i = represents the base strength of oxide i or the stability of the resulting cation.

A_j = represents the acid strength of oxide j ($-A_j$); it can also be regarded as the stability parameter of the polyoxygenated anion of the final compound.

n_j = characteristic of the anion of the compound.

The standard heat of formation of compound ij is then

$$\Delta H^\circ_{f_{ij}} = a_{ij}\Delta H^\circ_{fi} + b_{ij}\Delta H^\circ_{fj} + \Delta H^\circ_{R_{ij}} \quad . \tag{52}$$

In which oxide i (NiO) is the basic oxide, which loses b_{ij} oxide (O^{2-}) anions to acidic oxide j (Nb_2O_5).

The parameters K_i, A_j and n_j for Ni^{2+} and for five anions of the Groups IVB, VB and VIB are listed in Table XIII. The calculated standard heats of reaction of these binary oxides obtained using Equation 51 are also shown in Table XIII.

A correlation diagram of heats of reaction of binary oxides of Groups IVB, VB, and VIB is shown in Figure 18. For the formation of $NiNb_2O_6$ from NiO and Nb_2O_5:

$$Nb_2O_5(c) + NiO(c) \rightleftharpoons NiNb_2O_6(c) \tag{53}$$

the approximate heat of reaction can be obtained from Figure 18, by extrapolation which gives

$$\Delta H_R^{298} = -22.5 \pm 4.1 \text{ (kcal/mole)} \quad .$$

If we assume that the entropy of reaction and that the temperature effect on ΔH_R are small and negligible, then combining ΔG^f of Nb_2O_5 and NiO[35] with the approximate free energy of reaction 53, one may estimate

TABLE XIII

CATION AND ANION PARAMETERS AND CALCULATED ΔH_R FOR SOME BINARY OXIDES

Cation	K_i	Anion	A_j	n_j	Binary Oxide	ΔH_R^{298} (kcal/mole)
Ni^{2+}	7.46	CrO_4^{-2}	0.13	1.43	$NiCrO_4$	-17.26
		MO_4^{-2}	-2.87	1.38	$NiMO_4$	-25.08
		WO_4^{-2}	0.87	1.48	$NiWO_4$	-16.29[a]
		TiO_3^{-2}	5.13	1.40	$NiTiO_3$	-3.27[a]
		$V_2O_6^{-2}$	1.55	1.47	NiV_2O_6	-13.62

[a]Experimental values for ΔH_R^{298} ($NiTiO_3$) = -5.07 (kcal/mole), for ΔH_R^{298} ($NiWO_4$) = -12.89 (kcal/mole).

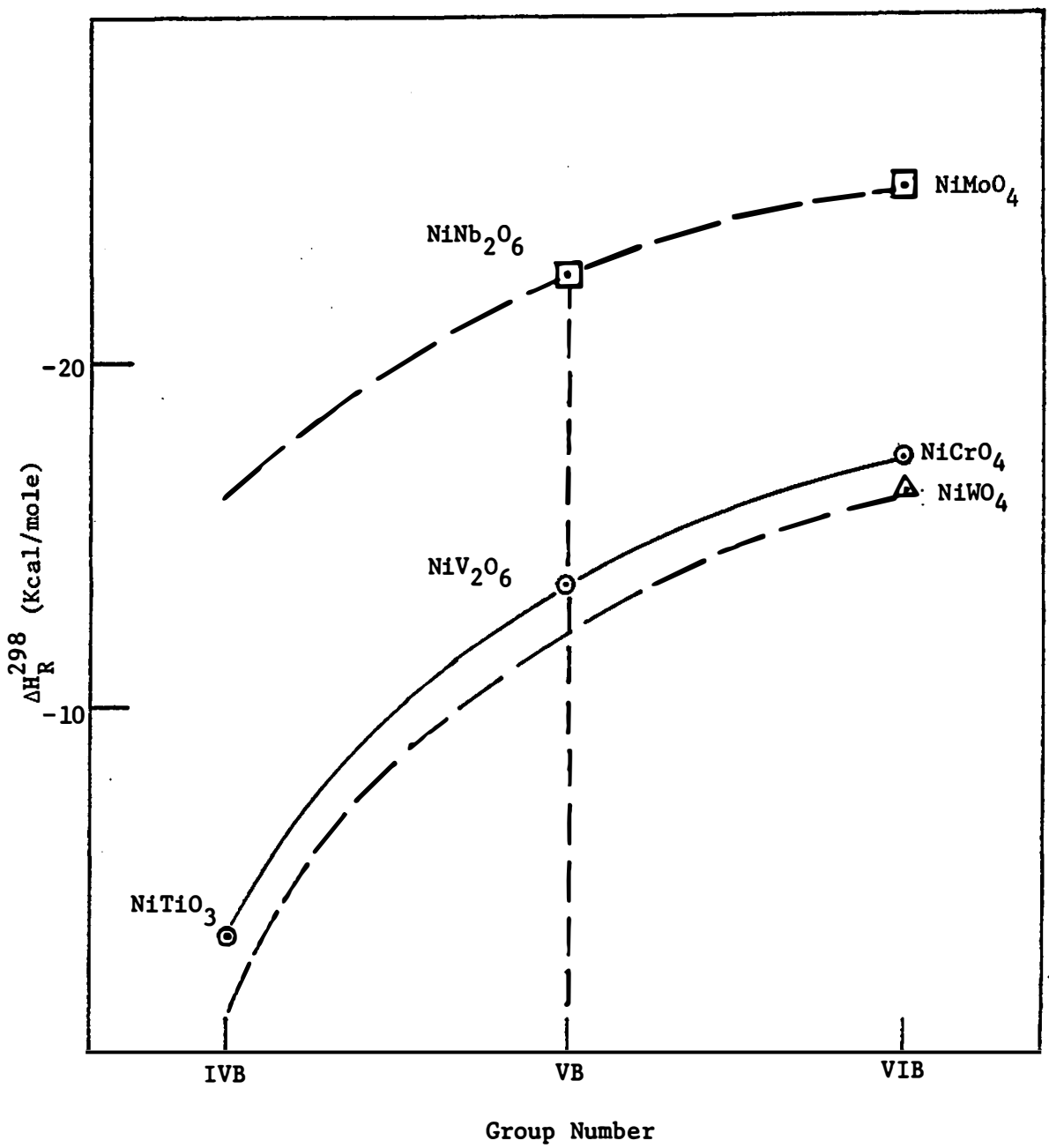


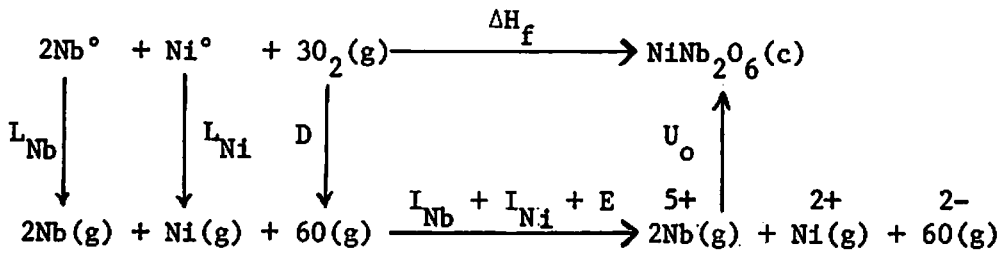
Figure 18. Correlation diagram of heats of reaction of some binary oxides with group number and period.

the free energy of formation of $NiNb_2O_6$ which gives

$$\Delta G^{f'}_{NiNb_2O_6} = -530.6 + 122.60\ (T/10^3)\ (kcal/mole). \qquad (54)$$

At 600°C, the difference between $\Delta G^{f'}_{NiNb_2O_6}$ and $\Delta G^{f}_{NiNb_2O_6}$ (estimated from the previous experiment, p 97) is approximately - 13 kcal/mole. This may be attributed to the fact that $\Delta G^{f'}$ is only an approximation.

The lattice energy of $NiNb_2O_6(c)$ can be estimated by using the Born-Haber cycle as follows:



Applying Hess's law and moving around the cycle in a clockwise direction:[200]

$$U_o = \Delta H_f - 6E - 3D - (2I_{Nb} + I_{Ni}) - (2L_{Nb} + L_{Ni}) \qquad (55)$$

where U_o is the lattice energy of $NiNb_2O_6$

E is the electron affinity of oxygen

D is the dissociation energy of O_2

I is the ionization energy

and L is the sublimation energy.

The lattice energy of $NiNb_2O_6$ was calculated to be U_o = 5019.6 kcal/mole using the following data:

ΔH_f = - 509 kcal/mole estimated from the experiments (p 97), I_{Nb} = 1140 kcal/g atom,[201] I_{Ni} = 418.5 kcal/g atom,[201] L_{Nb} = 172.4 kcal/g atom,[82] L_{Ni} = 102.6 kcal/g atom,[82] E = 168 kcal/mole,[202] and D = 118.9 kcal/mole.[202]

No comparison with lattice energies of related compounds is possible since lattice energies for such compounds have not been reported.

B. Studies of Nb(V) in Molten LiF-BeF_2-ZrF_4 (65.6-29.4-5.0 Mole %)

These studies were conducted in the experimental setup shown in Figure 6, p 62, using a platinum container (4 in dia, 10 in long). Platinum wire and pyrolytic graphite were used as indicator electrodes. The reference electrode was either a platinum quasi-reference electrode or a NiF_2(sat)/Ni electrode (employing a LaF_3 membrane). Nb(V) was added to the melt as K_2NbF_7, but IR analysis showed that Nb = O stretching vibration at 920 cm^{-1} was present in K_2NbF_7. Finally, Nb_2O_5 was also added to examine the effect of oxide on the voltammetric reduction. Except for the pyrolytic graphite working electrode, all of the materials in contact with the melt were made out of platinum. Cyclic voltammograms were obtained for concentrations of K_2NbF_7 ranging from 1.83×10^{-2} to 6.68×10^{-2} M in the temperature range 500 to 670°.

Figure 19 shows background cyclic voltammograms for the solvent mixture alone. Essentially no reducible material was present until the potential of approximately -1.45 V with respect to Ni(II)/Ni reference electrode was reached. This is probably due to the predeposition of Zr(IV).

A typical cyclic voltammogram (first cycle) at pyrolytic graphite electrode is shown in Figure 20; the shape of the voltammogram was reproducible for the duration of the experiment (longer than one month). Three reduction steps were observed. The first reduction step does not

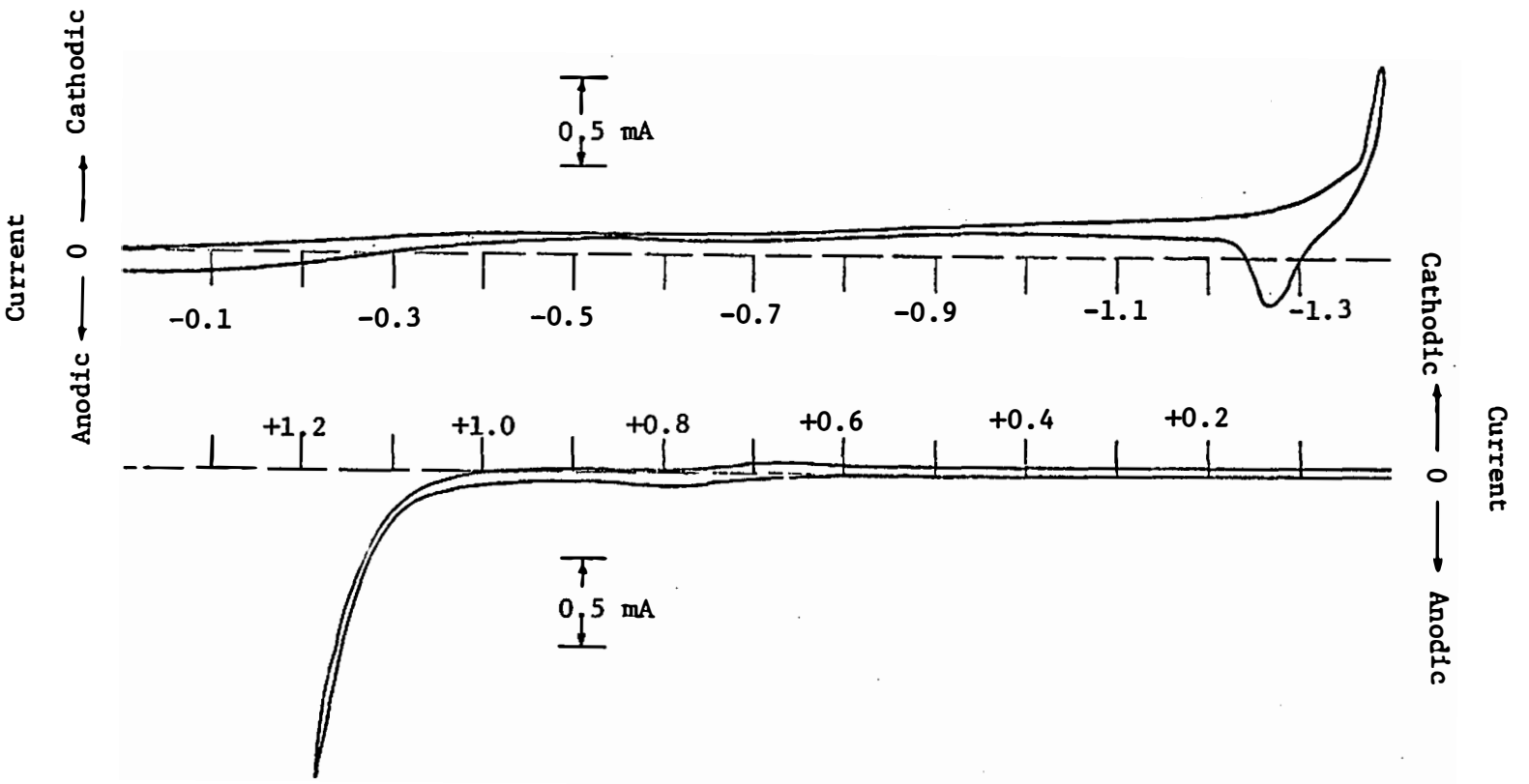


Figure 19. Cyclic voltammograms of molten LiF-BeF_2-ZrF_4 (65.6-29.4-5.0 mole %) at a platinum electrode at 500°C, electrode area: 0.08 cm^2; scan rate: 0.1 V/sec; Ni(II)/Ni reference electrode.

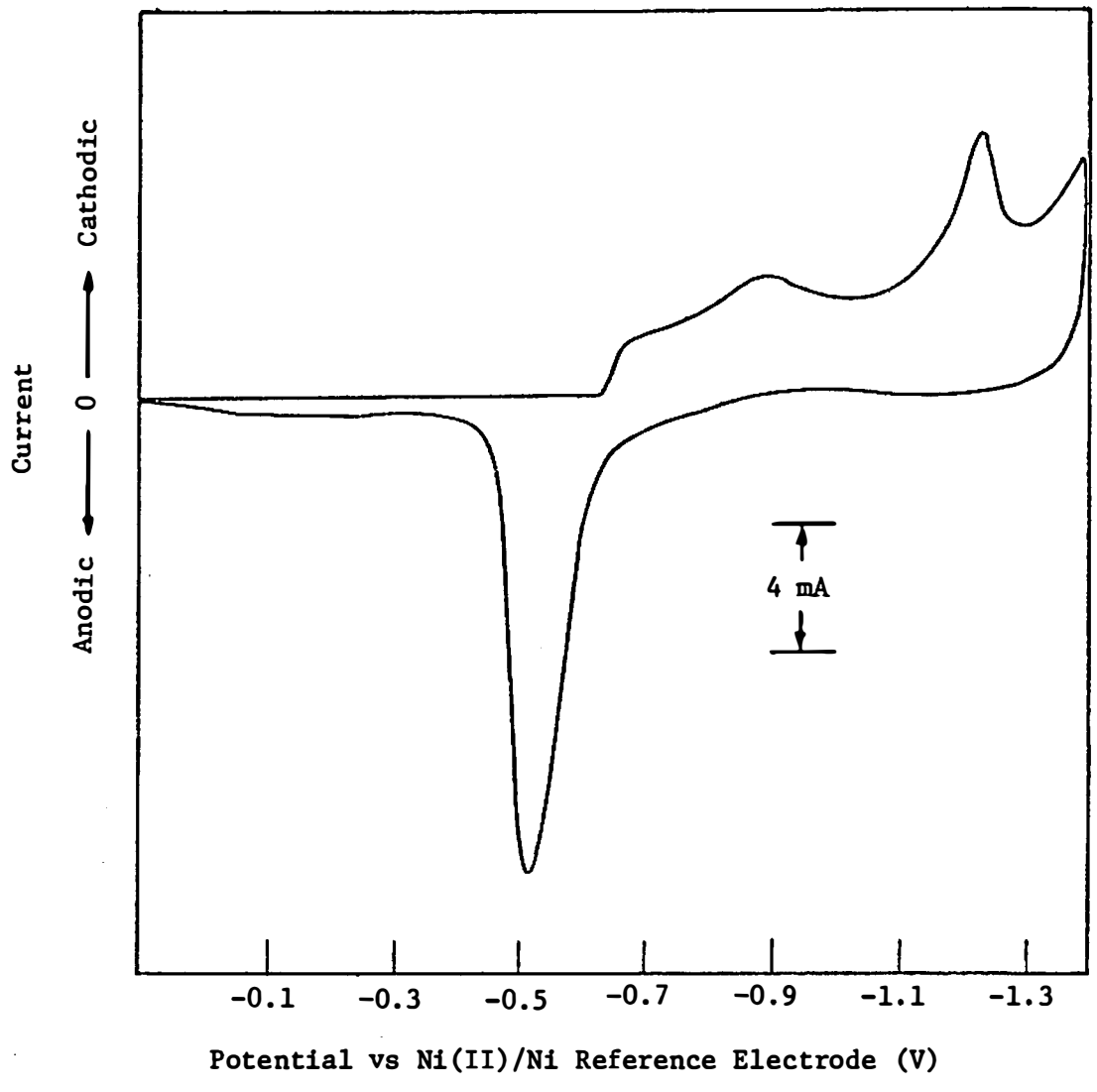


Figure 20. Cyclic voltammogram for the reduction of Nb(V) in molten $LiF-BeF_2-ZrF_4$ at pyrolytic graphite electrode at 500°C; electrode area: 0.16 cm^2; Nb(V) concentration: 5.17×10^{-2} M; scan rate: 0.1 V/sec.

exhibit a peak; the initial two reduction steps appear to be closely related (see below). At 500°, $i^c_{p(1)}$ = 1.25 mA, $i^c_{p(3)}$ = 5.0 mA (measured using the descending branch technique[159]); at Nb(V) concentration of 5.17×10^{-2} M; $i^c_{p(1)}$ = 1.7 mA, $i^c_{p(3)}$ = 6.4 mA at Nb(V) concentration of 6.68×10^{-2} M. Because of overlap between the first and second reduction step, the peak current of the second reduction step was hard to measure accurately.

Because the melt contained niobium in its pentavalent state, the first wave, therefore, is likely to be the reduction of an ion containing pentavalent niobium to some lower valence state with the transfer of less than five electrons. Comparing with Senderoff and Mellor's report[112] of the reduction of Nb(V) in the LiF-NaF-KF eutectic, the reduction potential of the first reduction step in this work was about 0.49 V more negative than the reduction potential corresponding to Nb(V)/Nb(IV) in LiF-NaF-KF. This comparison suggests that either the Nb(V) species in the two melts are different, or the reduction intermediates are different. In this study, Nb_2O_5 was also added at the end of the experiment to examine the effect of oxide addition. The same voltammogram as shown in Figure 20 was obtained. Based on the high stability of NbO_2F(d) in molten Li_2BeF_4, this suggests the possibility of the formation of NbO_2F in LiF-BeF_2-ZrF_4 melts.

In molten fluorides, Zr(IV) is known to be an oxide "getter."[35] If the melt were contaminated with a small amount of oxide ($X_O^{2-} > 3.6 \times 10^{-10}$ at 500°C[35]), ZrO_2 precipitation should occur. Under such circumstances, the free energy calculation of the following reaction indicates that

$NbF_5(d)$ will be converted to $NbO_2F(d)$.

$$ZrO_2(c) + NbF_5(d) \rightleftharpoons NbO_2F(d) + ZrF_4(d) \quad (56)$$

$$Q_{56} = X_{NbO_2F}/X_{NbF_5} \quad (56a)$$

At 500°, $\Delta G^f_{NbO_2F}$ = - 215.2 (kcal/mole) (p 92), $\Delta G^f_{ZrO_2(c)}$ = - 226.09 (kcal/mole), $\Delta G^f_{ZrF_4(d)}$ = - 402.67 (kcal/mole),[35] $\Delta G^f_{NbF_5(d)}$ = - 353.15[112] (kcal/mole), which gives

$$\Delta G_R = - 38.63 \text{ kcal/mole} \quad (56b)$$

$$Q_{56} = X_{NbO_2F}/X_{NbF_5} = 8.33 \times 10^{10} \quad (56c)$$

Equations 56b and 56c show that $NbO_2F(d)$ will be the predominant species in the melt contaminated with a small amount of oxide.

Figure 21 shows that the first reduction step is wave shaped for the first scan, but peak shaped for the second or following scans. Three reduction steps and one oxidation step (a shoulder before the oxidation peak was also observed at scan rates <0.1 V/sec) were obtained at scan rate <0.5 V/sec. One reduction step and two oxidation steps were observed at scan rates >5 V/sec (see Figure 22). Voltammetric results (first cycle) for the reduction of Nb(V) at pyrolytic graphite electrode at 500° are summarized in Table XIV. Cyclic voltammograms (first scan) at fast scan rates are shown in Figure 22. The $E_{p/2}$ values of the first step shift cathodically with increasing scan rate parameters. $i^c_{p(1)}/v^{1/2}$ is almost independent of scan rate. E vs log $(i^c_{p(1)} - i)/i$ plot for the first step (first scan) is linear with a slope 2.3RT/nF, which gives n_1 = 2.0. E vs log $(i^c_p - i)/i$ plot for the first step (second scan) is also

Figure 21. Two cycle voltammograms for the reduction of Nb^{5+} in molten $LiF-BeF_2-ZrF_4$ at pyrolytic graphite electrode at 500°. Plot of $\log(i_p - i)/i$ vs potential for the first reduction step at second cycle.

Electrode area: 0.16 cm^2; Nb(V) concentration: 6.68×10^{-2} M; scan rate: 0.1 V/sec.

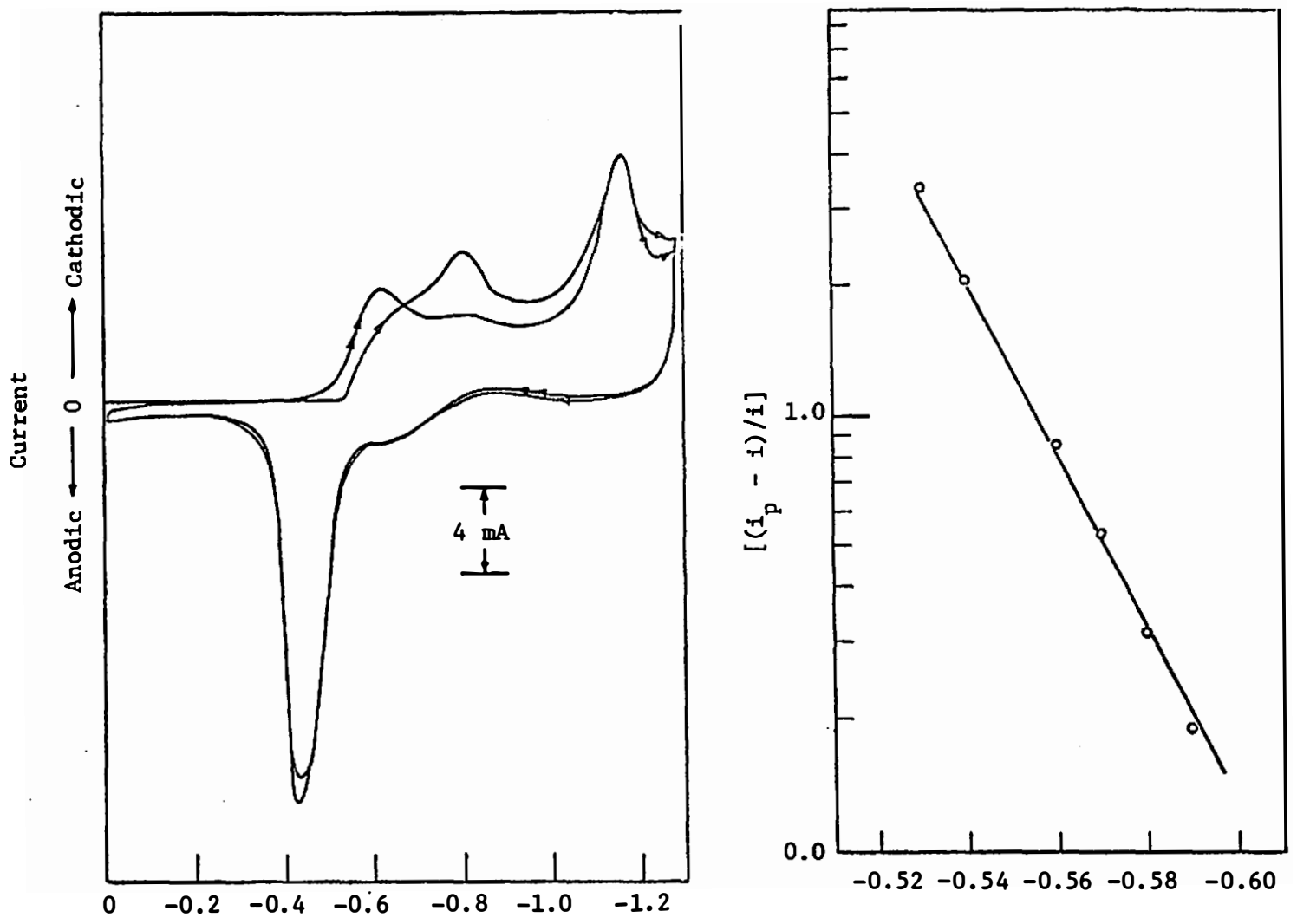

Current
Anodic
0
Cathodic
4 mA
0
-0.2
-0.4
-0.6
-0.8
-1.0
-1.2
$[(i_p - i)/i]$
1.0
0.0
-0.52
-0.54
-0.56
-0.58
-0.60
Potential vs Ni(II)/Ni Reference Electrode (V)

Figure 21

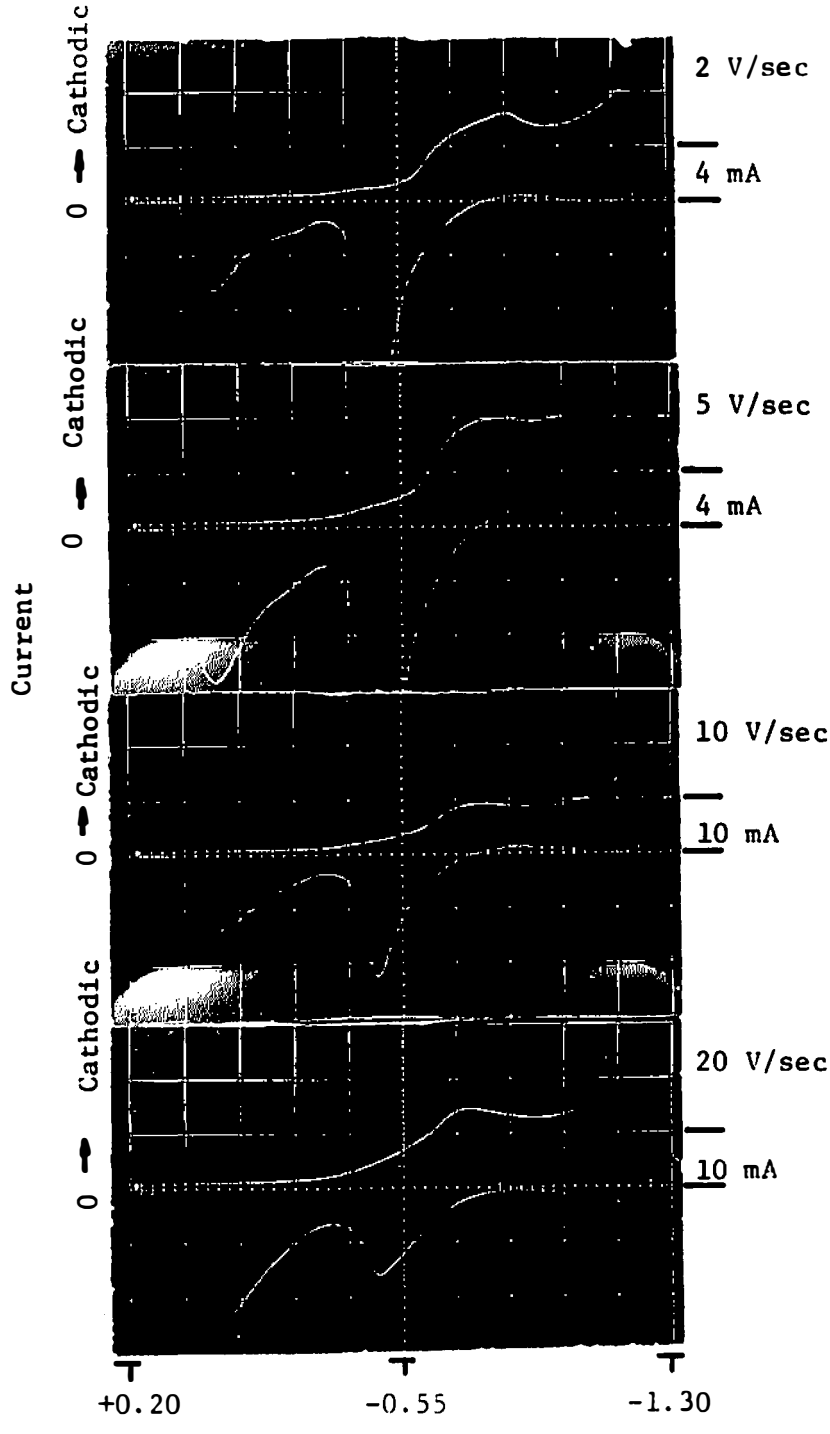


Figure 22. Cyclic voltammograms at fast scan rates for the reduction of Nb(V) at pyrolytic graphite electrode at 500°; electrode area: 0.16 cm^2; Nb(V) concentration: 5.17 x 10^{-2} M.

TABLE XIV

VOLTAMMETRIC RESULTS FOR THE REDUCTION OF Nb(V) IN MOLTEN LiF-BeF_2-ZrF_4 (65.6-29.4-5.0 MOLE %) AT PYROLYTIC GRAPHITE ELECTRODE AT 500°. Ni(II) (SATURATED)/Ni REFERENCE ELECTRODE

Scan Rate (V/Sec)	$E^c_{p(1)}$ (V)	$E^c_{p(2)}$ (V)	$E^c_{p(3)}$ (V)	$E^a_{p(1)}$ (V)	$E^a_{p(2)}$ (V)	$i^c_{p(1)}$ (mA)	$i^a_{p(1)}$ (mA)	$i^a_{p(2)}$ (mA)	$\frac{i^c_{p(1)}}{v^{1/2}}$ mA sec$^{1/2}$ V$^{-1/2}$	$\frac{i^a_{p(1)}}{v^{1/2}}$ mA sec$^{1/2}$ V$^{-1/2}$	$\frac{i^a_{p(2)}}{v^{1/2}}$ mA sec$^{1/2}$ V$^{-1/2}$
0.01	-0.58	-0.80	-1.17	-0.47	-----	0.30	7.60	-----	3.0	76.0	-----
0.02	-0.59	-0.81	-1.17	-0.47	-----	0.45	8.40	-----	3.2	59.6	-----
0.05	-0.60	-0.82	-1.16	-0.47	-0.03	0.80	8.60	0.20	3.6	38.6	0.9
0.1	-0.61	-0.82	-1.16	-0.47	-0.04	1.20	9.00	0.25	3.7	28.5	0.8
0.2	-0.62	-0.83	-1.15	-0.47	-0.05	1.70	9.30	0.55	3.8	20.8	1.2
0.5	-0.63	-0.84	-1.14	-0.46	-0.06	2.50	10.2	0.95	3.5	14.1	1.3
1	-0.63	-0.84	-----	-0.46	-0.06	----	-----	2.40	3.2	----	2.4
2	-0.64	-0.84	-----	-0.48	-0.05	----	-----	4.80	3.7	----	3.4
5	-0.81			-0.48	-0.04	----	----	8.40	---	----	3.7
10	-0.76			-0.49	-0.04	----	24.0	10.00	---	7.6	3.2
20	-0.73			-0.49	-0.03	----	16.0	18.00	----	3.6	4.0

linear (Figure 21) in the region 0.35 i_p - 0.7 i_p with a slope of 0.58 (nF/RT),[146] which gives n_1 = 2.1. The first two reduction steps are closely related and combine into one broad peak at high scan rates (Figure 22), p 109). $E^c_{p(3)}$ shifts slightly in the anodic direction with increasing scan rate; the peak disappears at high scan rates. $E^a_{p(1)}$ and $E^a_{p(2)}$ are almost independent of scan rate. $i^c_{p(3)}/v^{1/2}$ and $i^a_{p(1)}/v^{1/2}$ decrease with increasing scan rate. $i^a_{p(2)}/v^{1/2}$ increases with increasing scan rate. The differences in the voltammogram between the first and the second scan suggest that either electrode surface phenomena or kinetic complications are involved.

Similar voltammograms were observed at 600 and 670°; three reduction steps and one oxidation step were obtained at 0.1 V/sec. The first reduction step was wave shaped for the first scan but peak shaped for the second scan. Because the potentials were measured with respect to a Pt quasi-reference electrode at these two temperatures, no attempt was made to examine the temperature effect on the reduction potentials.

Based on the voltammetric results, a tentative reduction mechanism is as follows:

$$NbO_2^+ + 2e^- \rightleftharpoons NbO_2^- \quad (57)$$

$$NbO_2^- \xrightarrow{k_f} NbO^+ + O^{2-} \quad (58)$$

$$\xrightarrow{2NbO_2^+} Nb_2O_5(c) \quad (59)$$

$$NbO^+ + e^- \longrightarrow NbO(c) \quad (60)$$

$$Nb_2O_5(c) + 6e^- \longrightarrow 2NbO(c) + 3O^{2-} \quad (61)$$

The fluoride ions have been left out of the above equations for convenience.

The number of electrons in the first reduction step is suggested by the log plot (Figure 21, p 107). Based on the previous solubility measurements of Nb_2O_5 in molten Li_2BeF_4, the solubility of Nb_2O_5 in molten fluorides is expected to be very low, especially in the acidic melts. Therefore, the oxide released by the reaction (58) will very probably combine with NbO_2^+, and precipitate as $Nb_2O_5(c)$ at the electrode surface. The reduction potential of the first reduction step with a following chemical reaction will shift cathodically with increasing scan rate.[145] The reduction potential of the second reduction step (reaction (60)) with a preceding chemical reaction, will shift anodically with increasing scan rate.[145] These effects apparently result in the merging of two reduction steps to one broad peak (Figure 22, p 109). At high scan rates, the formation of Nb_2O_5 is apparently too small to be observed. Support for the postulate of the reduction of $Nb_2O_5(c)$ to NbO(c) in the last reduction step may be obtained from the following free energy calculation of reaction (62):

$$Nb_2O_5(c) + 3Ni^\circ + 3/2ZrF_4(d) \rightleftharpoons 2NbO(c) + 3NiF_2(c) + 3/2ZrO_2(c) \qquad (62)$$

At 500°, using the available ΔG^f of NbO(c),[46] $Nb_2O_5(c)$, $ZrF_4(d)$, $ZrO_2(c)$, and $NiF_2(c)$,[35] one gets E = - 1.28 V for reaction (62), which is close to the experimental value. The formation of NbO(c) as the final product can also explain the shape and the anodic potential of the oxidation peak at low scan rates. The second anodic peak observed at fast scan rates may be attributed to adsorption of NbO.[177]

The voltammetric reduction of Nb(V) at platinum electrode (electrode area 0.1 cm^2) was quite different from that at pyrolytic graphite electrode, and the results were more complicated and irreproducible. The potential was measured with respect to a Pt quasi-reference electrode.

The number of reduction steps observed was dependent on scan rate. Four reduction steps (E_p^c: -0.52, -0.83, -0.95, -1.03 V) were observed at 0.05 V/sec. Three reduction steps were observed at scan rate 0.1 - 0.5 V/sec. Two reduction steps were obtained at scan rates 0.005 - 0.02 V/sec. $E_{p(1)}^c$ shifts cathodically with increasing scan rate (-0.41 V at 0.005 V/sec to -0.72 V at 0.5 V/sec). $i_{p(1)}^c/v^{1/2}$ increases slightly with increasing scan rate. $\text{Log}(i_p - i)/i$ vs E plot for the first reduction step was linear in the range 0.35 - 0.7 i_p with a slope $0.58(\frac{nF}{RT})$, which gives $n_1 = 1.8$. $E_{p(2)}^c$ also shifts cathodically with increasing scan rate (-0.83 V at 0.05 V/sec to -0.96 V at 0.5 V/sec). This peak disappeared at low scan rates (<0.02 V/sec). The third and fourth reduction steps combined at high scan rates (>0.1 V/sec), and the fourth step disappeared at low scan rates (<0.02 V/sec). Three oxidation waves were observed (E_p^a: -0.49, -0.40, -0.07 V at 0.1 V/sec). The first oxidation wave was a shoulder, which decreased with increasing scan rate. The above voltammetric results could only be reproduced two to three days. Later, the current for the reduction peaks increased 10 to 20 times and the peak potential shifted cathodically. This is possibly due to the formation of some oxide films or precipitation of some oxides at the electrode surface. Because of the irreproducibility of the voltammetric results, no attempts have been made to explain the reduction mechanism.

C. Electrochemistry of Niobium Pentachloride in Molten $AlCl_3$-NaCl Mixtures

Molten chloroaluminates have been shown to be good solvents for electrochemical[117,118,121-123,127] and spectral studies.[117,124-129] These melts can be characterized by low liquidus temperatures, a relatively high decomposition potential and a wide range of optical transparency.[117] The Lewis acidity can be readily changed by varying the $AlCl_3$-MCl (M = alkali cation) ratio. The importance of the acid-base properties of these melts has been discussed in Chapter I. In the present work, the redox chemistry of Nb(V) in chloroaluminate melts was studied by varying melt composition, temperature and Nb(V) concentration using several electrochemical techniques.

1. Electrochemistry of Nb(V) in Molten $AlCl_3$-NaCl (63-37 Mole %)

Electrochemical studies of the reduction of Nb(V) in molten $AlCl_3$-NaCl (63-37 mole %) were carried out in a sealed glass cell (Figure 5, p 60) using platinum and tungsten working electrodes (electrode area: 0.10 cm^2), a large Pt foil quasi-reference electrode (QRE), and a large Pt foil counter electrode. Nb(V) was added as $NbCl_5$ in all cases resulting in a yellow solution. Potentials were measured with respect to Al(III) ($AlCl_3$-NaCl, 63-37 mole %)/Al reference electrode separated from the bulk melt by a Pyrex membrane.

a. Polarographic studies using current time curves. The polarogram constructed from current-time curves for the reduction of Nb(V) at a platinum electrode at 180°C is shown in Figure 23. The same results

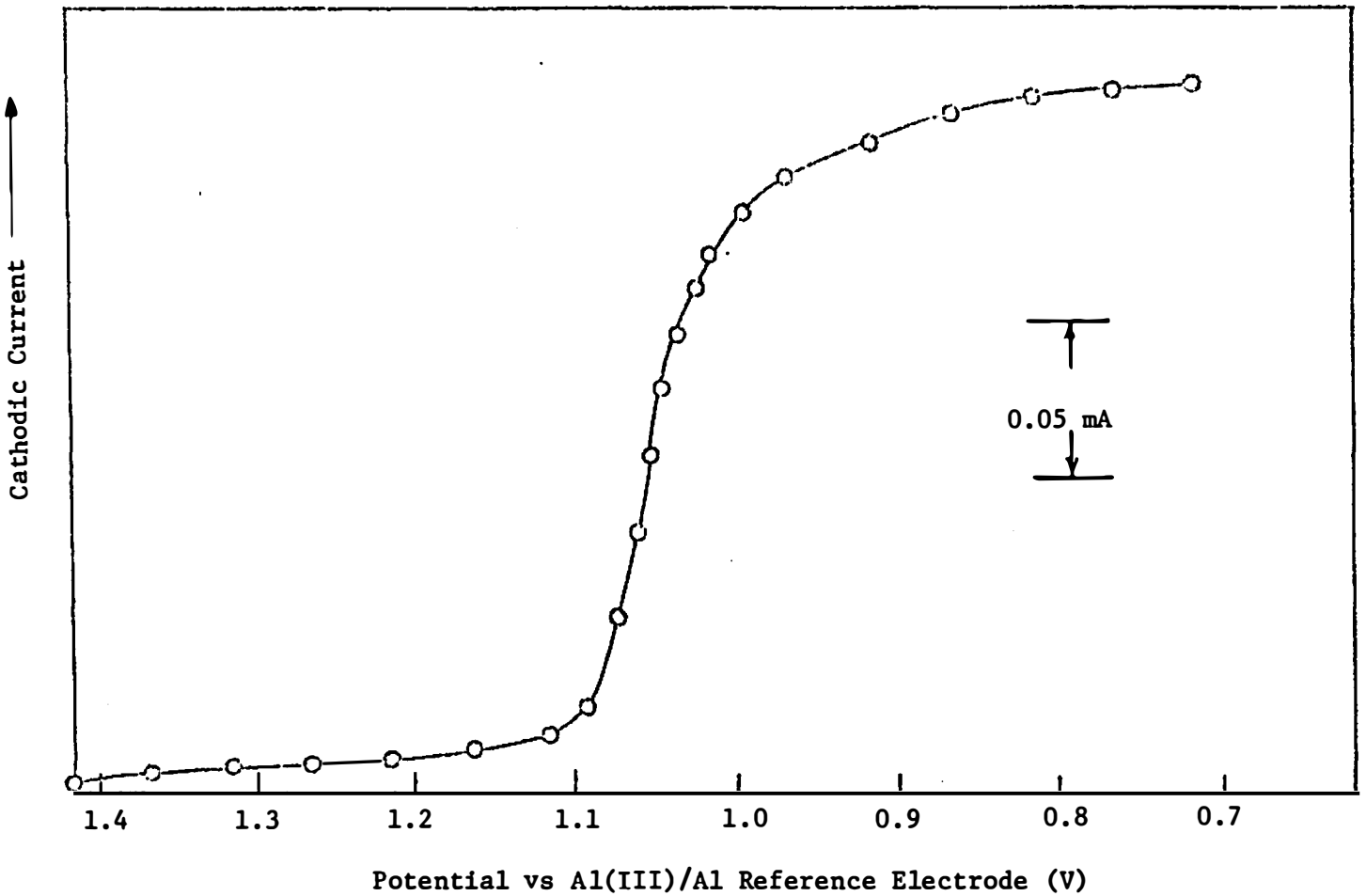


Figure 23. Polarogram constructed from current-time curves for the reduction of Nb(V) at platinum electrode at 180°C.

Melt composition: $AlCl_3$-NaCl (63-37 mole %); electrode area: 0.10 cm^2; Nb(V) concentration: 1.5×10^{-2} M; current measured at 5 sec.

were obtained with a tungsten electrode. One reduction step was observed in the potential range 1.4 - 0.7 V. The half-wave potential is 1.035 V at 180°. E vs log $(i_d - i)/i$ and E vs log $(i_d - i)$ plots were not linear. The non-linearity of the log plot is consistent with Gut's report[101] who studied the reduction of Nb(V) in $AlCl_3$-NaCl-KCl (60-26-14 mole %) at 120°. E vs log $(i_d - i)^n/i$ plots were also found to be non-linear.

Thus, polarographic studies show that one reduction step is obtained in the potential range 1.4 - 0.7 V. The presence of chemical complications is indicated by the non-linearity of the log plot.

b. Chronopotentiometric studies. Reduction of Nb(V) in $AlCl_3$-NaCl (63-37 mole %) was also studied at platinum and tungsten working electrodes chronopotentiometrically. Typical chronopotentiograms at a platinum electrode at 180° are shown in Figure 24. The same results were obtained at a tungsten electrode. The transition time was measured by Reinmuth's method.[203] The $E_{1/2}$ value measured at one-fourth of the transition time is about 1.04 V, in agreement with the polarographic results. $E_{1/2}$ value is almost independent of the current density (i_o = 2 - 23 mA/cm^2). The $\log(\tau^{1/2} - t^{1/2})/t^{1/2}$ vs E plot was not linear. The $\log(\tau^{1/2} - t^{1/2})$ vs E plot was linear with a slope 2.3RT/nF which gives n = 0.96 at i_o = 3 mA/cm^2. This results suggests that the reduction process is either an irreversible process with $\alpha n = 0.96$ (n = 2), or a reversible process followed by a rapid irreversible chemical reaction with n = 1.[167] The variation of $i_o\tau^{1/2}$ with i_o is also shown in Figure 24. As seen in Table VII (p 41), an increase of $i_o\tau^{1/2}$ with increasing current density is generally indicative of adsorption.[168,181,182] Three models (AR-SR,

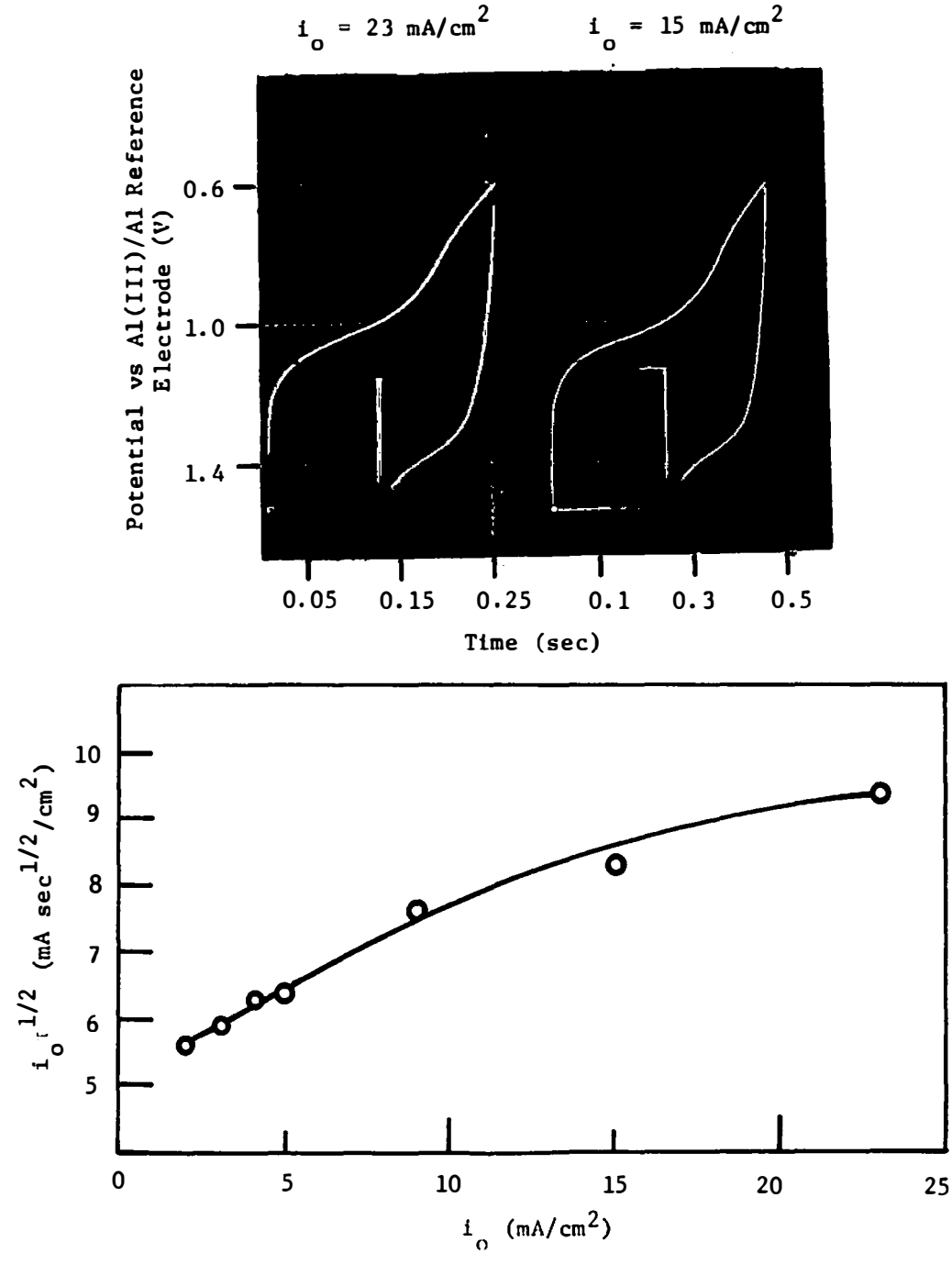


Figure 24. Chronopotentiograms for the reduction of Nb(V) at platinum electrode at 180° and the plot of $i_o\tau^{1/2}$ vs i_o.

Melt composition: $AlCl_3$-NaCl (63-37 mole %); electrode area: 0.10 cm^2; Nb(V) concentration: 1.5×10^{-2} M.

SAR, SR-AR) have been tested. The plots of $i\tau$ vs $1/i$ (AR-SR model), $i\tau$ vs $\tau^{1/2}$ (SAR model), and $(i\tau)^{1/2}$ vs $i^{-1/2}$ (SR-AR model) were all linear (see Figure 25); therefore, no choice could be made among the models.

No attempts were made to examine the reduction beyond 0.6 V. Thus, chronopotentiometric results are consistent with polarographic studies; one step reduction is observed at $E_{1/2}$ = 1.04 V.

c. Voltammetric studies. Voltammograms were run at concentrations of $NbCl_5$ ranging from 1.2×10^{-2} M to 2.4×10^{-2} M and temperatures from 180° to 260° . Figure 26 shows typical cyclic voltammograms (first scan) for $AlCl_3$-NaCl (63-37 mole percent) before and after the addition of Nb(V) at platinum and tungsten working electrodes. The residual current is quite low in the potential range of interest.

At platinum, but not tungsten electrodes, a small wave at ~1 V has been attributed to the reduction of H^+.[192] For the presence of Nb(V) two reduction waves were observed at the platinum electrode in the potential range 1.5 - 0.1 V. The same results were obtained at the tungsten electrode.

The first reduction step is well-defined. Figure 27 shows that $i^c_{p(1)}$ is proportional to Nb(V) concentration. Figure 28 shows that $i^c_{p(1)}/v^{1/2}$ decreases slightly with increasing scan rate (0.005 V/sec to 5 V/sec). $E^c_{p(1)}$ shifts cathodically from 1.045 V at 0.005 V/sec to 0.89 V at 5 V/sec. $E^a_{p(1)}$ shifts slightly anodically with increasing scan rate (from 1.310 V at 0.005 V/sec to 1.384 V at 5 V/sec). Compared to $i^c_{p(1)}$, $i^a_{p(1)}$ is small. The peak separation $(E^c_{p(1)} - E^a_{p(1)})$ is

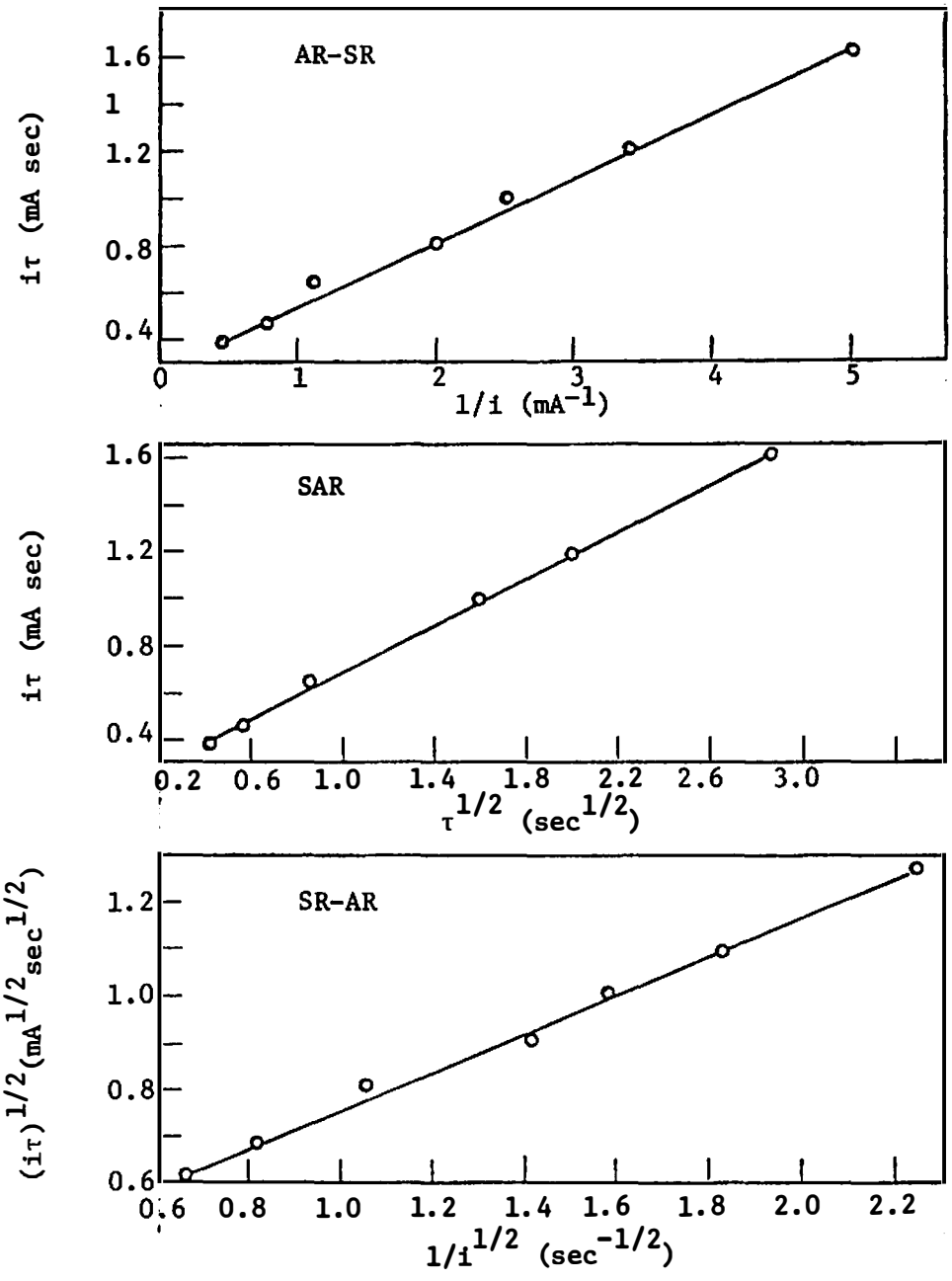


Figure 25. Tests of the AR-SR, SAR, and SR-AR models for the reduction of Nb(V) at platinum electrode at 180° Melt composition: $AlCl_3$-NaCl (63-37 mole %); electrode area: 0.10 cm^2; Nb(V) concentration: 1.50×10^{-2} M.

Figure 26. Cyclic voltammograms in the absence and presence of Nb(V)

Melt composition: $AlCl_3$-NaCl (63-37 mole %); scan rate: 0.1 V/sec; electrode area: 0.10 cm^2; (a) pure melt, platinum electrode; (b) pure melt, tungsten electrode; (c) Nb(V) concentration: 1.50×10^{-2} M, platinum electrode.

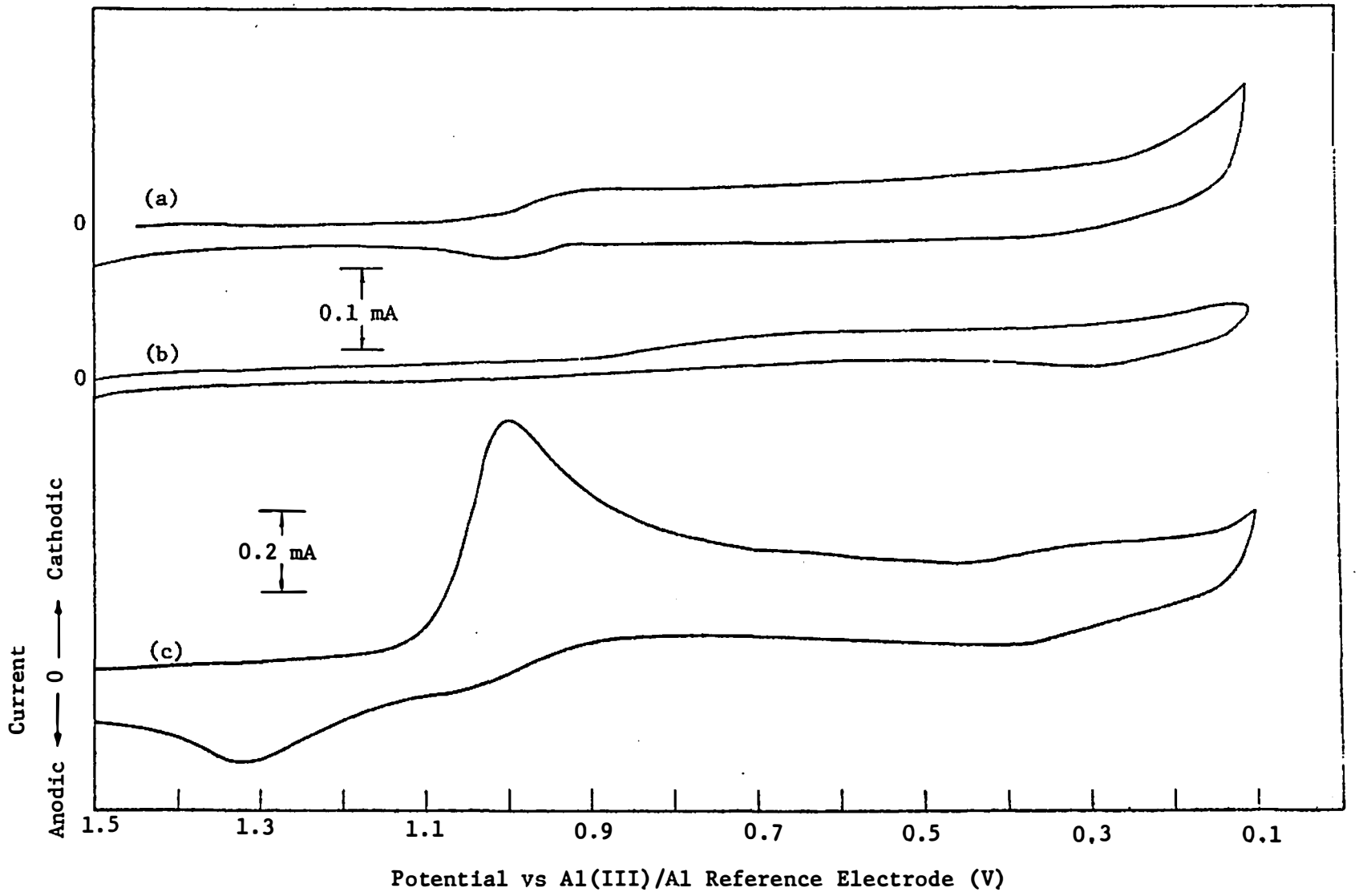

(a)
0
0.1 mA
(b)
0
0.2 mA
(c)
Current
Anodic ← 0 → Cathodic
1.5
1.3
1.1
0.9
0.7
0.5
0.3
0.1
Potential vs Al(III)/Al Reference Electrode (V)

Figure 26

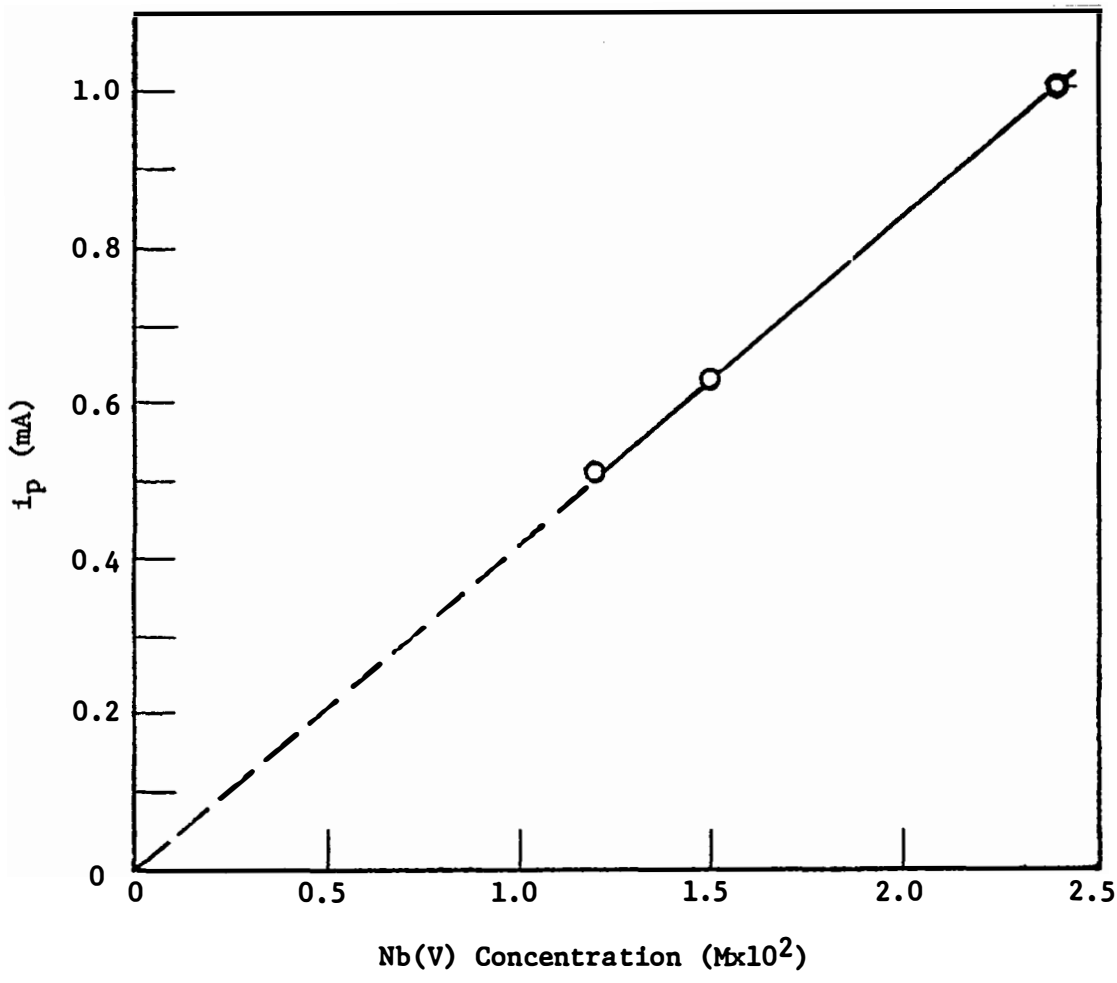


Figure 27. Variation of i_p with Nb(V) concentration at platinum electrode at 180°C.

Electrode area: 0.10 cm^2; melt composition: $AlCl_3$-NaCl (63-37 mole %); scan rate: 0.1 V/sec.

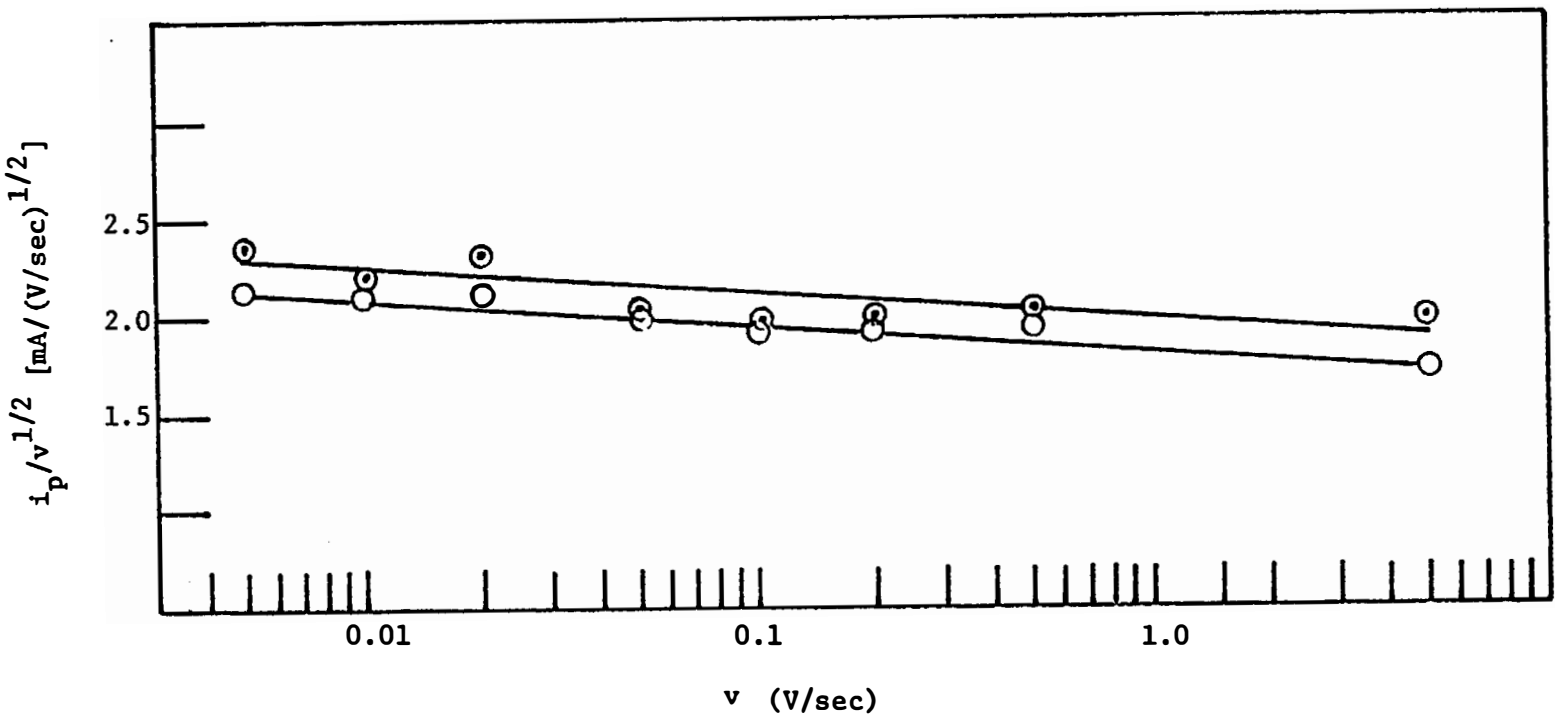


Figure 28. Plot of $i_p/v^{1/2}$ vs v for the first wave.

Melt composition: $AlCl_3$-NaCl (63-37 mole %); electrode area: 0.10 cm^2; Nb(V) concentration: 1.5×10^{-2} M; temperature: 180°C.

⊙, Pt electrode; O, tungsten electrode.

quite large, and increases with increasing scan rate (-265 mV at 0.005 V/sec to -484 mV at 5 V/sec). The peak width ($E_p - E_{p/2}$) for the first reduction step increases with increasing scan rate (-30 mV at 0.005 V/sec to -146 mV at 5 V/sec). $E^c_{p(1)}$ also shifts anodically with increasing concentration (0.98, 1.03 V at 1.43×10^{-2}, 2.44×10^{-2} M, respectively, for temperature 180° scan rate 0.1 V/sec). The voltammetric results are summarized in Table XV. These results indicate that kinetic complications are involved in the first reduction step. The second reduction step, at $E^c_p = 0.31$ V (0.1 V/sec), is broad and ill-defined. No attempt was made to analyze this reduction step in detail.

On the basis of polarographic, chronopotentiometric and voltammetric results for the first reduction step, the most likely reduction scheme appears to be as follows:

$$Nb^{5+} + e^- \rightleftharpoons Nb^{4+} \qquad (E_1) \qquad (63)$$

$$2Nb^{4+} \underset{k_b}{\overset{k_f}{\rightleftharpoons}} Nb_2^{8+} \qquad (C) \qquad (64)$$

$$Nb_2^{8+} + 2e^- \rightleftharpoons Nb_2^{6+} \qquad (E_2) \qquad (65)$$

The presence of $NbCl_6^-$,[92-94] $NbCl_6^{2-}$,[88-90] Nb_2Cl_8,[48] and $Nb_2Cl_9^{3-}$ [204,205] in solid state or solutions has been reported. From voltammetric results, the small anodic peak and the large peak separation indicate that the equilibrium constant ($K = k_b/k_f$) should be small, or k_f should be large. If k_b is very small the chemical reaction becomes totally irreversible. Rationalization for large k_f values for dimerization in acidic melts can be obtained from the following reaction:

TABLE XV

VOLTAMMETRIC RESULTS FOR THE REDUCTION OF Nb(V). MELT COMPOSITION: $AlCl_3$-NaCl (63-37 mole %)

Temperature °C	Scan Rate V/sec	Electrode	$E^c_{p(1)}$ V	$E^a_{p(1)}$ V	$E_p - E_{p/2}$ mV	$E^c_{p(2)}$ V	$E^a_{p(2)}$ V	$i^c_{p(1)}$ mA	$i^c_{p(1)}/v^{1/2}$ mA $sec^{1/2}V^{-1/2}$
180	0.005	Pt	1.045	1.310	-25			0.17	2.39
	0.01		1.040	1.330	-43			0.22	2.20
	0.02		1.030	1.340	-55			0.33	2.34
	0.05		1.030	1.340	-50			0.46	2.05
	0.10		1.015	1.335	-55	0.305	0.395	0.63	1.99
	0.20		1.015	1.355	-65			0.90	2.01
	0.50		1.000	1.355	-75	0.335	0.360	1.42	2.01
	5		0.906	1.385	(-146)	0.301		4.40	1.96
	0.005	W	1.060	1.365	-31			0.15	2.18
	0.01		1.045	1.355	-40			0.21	2.10
	0.02		1.030	1.355	-45			0.30	2.12
	0.05		1.015	1.355	-55	0.285	0.365	0.45	2.00
	0.10		1.000	1.365	-65	0.305	0.390	0.61	1.93
	0.20		1.015	1.365	-65			0.85	1.90
	0.50		1.000	1.385	-80			1.37	1.94
	5		0.890	1.384	(-147)	0.271		3.80	1.70

TABLE XV (Continued)

Temperature °C	Scan Rate V/sec	Electrode	$E^c_{p(1)}$ V	$E^a_{p(1)}$ V	$E_p - E_{p/2}$ mV	$E^c_{p(2)}$ V	$E^a_{p(2)}$ V	$i^c_{p(1)}$ mA	$i^c_{p(1)}/v^{1/2}$ mA $sec^{1/2}V^{-1/2}$
220	0.1	Pt	1.007	1.247	-50	0.317	0.367	0.86	2.71
		W	1.002	1.267	-52	0.316	0.360	0.85	2.68
260	0.1	Pt	0.988	1.148	-45			0.92	2.91
		W	0.983	1.143	-50			0.91	2.87

[a]Electrode area: 0.10 cm^2; Nb(V): 1.50×10^{-2} M; reference electrode: Al(III) ($AlCl_3$-NaCl (63-37 mole %)/Al.

$$2NbCl_6^{2-} \underset{k_b}{\overset{k_f}{\rightleftharpoons}} Nb_2Cl_9^- + 3Cl^- \qquad (64a)$$

Equation 64a indicates that the k_f value should increase with increasing acidity of the melt.

Polarographic and chronopotentiometric results have already indicated that chemical complication is involved in the first reduction step. The anodic shift of the peak potential for the first reduction step with increasing concentration suggests that a second order following chemical reaction is possibly involved.[151,153,155] The cathodic shift of $E^c_{p(1)}$ with increasing scan rate, the decreasing $i_p/v^{1/2}$ with increasing scan rate, and the increasing peak width with increasing scan rate support the proposed mechanism.[145,149,151]

At higher temperatures (220°, 260°) two shoulder anodic waves were observed. The cathodic peak width decreases with increasing temperature. These observations also support the proposed mechanism. Equation 66 shows that k_f should decrease at higher temperatures and the decreasing k_f values will cause an increase in the sharpness of the reduction peak.[149] The cathodic shift of the reduction potential with increasing temperature was observed (see Table XV), which indicates that the lower oxidation state is more stable at lower temperatures. This is because the lower the temperature the higher the acidity of the melt, which will stabilize the lower oxidation state as discussed previously (p 20). The broad peak at E^c_p = 0.31 V (at 180°C) may be attributed to the reduction of Nb_6^{+2} to Nb_3^{+8} (see below).

2. Electrochemistry of Nb(V) in Molten $AlCl_3$-NaCl (61-39 Mole %)

Voltammetric studies of the reduction of Nb(V) in $AlCl_3$-NaCl

(61-39 mole %) were carried out in a separate series of experiments. The same kind of electrochemical cell was used as before. The reference electrode was Al(III)($AlCl_3$-NaCl, 61-39 mole %)/Al, which was slightly different from other studies.

The cyclic voltammograms before addition of Nb(V) is almost identical to $AlCl_3$-NaCl (63-37 mole %). The residual current is low in the potential range of interest. Typical cyclic voltammograms after addition of Nb(V) at tungsten electrode in the potential range 1.4 - 0.8 V are shown in Figure 29. The same voltammograms were obtained at the platinum electrode.

Except for the change of anodic part of the voltammograms with scan rate and the appearance of a new sharp and symmetric reduction peak at E_p^c = 0.41 the voltammetric behavior of Nb(V) reduction at this melt composition was almost the same as the voltammetric behavior in $AlCl_3$-NaCl (63-37 mole %); E_p^c shifts cathodically with increasing scan rate (1.00 V at 0.01 V/sec to 0.89 V at 5 V/sec). $i_p/v^{1/2}$ decreases with increasing scan rate. Two anodic peaks (1.21 and 1.31 V) were observed at 0.1 V/sec. One anodic peak is observed at scan rates >0.5 V/sec (E_p^a = 1.36 V at 5 V/sec). One broad anodic peak is observed at 0.01 V/sec (E_p^a = 1.15 V). The change of anodic voltammograms with scan rate provides evidence for the presence of an ECE mechanism in the electrode reduction process. The ECE mechanism with an irreversible chemical reaction has been discussed by Nicholson and Shain.[149] In the R-R case with a small peak separation, one cathodic peak should be observed. One anodic wave corresponding to the second charge transfer should be observed at

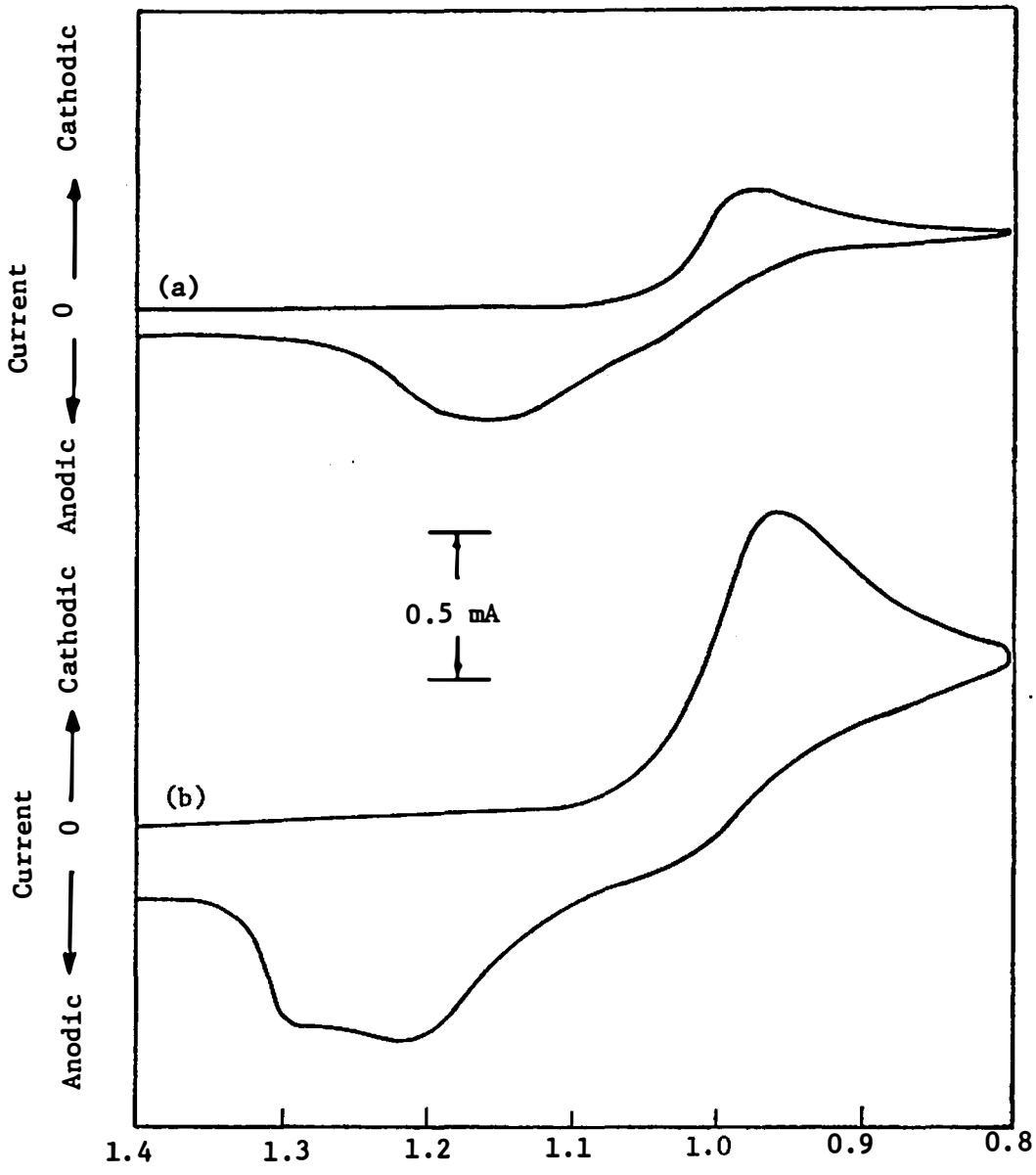


Figure 29. Cyclic voltammograms for the reduction of Nb(V) at tungsten electrode at 180°C.

Melt composition: $AlCl_3$-NaCl (61-39 mole percent); electrode area: 0.10 cm^2; Nb(V) concentration: 2.44×10^{-2} M. (a) 0.01 V/sec; (b) 0.1 V/sec.

low scan rates (k_f/a is large, where a = nFv/RT). At high scan rates (k_f/a is small), one anodic wave corresponding to the first charge transfer should be observed. At intermediate scan rates, two anodic peaks or odd voltammograms should be observed. These theoretical predictions are in agreement with the experimental results.

The nature and characteristics of the sharp and symmetric peak at E_p^c = 0.41 V will be examined in more detail in $AlCl_3$-NaCl (55-45 mole %).

3. Electrochemistry of Nb(V) in Molten $AlCl_3$-NaCl (55-45 Mole %)

Electrochemical studies of the reduction of Nb(V) in molten $AlCl_3$-NaCl (55-45 mole %) in the temperature range 140 - 260° were carried out in the same cell as that used for $AlCl_3$-NaCl (63-37 mole %). The melt composition was obtained by adding NaCl in the drybox. Potentials were measured with respect to an Al(III) ($AlCl_3$-NaCl, 63-37 mole %)/Al reference electrode.

a. Polarographic studies using current-time curves. The polarogram constructed from current-time curves for the reduction of Nb(V) in molten $AlCl_3$-NaCl (55-45 mole percent) at a platinum working electrode at 180° is shown in Figure 30. The same results were obtained at 260° and at a tungsten electrode. Two reduction steps were observed in the potential range 1.3 - 0.1 V at 180° and 260° The $E_{1/2}$ values are 0.96 and 0.26 V at 180° and 0.95 and 0.25 V at 260° E vs $\log(i_d - i)/i$ plot for the first step is partially linear (in the region 1.0 - 0.93 V) with a slope 2.3 RT/nF which gives n = 1.9. E vs $\log(i_d - i)$ plot is not

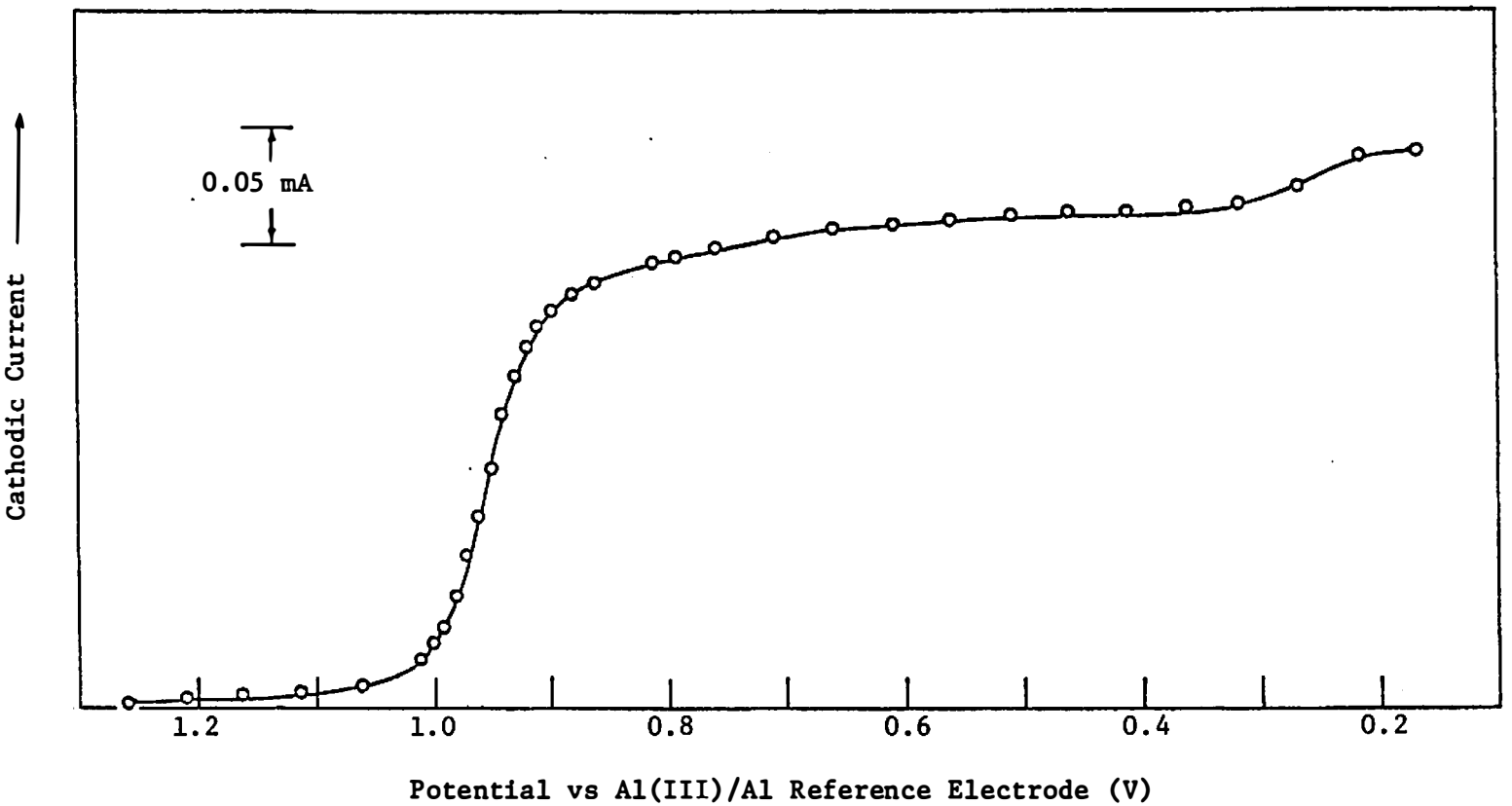


Figure 30. Polarograms constructed from current-time curves for the reduction of Nb(V) at platinum electrode at 180°C.

Melt composition: $AlCl_3$-NaCl (55-45 mole %); electrode area: 0.10 cm^2; Nb(V) concentration: 1.42×10^{-2} M; current measured at 5 sec.

linear. The non-linearity of the log plot indicates that chemical complications are involved in the reduction process.

The polarogram obtained at a platinum electrode at 140° in the potential range 1.3 - 0.6 V is shown in Figure 31. The same results were obtained at 150° and with the tungsten electrode. The first reduction step at higher temperatures (180° , 260°) is separated into two steps; the $E_{1/2}$ values corresponding to the two steps are 1.06 and 0.92 V at 140° . The diffusion current ratio for the two waves is one; this indicates that equal number of electrons is involved in the two reduction processes. The log plots are not linear. No attempt was made to analyze the reduction step beyond 0.6 V.

Thus, the polarographic results show that the reduction of Nb(V) at the platinum and tungsten electrodes in $AlCl_3$-NaCl (55-45 mole %) proceeds in two steps at higher temperatures (180 and 260°). The first reduction step is split into two steps at lower temperatures (140 and 150°). The nonlinearity of the log plots indicates that chemical complications are involved in the charge transfer process.

b. Chronopotentiometric studies. Chronopotentiograms were obtained for the reduction of Nb(V) in $AlCl_3$-NaCl (55-45 mole %) at platinum and tungsten electrodes in the temperature range 140 - 260° . Two reduction steps were obtained at higher temperatures (180 and 260°) (see Figure 32(a)). The first reduction step at higher temperature was split into two steps at 140° (see Figure 32(b)). The transition time was determined by Reinmuth's method.[203] The $E_{1/2}$ values are 0.97 V and 0.26 V at 180°, 0.94 V and 0.38 V at 260°. The first reduction step

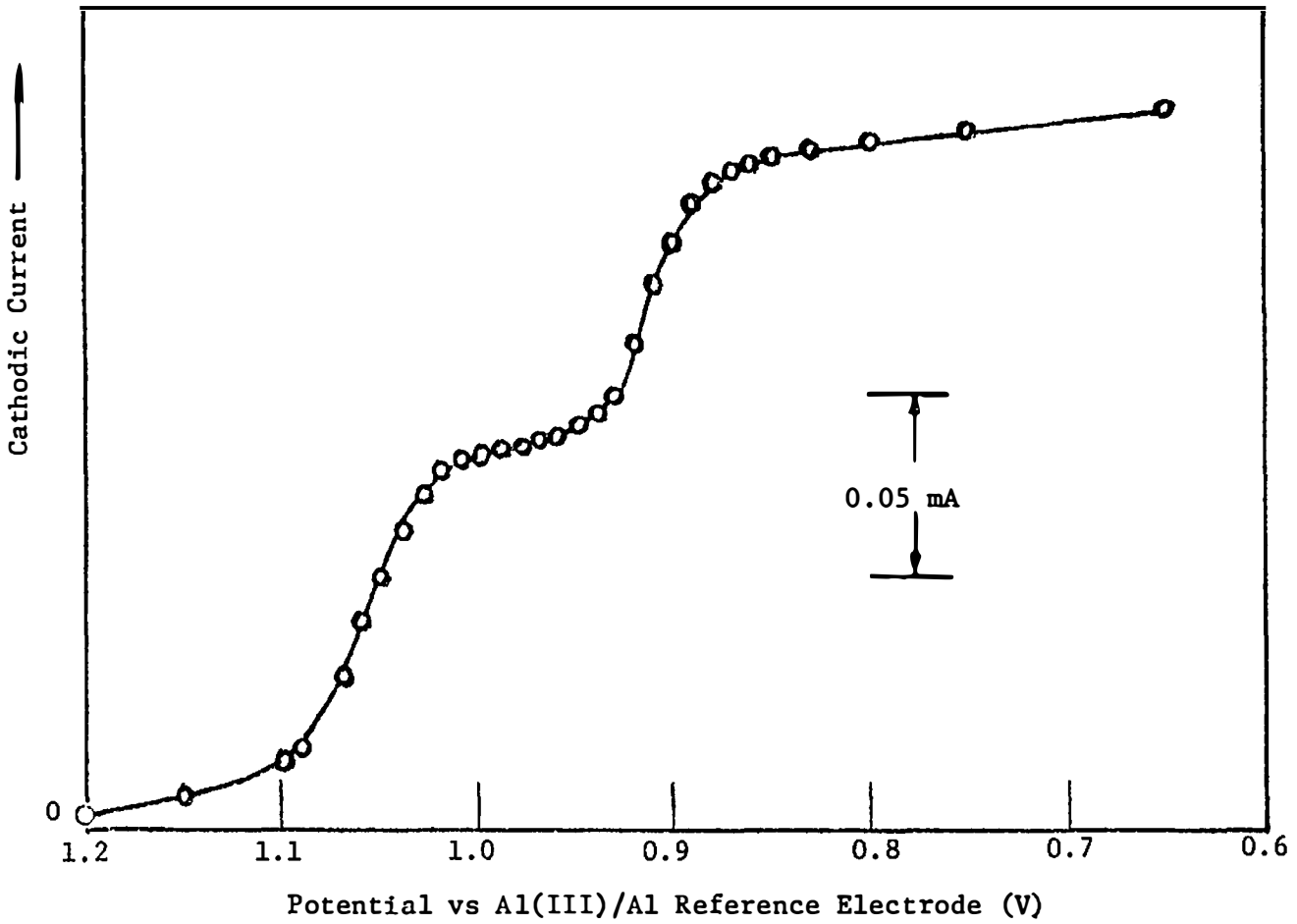


Figure 31. Polarogram constructed from current-time curves for the reduction of Nb(V) at platinum electrode at 140°C.

Melt composition: $AlCl_3$-NaCl (55-45 mole percent); electrode area: 0.10 cm^2; Nb(V) concentration: 1.42×10^{-2} M; current measured at 5 sec.

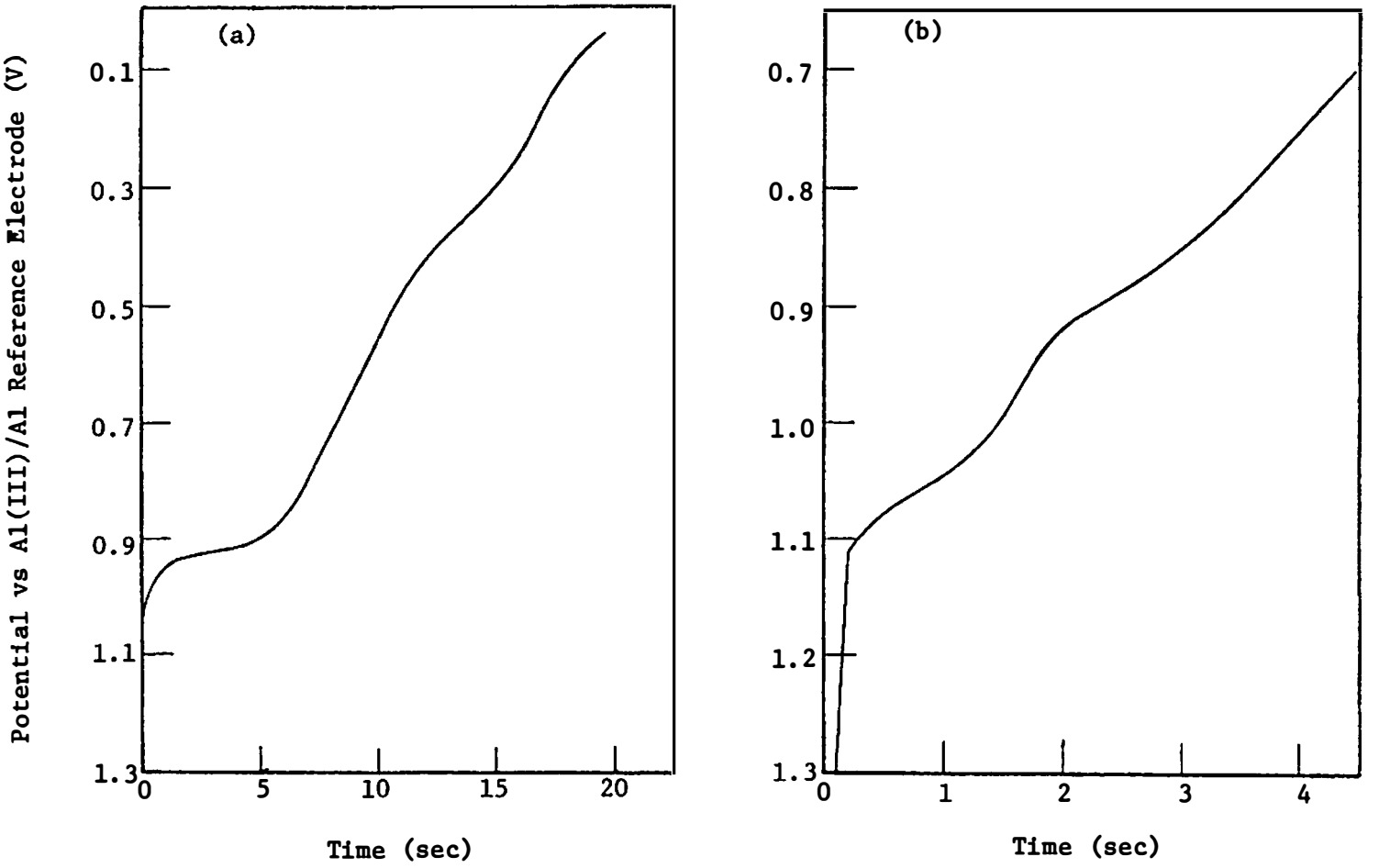


Figure 32. Chronopotentiograms for the reduction of Nb(V) at platinum electrode.

Melt composition: $AlCl_3$-NaCl (55-45 mole percent); electrode area: 0.10 cm^2; Nb(V) concentration: 1.42×10^{-2} M; (a) 260°C; i_o = 3 mA/cm^2; (b) 140°C; i_o = 0.3 mA/cm^2.

at higher temperature is split into two steps at 140-150° with $E_{1/2}$ = 1.09 V and 0.91 V. The half wave potentials at 260° are independent of current density (i_o = 3 mA/cm^2 - 50 mA/cm^2). E vs $\log(\tau^{1/2} - t^{1/2})/t^{1/2}$ and $\log(\tau^{1/2} - t^{1/2})$ plots for each reduction step are nonlinear, which suggests that a slow chemical reduction following the first charge transfer process is possibly involved.[167]

A series of cathodic chronopotentiograms of Nb(V) were obtained at different current densities. The variation of $i_o\tau^{1/2}$ with current density (i_o = 3 mA/cm^2 - 50 mA/cm^2) for the first reduction step at 260° is similar in that shown in Figure 24 (p 117). The observed increase of $i_o\tau^{1/2}$ with increasing current density is generally indicative of adsorption.[168] Three models (SR-AR, SAR, and AR-SR) were tested; all plots were found to be linear; thus no choice could be made among the models. This result is similar to that found in $AlCl_3$-NaCl (63-37 mole %).

Thus, the number of reduction steps, reduction potentials, and the effect of temperature on the chronopotentiometric reductions are in agreement with the polarographic results.

c. Voltammetric studies. Voltammetric reduction of Nb(V) in $AlCl_3$-NaCl (55-45 mole %) was quite sensitive to temperature. Two reduction steps were observed at 180° and 260° the first reduction step was split into two steps at lower temperatures. This is consistent with the polarographic and chronopotentiometric results. Figure 33(a) shows a typical voltammogram at the platinum electrode at 180° · The same results were obtained at the tungsten electrode. The anodic wave

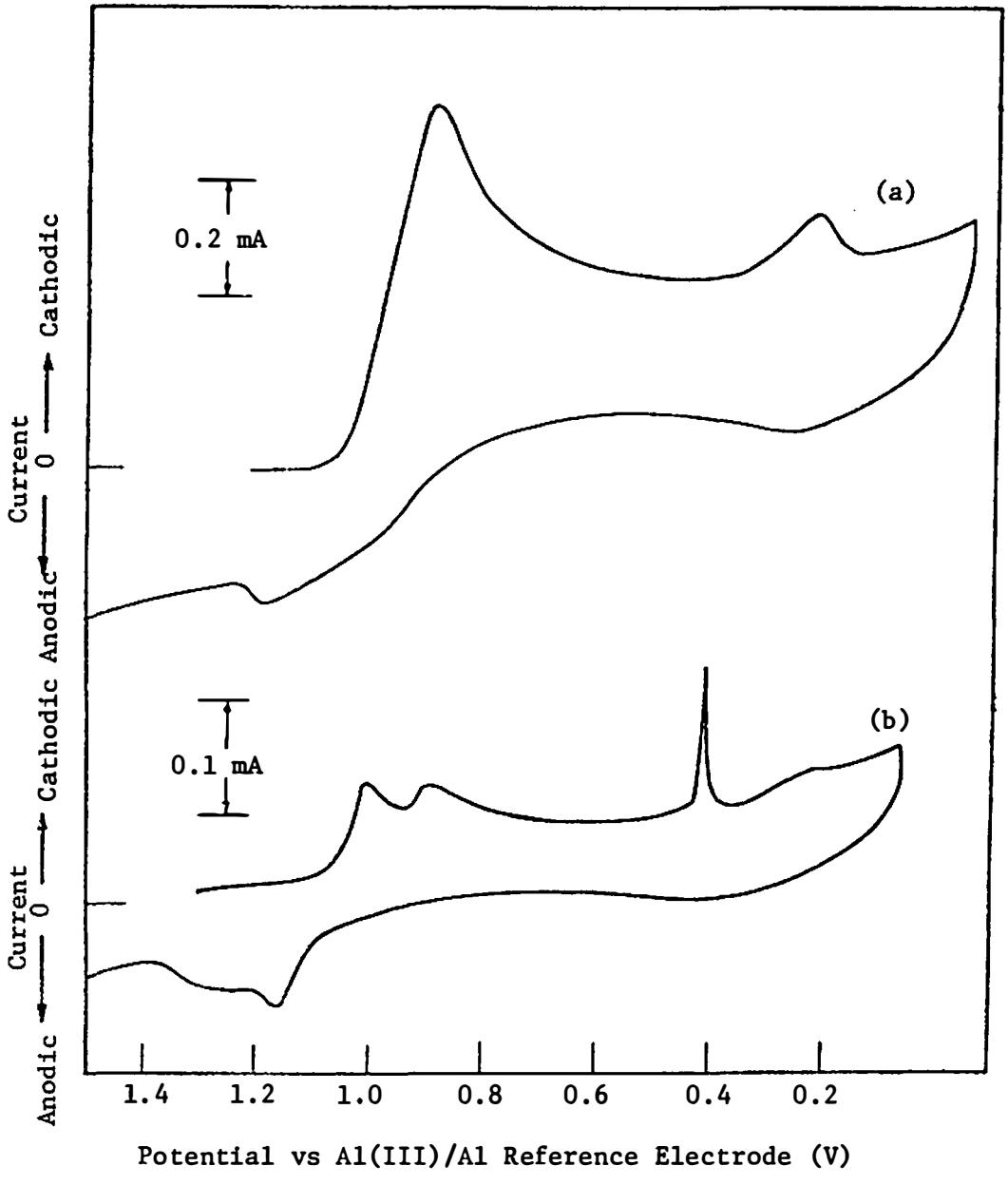


Figure 33. Cyclic voltammograms for the reduction of Nb(V) at platinum electrode.

Melt composition: $AlCl_3$-NaCl (55-45 mole %); electrode area: 0.10 cm^2; Nb(V) concentration: 1.42×10^{-2} M; (a) 180° 0.1 V/sec; (b) 140°, 0.01 V/sec.

at ~1.1 V was better defined at 260° than at 180°. Table XVI summarizes some of the voltammetric results for the reduction of Nb(V) at 180°C and 260°C. The cathodic peak potential for the first reduction step ($E^c_{p(1)}$) shifts cathodically with increasing scan rate. $i^c_{p(1)}/v^{1/2}$ decreases with increasing scan rate. Peak width increases slightly with increasing scan rate. The second reduction step is not very well-defined, and is similar to that in $AlCl_3$-NaCl (63-37 mole %). $E^c_{p(4)}$ (fourth reduction step) and $i^c_{p(4)}/v^{1/2}$ are almost independent of scan rate (0.05 V/sec - 0.2 V/sec). This peak is hard to see at high scan rates (> 0.2 V/sec).

Figure 33(b) shows a typical cyclic voltammogram at 140°. The same voltammogram was obtained at 150° and at a tungsten electrode. Table XVII summarizes some of the voltammetric results for the reduction of Nb(V) at 150° at the platinum and tungsten electrodes. The first reduction step at higher temperatures was separated into two steps when the temperature was lowered. Voltammetric results show that $E^c_{p(1)}$ at lower temperatures shifts cathodically with increasing scan rate. $i^c_{p(1)}/v^{1/2}$ is almost independent of scan rate. $E^c_{p(2)}$ also shifts cathodically with increasing scan rate. The peak current for the second reduction step can not be determined accurately. The third reduction step with the peak potential at $E^c_{p(3)}$ = 0.44 V is a sharp and symmetric peak which has similar characteristics as the one found in $AlCl_3$-NaCl (61-39 mole %). The peak potential is independent of scan rate. The peak current increases with the number of scans. This reduction step is apparently not a diffusion-controlled process. Because the peak current decreases with increasing scan rate (the peak disappears at scan rate >0.5 V/sec), it is

TABLE XVI

VOLTAMMETRIC RESULTS FOR THE REDUCTION OF Nb(V) AT PLATINUM ELECTRODE, MELT COMPOSITION: $AlCl_3$-NaCl (55-45 mole %); Nb(V) CONCENTRATION: 1.42×10^{-2} M; Al(III)/Al REFERENCE ELECTRODE

Temperature °C	Scan rate (V/sec)	$E^c_{p(1)}$ (V)	$E^a_{p(1)}$ (V)	$(E_p - E_{p/2})_{(1)}$ (mV)	$E^c_{p(4)}$ (V)	$i^c_{p(1)}/v^{1/2}$ mA $sec^{1/2}$ $V^{-1/2}$	$i_{p(4)}/v^{1/2}$ mA $sec^{1/2}$ $V^{-1/2}$
260	0.05	0.935	1.07	- 70	0.32	2.56	0.44
	0.1	0.925	1.08	- 70	0.32	2.45	0.63
	0.2	0.925	1.07	- 85	0.31	2.46	0.50
	5.0	0.850	1.11			2.23	
180	0.01	0.930	1.13	- 60		2.20	0.40
	0.1	0.910	1.19	- 85	0.26	1.70	0.37
	0.2	0.890	1.20	- 85	0.25	1.58	0.39

TABLE XVII

VOLTAMMETRIC RESULTS FOR THE REDUCTION OF Nb(V). MELT COMPOSITION: $AlCl_3$-NaCl (55-45 mole %); Nb(V) CONCENTRATION 1.42×10^{-2} M; TEMPERATURE 150°

Electrode	Scan Rate (V/sec)	$E^c_{p(1)}$ (V)	$(E_p - E_{p/2})_{(1)}$ (mV)	$E^c_{p(2)}$ (V)	$E^c_{p(3)}$ (V)	$E^c_{p(4)}$ (V)	$i^c_{p(1)}/v^{1/2}$ mA $sec^{1/2}$ $V^{-1/2}$
Pt	0.01	1.01	- 50	0.93	0.44	0.33	1.00
	0.1	1.00	- 55	0.93	0.45	0.32	1.07
	0.5	1.00	- 65	0.92		0.32	0.92
	2	0.99	- 60	0.87			1.27
	20	0.93		0.75			1.23
W	0.01	1.01	- 50	0.93	0.44	0.31	1.00
	0.1	0.99	- 55	0.90	0.44	0.30	0.92
	0.5	0.99	- 63	0.88	0.43		1.02
	2	0.98	- 60	0.87			1.27
	20	0.93		0.75			1.23

also not due to an adsorption process.[177] This peak also disappears at higher temperatures (180 and 260°). Because it appears with the appearance of the first reduction step, this peak is possibly due to the reduction of an insoluble film which comes from the reaction products of the first reduction step. The fourth reduction step at E_p^c = 0.32 V has the same reduction potential as the last step in $AlCl_3$-NaCl (63-37 mole percent). The reduction peak is not well-defined, but it is better defined than in $AlCl_3$-NaCl (63-37 mole %). If this peak is due to the reduction of the lower oxidation state of niobium species, the number of electrons must be less than one, and the reaction order is possibly higher than first order, because the peak is small and broad.

Based on the polarographic, chronopotentiometric and voltammetric results, a possible reaction mechanism is given as follows:

$$Nb^{5+} + e^- \rightleftharpoons Nb^{4+} \qquad E_1,\ n_1 = 1 \tag{63}$$

$$2Nb^{4+} \underset{k_b}{\overset{k_f}{\rightleftharpoons}} Nb_2^{8+} \qquad (K = k_b/k_f) \tag{64}$$

$$Nb_2^{8+} + 2e^- \rightleftharpoons Nb_2^{6+} \qquad E_2,\ n_2 = 1 \tag{65}$$

$$3Nb_2^{6+} + 2e^- \rightleftharpoons 2Nb_3^{8+} \qquad E_4,\ n_4 = 0.33 \tag{66}$$

The number of electrons in the first two charge transfer processes is $n_1 = n_2 = 1$, based on the equality of polarographic diffusion currents and the log plot obtained at higher temperatures. The splitting of the first reduction step at higher temperatures into two steps at lower temperatures is probably caused by the increase in k_f value (or decreasing K, $K = k_b/k_f$) at lower temperatures due to the increasing acidity of the

melt at lower temperatures. Saveant et al.[150,206] have reported that the peak potential should shift anodically with increasing k_f value (decreasing K value) for an ECE mechanism including a reversible chemical reaction. Nicholson and Shain[149] have reported that no second wave appears at low k_f, but the anodic shift of the first wave and the appearance of the second wave should be observed at large values of k_f for an ECE mechanism with irreversible chemical reaction. These theoretical diagnostic criteria are in agreement with the observed results. The third reduction step is probably due to the reduction of an insoluble film on the electrode. The assignment of the fourth reduction step is very tentative at the present time.

The proposed formation of Nb_3^{8+} is based on the observed diffusion current ratio ($i_{d(4)}/i_{d(1)}$ = 0.26 - 0.30) obtained at 180° and 260° by polarography. The formation of Nb_3^{8+} in LiCl-KCl eutectic has been reported by Suzuki.[106,107] Also, one would expect a small wave for a process involving a small number of electrons as well as for a process of a higher order.[156]

4. Electrochemistry of Nb(V) in Molten $AlCl_3$-NaCl (50-50 Mole %)

Electrochemical studies of the reduction of Nb(V) in molten $AlCl_3$-NaCl (50-50 mole %) were carried out in the same cell used for studies of the $AlCl_3$-NaCl (63-37 mole %) system. Nb(V) was added as $NbCl_5$ in all cases; Nb(V) was stable in the melt as a yellow solution. Potentials were measured with respect to an Al(III) ($AlCl_3$-NaCl, 63-37 mole %) reference electrode (with a glass membrane). This melt

composition was obtained in two ways: (1) by changing from the previous melt composition $AlCl_3$-NaCl (55-45 mole %) by adding NaCl to the cell in the drybox; and (2) by starting directly from $AlCl_3$-NaCl (50-50 %). The same electrochemical behavior was observed in these two series of experiments.

a. Polarographic studies using current-time curves. Polarographic studies using current-time curves (current measured at 0.02, 0.1 and 5 sec) were carried in the concentration range 6.8×10^{-3} - 5.19×10^{-2} M using platinum and tungsten electrodes at temperatures 160°C and 180°C. The polarogram obtained at temperatures higher than 180°C was ill-defined. Four reduction steps were observed at higher concentrations (1.34×10^{-2} - 5.19×10^{-2}) and longer times (5 sec) in the potential range 0.7 - 0.3 V (see Figure 34). The concentration dependence of the diffusion current of the four reduction steps is shown in Table XVIII. The first reduction step is well-defined; the corresponding $\log(i_d - i)/i$ vs potential plot for the first reduction step is also shown in Figure 34. The straight line drawn through the data points has the theoretical slope 2.3RT/nF, for a one electron reversible process where the product is soluble in either the solution or in the electrode (see Table VIII, p 44). This result suggests that Nb^{5+} is reduced reversibly to Nb^{4+}. The latter reduction steps are not well-defined. Two reduction steps were observed at a low concentration (6.8×10^{-3} M) and short times (0.1 and 0.02 sec) at 180° (see Figure 35). E vs log $(i_d - i)/i$ plots for the two reduction steps are also shown in Figure 35. The two straight lines, with a slope 2.3RT/nF, give $n_1 = 0.97$, $n_2 = 0.92$. These results suggest that the

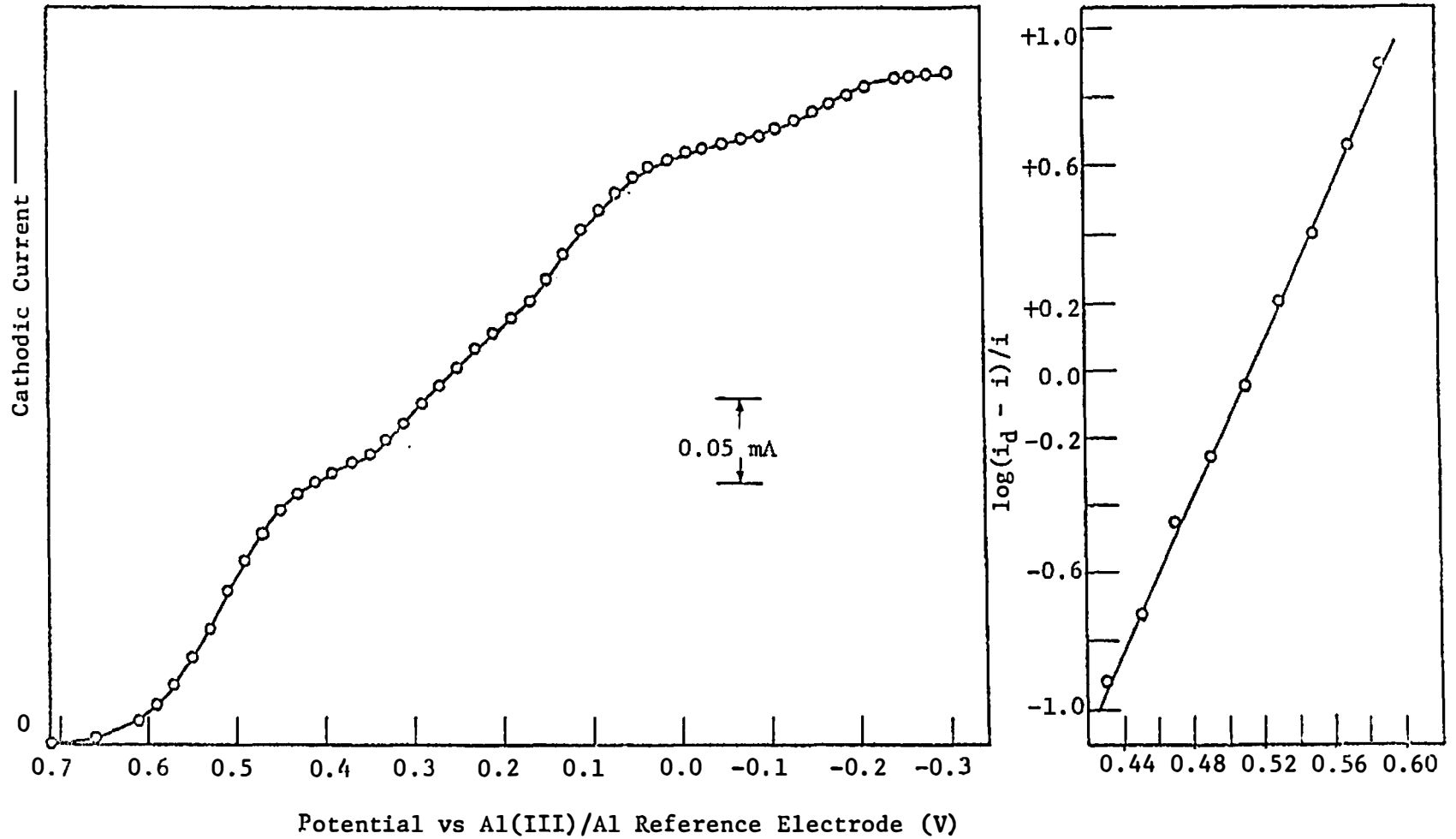


Figure 34. Polarogram constructed from current-time curves for the reduction of Nb(V) at platinum electrode at 180°C; plot of E vs log $(i_d - i)/i$ for the first wave.

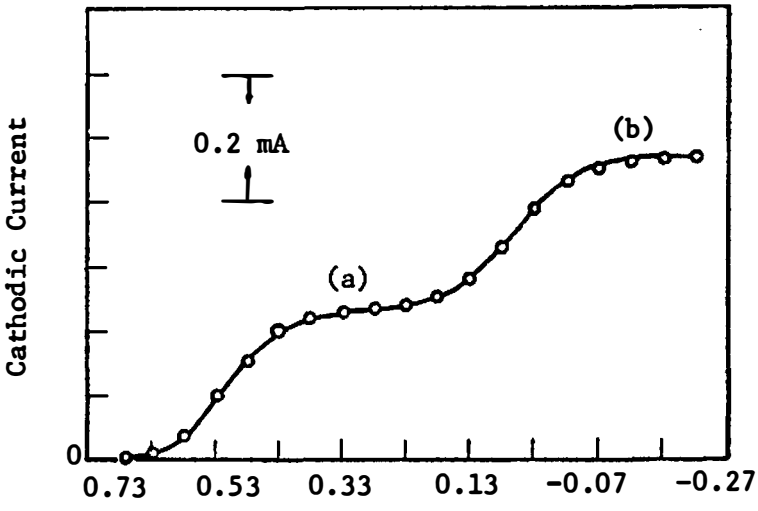
Melt composition: $AlCl_3$-NaCl (50-50 mole percent); electrode area: 0.10 cm^2; Nb(V) concentration: 2.68×10^{-2} M; current measured at 5 sec.

TABLE XVIII

CONCENTRATION DEPENDENCE OF THE DIFFUSION CURRENT

Nb(V) Concentration M	$i_{d(1)}$ μA	$i_{d(1)}/C$ μA·liter·mole^{-1}	$i_{d(2)}$ μA	$i_{d(2)}/C$ μA·liter·mole^{-1}	$i_{d(3)}$ μA	$i_{d(3)}/C$ μA·liter·mole^{-1}	$i_{d(4)}$ μA	$i_{d(4)}/C$ μA·liter·mole^{-1}
6.8×10^{-3}	37	5.45×10^{3}	21	3.00×10^{3}	20	2.94×10^{3}	7	1.02×10^{3}
2.68×10^{-2}	150	5.59×10^{2}	80	2.98×10^{3}	84	3.13×10^{3}	30	1.11×10^{3}
5.19×10^{-2}	288	5.54×10^{2}	144	2.77×10^{3}	168	3.23×10^{3}	64	1.15×10^{3}

[a]Melt composition: $AlCl_3$-NaCl (50-50 mole %); Pt electrode area: 0.10 cm^2; temperature: 180°; current measured at 5 sec.



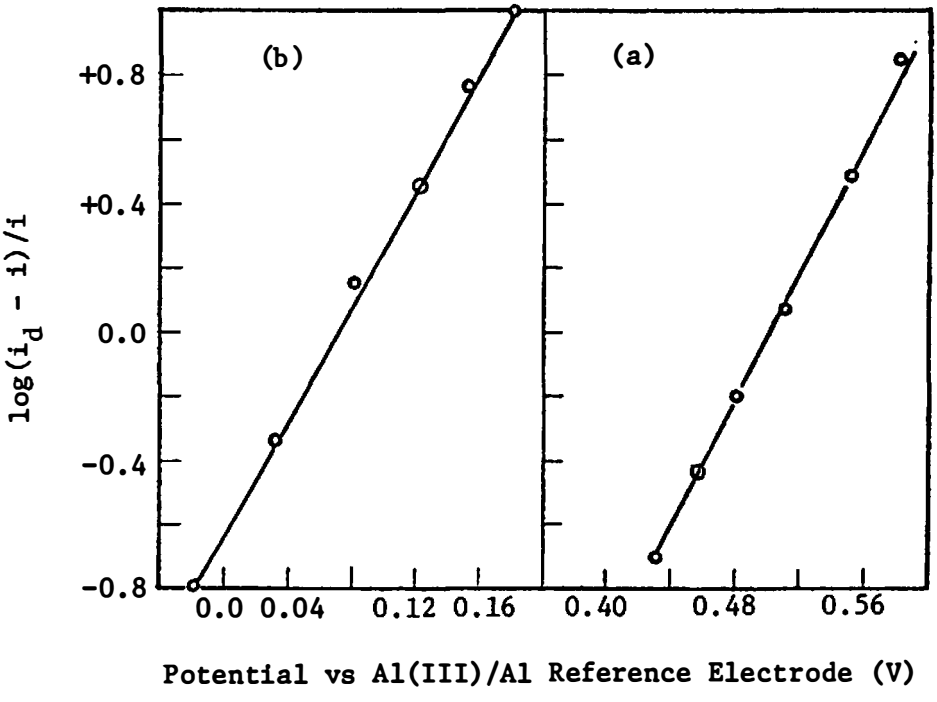


Figure 35. Polarogram constructed from current-time curves at tungsten electrode at 180°C. Plot of E vs $\log(i_d - i)/i$ for the two waves shown.

Melt composition: $AlCl_3$-NaCl (50-50 mole %); electrode area: 0.10 cm^2; Nb(V) concentration: 6.8 x 10^{-3} M; current measured at 0.1 sec.

chemical reaction following the first charge transfer may not have sufficient time to occur at the lower Nb(V) concentration and short current measuring times. Instead two simple reversible diffusion-controlled reduction waves are observed, corresponding to Nb^{5+}/Nb^{4+} and Nb^{4+}/Nb^{3+}. Table XIX summarizes the polarographic results for the reduction of Nb(V) at different experimental conditions. The potentials were measured with respect to Al(III)($AlCl_3$-NaCl, 63-37 mole %)/Al reference electrode. Based on Osteryoung's results,[118] 0.43 V should be added for converting the potential differences between $AlCl_3$-NaCl (50-50 mole %) and $AlCl_3$-NaCl (63-37 mole %) at 175°. Because the first reduction step is a one electron charge transfer process (Nb^{5+}/Nb^{4+}), the number of electrons transferred in the latter reduction steps can be estimated from the diffusion current ratios with respect to the first reduction step, which give $n_1:n_2:n_3:n_4$ = 1:0.5:0.5:(0.2 - 0.3). The diffusion coefficient of Nb(V) shown in Table XIX was obtained from the current-time curves using the Cottrell equation (Equation 27, p 43).

b. Differential pulse polarographic studies. A differential pulse polarogram for the reduction of Nb(V) at the platinum electrode at 160°C is shown in Figure 36. The same results were obtained at the tungsten electrode. Four reduction steps were observed. The peak width (ΔE_w) for the first reduction step at 160°C at pulse amplitude 5 mV is 130 mV. The peak width for a reversible electron transfer process is (90.4/n)(T/298) mV,[176] which gives n = 1 for the first reduction step at 160°C.

TABLE XIX

POLAROGRAPHIC RESULTS FOR THE REDUCTION OF Nb(V) AT PLATINUM AND TUNGSTEN ELECTRODES.
MELT COMPOSITION: $AlCl_3$-NaCl (50-50 mole %)[a]

Temperature °C	$NbCl_5$ Concentration M	Electrode	Current Measuring Time, sec	$(E_{1/2})_1$ (V)	$(E_{1/2})_2$ (V)	$(E_{1/2})_3$ (V)	$(E_{1/2})_4$ (V)	$(i_d)_1/(i_d)_2/(i_d)_3/(i_d)_4$	$D_1 \times 10^6$ cm^2/sec
160	1.34×10^{-2}	Pt	5	0.510	0.220	0.07	- 0.21	1/0.53/0.58/0.25	3.36
180	6.8×10^{-3}	W	5	0.511	0.270	0.09	- 0.16	1/0.60/0.59/0.24	3.37
	6.8×10^{-3}	W	0.1	0.511	--	0.07	--	1/0.95	4.19
	6.8×10^{-3}	W	0.02	0.501	--	0.03	--	1/0.94	4.56
	2.68×10^{-2}	Pt	5	0.512	0.260	0.10	- 0.17	1/0.53/0.56/0.21	5.26
	2.68×10^{-2}	Pt	0.1	0.512	--	0.042	--	1/0.8	4.68
	2.68×10^{-2}	Pt	0.02	0.512	--	0.032	--	1/0.9	4.95
	5.19×10^{-2}	Pt	5	0.530	0.300	0.11	- 0.13	1/0.50/0.55/0.22	5.17

[a]Electrode area: 0.10 cm^2; Al(III) ($AlCl_3$-NaCl, 63-37 mole %) /Al reference electrode.

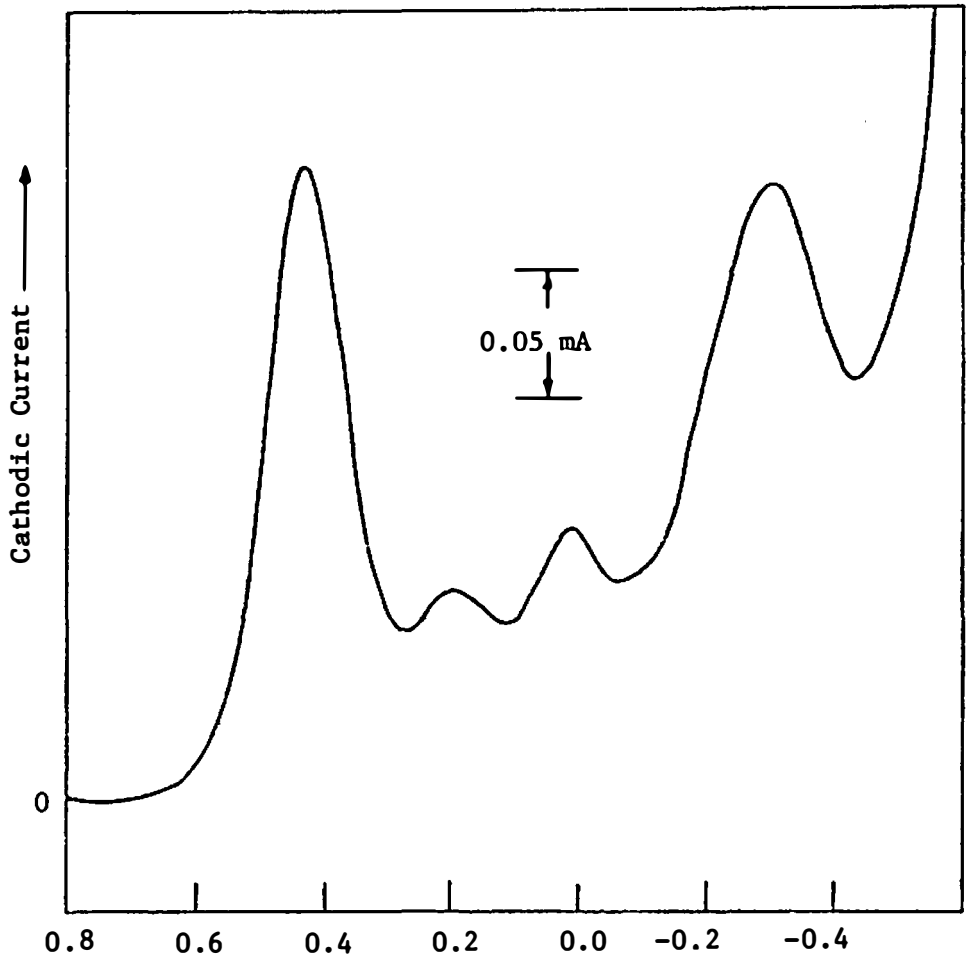


Figure 36. Differential pulse polarogram for the reduction of Nb(V) at platinum electrode at 160°

Melt composition: $AlCl_3$-NaCl (50-50 mole %); Nb(V) concentration: 6.8×10^{-3} M; scan rate: 10 mV/sec; drop time : 0.5 sec; pulse amplitude: 5 mV.

The $E_{1/2}$ values at 160°C (Nb(V) concentration: 6.8×10^{-3} M) are $(E_{1/2})_1 = 0.46$ V, $(E_{1/2})_2 = 0.20$ V, $(E_{1/2})_3 = 0.08$ V and $(E_{1/2})_4 = -0.28$ V obtained by using Equation 30, p 45. Except for the last step, the other values are in reasonable agreement with the polarographic results obtained by using current-time curves.

c. Chronopotentiometric studies. Chronopotentiograms were obtained for the reduction of Nb(V) in $AlCl_3$-NaCl (50-50 mole %) at both tungsten and platinum electrodes. The chronopotentiogram for the first reduction step is well-defined (see Figure 37). E vs $\log(\tau^{1/2} - t^{1/2})/t^{1/2}$ plot for the first reduction step is also shown in the same figure. The slope, 2.3RT/nF, of the straight line, gives n = 1.01, which indicates that the first reduction step is a reversible one electron charge transfer process (Nb^{5+}/Nb^{4+}). These results are consistent with the previous polarographic studies. Figure 38 shows the $i_o\tau^{1/2}$ vs current density (i_o) plot for the first reduction step. The values of $i_o\tau^{1/2}$ were reasonably constant over the current density studied; it appears that Sands' equation (see Equation 23, p 39) is followed.

The chronopotentiogram for the entire potential range (+0.9 ~ -0.5 V) at the tungsten electrode at 160° is shown in Figure 39. The same results were obtained at the platinum electrode. The chronopotentiograms at temperatures higher than 180° were not well-defined. Four reduction steps were observed at low current densities. The second step was not well defined. Three reduction steps were observed at high current desnities. Table XX shows chronopotentiometric results for the reduction of Nb(V)

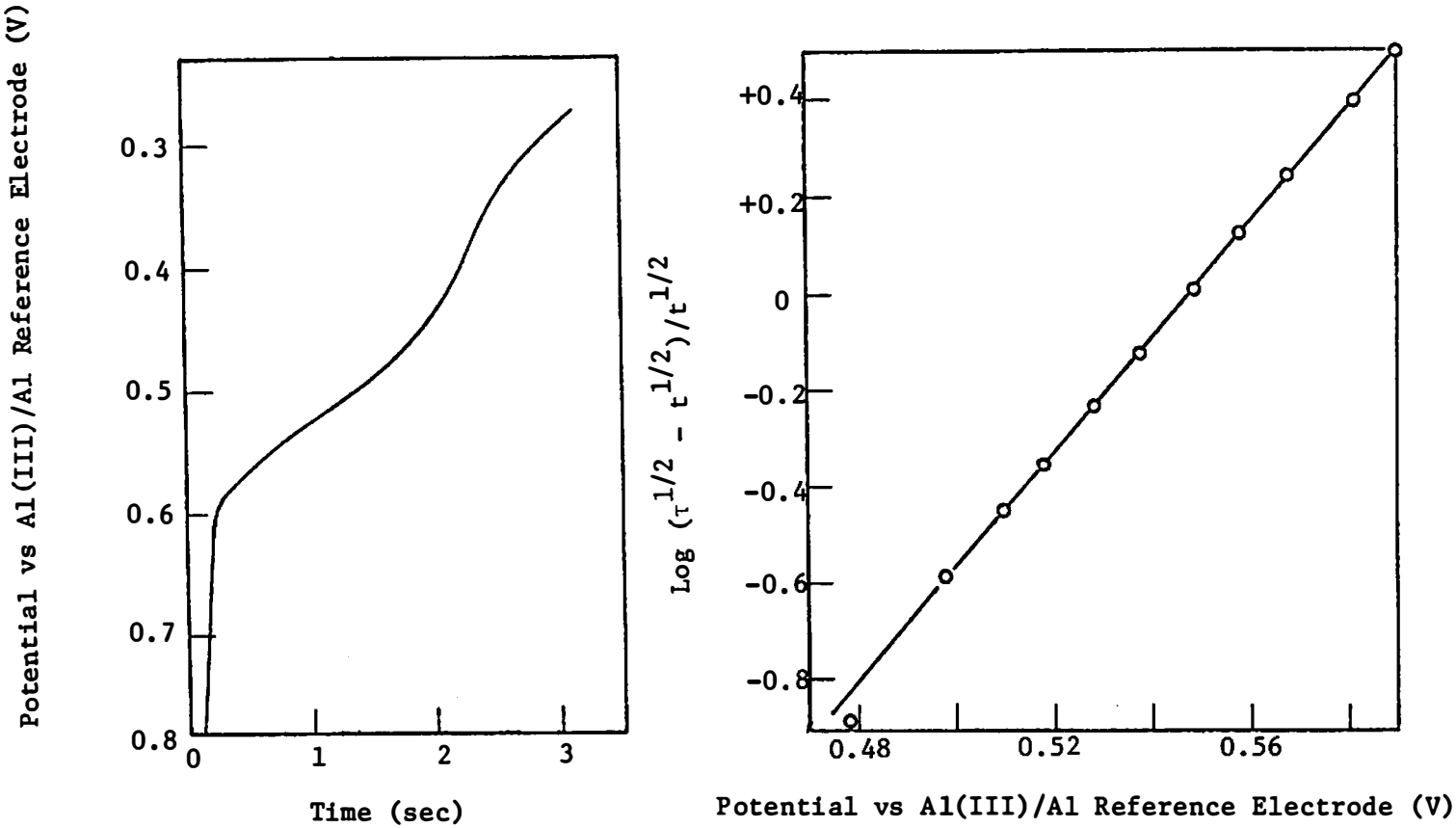


Figure 37. Chronopotentiogram for the first reduction step of Nb(V) at platinum electrode at 160°C.

Plot of E vs $\log(\tau^{1/2} - t^{1/2})/t^{1/2}$ for the chronopotentiogram shown. Melt composition $AlCl_3$-NaCl (50-50 mole percent); electrode area: 0.10 cm^2; Nb(V) concentration: 5.19×10^{-2} M; current density: 6 mA/cm^2.

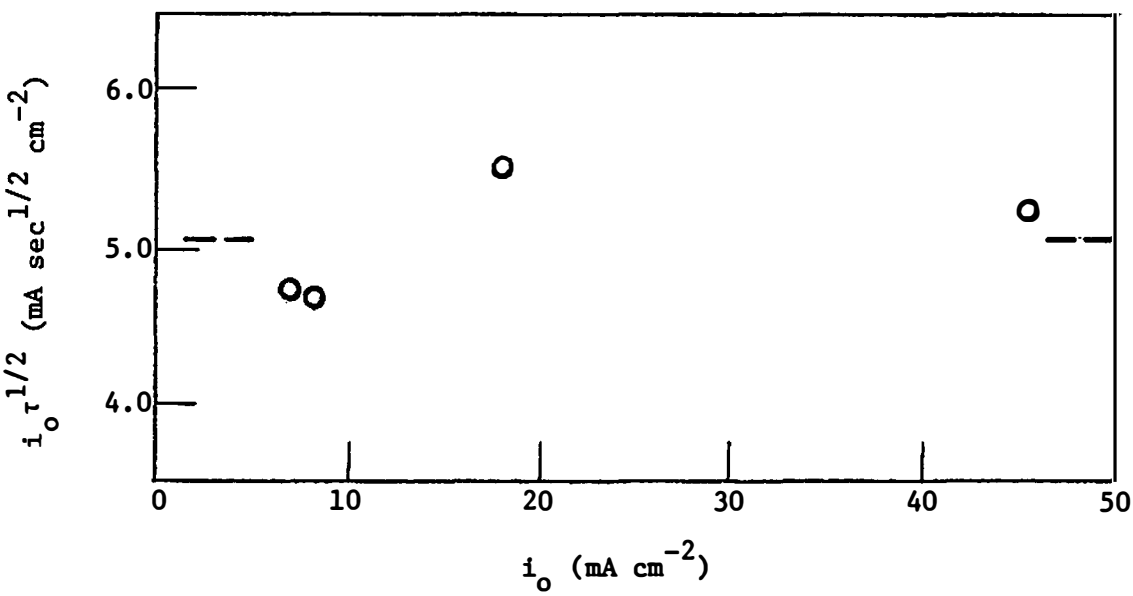


Figure 38. Plot of $i_o\tau^{1/2}$ vs i_o for the first reduction step of Nb(V) at platinum electrode at 180°C.

Melt composition: $AlCl_3$-NaCl (50-50 mole percent); electrode area: 0.10 cm^2; Nb(V) concentration: 2.68×10^{-2} M.

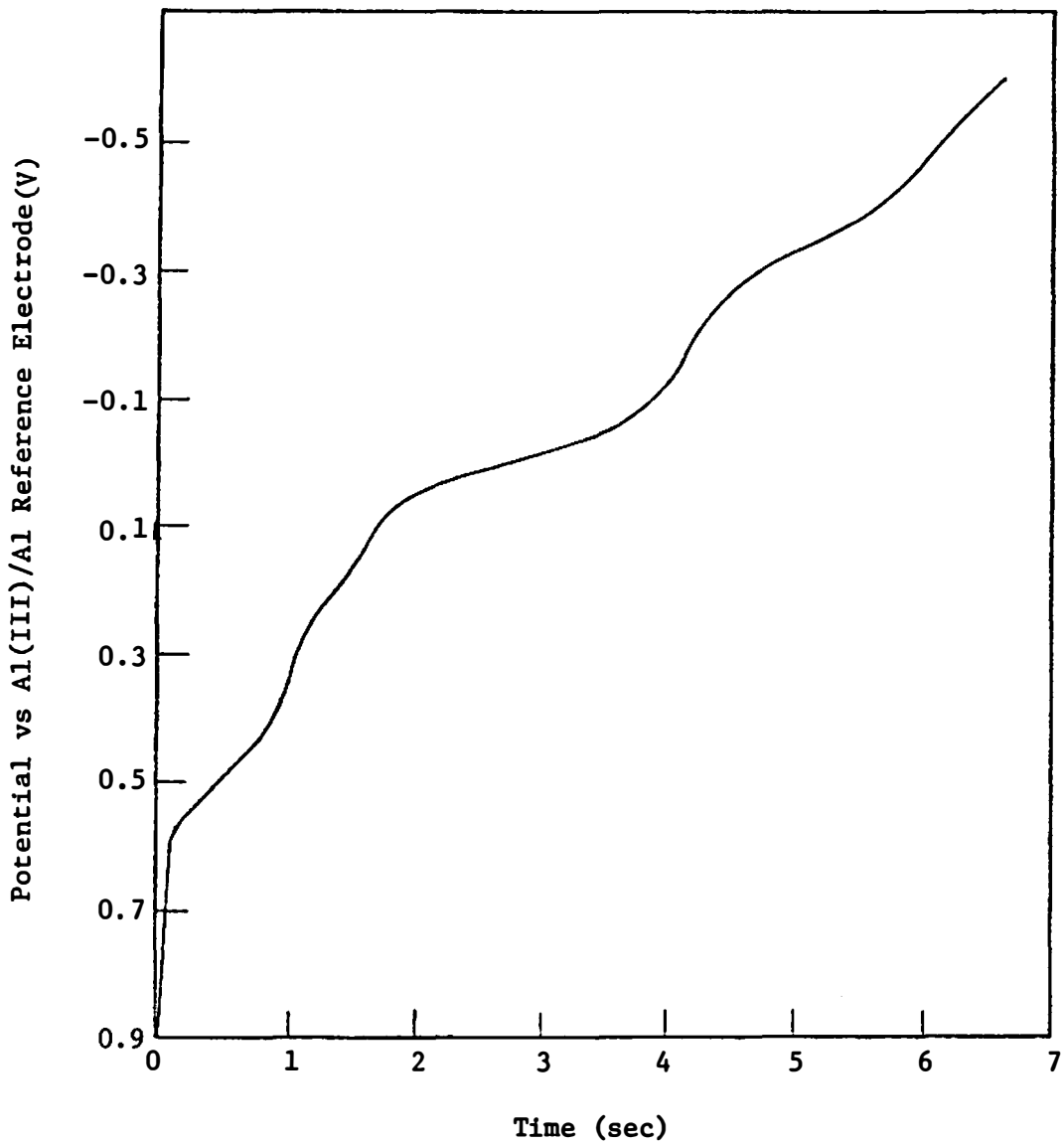


Figure 39. Chronopotentiogram for the reduction of Nb(V) at tungsten electrode at 160°C.

Melt composition: $AlCl_3$-NaCl (50-50 mole %); electrode area: 0.10 cm^2; Nb(V) concentration: 5.19×10^{-2} M; current density: 10 mA/cm^2.

TABLE XX

CHRONOPOTENTIOMETRIC RESULTS FOR THE REDUCTION OF Nb(V) AT PLATINUM AND TUNGSTEN ELECTRODES.
MELT COMPOSITION: $AlCl_3$-NaCl (50-50 mole %)[a]

$NbCl_5$ Concentration M	Electrode	i_o mA/cm^2	τ_1 sec	τ_2 sec	τ_3 sec	τ_4 sec	$(E_{1/2})_1$ (V)	$(E_{1/2})_2$ (V)	$(E_{1/2})_3$ (V)	$(E_{1/2})_4$ (V)	$i_o\tau_1^{1/2}$ mA sec$^{1/2}$ cm^{-2}	$i_o\tau_2^{1/2}$ mA sec$^{1/2}$ cm^{-2}	$i_o\tau_3^{1/2}$ mA sec$^{1/2}$ cm^{-2}	$i_o\tau_4^{1/2}$ mA sec$^{1/2}$ cm^{-2}
2.68×10^{-2}	Pt	6	0.76	0.15	1.06	0.65	0.509	0.23	0.07	- 0.22	5.23	2.32	6.18	4.84
		7	0.45	0.08	0.80	0.45	0.504	0.23	0.07	- 0.22	4.69	1.98	6.26	4.69
		8	0.34	0.06	0.61	0.34	0.494	0.22	0.07	- 0.22	4.66	1.96	6.25	4.66
		18	0.098	0.011	0.12	0.07	0.514	0.22	0.06	- 0.22	5.63	1.90	6.24	4.76
		25	0.042	0.0054	0.062	0.04	0.512	0.22	0.06	- 0.23	5.12	1.84	6.24	4.89
		30	0.027	--	--	--	0.524	--	--	--	5.02	--	--	--
		45	0.014	--	--	--	0.516	--	--	--	5.24	--	--	--
5.19×10^{-2}	Pt	10	0.83	0.32	1.30	0.95	0.535	0.28	0.10	- 0.20	9.0	5.6	11.5	9.7
		12	0.55	0.19	0.94	0.65	0.530	0.29	0.10	- 0.19	8.9	5.2	11.6	9.7
		13.6	0.41	0.11	0.77	0.46	0.530	0.29	0.10	- 0.19	8.9	4.5	11.9	9.3
5.19×10^{-2}	W	10	0.97	0.31	1.65	1.10	0.535	0.28	0.10	- 0.19	9.8	5.6	1.29	1.05
		13	0.58	0.14	0.97	0.70	0.530	0.29	0.09	- 0.18	9.9	4.9	1.08	1.08
		15	0.42	0.10	0.75	0.49	0.535	0.27	0.10	- 0.19	9.8	4.7	1.29	1.05

[a]Electrode area: 0.10 cm^2; Al(III) ($AlCl_3$-NaCl 63-37 mole %)/Al; temperature: 180°.

at 180° for two Nb(V) concentrations. The transition time was measured by Reinmuth's method.[203] The second reduction step could not be seen at high current densities (>25 mA/cm^2), and the transition times for the last two steps were very hard to measure accurately at high current densities. $i_o\tau_1^{1/2}$, $i_o\tau_2^{1/2}$ and $i_o\tau_4^{1/2}$ are independent of current density. $i_o\tau_2^{1/2}$ decreases with increasing current density, which indicates that a preceding chemical reaction is involved before the second reduction step.[168] The relationship for $i_o\tau^{1/2}$ for the case of a preceding chemical reduction is given by[132,166]

$$i_o\tau^{1/2} = \frac{nF(\pi D)^{1/2}C}{2} - \frac{\pi^{1/2}}{2K(k_f + k_b)^{1/2}} i_o \qquad (67)$$

where $K = k_f/k_b$. By dividing both sides by i_o

$$\tau^{1/2} = \frac{nF(\pi D)^{1/2}C}{2i_o} - \frac{\pi^{1/2}}{2K(k_f + k_b)^{1/2}} \qquad (67a)$$

or

$$\tau_K^{1/2} = \tau_D^{1/2} - \frac{\pi^{1/2}}{2K(k_f + k_b)^{1/2}} \qquad (67b)$$

This indicates that the kinetic transition time (τ_K) is less than that for pure diffusion controlled transition time (τ_D), provided $K(k_f + k_b)^{1/2}$ is not too large.

The diffusion coefficient for Nb(V) in $AlCl_3$-NaCl (50-50 mole %) at 180°° calulated using Sand's equation (Equation 23, p 39) is 4.9×10^{-6} and 4.5×10^{-6} cm^2/sec at Nb(V) concentration 2.68×10^{-2} and 5.19×10^{-2} M, respectively. These data are in reasonable agreement with the chronoamperometric results.

d. Voltammetric studies. Voltammetric studies of the reduction of Nb(V) in $AlCl_3$-NaCl (50-50 mole %) were carried out by examining the effect of scan rate, Nb(V) concentration, and temperature. Typical entire voltammograms extending from +1.0 to -0.5 V vs Al(III)/Al reference electrode ($AlCl_3$-NaCl, 63-37 mole %) are shown in Figures 40 and 41. Four reduction steps were observed at slow san rates (see Figure 40). Three reduction steps were observed at fast scan rates (see Figure 41). The lower the concentration, the lower the scan rate at which the second step disappeared (1 V/sec at Nb(V) concentration 1.34×10^{-2} M, 20 V/sec at Nb(V) concentration 5.19×10^{-2} M). The same results were obtained at platinum and tungsten electrodes.

The voltammogram for the first step reduction (potential scan from 1.0 to 0.4 V) is shown in Figure 42. The peak current, $i^c_{p(1)}$, of the first reduction step was directly proportional to Nb(V) concentration in the range 6.8×10^{-3} - 5.19×10^{-2} M; this is shown in Figure 43. The plot of $i_p/v^{1/2}$ vs v at Nb(V) concentration 1.34×10^{-2} M for three temperatures is shown in Figure 44, which shows that parameter $i_p/v^{1/2}$ is almost independent of v. Table XXI shows the voltammetric results for the first reduction step at a platinum electrode. The same results were obtained at the tungsten electrode. This table summarizes peak separation ($E^c_p - E^a_p$), peak width ($E_p - E_{p/2}$), cathodic peak potential (E^c_p), half-wave potential ($E_{1/2}$), anodic and cathodic peak current ratio (i^a_p/i^c_p), and diffusion coefficient of Nb^{5+} at various temperatures and concentrations. The expected values for peak potential separation and peak width are $-(59/n)(T/298)$ and $-(56/n)(T/298)$ mV,[145] respectively. The results show

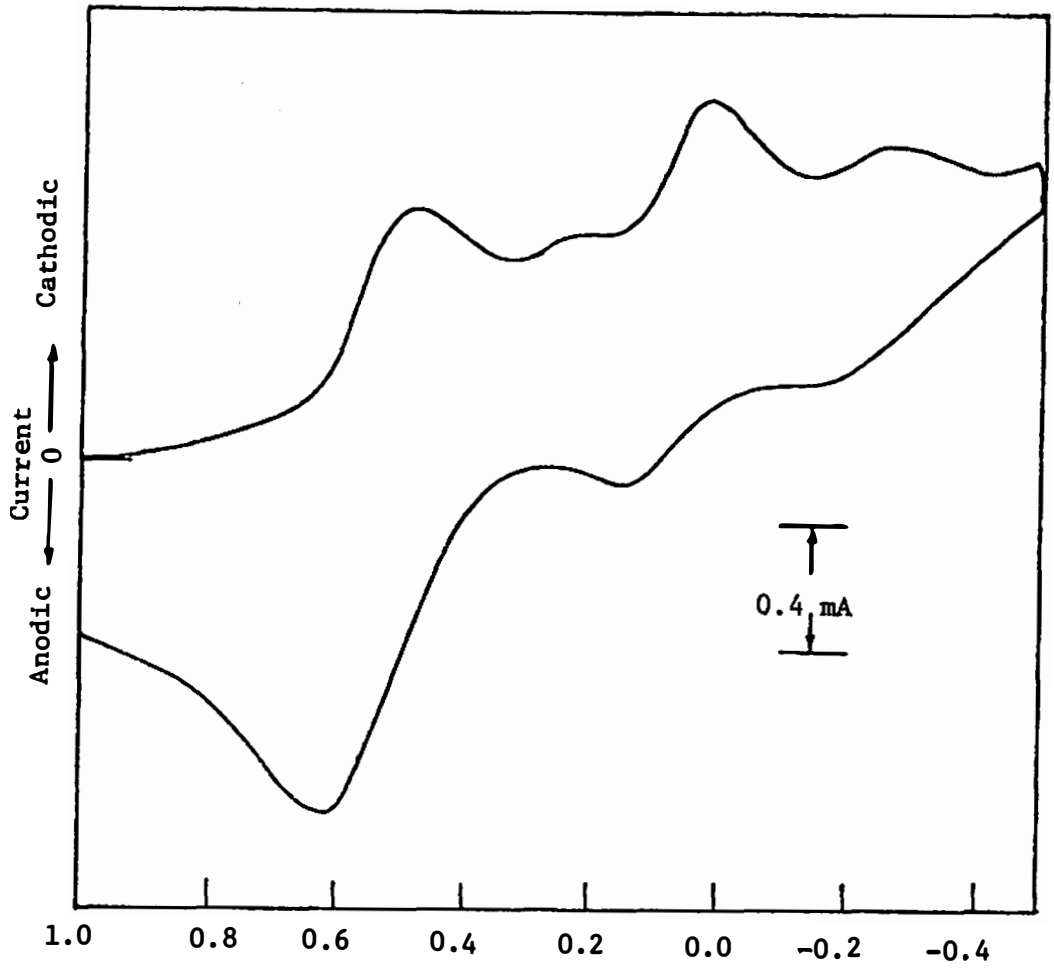


Figure 40. Cyclic voltammogram (first scan) for the reduction of Nb(V) at platinum electrode at 160°C.

Melt composition: $AlCl_3$-NaCl (50-50 mole %); electrode area: 0.10 cm^2; Nb(V) concentration: 5.19×10^{-2} M, scan rate: 0.1 V/sec.

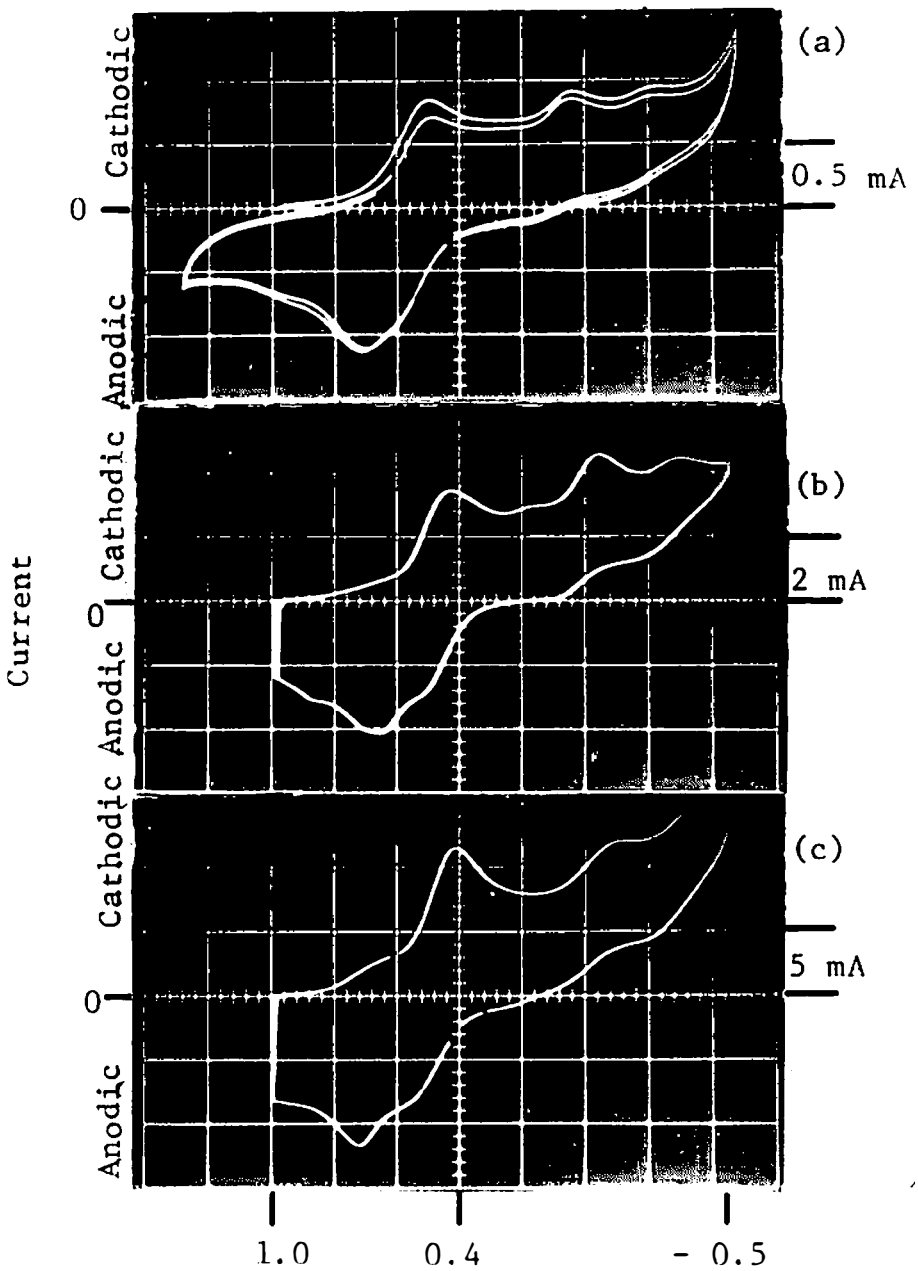


Figure 41. Cyclic voltammograms for the reduction of b(V) at a platinum electrode at fast scan rates.

Melt composition: $AlCl_3$-NaCl (50-50 mole %); electrode area: 0.10 cm^2; temperature 180°. (a) 1 V/sec, Nb(V) concentration 1.34 x 10^{-2} M; (b) 2V/sec, b(V) concentration 5.19 x 10^{-2} M; (c) 20V/sec, b(V) concentration 5.19 x 10^{-2} M.

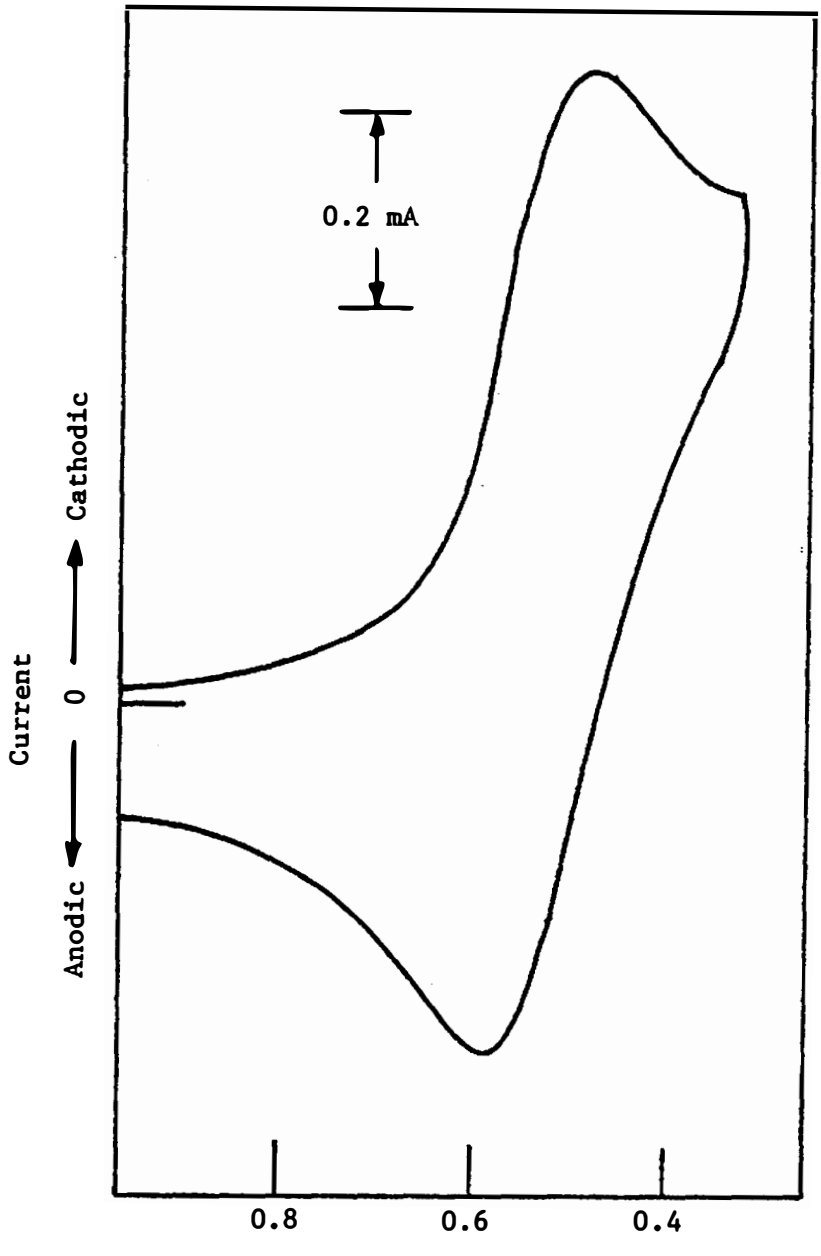


Figure 42. Cyclic voltammogram for the reduction of Nb(V) at tungsten electrode at 180°C.

Melt composition: $AlCl_3$-NaCl (50-50 mole %); electrode area: 0.10 cm^2; Nb(V) concentration: 2.68×10^{-2} M; scan rate: 0.2 V/sec.

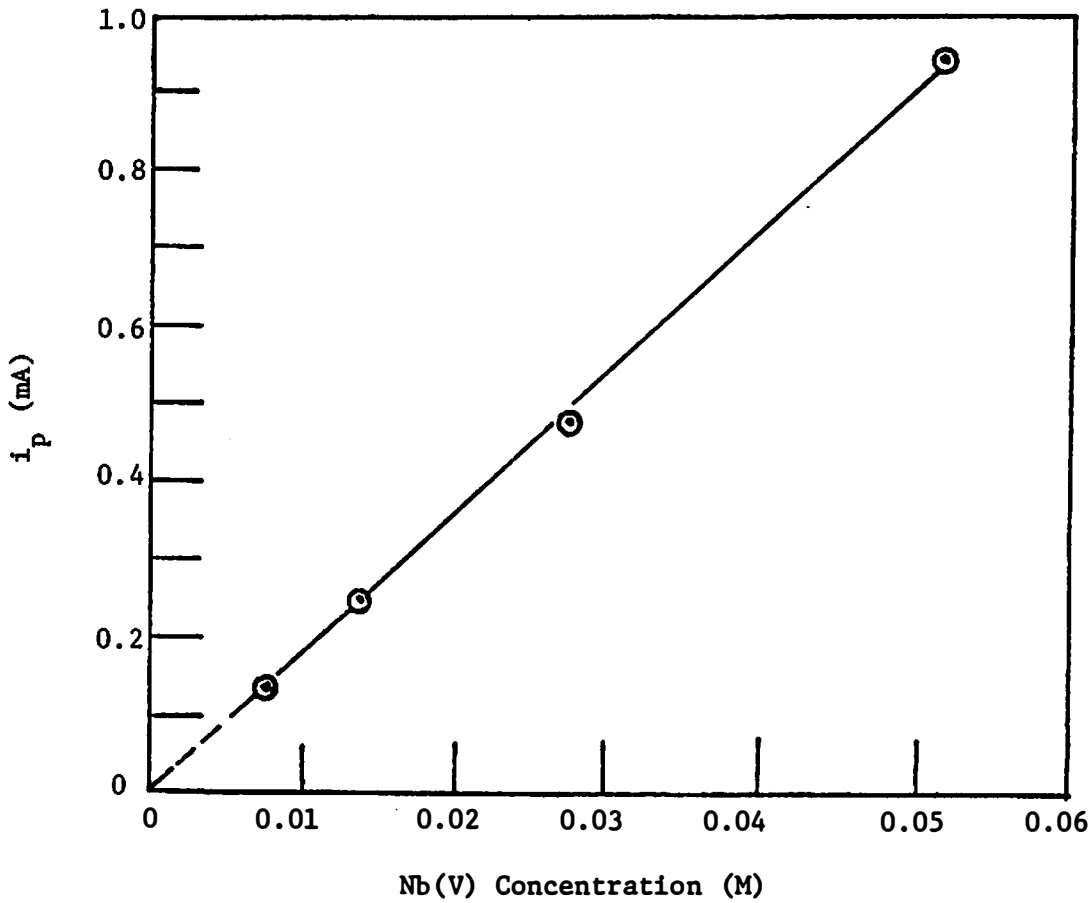


Figure 43. Variation of i_p of the first reduction step with (V) concentration at platinum electrode at 180°C.

Melt composition: $AlCl_3$-NaCl (50-50 mole %); electrode area: 0.10 cm^2; scan rate: 0.1 V/sec.

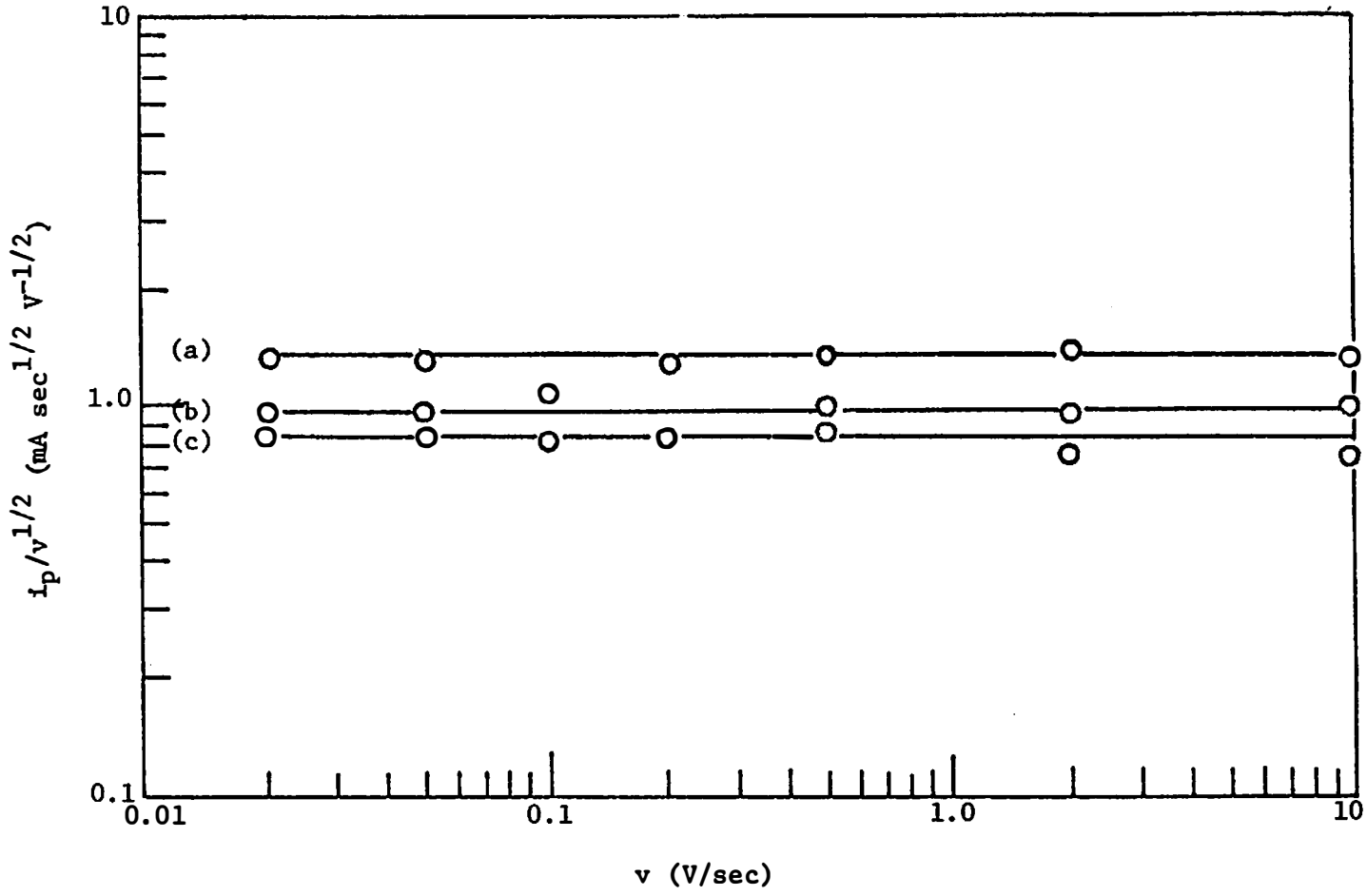


Figure 44. Plot of $i_p/v^{1/2}$ vs v for the first reduction step at platinum electrode.

Melt composition: $AlCl_3$-NaCl (50-50 mole percent); electrode area: 0.10 cm^2; Nb(V) concentration: 1.34×10^{-2} M. (a) 260°C; (b) 220°C; (c) 180°C.

TABLE XXI

VOLTAMMETRIC RESULTS FOR THE REDUCTION OF Nb^{5+} TO Nb^{4+} AT THE PLATINUM ELECTRODE.
MELT COMPOSITION: $AlCl_3$-NaCl (50-50%)[a]

$NbCl_5$ Concentration (M)	Temperature °C	$(E_p^c - E_p^a)_{(mV)}$ calc.	$(E_p^c - E_p^a)_{(mV)}$ exp.	$(E_p - E_{p/2})_{(mV)}$ calc.	$(E_p - E_{p/2})_{(mV)}$ exp.	$\frac{i_p^a}{i_p^c}$	E_p^c (V)	$E_{1/2}$ (V)	D (cm^2/sec)
6.8×10^{-3}[a]	180	- 89.7	- 90 ± 5	- 86.1	- 90 ± 5	1.00	0.440	0.496	7.0×10^{-6}
1.34×10^{-2}[b]	160	- 85.7	- 89 ± 5	- 82.3	- 90 ± 5	1.00	0.480	0.525	6.6×10^{-6}
	180	- 89.7	- 90 ± 5	- 86.1	-100 ± 10	0.99	0.460	0.516	7.1×10^{-6}
	220	- 97.6	-100 ± 5	- 93.7	-110 ± 10	1.00	0.438	0.498	11.2×10^{-6}
	260	-105.5	-110 ± 5	-101.3	-120 ± 10	0.98	0.416	0.476	19.3×10^{-6}
	300	-114.0	-130 ± 10	-109.4	-140 ± 10	1.03	0.413	0.458	24.5×10^{-6}
2.68×10^{-2}[b]	160	- 85.7	- 90 ± 5	- 82.3	- 90 ± 5	1.01	0.50	0.540	4.9×10^{-6}
	180	- 89.7	- 95 ± 5	- 86.1	-100 ± 10	1.02	0.474	0.524	5.8×10^{-6}
	300	-113.4	-130 ± 10	-108.9	-120 ± 10	1.01	0.406	0.466	20.8×10^{-6}
5.19×10^{-2}[b]	160	- 85.7	-100 ± 10	- 82.3	- 95 ± 10	0.97	0.504	0.548	4.8×10^{-6}
	180	- 89.7	-100 ± 10	- 86.1	-100 ± 10	0.98	0.490	0.538	6.6×10^{-6}
5.0×10^{-2}[c]	145	- 82.8	- 85 ± 5	- 79.5	- 86 ± 5	1.00	0.665	0.709	4.0×10^{-6}
	310	-116.0	-120 ± 5	-111.3	-121 ± 5	1.01	0.625	0.695	11.7×10^{-6}
7.46×10^{-2}[c]	190	- 91.5	- 95 ± 5	- 87.8	- 96 ± 5	1.06	0.660	0.69	2.7×10^{-6}
	280	-109.9	-115 ± 5	-105.5	-114 ± 5	1.01	0.63	0.68	7.6×10^{-6}

[a]Electrode area = 0.10 cm^2; scan rate = 0.1 V/sec; Al(III) ($AlCl_3$-NaCl, 63-37 mole %)/Al reference electrode.
(a), (b), and (c) designate three series of experiments.

that the first reduction step is essentially a one electron reversible diffusion-controlled process; Nb^{5+} is reversibly reduced to Nb^{4+}. The ratio of anodic to cathodic peak current (i_p^a/i_p^c) was calculated using Nicholson's semi-empirical formula;[206] it was in the range 0.97 - 1.06. $E_{1/2}$ values were obtained by measuring the potentials at 0.85 i_p.[145] E_p^c shifts anodically with increasing concentration; the dependence of E_p^c with the Nb(V) concentration suggests that a chemical complication is involved.

Assuming that the effect of the chemical complication is small, the diffusion coefficient of Nb(V) in molten $AlCl_3$-NaCl (50-50 mole %) at various temperatures and concentrations may be calculated from the Randles-Sevcik equation (Equation 16, p 28). The calculated values are also listed in Table XXI. The diffusion coefficients of Nb(V) for the concentration 1.34×10^{-2} M resulted in a linear log D vs 1/T plot in the temperature range 160° - 300° The resulting equation is

$$\log D = - 2.70 - 1100/T \qquad (68)$$

Thus, the activation energy, E_a, for the diffusion of Nb(V) is 5.03 kcal/mole.[188] Table XXII summarizes the effect of the scan rate on the experimental parameters over the entire potential range (1.0 - -0.5 V) at a platinum electrode. Similar results were obtained at the tungsten electrode. $i_{p(2)}^c$ is estimated by using the descending branch technique.[159] Table XXII shows that $i_{p(2)}^c/v^{1/2}$ decreases with increasing scan rate, and the ill-defined peak actually disappears at high scan rates (>1 V/sec at Nb(V) concentration 1.34×10^{-2} M; >20 V/sec at Nb(V) concentration 5.19×10^{-2} M). These results suggest that chemical complications are present between the first and second charge transfer processes. Because

TABLE XXII

VOLTAMMETRIC RESULTS FOR THE FOUR REDUCTION STEPS AT PLATINUM ELECTRODE.
MELT COMPOSITION: $AlCl_3$-NaCl (50-50 mole %)[a]

Temperature (°C)	$NbCl_5$ Concentration (M)	Scan Rate (V/sec)	$E^c_{p(1)}$ (V)	$E^c_{p(2)}$ (V)	$E^c_{p(3)}$ (V)	$E^a_{p(3)}$ (V)	$E^c_{p(3)} - E^a_{p(3)}$ (mV)	$E^c_{p(4)}$ (V)	$E^a_{p(4)}$ (V)	$E^c_{p(4)} - E^a_{p(4)}$ (mV)	$i^c_{p(2)}/v^{1/2}$ mA $sec^{1/2}$ $V^{-1/2}$
160	2.68×10^{-2}	0.02	0.48	0.25	0.075	0.19	- 115	- 0.24	- 0.17	- 70	0.35
		0.05	0.49	0.25	0.055	0.17	- 115	- 0.24	- 0.17	- 70	0.26
		0.1	0.49	0.24	0.045	0.16	- 115	- 0.23	- 0.15	- 80	0.22
		0.2	0.49		0.035	0.15	- 115	- 0.24	- 0.16	- 80	0.17
		0.5	0.49		0.015		- 125	- 0.24	- 0.16	- 80	0.12
160	5.19×10^{-2}	0.1	0.50	0.27	0.05	0.17	- 120	- 0.24	- 0.17	- 70	0.47
		0.2	0.50	0.26	0.04	0.13	- 90	- 0.24	- 0.17	- 70	0.43
		2.0	0.45	0.18	- 0.05	0.05	- 100	- 0.29	- 0.21	- 80	0.24
		20	0.43	--	- 0.09	--	--	- 0.34	- 0.25	- 90	--
180	5.19×10^{-2}	0.02	0.47	0.27	0.06	0.20	- 140	- 0.27	- 0.20	- 70	0.60
		0.05	0.48	0.27	0.06	0.20	- 140	- 0.25	- 0.18	- 70	0.80
		0.1	0.49	0.26	0.06	0.19	- 130	- 0.24	- 0.19	- 50	0.69
		0.2	0.49	0.23	0.04	0.17	- 130	- 0.26	- 0.19	- 70	0.61
		0.5	0.49	0.21	- 0.07	0.13	- 200	- 0.24	- 0.18	- 60	0.68
		2	0.47	0.21	- 0.01	0.12	- 130	- 0.27	- 0.17	-100	0.49
		20	0.45	--	--	--	--	- 0.31	- 0.21	-100	--

[a]Electrode area, 0.10 cm^2; Al(III)/Al reference electrode ($AlCl_3$-NaCl, 63-37 mole %).

the second peak is flat and broad, one cannot accurately estimate the peak currents for the third and fourth peaks by using the descending branch technique. The changes in the peak potential (E_p^c) and peak separation ($E_p^c - E_p^a$) with scan rate for the third and fourth steps, however, can be obtained from the analysis of the voltammograms. Table XXII shows that $E_{p(3)}^c$ shifts cathodically with increasing scan rate. $E_{p(4)}^c$ is almost independent of the scan rate. No significant changes in the shape of the voltammograms for the third and fourth reduction steps with scan rate were observed. Verification of $n_1 = 1$ for the first reduction step can also be achieved from the ratio of voltammetric $i_p/v^{1/2}$ to chronoamperometric $it^{1/2}$ and chronopotentiometric $i\tau^{1/2}$. For these determinations of n, concentration, diffusion coefficient, and electrode area do not need to be known. The ratio is obtained by dividing Equation 16, p 28, by Equation 23, p 39, and by Equation 27, p 43, and are given by the following expressions:

$$\frac{i_p/v^{1/2}}{i\tau^{1/2}} = 54.86\left(\frac{n}{T}\right)^{1/2} \tag{69}$$

$$\frac{i_p/v^{1/2}}{it^{1/2}} = 86.31\left(\frac{n}{T}\right)^{1/2} \tag{70}$$

Using experimental values under identical experimental conditions for $i_p/v^{1/2}$, $i\tau^{1/2}$, and $it^{1/2}$, n_1 is calculated to be 1.01 and 1.05, respectively. Thus, voltammetric results indicate that the possible reduction mechanism is the ECEEE type. No theoretical treatment has appeared yet to describe such a complicated system (see Table VI, p 31). At the

present time step by step analysis by comparison with known theoretical treatments is probably the only way to try to understand this complicated system. Table XXI, p 161, shows that the peak potential of the first reduction step shifts anodically with increasing Nb(V) concentration. There are two possible mechanisms that can give such results; (1) reversible charge transfer followed by reversible or irreversible dimerization;[152-155,157,158] and (2) a disproportionation reaction following a reversible charge transfer.[150] The observed proportionality of the peak current with concentration for the first reduction step eliminates the possibility of the second mechanism. Saveant and Vianello[155] have reported the theoretical treatment of the reversible charge transfer followed by a reversible dimerization mechanism. They concluded that a pure diffusion current should be observed. When the extent of the dimerization is small, the peak current and peak potential for this process are given by:

$$i_p = 0.500\ nFD_o^{1/2}C(\frac{nF}{RT}v)^{1/2} \qquad (71)$$

$$E_p = E_{1/2} - 0.70\ \frac{RT}{nF} - \frac{RT}{4nF}\ln\frac{D_o}{D_z} - \frac{RT}{2nF}\ln K + \frac{RT}{2nF}\ln C \qquad (72)$$

where D_o and D_z are the diffusion coefficients of the oxidized and dimer forms, i_p is proportional to concentration and $v^{1/2}$, E_p is independent of scan rate, but shifts anodically with increasing concentration. E_p vs log C plot should be linear with a slope 2.3RT/2nF. Figure 45 shows the E_p^c vs log C plot for Nb^{5+} to Nb^{4+} step at the platinum electrode at 180°. The plot is linear with a slope 2.3RT/2nF, which gives $n_1 = 0.92$.

Based on the voltammetric analyses and the polarographic and chronopotentiometric results, tentative mechanism for the electrode reduction

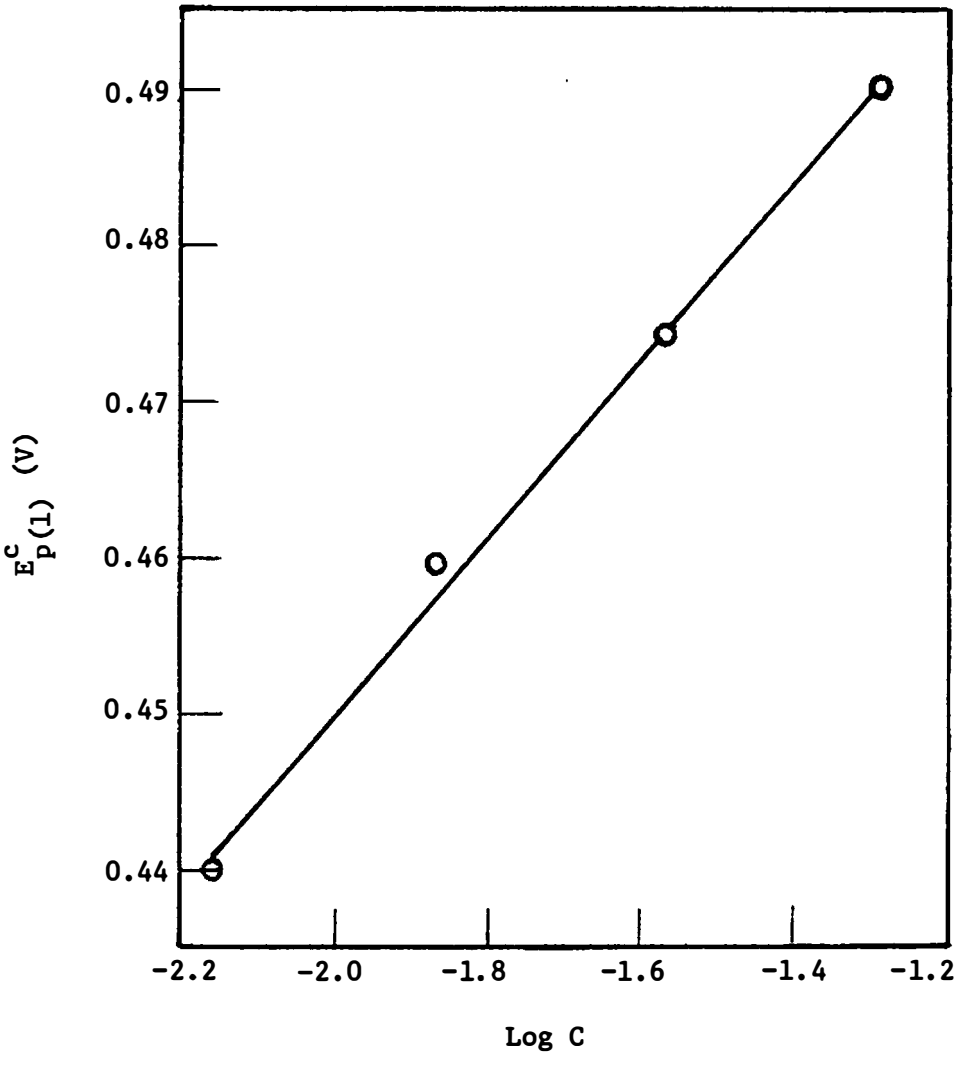


Figure 45. Plot of $E^c_{p(1)}$ vs log C for the reduction of Nb^{5+} to Nb^{4+} at platinum electrode at 180°C.

Melt composition: $AlCl_3$-NaCl (50-50 mole percent); electrode area: 0.10 cm^2.

of Nb(V) in molten $AlCl_3$-NaCl (50-50 mole %) is as follows: (1) At lower Nb(V) concentration (<6.8×10^{-3} M) and fast scan rates (>1 V/sec), the following chemical reaction does not have enough time to occur. Then the electrode reaction is

$$Nb^{5+} + e^- \rightleftharpoons Nb^{4+} \quad E_1, \quad n_1 = 1 \tag{63}$$

$$Nb^{4+} + e^- \rightleftharpoons Nb^{3+} \quad E_2, \quad n_2 = 1 \tag{73}$$

The third reduction step observed in the chronopotentiograms and voltammograms is possibly due to a higher order electrode reduction of Nb^{3+} to Nb_3^{8+} or Nb_6^{14+}. To confirm this hypothesis, further experiments need to be done. The reduction of Nb^{4+} to Nb^{3+} has been suggested by Gut[101] in $AlCl_3$-NaCl-KCl (50-25-25 mole percent) at 200°C, by Caton and Freund[102] in LiCl-KCl eutectic at 450°C, and by Inman[111] in alkali chloride mixtures at 720 - 760°C. Gut[101] also found another reduction step close to the limit of the melt. He suggested that it was probably due to the reduction of Nb(III), but no further explanation was given. No reduction wave could be detected for Nb^{3+} by Inman. Caton and Freund reported that the reduction of Nb^{3+} was not reproducible. They suggested that Nb^{3+} was probably reduced to Nb_3^{8+} or Nb_6^{14+}. Because $AlCl_3$-NaCl (50-50 mole %) is a more acidic medium than alkali chlorides, it may stabilize more readily the cluster species of niobium.

(2) At higher Nb(V) concentrations and slower scan rates the following chemical reaction occurs after the first step. The postulated mechanism is:

$$Nb^{5+} + e^- \rightleftharpoons Nb^{4+} \qquad E_1 \quad (n_1 = 1) \tag{63}$$

$$2Nb^{4+} \underset{k_b}{\overset{k_f}{\rightleftharpoons}} Nb_2^{8+} \qquad C \quad (K = \frac{k_b}{k_f}) \qquad (64)$$

$$Nb_2^{8+} + e^- \rightleftharpoons Nb_2^{7+} \qquad E_2 \ (n_2 = 0.5) \qquad (74)$$

$$Nb_2^{7+} + e^- \rightleftharpoons Nb_2^{6+} \qquad E_3 \ (n_3 = 0.5) \qquad (75)$$

$$3Nb_2^{6+} + 2e^- \rightleftharpoons 2Nb_3^{8+} \qquad E_4 \ (n_4 = 0.33) \qquad (66)$$

It has been shown that the first reduction step is essentially a reversible one electron diffusion controlled process. The anodic shift of the reduction potential with increasing Nb(V) concentration and the linearity of $E^c_{p(1)}$ vs log C plot suggest that a following dimerization reaction is coupled to the reversible charge transfer.[155] The expected small k_f or large $K = k_b/k_f$ for the dimerization reaction in this basic melt composition explains why the complications for the first step are only minor.[155] Saveant *et al.*[207] reported that a pure diffusion-controlled process should be seen for an ECE mechanism with a large K for the following chemical reaction . This is due to the increasing thermodynamic stability of Nb^{4+}, as K is large. The number of electrons in the second and third reduction steps is based on the polarographic diffusion current ratios (see Table XIX, p 147). Nicholson and Shain[145] have reported that the voltammogram for a charge transfer preceded by a reversible chemical reaction is flat for a small k_f value, and the flatness of the wave increases with increasing scan rate. The decrease in the ratio of n_2/n_1 can also cause the flatness of the wave for the second reduction step.[149] The experimental results are consistent with these predictions.

The proposed reaction for the fourth step (Equation 66) is based on the observed diffusion current ratio at long times.

The existence of Nb_2^{7+} (valence: 3.5) has not been reported yet, but Caton and Freund[102] have reported that niobium ions were generated by controlled potential electrolysis in LiCl-KCl eutectic with an average n value of 3.64. Yang and coworkers[105] also found that mixed valence states between Nb^{3+} and Nb^{4+} prevailed in concentrated LiCl-KCl eutectic melts. Thus, other results suggest the possibility of the existence of Nb_2^{7+} as well.

The effect of the temperature (160 - 300°C) on the voltammetric reduction of Nb(V) at the platinum and tungsten electrodes was also examined. $E^c_{p(1)}$ shifts cathodically with increasing temperature (see Table XXI, p 161). $E^c_{p(2)}$ also shifts cathodically with increasing temperature from 0.24 V at 160°C to 0.17 V at 300°C (Nb(V) concentration: 1.34×10^{-2} M, 0.1 V/sec). These results suggest that the higher oxidation state is more stable in a more basic melt, because the basicity of the melt increases with increasing temperature.[118,121,122] The increase in stability of the higher oxidation state in more basic melts has been found in other systems.[127,192] The dissociation equilibrium constant K of the dimer ($K = k_b/k_f$) should also increase with increasing temperature, as one can note from Equation 64a, p 127.

Equation 72, p 165, also indicates that the peak potential of the first reduction step will shift cathodically as K increases. The voltammograms for the third and fourth reduction steps were not well-defined at higher temperatures (> 260°C). The waves are small and broad (see

Figure 46). One should expect the lowering of the peak current for the third and fourth reduction steps as K increases because of the decrease of the dimerization products. The increase in the peak current with increasing temperature for the second reduction step may be due to the reduction of monomeric Nb(IV).

e. Adsorption studies. The presence of adsorption of intermediate niobium species at the platinum electrode was found in $AlCl_3$-NaCl (50-50 mole %) at the temperature of 220° and at Nb(V) concentration 2.68×10^{-2} M. These adsorption effects were not found in other melt compositions, as well as not at the tungsten electrode. The appearance of these adsorption phenomena was also dependent on the duration of the experiment; usually, the effect was observed when experiments were carried out for more than one day. Figure 47 shows some of the typical results at 220°C. The experimental adsorption parameters are summarized in Table XXIII. The voltammetric results show the transition from equilibrium adsorption-desorption process (Langmuir adsorption) at low scan rates (0.1 - 2 V/sec) to a rate-controlled adsorption-desorption process. At low scan rates, the adsorption and desorption peak currents and potentials are symmetric (Figure 47(a) and (b)). As the scan rate is increased, the adsorption peak shifts cathodically, and the desorption peak anodically. The amount of this shift along the potential axis increases with increasing scan rate (see Figure 47(c) and (d) and Table XXIII). The adsorption-desorption peaks become broad and skewed. The height of the adsorption-desorption peaks increased more rapidly than that of the normal diffusion controlled peaks with scan rate, and finally overlapped with the diffusion peak

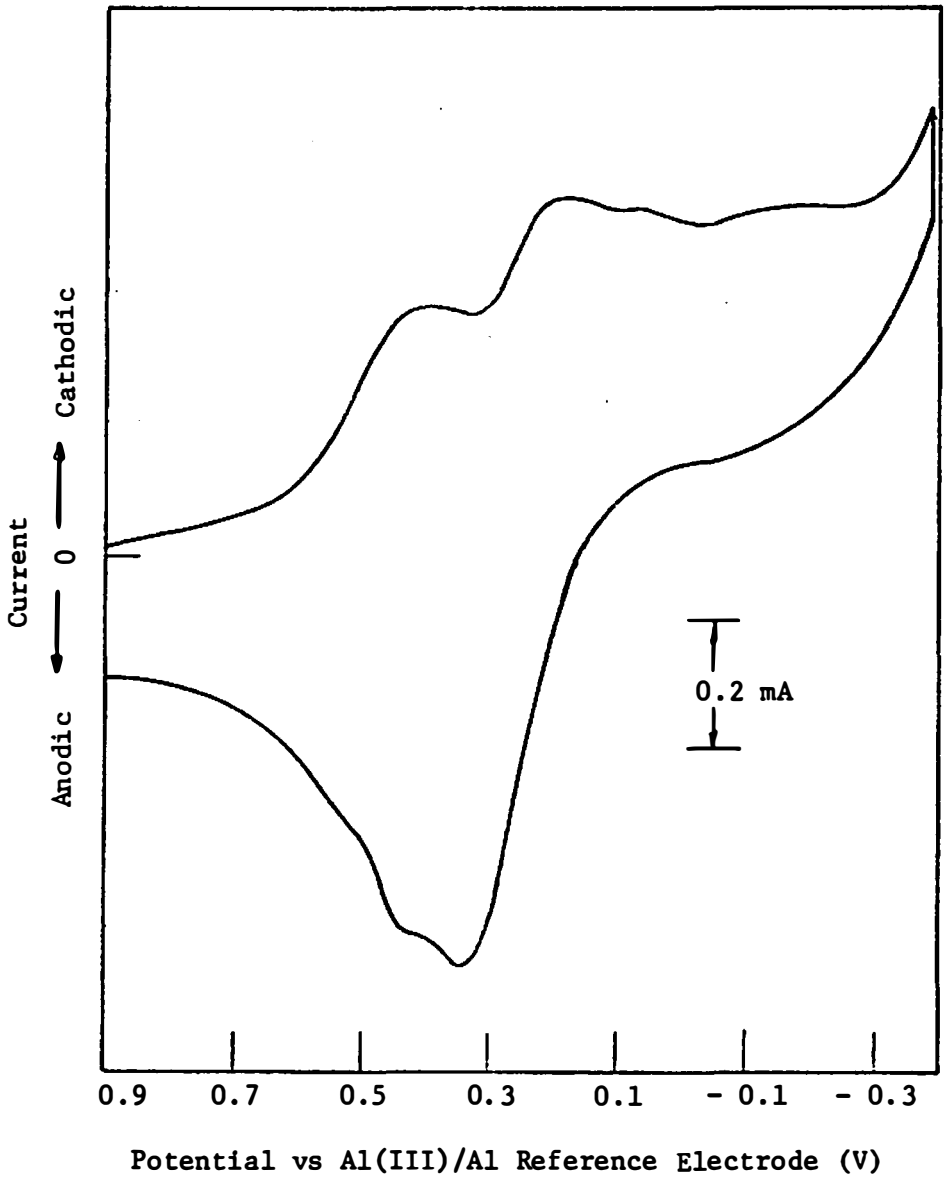


Figure 46. Cyclic voltammogram for the reduction of Nb(V) at platinum electrode at 300°.

Melt composition: $AlCl_3$-NaCl (50-50 mole %); electrode area: 0.10 cm^2; Nb(V) concentration: 1.34 x 10^{-2}M; scan rate: 0.1 V/sec.

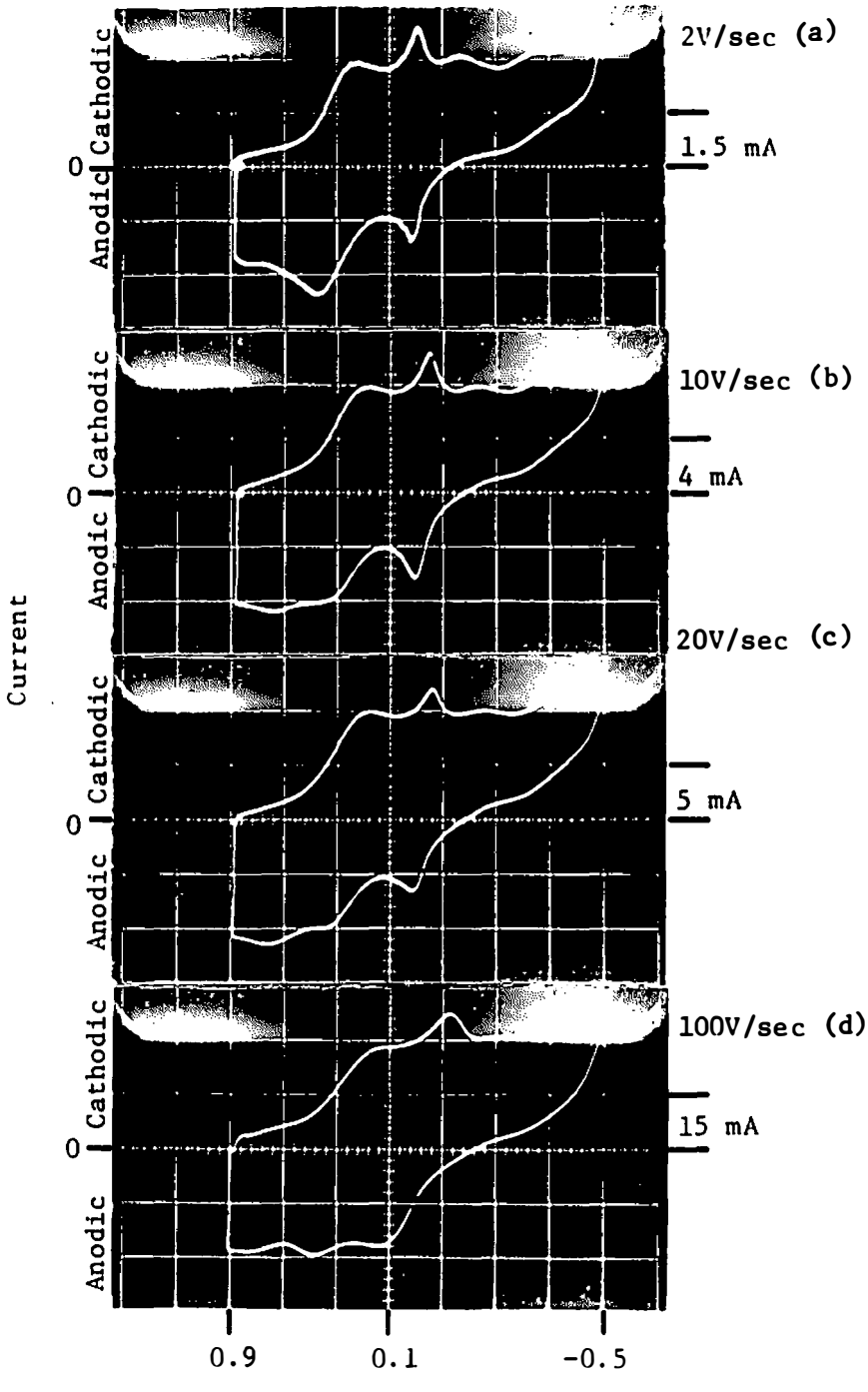


Figure 47. Cyclic voltammogram for the reduction of Nb(V) at platinum electrode at 220°.

Melt composition: $AlCl_3$-NaCl (50-50 mole %); electrode area: 0.10 cm^2; Nb(V) concentration: 2.68×10^{-2} M.

TABLE XXIII

VOLTAMMETRIC RESULTS FOR THE ADSORPTION PROCESS AT THE PLATINUM ELECTRODE

$NbCl_5$ Concentration M	Scan Rate V/sec	$E_{p(a)}$ V	$E_{p(d)}$ V	ΔE mV	$\Delta E_{w(a)}$ mV	$\Delta E_{w(d)}$ mV	$i_{p(a)}$ mA	$i_{p(a)}/v^{1/2}$ mA $sec^{1/2}$ $V^{-1/2}$
2.68×10^{-2}	0.1	0.193	0.193	0	28	30	--	0.86
	0.5	0.193	0.193	0	49	51	0.61	0.86
	2	0.213	0.213	0	63	64	1.26	0.89
	10	0.165	0.213	48	64	84	3.28	1.03
	20	0.153	0.305	152	64	88	3.90	0.87
	100	0.111	0.313	202	100	--	9.60	0.96

[a]Melt composition: $AlCl_3$-NaCl (50-50 mole %); electrode area: 0.10 cm^2; Al(III) ($AlCl_3$-NaCl, 63-37 mole %)/Al reference electrode.

of the third reduction step. These observations are consistent with the theory of the stationary electrode polarography of systems involving kinetic adsorption of the products.[178] The adsorption peak currents ($i_{p(a)}$) are also shown in Table XXIII; $i_{p(a)}$ is proportional to $v^{1/2}$ at high scan rates. These results are consistent with the theoretical predications[178] (Equation 35, p 47). The adsorption peak appeared as a prepeak for the third reduction step, and overlapped with the second reduction step. This result suggests that the species involved in the electrode adsorption process is the product in the third reduction step, probably Nb_2^{6+}.

f. Standard electrode Potential of the Nb(V)/Nb(IV) couple. The half-wave potential $E_{1/2}$ for a reversible process $O + ne^- = R$ may be taken as the voltammetric equivalent of the standard electrode potential E°, assuming that diffusion coefficients and activity coefficients of O and R are equal.[145] The $E_{1/2}$ values for the reversible process Nb(V) + e^- = Nb(IV) are listed in Table XXI, p 161, with respect to Al(III)/Al ($AlCl_3$-NaCl, 63-37 mole percent) reference electrode. The complications due to dimerization of Nb(IV) should be small at low solute concentrations. At Nb(V) concentration 1.34×10^{-2} M, E vs T plot is linear in the temperature range 160°C - 300°C, which gives:

$$E = 0.732 - 4.79 \times 10^{-4} T(V) \qquad (76)$$

The temperature coefficient of E is

$$\left(\frac{\partial E}{\partial T}\right)_p = -4.79 \times 10^{-4} \ (V/°K) \qquad (76a)$$

The entropy change of the cell reaction is

$$\Delta S = nF \cdot \left(\frac{\partial E}{\partial T}\right)_p = -11.05 \text{ (eu)} \qquad (76b)$$

Equation 76 is the cell voltage as a function of temperature without correction for the potential difference due to the melt composition difference between bulk and reference comparments. Osteryoung et al.[118] reported that the potential difference between $AlCl_3$-NaCl (50-50 mole %) and $AlCl_3$-NaCl (63-37 mole %) is about 0.43 V at 175°. Assuming that the temperature coefficient of the cell voltage $(\partial E/\partial T)p$ is independent of the melt composition, the corrected cell voltage as a function of temperature is given by:

$$E = 1.162 - 4.79 \times 10^{-4}\, T(V) \qquad (77)$$

in the temperature range 160°C - 300°C.

Using Equation 77, the equilibrium quotient for the following reaction can be estimated.

$$NbCl_5(d) + 1/3NaCl(d) + 1/3Al^\circ \rightleftharpoons NbCl_4(d) + 1/3NaAlCl_4(d) \qquad (78)$$

in which

$$Q = X_{NbCl_4}/X_{NbCl_5} \qquad (78a)$$

The free energy change for reaction (78) is given by:

$$\Delta G = -nFE = -26.80 + 11.05 \left(\frac{T}{10^3}\right) \quad \text{(kcal/mole)} \qquad (78b)$$

or

$$\log \frac{X_{NbCl_4}}{X_{NbCl_5}} = -2.41 + 5.86 \left(\frac{10^3}{T}\right) \qquad (78c)$$

Equation 78(c) shows the lower the temperature the higher the stability of Nb(IV) in $AlCl_3$-NaCl (50-50 mole %). This is consistent with

the discussion of the effect of acid-base properties of melts on solute behavior (p 19).

5. Effect of Melt Composition and Temperature on the Reduction of Nb(V) in Molten $AlCl_3$-NaCl Mixtures

The electrochemical reduction of Nb(V) was found to be very sensitive to melt composition and temperature. This suggests that the stability of the niobium species in the melts and the electrode reduction mechanism are very dependent on the melt composition (acid-base properties or pCl^- values) and temperature of the melt. Table XXIV summarizes some of the results obtained by the electrochemical studies.

Two reduction steps were observed in $AlCl_3$-NaCl (63-37 mole %). The first reduction step is well-defined and concentration dependent. The second reduction step is small, broad and ill-defined. Polarographic, chronopotentiometric, and voltammetric results suggest that the first reduction step involves formation of Nb(III) through an ECE mechanism.

Two reduction steps were observed in $AlCl_3$-NaCl (55-45 mole percent) at 180 and 260°C. The first reduction step at 180° and 260°C was split into two reduction steps at lower temperatures (140 and 150°C). Based on the polarographic, chronopotentiometric, and voltammetric results, the ECE mechanism involving $Nb^{5+}/Nb^{4+}(E_1)$, $2Nb^{4+}/Nb_2^{8+}(C)$, and $Nb_2^{8+}/Nb_2^{6+}(E_2)$, is believed to be present in the first step at higher temperatures or the first two steps at lower temperatures. The splitting into two reduction peaks at lower temperatures is probably caused by the temperature effect on the equilibrium constant of the chemical reaction. A sharp and symmetric third reduction peak not included in the total number of steps

TABLE XXIV

EFFECT OF MELT COMPOSITION ON THE REDUCTION OF Nb(V) IN MOLTEN $AlCl_3$-NaCl MIXTURES AT THE PLATINUM ELECTRODE

Melt Composition ($AlCl_3$-NaCl)	Temperature °C	Nb(V) Concentration M	Experimental Technique	$E_{1/2}$[a] V	Remarks
63-37 mole %	180	1.5×10^{-2}	Polarography	1.035	
	180	1.5×10^{-2}	Chronopotentiometry	1.040	
	180	1.5×10^{-2}	Voltammetry	1.040,[b] 0.31[c]	
55-45 mole %	180	1.42×10^{-2}	Polarography	0.96, 0.25 (1.035, 0.325)[d]	
	180	1.42×10^{-2}	Chronopotentiometry	0.97, 0.26 (1.045, 0.335)[d]	
	180	1.42×10^{-2}	Voltammetry	0.96,[b] 0.27,[b] (1.035, 0.345)[d]	
	140	1.42×10^{-2}	Polarography	1.06, 0.92, (1.135, 0.995)[d]	
	140	1.42×10^{-2}	Chronopotentiometry	1.09, 0.91, (1.165, 0.985)[d]	
	140	1.42×10^{-2}	Voltammetry	(0.99, 0.90, 0.44, 0.30)[c]	
				(1.065, 0.975, 0.515, 0.375)[d]	Current measured at 0.1 sec
50-50 mole %	180	6.8×10^{-3}	Polarography	0.511, 0.07 (0.941, 0.50)[d]	
	180	2.68×10^{-2}	Polarography	0.512, 0.260, 0.10, - 0.17	Current measured at 5 sec

TABLE XXIV (Continued)

Melt Composition ($AlCl_3$-NaCl)	Temperature °C	Nb(V) Concentration M	Experimental Technique	$E_{1/2}$[a] V	Remarks
50-50 mole %	180	2.68×10^{-2}	Chronopotentiometry	0.509, 0.230, 0.07, - 0.22 (0.939, 0.66, 0.50, 0.21)[d]	i_o 6 mA/cm^2
	180	1.34×10^{-2}	Voltammetry	0.516, 0.23,[c] 0.05,[c] - 0.24[c]	0.1 V/sec

[a]Potentials measured with respect to Al(III) ($AlCl_3$-NaCl, 63-37 mole %)/Al reference electrode.

[b]Scan rate: 0.1 V/sec, potential at 0.85 i_p.

[c]Peak potential at 0.1 V/sec.

[d]Potential after correcting for the potential difference between bulk and reference compartments; 0.075 V for $AlCl_3$-NaCl (55-45 mole %); 0.43 V for $AlCl_3$-NaCl (50-50 mole %).[118]

above is coupled with the appearance of the first reduction step at lower temperatures. This peak disappears at higher temperatures (180 and 260°C) and higher scan rate (>0.5 V/sec). It is possibly due to the reduction of an insoluble film which was formed after the first reduction step. The last reduction step has the same characteristics as the one found in $AlCl_3$-NaCl (63-37 mole %); it probably involves the formation of Nb_3^{8+}.

In $AlCl_3$-NaCl (50-50 mole %), two reduction steps were observed at fast scan rates and low Nb(V) concentrations (6.8×10^{-3} M). Polarographic results show that the first two reduction steps correspond to two reversible couples, Nb^{5+}/Nb^{4+} and Nb^{4+}/Nb^{3+}. At higher concentrations or slower scan rates, four reduction steps were observed. Polarographic, chronopotentiometric, and voltammetric results show that the first reduction step is a one electron reversible diffusion controlled process (Nb^{5+}/Nb^{4+}). ECE mechanism involving $Nb^{5+}/Nb^{4+}(E_1)$, $2Nb^{4+}/Nb_2^{8+}(C)$, $Nb_2^{8+}/Nb_2^{7+}(E_2)$ has been tentatively attributed to the first initial two reduction steps; this is followed by two charge transfers; $Nb_2^{7+}/Nb_2^{6+}(E_3)$ and $Nb_2^{6+}/Nb_3^{8+}(E_4)$. Polarograms and chronopotentiograms at higher temperatures (>180°C) were not well-defined. Voltammograms at 300°C show that other kinetic complications arise. Rate controlled adsorption at the platinum electrode of products of the third reduction step has also been found in this melt composition.

Cathodic shift of the reduction potentials of the first reduction step in $AlCl_3$-NaCl (63-37 mole %) and of the first and second reduction steps in $AlCl_3$-NaCl (50-50 mole %) with increasing temperature

indicates that the lower oxidation state is more stable in the acidic melts. The reversible reduction of Nb^{5+} to Nb^{4+} observed only in the basic melt suggests that monomeric Nb^{4+} is more stable in the basic melt.

D. Electrochemistry of Niobium Oxychloride in Molten $AlCl_3$-NaCl Mixtures

Electrochemistry of niobium in aqueous solutions and nonaqueous solvents is complicated by the tendency of niobium(V) to hydrolyze and form niobium(V) oxy-species.[99,100] Because of the tendency of Nb(V) to form niobium oxychloride, most of the electrochemistry of niobium in molten salts has been studied by anodic dissolution of Nb metal.[102,103,105-111] No electrochemical studies on $NbOCl_3$ in molten salts have been reported. For comparison with previous studies on $NbCl_5$ in molten chloroaluminates, it was considered of interest to study the electrochemical behavior of $NbOCl_3$ in molten chloroaluminates, and to examine the effect of melt composition and temperature on the stability and electrode reduction mechanism of niobium(V) oxychloride.

Electrochemical studies of niobium(V) oxychloride were carried out in the same kind of cell used for studying niobium pentachloride (Figure 5, p 60). Tungsten and platinum wires were used as working electrodes; two large platinum foils were used as counter and quasi-reference electrodes. The potentials were measured with respect to Al(III) ($AlCl_3$-NaCl, 63-37 mole %)/Al reference electrode. Niobium oxychloride was added as $NbOCl_3$. The melt composition was changed from $AlCl_3$-NaCl (63-37 mole %) to $AlCl_3$-NaCl (50-50 mole %). The electrochemistry of Nb(V) oxychloride was examined by means of linear sweep

voltammetry, differential pulse polarography, chronopotentiometry, and chronoamperometry.

1. Electrochemistry of Niobium Oxychloride in Molten $AlCl_3$-NaCl (63-37 and 56-44 mole %)

a. Polarographic studies using current-time curves. The polarograms constructed from current-time curves for the reduction of niobium oxychloride in the melt compositions $AlCl_3$-NaCl 63-37 and 56-44 mole % are similar to those shown in Figure 23 (p 115) and Figure 30 (p 131). A one step reduction was observed in the melt composition $AlCl_3$-NaCl (63-37 mole %) at the platinum electrode at 250° (Nb(V) concentration: 2.07×10^{-2} M) with $E_{1/2}$ = 0.99 V. The E vs log (i_d-i) plot was not linear. E vs log $(i_d-i)/i$ plot was partially linear in the potential range 0.96 - 1.01 V with a slope 2.3 RT/nF, which gives n = 1.9. A one step reduction was also observed in the melt composition $AlCl_3$-NaCl (56-44 mole %) in the potential range 1.0 - 0.5 V at 290° (Nb(V) concentration: 1.95×10^{-2} M) with $E_{1/2}$ = 0.89 V. E vs log $(i_d-i)/i$ and log (i_d-i) plots were not linear. Thus, polarographic results suggest that niobium(V) oxychloride is unstable in $AlCl_3$-NaCl (63-37 and 56-44 mole %), and is converted to niobium(V) chloride; it then follows the same electrode reduction mechanism as Nb(V) chloride.

b. Chronopotentiometric studies. The chronopotentiograms for the reduction of niobium(V) oxychloride in the melt compositions $AlCl_3$-NaCl (63-37 and 56-44 mole %) at a platinum electrode are similar to those shown in Figure 24 (p 117) and Figure 32 (p 134). A one step reduction was observed in the potential range 1.4 - 0.5 V at 130° and

250° with $E_{1/2}$ values; 1.00, and 0.98 V, respectively, (Nb(V) concentration: 2.07×10^{-2} M, $i_o = 4 mA/cm^2$). E vs $\log(\tau^{1/2} - t^{1/2})$ plot was linear at 130° with a slope 2.3 RT/nF, which gives $n_1 = 0.9$. Similar results were obtained with Nb(V) chloride. Two reduction steps were observed in $AlCl_3$-NaCl (56-44 mole %) in the potential range 1.2 - 0.2 V at 295° with $E_{1/2}$: 0.89 V and 0.32 V (Nb(V) concentration: 1.95×10^{-2} M, i_o = 6-7 mA/cm^2). E vs $\log (\tau^{1/2} - t^{1/2})$ and $\log (\tau^{1/2} - t^{1/2})/t^{1/2}$ plots were not linear for both steps.

Thus, the chronopotentiometric results are in agreement with the polarographic results, which indicate that Nb(V) oxychloride was converted to Nb(V) chloride, and reduced according to the same mechanism as Nb(V) chloride in these acidic melts.

c. Voltammetric studies. Voltammetric studies of niobium(V) oxychloride in molten $AlCl_3$-NaCl (63-37 and 56-44 mole %) have been done at platinum and tungsten electrodes in the temperature range 130°-325°. Cyclic voltammograms in $AlCl_3$-NaCl (63-37 mole %) in the absence and the presence of niobium oxychloride at 170° at a platinum electrode are similar to those shown in Figure 26 (p 120). The residual current is low (< 0.1 mA) in the potential range of interest. The concentration dependence of the peak current ($i^c_{p(1)}$) was established for the Nb(V) concentration range: 1.20×10^{-2}-2.07×10^{-2}M (Figure 48). Table XXV shows some of the voltammetric results obtained at the platinum electrode. The same results were obtained with a tungsten electrode. A one step reduction was observed in the potential range 1.8 - 0.5 V. E^c_p shifts cathodically with increasing scan rate. $i^c_p/v^{1/2}$ decreases slightly with increasing

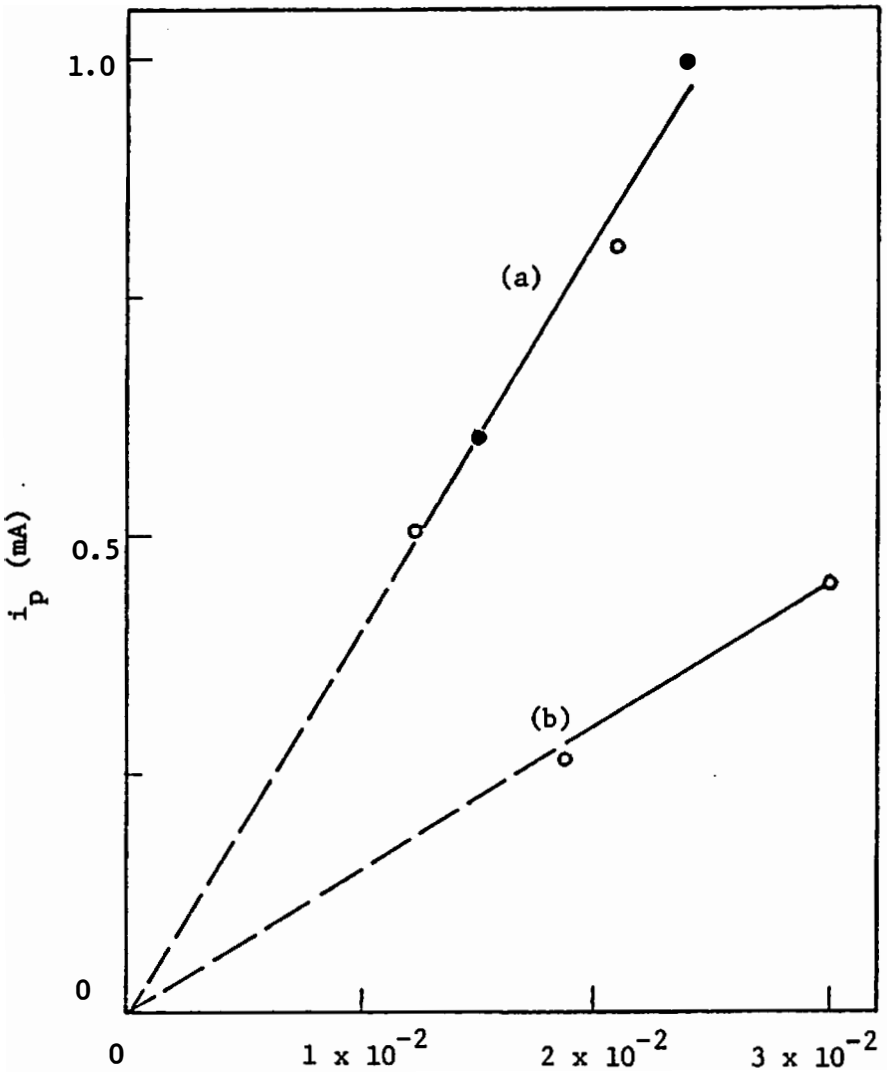


Figure 48. Variation of i_p with Nb(V) (added as $NbOCl_3$) concentration at platinum electrode.

Electrode area: 0.10 cm^2; scan rate: 0.1 V/sec. (a) $AlCl_3$-NaCl (63-37 mole %); 180°;●data taken from previous experiments. (b) $AlCl_3$-NaCl (50-50 mole %); 190°; peak current for the first reduction step.

TABLE XXV

VOLTAMMETRIC RESULTS FOR THE REDUCTION OF Nb(V) (ADDED AS $NbOCl_3$) AT THE PLATINUM ELECTRODE. MELT COMPOSITION: $AlCl_3$-NaCl (63-37 mole %)[a]

Temperature °C	Scan Rate V/sec	E_p^c V	$E_{1/2}$ V	$E_p - E_{p/2}$ mV	$i_p^c/v^{1/2}$ mA $sec^{1/2}$ $V^{-1/2}$
170	0.01	0.995	1.02	- 45	2.30
	0.05	0.985	1.01	- 45	2.23
	0.1	0.965	0.99	- 60	2.21
	0.5	0.940	0.97	- 90	2.10
210	0.01	0.980	0.99	- 30	3.00
	0.05	0.968	0.98	- 37	2.85
	0.1	0.955	0.98	- 48	2.75
310	0.01	0.920	0.95	- 40	4.00
	0.05	0.914	0.94	- 50	3.97
	0.1	0.905	0.94	- 64	3.83
	0.5	0.894	0.93	- 66	3.85

[a]Electrode area: 0.10 cm^2; niobium(V) concentration: 2.07×10^{-2} M; Al(III) ($AlCl_3$-NaCl, 63-37 mole %)/Al reference electrode.

scan rate. Except for the observation that the anodic peak becomes broad and big at 325°, the voltammetric results are similar to those obtained for niobium(V) chloride in $AlCl_3$-NaCl (63-37 mole %).

In $AlCl_3$-NaCl (56-44 mole %), two reduction steps were observed at higher temperature (190° and 295°). The first reduction step at the higher temperature was separated into two reduction steps at 130°. The sharp and symmetric peak at E_p^c = 0.42 V and the ill-defined last reduction step, which were observed in studying niobium(V) chloride, were also observed in this study (see Figure 33, p 136). Table XXVI summarizes some of the results at the platinum electrode. The same results were obtained with a tungsten electrode. The cyclic voltammogram at 295° shows that the anodic peak is not as well-defined as in previous studies with Nb(V) chloride in this melt. Sometimes, a small amount of black precipitate was observed at the end of the experiment.

Levoy et al.[24,208] have reported that Al(III) acts effectively as a very strong O^{2-} acceptor in the acidic melt $AlCl_3$-NaCl-KCl (60-26-14 mole %); many oxides will be soluble in this melt and the solute oxide complexes will be less stable in this strong oxide acceptor melt. The formation of $NbCl_5(g)$ and AlOCl(c) by the reaction of $NbOCl_3(c)$ with $Al_2Cl_6(g)$ has also been reported by Schafer et al.[97] The conversion of $NbOCl_3(c)$ to $NbCl_5(c)$ in molten chloroaluminates can also be seen from the free energy calculation of the following reaction:

$$NbOCl_3(c) + NaAl_2Cl_7(\ell) \rightleftharpoons NbCl_5(c) + AlOCl(c) + NaAlCl_4(\ell) \ . \qquad (79)$$

Using the available free energies of formation $\Delta G^f_{NbOCl_3}$[46] $\Delta G^f_{NbCl_5}$[85] (Table IV, p 12) ΔG^f_{AlOCl},[82] $\Delta G^f_{NaAl_2Cl_7}$,[118] and $\Delta G^f_{NaAlCl_4}$,[118] one can

TABLE XXVI

VOLTAMMETRIC RESULTS FOR THE REDUCTION OF Nb(V) (ADDED AS $NbOCl_3$) AT THE PLATINUM ELECTRODE. MELT COMPOSITION: $AlCl_3$-NaCl (56-44 mole %)[a]

Temperature °C	Scan Rate V/sec	$E^c_{p(1)}$ V	$(E_p - E_{p/2})_{(1)}$ mV	$E^c_{p(2)}$ V	$E^c_{p(3)}$ V	$E^c_{p(4)}$ V	$i_{p(1)}/v^{1/2}$ (mA $sec^{1/2}$ $V^{-1/2}$)
130	0.01	1.010	- 50	0.880	0.42	--	1.000
	0.05	1.005	- 50	0.870	0.42	0.27	0.94
	0.1	0.975	- 55	0.865	0.43	0.23	1.00
	0.5	0.970	- 65	0.850	0.43	0.26	0.92
190	0.01	0.920				0.25	3.00
	0.05	0.905				0.20	2.58
	0.1	0.885				0.21	2.02
	0.5	0.870				0.19	2.19
275	0.01	0.875				0.33	3.80
	0.05	0.865				0.30	3.57
	0.1	0.865				0.25	3.46
	0.5	0.820				0.25	3.25

[a]Electrode area: 0.10 cm^2; Nb(V) concentration: 1.95×10^{-2} M; Al(III) ($AlCl_3$-NaCl, 63-37 mole %)/Al reference electrode.

estimate the free energy of reaction (79), which gives: $\Delta G = -5.01$ (kcal/mole) at 200°, $\Delta G = -3.65$ (kcal/mole) at 130°. These values indicate that $NbOCl_3$(c) should be converted to $NbCl_5$(c) in acidic chloroaluminates.

Based on the known information and the results of the electrochemical studies in $AlCl_3$-NaCl (63-37 and 56-44 mole %), NbO(III) is probably converted to Nb^{5+} by the following reaction:

$$Al_2Cl_7^- + 2NbO^{3+} \rightarrow 2Nb^{5+} + 2AlO^+ + 7Cl^- \quad . \qquad (80)$$

Nb(V) is then reduced by following the same mechanism as Nb(V) chloride in these acidic melts.

2. Electrochemistry of Niobium Oxychloride in Molten $AlCl_3$-NaCl (50-50 Mole %)

Electrochemical studies of niobium(V) oxychloride in $AlCl_3$-NaCl (50-50 mole %) were carried out in the cell described before in the temperature range 150-340°. The melt composition was obtained by adding NaCl to $AlCl_3$-NaCl (56-44 mole %). The potential was measured with respect to Al(III) ($AlCl_3$-NaCl, 63-37 mole %)/Al reference electrode. The color of this melt in the presence of NbO(III) was deep blue which was different from the yellow color of $NbCl_5$ in the same melt composition; this suggests that NbO(III) was stable in this basic melt.

a. Polarographic studies using current-time curves: The polarogram constructed from current-time curves for the reduction of NbO(III) at the tungsten electrode at 245° is shown in Figure 49. A one step reduction was observed in the potential range 1.1 - 0.4 V with $E_{1/2}$

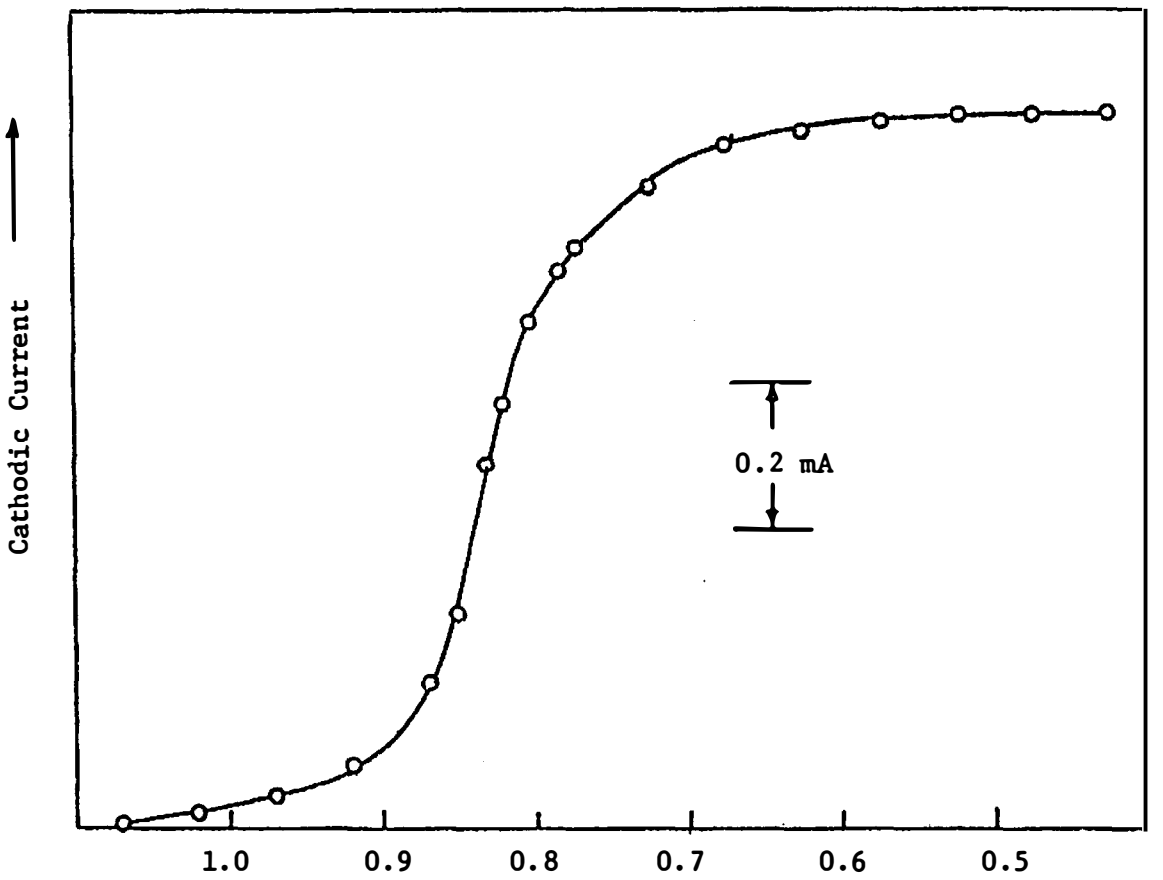


Figure 49. Polarogram constructed from current-time curves for the reduction of NbO(III) at tungsten electrode at 245°.

Melt composition: $AlCl_3$-NaCl (50-50 mole %); electrode area: 0.10 cm^2; NbO(III) concentration: 3.0×10^{-2} M; current measured at 2.5 sec.

of 0.830, 0.79, and 0.77 V at 245, 290, and 340°, respectively. The same results were obtained at the platinum electrode. E vs log $(i_d-i)/i$ and log (i_d-i) plots are not linear, indicating that chemical complications are probably involved in this reduction step. Figure 50 shows that the one reduction step at the higher temperatures is split into two steps at 190° with $E_{1/2}$ = 1.05, and 0.895 V, respectively. The diffusion current ratio for these two steps is close to one. E vs log (i_d-i) plot is not linear. E vs log $(i_d-i)/i$ plot is linear with a slope 2.3 RT/nF, which gives n_1 =1.1. These results suggest that the first reduction step at 190° is a reversible diffusion controlled one electron charge transfer process. (See Table VIII, p 44). The log plot of the second reduction step is not linear. The diffusion coefficient (D) of NbO(III) determined from the current-time curves using Equation 27, p 43, is 4.07×10^{-6} cm^2/sec at 190°.

b. Differential pulse polarographic studies. Differential pulse polarograms for the reduction of NbO(III) in $AlCl_3$-NaCl (50-50 mole %) were obtained at platinum and tungsten electrodes, at temperatures 180° and 280° (potential range: 1.2 - 0.5 V). Figure 51 shows the differential pulse polarogram at a tungsten electrode at 280°. The same result was obtained at a platinum electrode. A one step reduction was observed at faster scan rates and higher pulse amplitudes with $E_{1/2}$ = 0.78 V (Figure 51(a)), however this peak is partially resolved at slower scan rates and lower pulse amplitude (Figure 51 (b)). This suggests that this peak is due to the overlapping of two reduction processes. Figure 52 shows the differential pulse polarogram at a tungsten electrode at 180°.

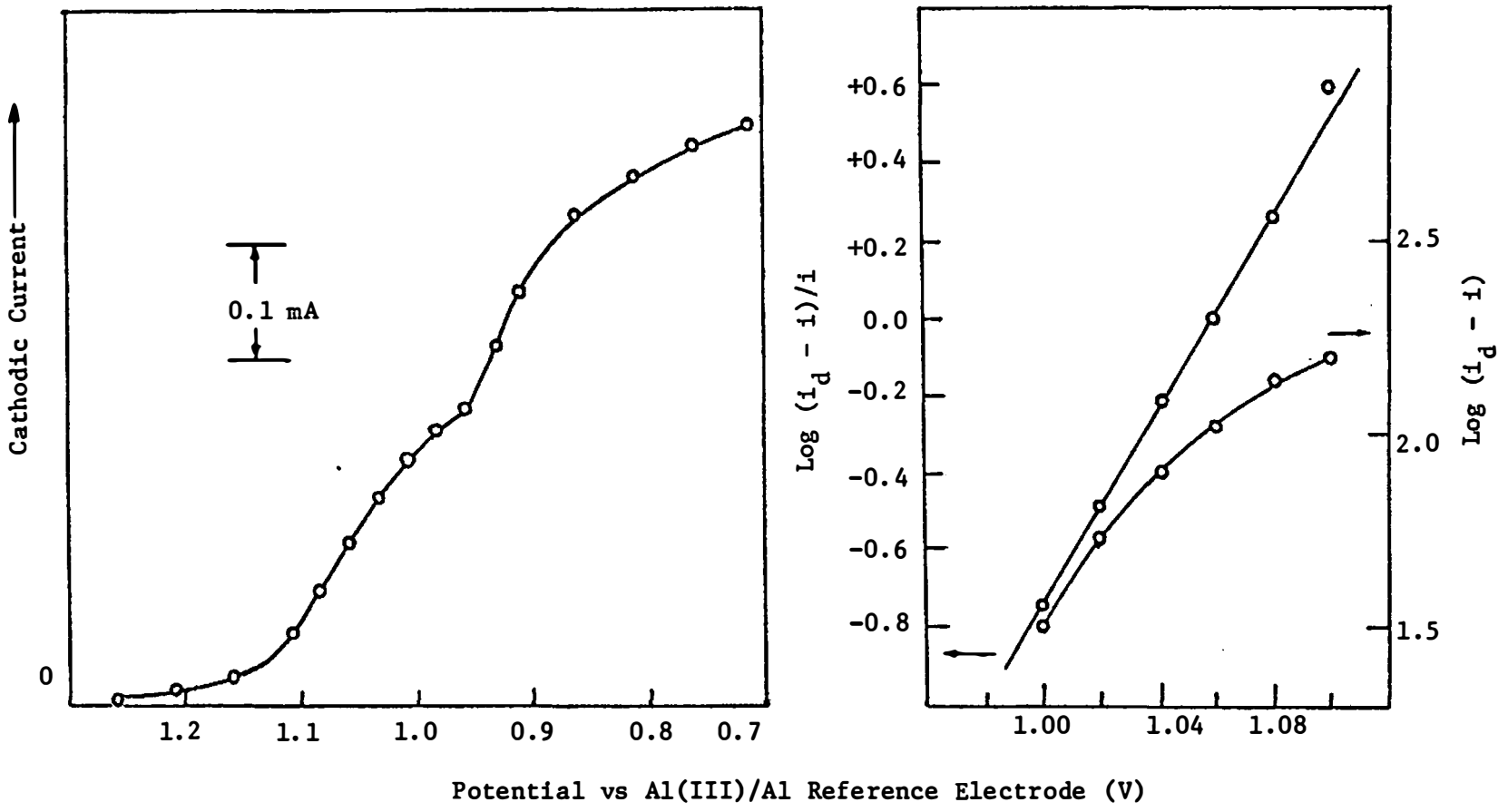


Figure 50. Polarogram constructed from current-time curves for the reduction of NbO(III) at platinum electrode at 190°. Plot of E vs log $(i_d - i)/i$ and log $(i_d - i)$ for the first wave.

Melt composition: $AlCl_3$-NaCl (50-50 mole %); electrode area: 0.10 cm^2; NbO(III) concentration: 3.0×10^{-2} M; current measured at 2.5 sec.

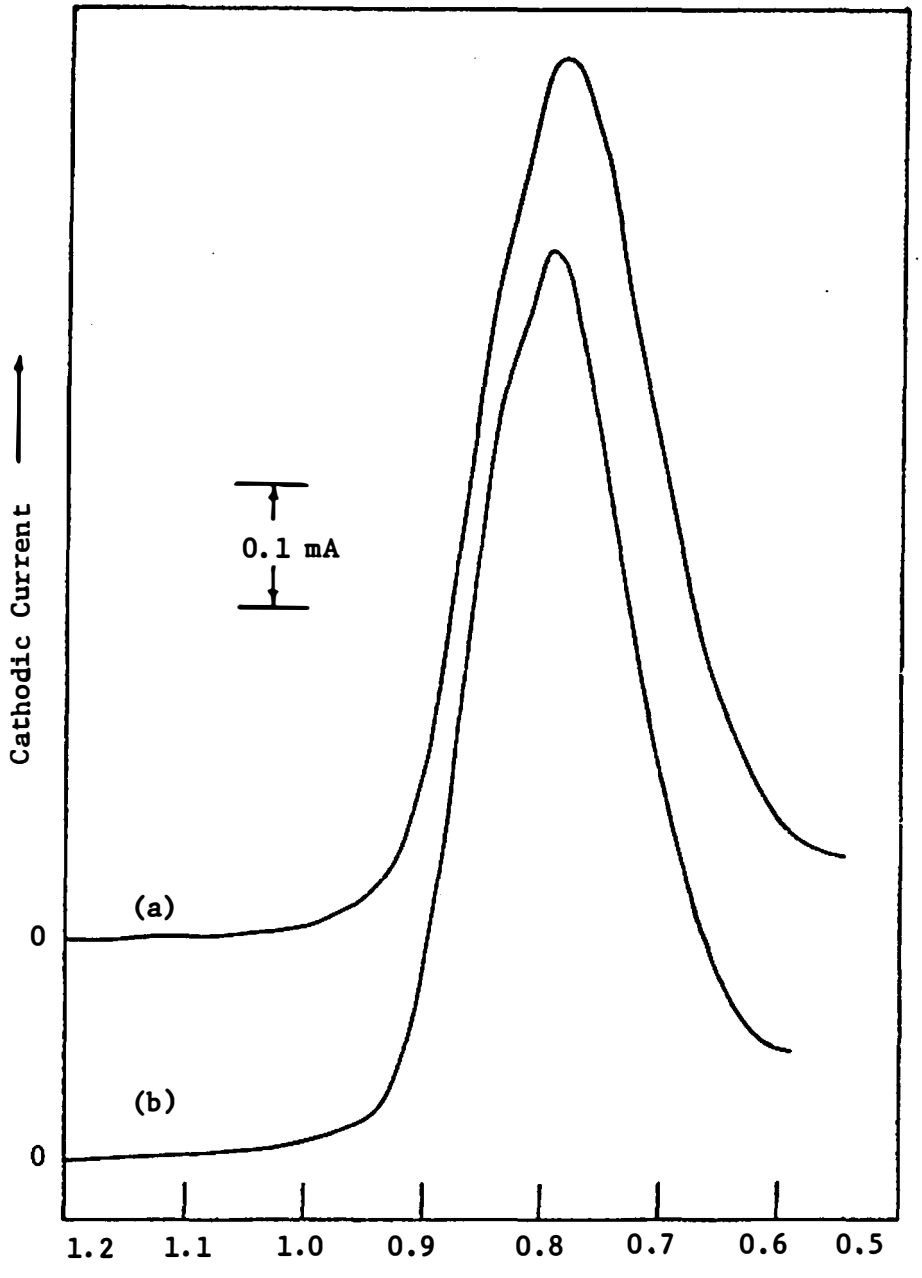


Figure 51. Differential pulse polarograms for the reduction of NbO(III) at tungsten electrode at 280°.

Melt composition: $AlCl_3$-NaCl (50-50 mole %); Nb(V) concentration: 3.0×10^{-2} M; drop time: 0.5 sec. (a) Scan rate: 10 mV/sec; pulse amplitude: 5 mV; (b) scan rate: 5 mV/sec; pulse amplitude: 2.5 mV.

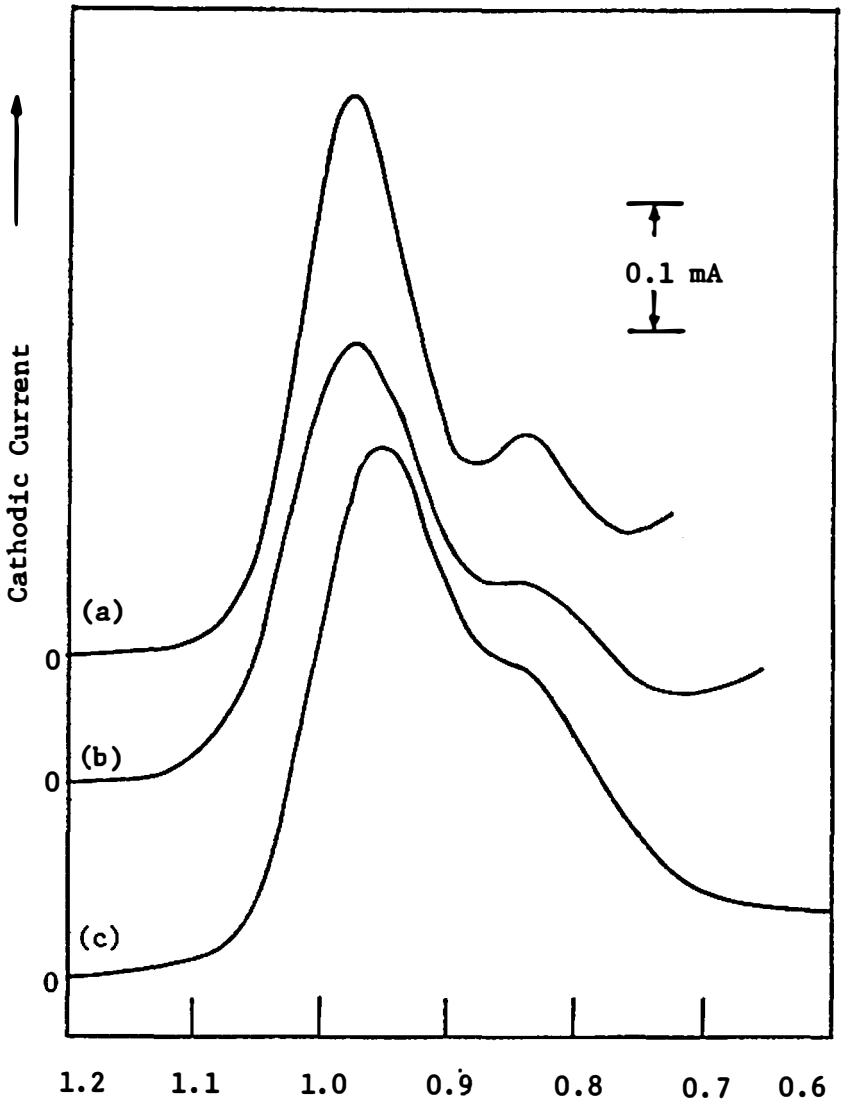


Figure 52. Differential pulse polarograms for the the reduction of NbO(III) at tungsten electrode at 180°.

Melt composition: $AlCl_3$-NaCl (50-50 mole %); Nb(V) concentration: 3.0×10^{-2} M; drop time: 0.5 sec. (a) Scan rate: 2 mV/sec; pulse amplitude: 1 mV; (b) scan rate: 5 mV/sec; pulse amplitude: 2.5 mV; (c) scan rate: 10 mV/sec; pulse amplitude: 5 mV.

A two step reduction process was observed. A cathodic shift of the peak potentials with scan rate were observed; $E_{1/2}$ shifts from 0.98 and 0.84 V at 2 mV/sec to 0.955, and 0.835 V at 10 mV/sec. The number of electrons for the first reduction step at 180° may be estimated from the peak half width by using the equation $\Delta E_w = (\frac{90.4}{n})(\frac{T}{298})$,[176] which gives n = 1.1 at the scan rate 5 mV/sec.

Thus, pulse polarographic results suggest that two reduction steps are present in the electrochemical reduction of NbO(III) in the potential range 1.2-0.5 V in the temperature range 180-280°.

c. Chronopotentiometric studies. Chronopotentiometric studies of NbO(III) (NbO(III) concentration: 3.0×10^{-2} M) in molten $AlCl_3$-NaCl (50-50 mole %) have been carried out at platinum and tungsten electrodes in the temperature range 190-340° (potential range: 1.2-0.6 V). A one step reduction was observed with $E_{1/2}$ values: 0.85, 0.80, and 0.77 V at the temperatures 245, 290, and 340°, respectively. E vs log $(\tau^{1/2}-t^{1/2})/-t^{1/2}$ and log $(\tau^{1/2}-t^{1/2})$ plots are not linear. The one reduction step at higher temperature was separated into two steps at 190° with $E_{1/2}$ 1.05 and 0.89 V. E vs log $(\tau^{1/2}-t^{1/2})/t^{1/2}$ and log $(\tau^{1/2}-t^{1/2})$ are not linear for both reduction steps. If $n_1 = 1$, the diffusion coefficient for NbO(III) calculated by using Equation 23 (p 39) is $D = 3.22 \times 10^{-6}$ cm^2/sec. Thus, chronopotentiometric results are consistent with the polarographic results.

d. Voltammetric studies. Voltammetric studies of NbO(III) in $AlCl_3$-NaCl (50-50 mole %) have been carried out at platinum and tungsten electrodes in the temperature range 150-340°. Linear sweep voltammograms

for the reduction of NbO(III) at a platinum electrode at 175° for the entire potential range (+1.3 ∿-0.1 V) are shown in Figure 53. The same results were obtained with tungsten electrodes. Figure 48(b) (p 183) shows the concentration dependence of the peak current of the first reduction step at 190°. Table XXVII summarizes some of the voltammetric results for the reduction of NbO(III) at lower temperatures (150-190°). The electrochemical behavior of NbO(III) in $AlCl_3$-NaCl (50-50 mole %) is quite different from that of Nb(V) chloride (see Figure 40, p 156). Four reduction steps were observed over the entire potential range (+1.3 ∿ -0.1 V) at 175° (Figure 53). The first two reduction steps are closely related. The cyclic voltammogram for the first reduction step at 150° (potential range: 1.3 ∿ 0.9 V) is shown in Figure 54. No anodic wave could be seen at the scan rates studied (0.005 V/sec ∿ 0.5 V/sec). The number of electrons for this first reduction step can be estimated from the experimental values (Table XXVII) and the expected value for a reversible charge transfer following an irreversible chemical reaction, $E_p - E_{p/2} = -(\frac{48}{n})(\frac{T}{298})$ mV,[157] which gives $n_1 = 0.91$ at 150°, $n_1 = 0.99$ at 190°. These results are consistent with the polarographic results. Verification of the number of electrons for the first reduction step at 190° can also be achieved by using Equation 70 (p 164) which gives $n_1 = 1.1$. Two typical cyclic voltammograms for the initial two reduction steps at the platinum electrode at 190° are shown in Figure 55. The variation of the anodic wave shape with the scan rate, the cathodic shift of $E^c_{p(1)}$ with increasing scan rate, and the decreasing $i^c_{p(1)}/v^{1/2}$ with increasing scan rate suggest that an ECE mechanism with an irreversible chemical reaction[149] is probably present. $E^c_{p(2)}$ shifts slightly with

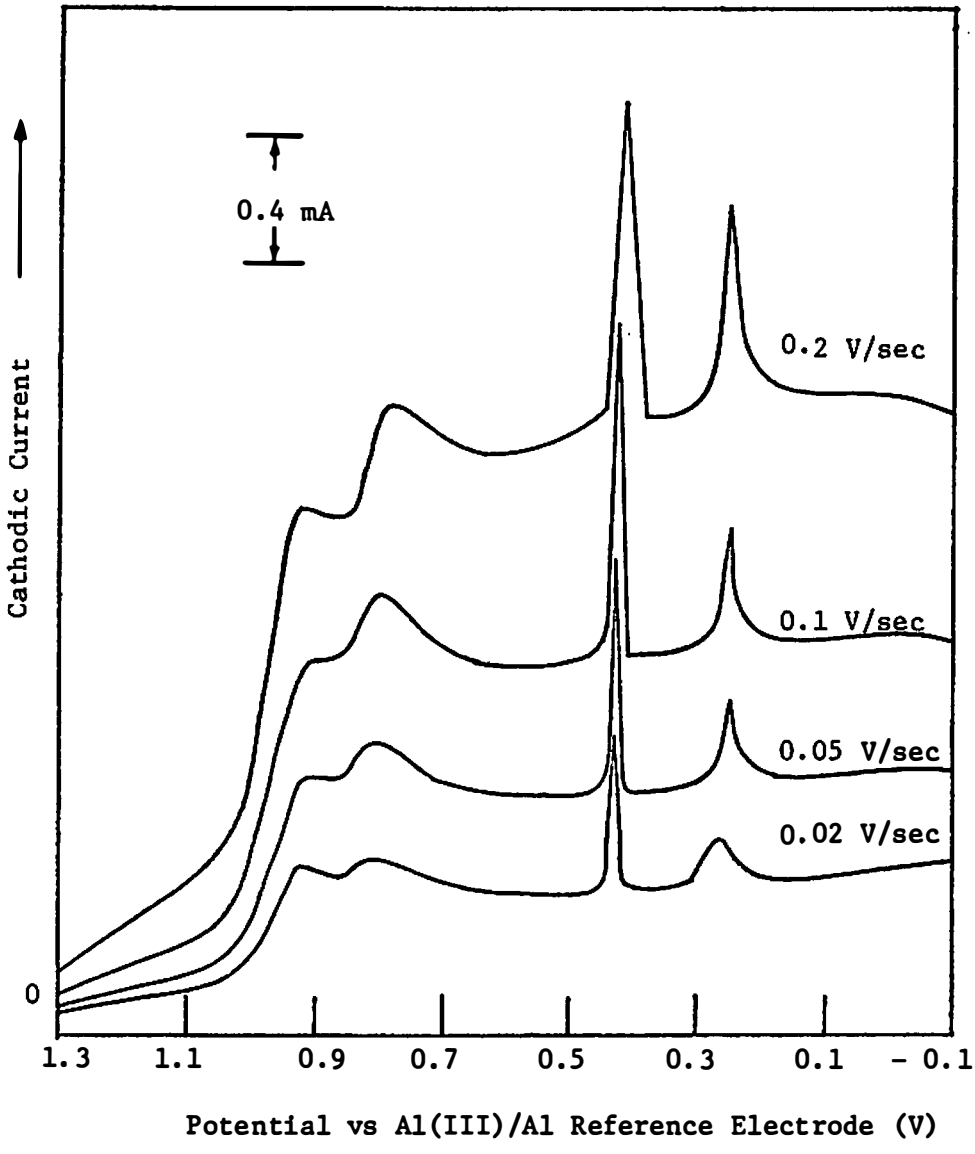


Figure 53. Linear sweep voltammograms for the reduction of bO(III) at the platinum electrode at 175°.

Melt composition: $AlCl_3$-NaCl (50-50 mole %); electrode area: 0.10 cm^2; NbO(III) concentration: 3.0 x 10^{-2} M.

TABLE XXVII

VOLTAMMETRIC RESULTS FOR THE REDUCTION OF NbO(III).
MELT COMPOSITION: $AlCl_3$-NaCl (50-50 mole %)[a]

Temperature °C	Electrode	Scan Rate V/sec	$E^c_{p(1)}$ (V)	$E^c_{p(2)}$ (V)	$E^c_{p(3)}$ (V)	$E^c_{p(4)}$ (V)	$(E_p - E_{p/2})(1)$ mV	$i^c_{p(1)}/v^{1/2}$ mA $sec^{1/2}$ $V^{-1/2}$	$i^c_{p(3)}/v^{1/2}$ mA $sec^{1/2}$ $V^{-1/2}$	$i^c_{p(4)}/v^{1/2}$ mA $sec^{1/2}$ $V^{-1/2}$
175	Pt	0.02	0.96	0.85	0.46	0.29			3.54	0.99
		0.05	0.95	0.84	0.46	0.29			3.12	1.25
		0.1	0.95	0.84	0.46	0.29			3.29	1.20
		0.2	0.95	0.82	0.46	0.29			2.41	1.43
		0.5	--	0.83	0.46	--			0.25	
175	W	0.02	0.96	0.84	0.47	0.31			2.83	0.43
		0.05	0.95	0.83	0.47	0.31			3.06	1.08
		0.1	0.94	0.82	0.47	0.30			3.10	1.01
		0.2	0.93	0.82	0.47	0.30			1.70	0.85
		0.5	0.93	0.81	0.47	0.30			—	0.36
150	Pt	0.005	1.00				- 75	0.22		
		0.01	0.99				- 75	0.19		
		0.02	0.98				- 76	0.19		
		0.05	0.97				- 75	0.18		
		0.1	0.96				- 82	0.17		
		0.2	0.95				- 85	0.16		
190	Pt	0.01	0.98	0.85			- 75	2.10		
		0.05	0.97	0.82			- 80	1.96		
		0.1	0.95	0.81			- 75	1.42		
		0.5	0.93	0.79			- 80	1.40		

[a]Electrode area: 0.10 cm^2; NbO(III) concentration: 3.0×10^{-2} M; Al(III) ($AlCl_3$-NaCl, 63-37 mole %)/Al reference electrode.

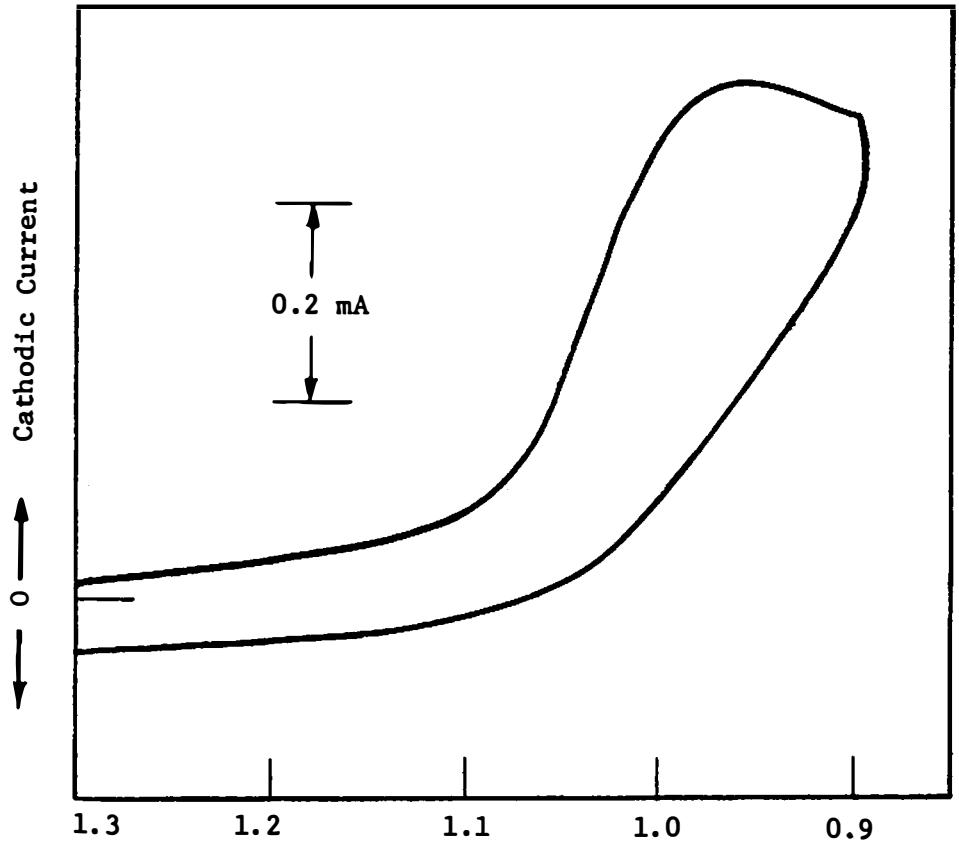


Figure 54. Cyclic voltammogram for the reduction of NbO(III) at the platinum electrode at 150°.

Melt composition: $AlCl_3$-NaCl (50-50 mole %); electrode area: 0.10 cm^2; NbO(III) concentration: 3.0×10^{-2} M; scan rate: 0.1 V/sec.

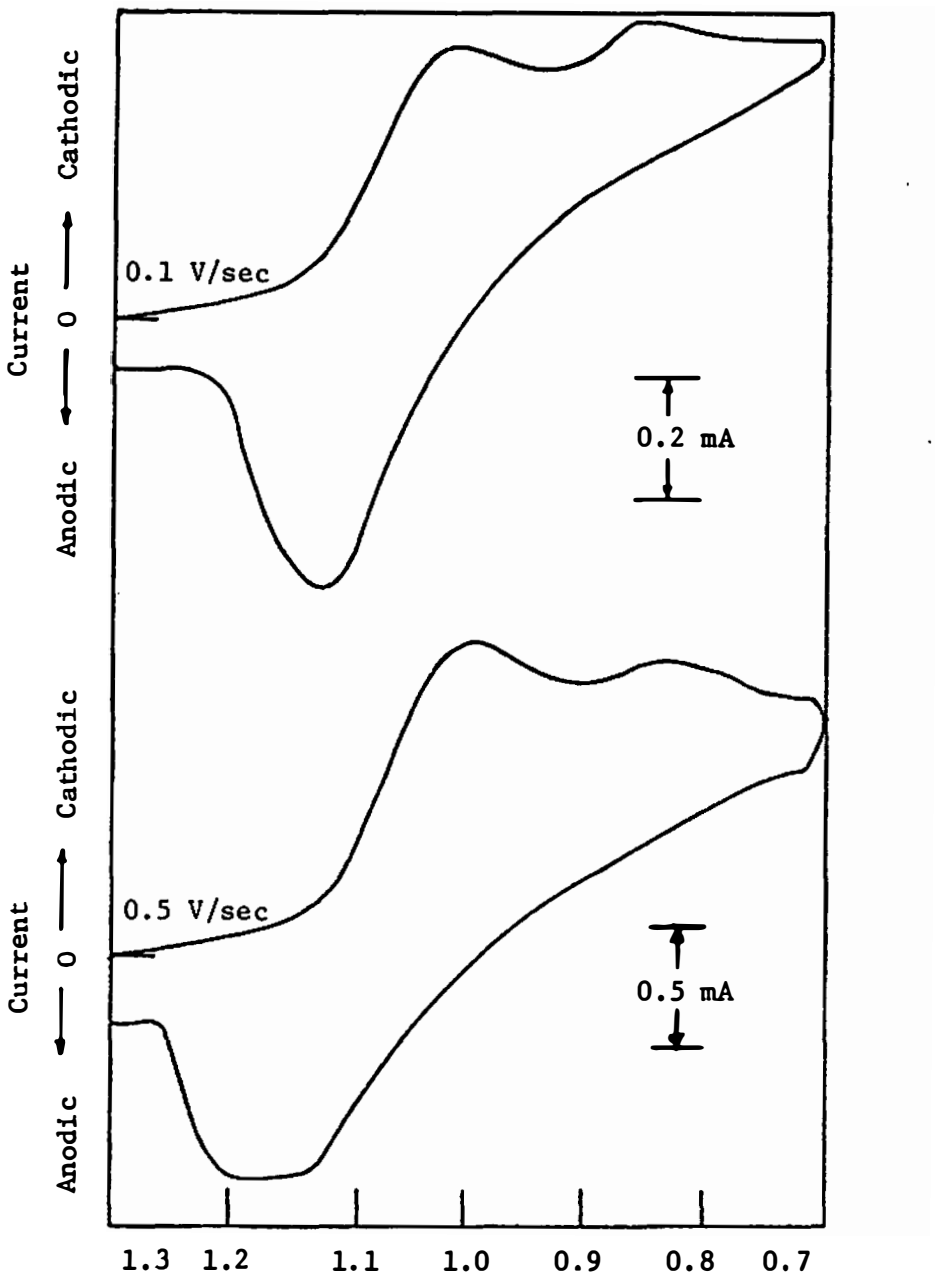


Figure 55. Cyclic voltammograms for the reduction of NbO(III) at the platinum electrode at 190°.

Melt composition: $AlCl_3$-NaCl (50-50 mole %); electrode area: 0.10 cm^2; NbO(III) concentration: 3.0 x 10^{-2} M.

increasing scan rate (0.01-0.5 V/sec at 190°), which indicates that the second reduction step is not a simple reversible process. Because of the overlap, the peak current of the second reduction step can not be determined accurately using the descending branch technique.[159]

Two sharp and symmetric peaks, with E_p^c 0.46 and 0.29 V, were observed at 175° at the platinum and tungsten electrodes (see Figure 53, p 195). The peak potentials of these two reduction steps were almost independent of scan rate (see Table XXVII, p 196). These peaks disappeared at high scan rates (>0.5 V/sec) and high temperatures (>190°). Voltammetric results indicate that the two reduction peaks are neither due to diffusion controlled processes, nor adsorption processes. They are possibly due to the reduction of some oxide films.

Cyclic voltammograms for the reduction of NbO(III) at the platinum electrode at 340° are shown in Figure 56 for fast scan rates (0.5-5 V/sec) and in Figure 57 for slow scan rate (0.01 V/sec). Table XXVIII summarizes some of the typical voltammetric results at 245 and 340° with tungsten and platinum electrodes. The two reduction peaks observed at lower temperature merged into a single peak at higher temperatures. E_p^c shifts cathodically with increasing scan rate. E_p^a shifts anodically with increasing scan rate. Peak separation ($E_p^c - E_p^a$) increases with increasing scan rate. $i_p^c/v^{1/2}$ decreases with increasing scan rate (see Table XXVIII. The splitting of the anodic peak at slow scan rates (see Figure 57), and the broadening of the reduction peak with increasing scan rate (see Figure 56), indicate the effect of the kinetic parameter (k_f/a) on the shape of the cyclic voltammograms. For an ECE mechanism with an irreversible chemical reaction between the two charge transfers, the

TABLE XXVIII

VOLTAMMETRIC RESULTS FOR THE REDUCTION OF NbO(III) AT HIGHER TEMPERATURES[a]

Temperature °C	Electrode	Scan Rate V/sec	E_p^c V	E_p^a V	$E_p^c - E_p^a$ mV	$i_p^c/v^{1/2}$ mA $sec^{1/2}V^{-1/2}$
245	W	0.01	0.81	- -	- -	6.40
		0.05	0.80	0.96	-160	5.92
		0.1	0.80	0.97	-170	5.85
		1.0	0.78	1.00	-220	5.50
		10	0.71	1.07	-360	5.06
340	Pt	0.01	0.75	0.89	-140	10.5
		0.05	0.71	0.88	-170	9.6
		0.1	0.71	0.87	-160	9.9
		0.5	0.67	0.86	-190	9.0
		1	0.65	0.91	-240	8.8
		2	0.60	0.97	-330	7.6
		5	0.58	1.02	-410	7.6

[a]Melt composition: $AlCl_3$-NaCl (50-50 mole %); electrode area: 0.10 cm^2; NbO(III) concentration: 3.0×10^{-2} M; Al(III) ($AlCl_3$-NaCl 63-37 mole %)/Al reference electrode.

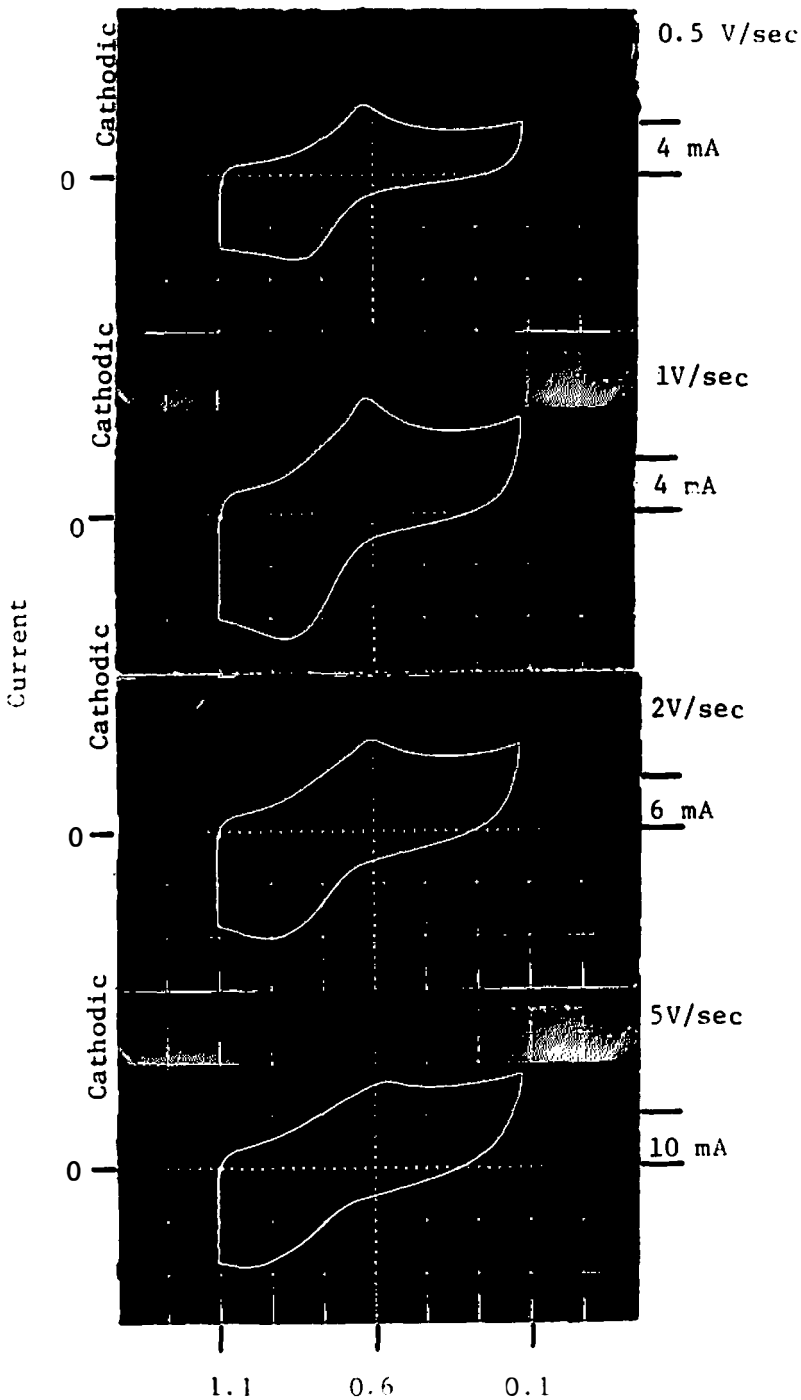


Figure 56. Cyclic voltammograms for the reduction of NbO(III) at the platinum electrode at 340°.

Melt composition: $AlCl_3$-NaCl (50-50 mole %); electrode area: 0.10 cm^2; NbO(III) concentration: 3.0×10^{-2} M.

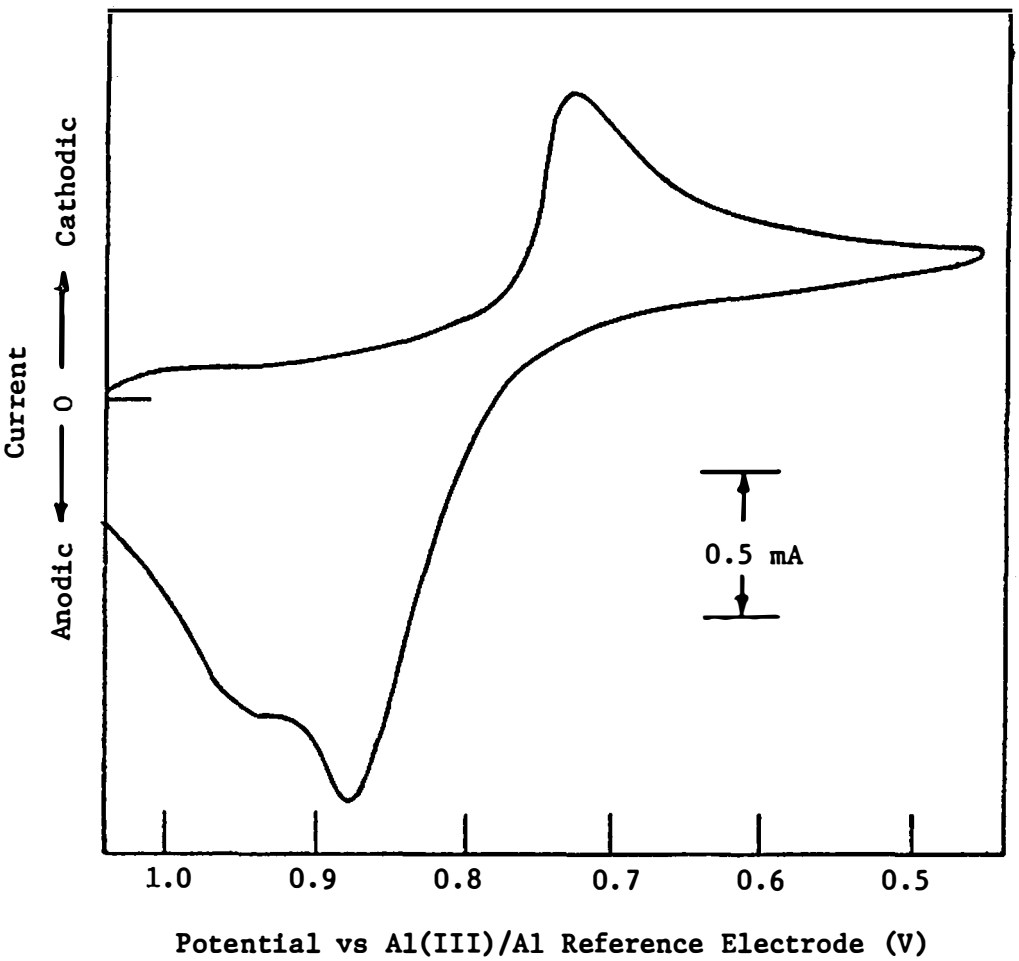


Figure 57. Cyclic voltammogram for the reduction of NbO(III) at the platinum electrode at 340°.

Melt composition: $AlCl_3$-NaCl (50-50 mole %); electrode area: 0.10 cm^2; NbO(III) concentration: 3.0×10^{-2} M; scan rate: 0.01 V/sec.

anodic peak of the second charge transfer should be observed at slow scan rates.[149] If the second charge transfer is a quasi-reversible process, the cathodic shift of the reduction peak of the second step and the increase of the peak separation with increasing span rate should be observed.[147,148] Increasing the scan rate (decreasing k_f/a) can also increase the peak current of the first reduction step,[149] which will cause the broadening of the total reduction peak current. Thus, the experimental results are consistent with the theoretical diagnostic criteria for an ECE mechanism with an irreversible chemical reaction and a quasi-reversible second charge transfer process.

Korshunov and Rokhlenko[98] have reported that $NbOCl_3$ was stable in $Na(K)AlCl_4$ melts. The stability of $NbOCl_3$ in basic chloroaluminates can also be seen from the free energy calculation of the following reaction:

$$NbOCl_3(c) + NaAlCl_4(\ell) \rightleftharpoons NbCl_5(c) + AlOCl(c) + NaCl(\ell) \quad . \qquad (81)$$

Using the available free energies of formation of $\Delta G^f_{NbOCl_3}$,[46] $\Delta G^f_{NbCl_5}$[85] (Table IV, p 12). ΔG^f_{AlOCl},[82] $\Delta G^f_{NaAlCl_4}$,[118] and ΔG^f_{NaCl},[118] one can estimate the free energy of reaction 81, which gives ΔG_R = 45.12 kcal/mole at 200°. This value indicates that $NbOCl_3$ should be stable in basic chloroaluminates, which is consistent with the experimental results obtained in this study.

Based on the experimental results, several mechanisms for the reduction of monomeric niobium(V) oxy-species were tested, but none of them could explain the data satisfactorily. The reduction of a dimeric niobium(V) oxy-species has been proposed as follows:

$$1/2[Cl_4Nb(V)ONb(V)OCl_4]^{2-} + e^- \rightleftharpoons 1/2[Cl_3Nb(IV)ONb(IV)OCl_3]^{2-} + Cl^- \quad E_1 (n_1=1) \quad (82)$$

$$\downarrow \rightarrow NbO_2(s) \xrightarrow{2xe^-} NbO_{(2-x)}(s) \xrightarrow{2(1-x)e^-} NbO(s) \quad (83)$$

$$1/2[Cl_3Nb(IV)ONb(IV)OCl_3]^{2-} \xrightarrow{k_f} 1/2\ [Cl_3Nb(V)ONb(III)OCl_3]^{2-} \quad (84)$$

$$1/2[Cl_3Nb(V)ONb(III)OCl_3]^{2-} + e^- \rightleftharpoons 1/2[Cl_2Nb(III)ONb(III)OCl_2]^{2-} + Cl^- \quad E_2\ (n_2 = 1) \quad (85)$$

The presence of dimeric Nb(V) oxy-species has been proposed by Sherman and Archer[100] in DMF who also proposed a similar reduction mechanism. Reactions 82, 84, and 85 constitute an ECE mechanism. The participation of Cl^- ions in the charge transfer process and the increasing stability of NbO(III) with increasing temperature will produce a large cathodic shift for reaction 82 with increasing temperature, which will cause the merging of the two peaks at higher temperature. The increase of the contribution of the second peak current to the total peak current with increasing temperature (see Figure 56, p 201) suggests that k_f values for reaction 84 increase with increasing temperature. The decreasing peak width at slow scan rates (large k_f/a) (Figure 57, p 202), the decreasing peak separation with increasing k_f/a (Figure 56, p 201), the splitting of the anodic peak at slow scan rates, the decrease of $i_p^c/v^{1/2}$ with increasing scan rate, and the cathodic shifts of the peak potential with increasing scan rate (see Table XXVII, p 196 and Table XXVIII, p 200) are in agreement with the proposed mechanism. The number of electrons for Reaction 82 was determined from the polarographic log plot

(Figure 50, p 190) and the voltammetric peak widths. The number of electrons for Reaction 85 was determined from Figure 50, p 190). $i_{d(1)}/i_{d(2)} \sim 1$. The two sharp and symmetric peaks observed at lower temperatures (see Figure 53, p 195) are possibly due to the reduction of the oxide films, such as Reaction 83.

3. Effect of Melt Composition and Temperature on the Electrochemical Reduction of Niobium Oxychloride in Molten Chloroaluminates

Electrochemical studies of niobium(V) oxychloride in molten chloroaluminates have been carried out by means of polarographic, chronopotentiometric, and voltammetric methods. The effect of melt composition and temperature on the stability and reduction mechanisms of niobium(V) oxychloride has been examined. The electrochemical results indicate that niobium(V) oxychloride is unstable in acidic melts, $AlCl_3$-NaCl (63-37 mole % and 56-44 mole %). Niobium(V) oxychloride will be converted to niobium(V) chloride, and then reduced by following the same mechanism as that followed by Nb(V) chloride in these acidic melts.

Niobium(V) oxychloride is stable in the basic melt, $AlCl_3$-NaCl (50-50 mole %). The electrochemical behavior of niobium(V) oxychloride in the basic melt composition is different compared to Nb(V) chloride. Four reduction steps were observed at 175°; the last two reduction steps were sharp and symmetric peaks with E_p^c: 0.46 and 0.29 V (0.89, 0.72 V after the correction for the potential difference due to the melt composition). The voltammetric results show that these two peaks are possibly due to the reduction of some oxide films. The initial

two reduction peaks are closely related; $E_{1/2}$ values are 1.05, 0.895 V (1.48, 1.325 V after correction for the melt composition effect) at 190°. Polarographic and voltammetric results show that the first reduction step is a reversible one electron process. The two reduction steps merged into one reduction step at higher temperatures with $E_{1/2}$ = 0.83 V (1.26 V after correction for the melt composition effect) at 245°. $E_{1/2}$ values shift cathodically with increasing temperature; these results suggest that the higher oxidation state is more stable in basic melts. It has been tentatively concluded that an ECE mechanism with an irreversible chemical reaction is involved in the initial two reduction steps. Comparison of the reduction potentials of niobium(V) chloride and niobium(V) oxychloride and the observed anodic shift of the redox potentials of NbO(III)/NbO(II) and NbO(II)/NbO(I) complex suggest that NbO(II) is more stable than Nb(IV), and NbO(I) is more stable than Nb(III) in $AlCl_3$-NaCl (50-50 mole %).

E. Vibrational Spectroscopic Studies of Solid Nb_2O_5 and $NiNb_2O_6$

Vibrational spectroscopic studies of solid Nb_2O_5 and $NiNb_2O_6$ were undertaken to support the studies of the oxide chemistry of Nb(V) in molten fluorides for identification of equilibrium solid phases. This work was done in collaboration with G. M. Begun, Chemistry Division, Oak Ridge National Laboratory, and K. W. Fung, Chemistry Department, University of Tennessee.

The crystal structure of solid Nb_2O_5 has been discussed by several authors.[46,49,54] The crystal structure of $NiNb_2O_6$ has been reported by Goldschmidt.[67,68] Infrared spectra of Nb_2O_5 have been reported.[209] No

Raman spectra of Nb_2O_5 have been reported. Raman and infrared spectra of $NiNb_2O_6$ have not been previously reported. Vibrational spectroscopic studies of $K_2NbO_2F_3$, K_3NbOF_6 and $K_2NbOF_5 \cdot H_2O$[61,78,198] have shown that the Nb-O stretching frequencies are around 850-1000 cm^{-1}. H-Nb_2O_5 and $NiNb_2O_6$ were prepared by the methods described in Chapter II, p. 64. The two compounds were identified by X-ray powder diffraction by members of the Analytical Chemistry Division. Infrared spectra of solid powders were obtained using the KBr-pellet (0.04 in thick) technique with a Perkin-Elmer Model 521 grating infrared spectrometer. A Cary Model 81 monochromator, coupled with a cooled 9558 EMI photomultiplier tube and a photo counting system, was used to record the Raman spectra. A Spectra-Physics Model 141 argon ion laser was used to excite the Raman spectra. The powder sample was contained in a quartz ampoule. Figures 58 and 59 show the Raman and infrared spectra of Nb_2O_5; Figures 60 and 61 show the Raman and infrared spectra of $NiNb_2O_6$. Vibrational frequencies of solid Nb_2O_5 and $NiNb_2O_6$ at 25° are summarized in Table XXIX. From Figure 58 and comparison with previous results,[61,78,198] it appears that the Nb-O symmetric stretching frequency in Nb_2O_5 is at 992 cm^{-1}. No corresponding infrared band was observed. From Figure 59 it appears that the antisymmetric stretch frequency of Nb-O in Nb_2O_5 is at 850 cm^{-1}. The infrared spectra reported here for Nb_2O_5 are in reasonable agreement with those reported previously. Figure 60 shows that the Nb-O symmetric stretching frequency in $NiNb_2O_6$ is at 882 cm^{-1}. The weak band at 856 cm^{-1} observed in Figure 61 may possibly be the corresponding antisymmetric stretching vibration of Nb-O. The decrease in the vibrational frequency of Nb-O in $NiNb_2O_6$ compared to Nb_2O_5 indicates that the Nb-O bond strength in Nb_2O_5 is higher than the Nb-O bond strength in $NiNb_2O_6$.

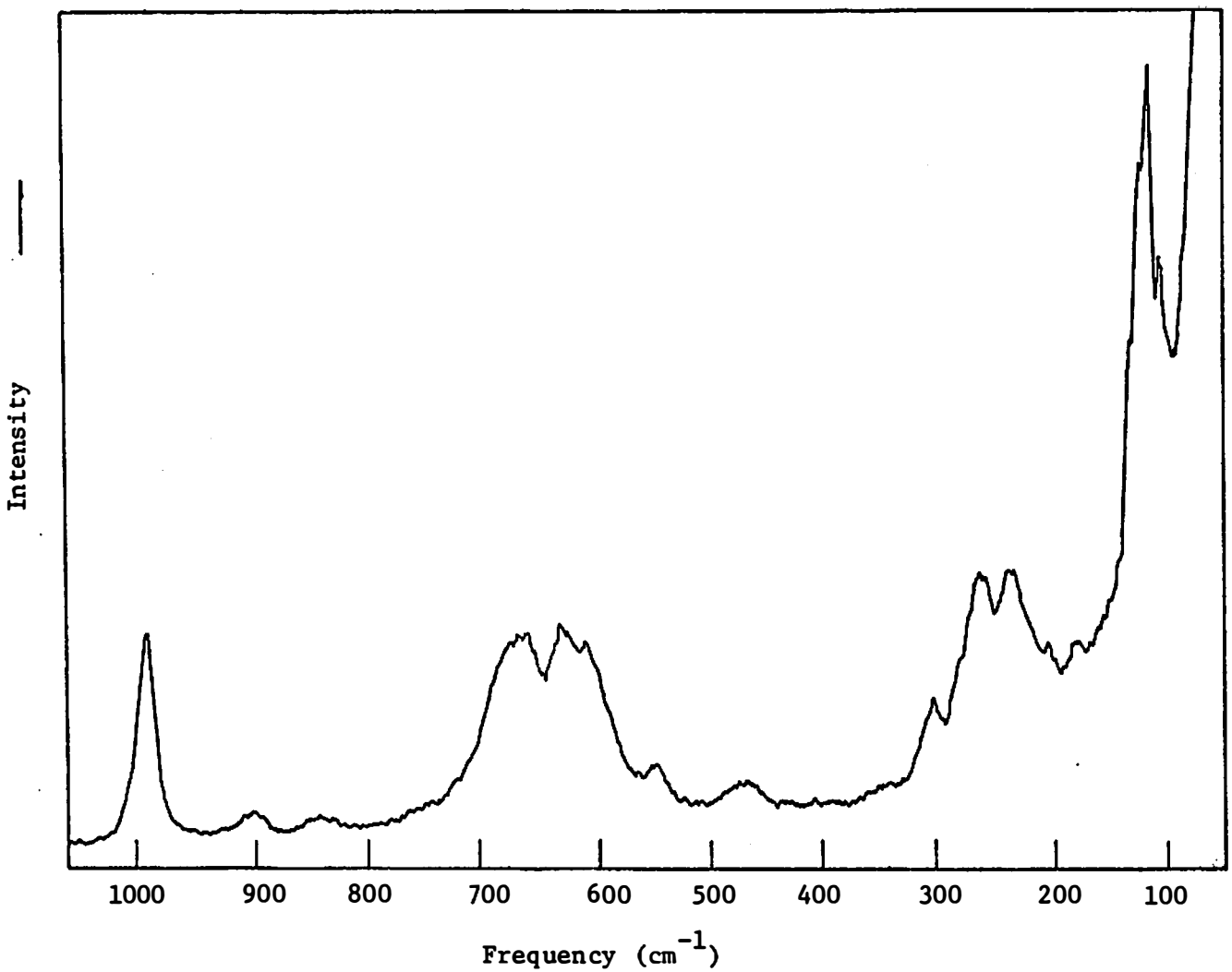


Figure 58. Raman spectrum of solid Nb_2O_5; 4880 Å laser excitation.

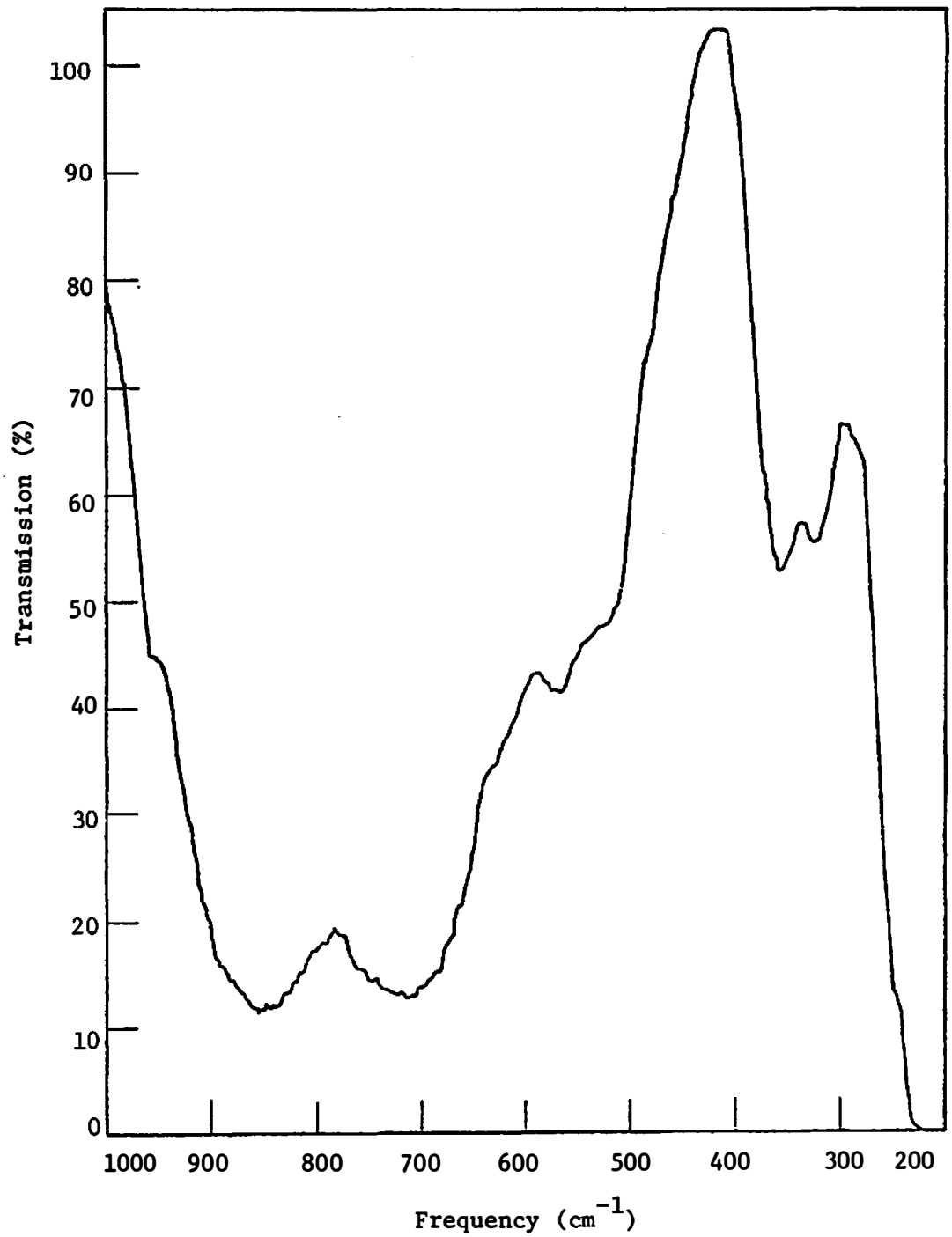


Figure 59. Infrared spectrum of solid Nb_2O_5 at 25°.

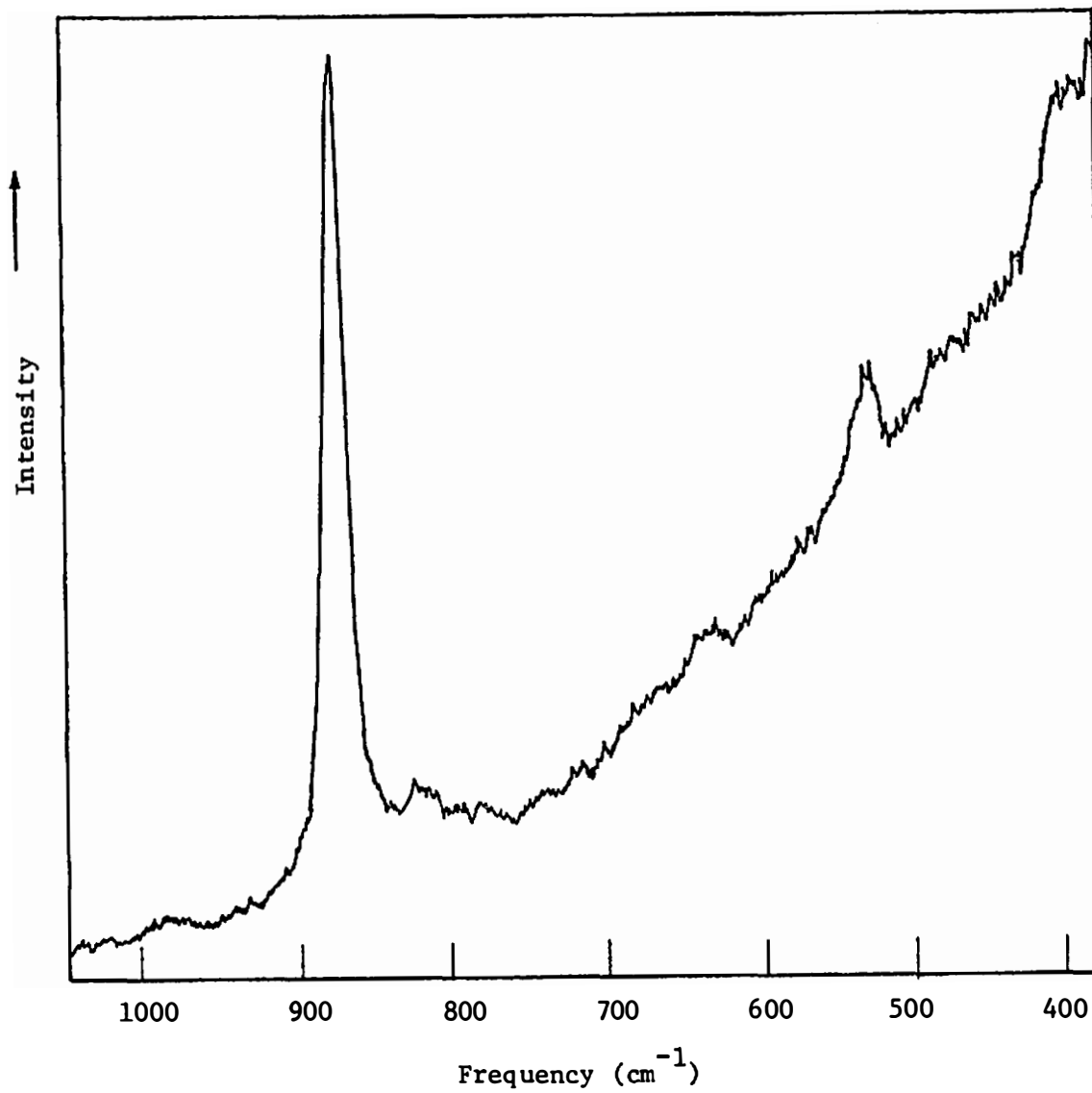


Figure 60. Raman spectrum of solid $NiNb_2O_6$ at 25°; 4800 Å laser excitation.

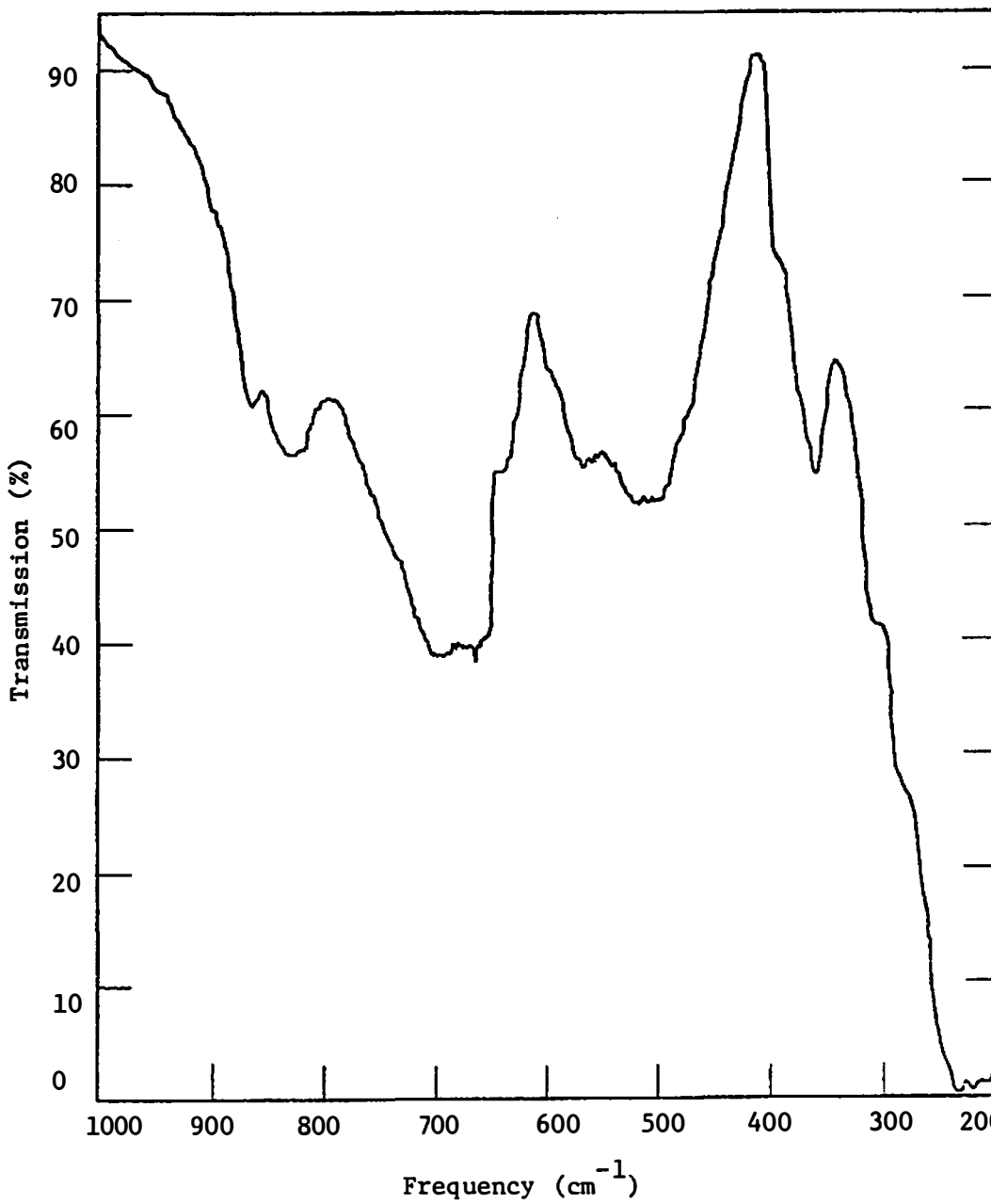


Figure 61. Infrared spectrum of solid $NiNb_2O_6$ at 25°.

TABLE XXIX

VIBRATIONAL FREQUENCIES (cm^{-1}) OF SOLID Nb_2O_5 AND $NiNb_2O_6$ AT 25° [a]

Nb_2O_5		$NiNb_2O_6$	
IR	Raman	IR	Raman
	107 (m) [b]		
	117 (vs) [b]		
	121 (sh) [b]		
	237 (s)		
	267 (s)		
325 (m)	307 (w)	360 (m)	406 (w)
360 (m)	472 (w)	510 (m)	
525 (sh)	547 (w)	570 (m)	528 (m)
	612 (sh)		
	632 (s)		
715 (vs)	664 (s)	680 (s)	
850 (vs)	842 (w)	830 (m)	882 (vvs)
	902 (w)	865 (m)	
	992 (s)		984 (w)

[a] w = weak; m = medium; sh = shoulder; s = strong; vs = very strong; vvs = very, very strong.

[b] Probably "ghost" lines due to the grating.

This is probably due to nickel cations, which coordinate with the oxide ions and cause the decrease of the vibrational frequency of Nb-O in $NiNb_2O_6$.

CHAPTER IV

SUMMARY

The oxide chemistry of niobium(V) has been studied in molten $LiF-BeF_2$ mixtures by solubility measurements. The stoichiometry of an oxygen-containing niobium(V) species (NbO_2F) in molten Li_2BeF_4 has been established from heterogeneous equilibrations of $NiNb_2O_6$ and NiO with the melt containing NiF_2. The equilibrium reaction is:

$$1/2\ NiNb_2O_6(c) + 1/2\ NiF_2(d) \rightleftharpoons NbO_2F(d) + NiO(c)\ .$$

The equilibrium quotient for the reaction, $Q = X_{NbO_2F}/X_{NiF_2}^{1/2}$, was determined as $\log Q = 1.81 - 4.58\ (10^3/T)$. The heterogeneous equilibrations of Nb_2O_5 and BeO with molten $LiF-BeF_2$ mixtures have also been studied; the equilibrium reaction is:

$$1/2\ Nb_2O_5(c) + 1/2\ BeF_2(d) \rightleftharpoons NbO_2F(d) + 1/2\ BeO(c)\ .$$

The equilibrium quotient $Q = X_{NbO_2F}$ was determined as $\log Q = 1.70 - 5.27\ (10^3/T)$ (in $LiF-BeF_2$: 67-33 mole%) and $\log Q = 0.90 - 4.81 \times (10^3/T)$ (in $LiF-BeF_2$: 52-48 mole %). The effect of the melt composition on the solubility of $Nb_2O_5(c)$ and on the activity coefficient of $NbO_2F(d)$ have been examined. It was found that the solubility of Nb_2O_5 decreases with increasing X_{BeF_2}. The free energies of formation of $NbO_2F(d)$ and $NiNb_2O_6(c)$ have been estimated from the experimental results.

$$\Delta G^f_{NbO_2F(d)} = -250.7 + 45.9\ (T/10^3)\ \text{(kcal/mole)}$$

$$\Delta G^f_{NiNb_2O_6(c)} = -509.0 + 112.7\ (T/10^3)\ \text{(kcal/mole)}$$

A Pourbaix diagram for niobium in molten Li_2BeF_4 at 500° and a phase diagram at 600° involving the equilibrium oxide phases (Nb_2O_5, $NiNb_2O_6$, NiO, and BeO) with NbO_2F and NiF_2 concentrations in molten Li_2BeF_4 were constructed. The heat of formation of $NiNb_2O_6$, ΔH^f = - 530.6 (kcal/mole), at 25° has been estimated by using an empirical method. The lattice energy of $NiNb_2O_6$(c), U_o = 5019.6 kcal/mole, has been estimated by using the Born-Haber cycle.

The electrochemical reduction of Nb(V) in molten LiF-BeF_2-ZrF_4 (65.6-29.4-5.0 mole %) has been studied by linear sweep voltammetry with pyrolytic graphite and platinum working electrodes. Ni(II) (saturated)/ Ni (LaF_3 membrane) was used as the reference electrode. Nb(V) was added to the melt as K_2NbF_7, but it was found to form NbO_2F. The results with a pyrolytic graphite electrode were reproducible; three reduction steps were observed at low scan rates (< 0.5 V/sec) and one reduction step was observed at high scan rates (> 5 V/sec). Mechanisms are proposed for the reduction of niobium(V). The results with platinum electrodes were more complicated and irreproducible, possibly due to the formation of oxide films at the electrode surface.

The electrochemical reduction of Nb(V) chloride in molten $AlCl_3$-NaCl (63-37, 61-39, 55-45 and 50-50 mole %) has been examined in the temperature range 140-300° by chronoamperometry, differential pulse polarography, chronopotentiometry, and linear sweep voltammetry using platinum and tungsten electrodes. The effect of the melt composition, temperature and Nb(V) concentration on the reduction steps were studied. The results show that the stability of the niobium species and the electrode reduction mechanisms of Nb(V) are very sensitive to the melt

composition (acid-base properties or pCl^- values) and to the temperature. In $AlCl_3$-NaCl (63-37 mole %) at 180°, two reduction steps were observed, the second reduction step being broad and ill-defined. In $AlCl_3$-NaCl (55-45 mole %), two reduction steps were observed at 180° and 260°. The first reduction step at 180° and at 260° was split into two reduction steps at lower temperatures (140 and 150°). An ECE mechanism has been tentatively proposed for the initial two reduction steps; Nb^{5+}/Nb^{4+} (E_1), $2Nb^{4+}/Nb_2^{8+}$(C), and Nb_2^{8+}/Nb_2^{6+} (E_2). A sharp and symmetric third reduction step appeared at lower temperatures (140 and 150°). This sharp peak always appeared together with the first reduction step at the lower temperatures; this peak may be attributed to the reduction of an insoluble film. The last reduction step has the same characteristics as the last step appeared in $AlCl_3$-NaCl (63-37 mole %). In $AlCl_3$-NaCl (50-50 mole %), two reduction steps were observed at fast scan rates and low Nb(V) concentrations (6.8×10^{-3} M) at 160-180°. Polarographic results show that the two reduction steps correspond to two reversible redox couples, Nb^{5+}/Nb^{4+}, and Nb^{4+}/Nb^{3+}. At higher Nb(V) concentrations, or with slow scan rates, four reduction steps were observed. Polarographic, chronopotentiometric, and voltammetric results show that the first reduction step is a one electron reversible diffusion controlled process (Nb^{5+}/Nb^{4+}). The temperature dependence of the diffusion coefficient of Nb^{5+} and the standard redox potential of the couple Nb^{5+}/Nb^{4+} have been determined. An ECE mechanism has been tentatively proposed for the initial two reduction steps. Polarograms and chronopotentiograms at higher temperatures (> 180°) were not well-defined. Voltammograms at 300° suggest also other kinetic complications. A rate controlled

adsorption of products of the third reduction step at the platinum electrode at 220° has been found. A cathodic shift of the reduction potential of the first reduction step in $AlCl_3$-NaCl (63-37 mole %) and of the first and second reduction steps in $AlCl_3$-NaCl (50-50 mole %) with increasing temperature was observed. This indicates that the lower oxidation states of niobium are more stable in the acidic melts. The observation of a reversible reduction of Nb^{5+} to Nb^{4+} in the basic melt but not in the acidic melt suggests that Nb^{4+} is more stable in the basic melts.

The electrochemical reduction of Nb(V) oxychloride in molten $AlCl_3$-NaCl (63-37, 56-44, and 50-50 mole %) in the temperature range 150-340° has been examined using chronoamperometry, differential pulse polarography, chronopotentiometry, and linear sweep voltammetry with platinum and tungsten electrodes. The effect of the melt composition and temperature on the reduction steps was examined. The results show that the stability and the electrode reduction mechanisms of Nb(V) oxy-species in the melt are very sensitive to the melt composition and temperature. Nb(V) oxychloride was unstable in $AlCl_3$-NaCl (63-37 and 56-44 mole %). NbO(III) was converted to Nb(V) chloride, and then reduced by following the same mechanism as Nb(V) chloride in these melts. NbO(III) was stable in $AlCl_3$-NaCl (50-50 mole %). The electrochemical behavior of Nb(V) oxychloride in the basic melt is completely different from that of Nb(V) chloride. Four reduction steps were observed at 175°. The last two reduction steps are sharp and symmetric peaks and may be attributed to the reduction of some oxide films. The initial two reduction steps are closely related. Polarographic and voltammetric results show that the first reduction step is a reversible one electron process. The diffusion

currents of the first and second reduction steps are approximately the same. The two reduction steps merged into one reduction step at higher temperatures (245 and 340°). The $E_{1/2}$ values shift cathodically with increasing temperature. An ECE mechanism with an irreversible chemical reaction has been postulated for the initial two reduction steps. The anodic shifts of the redox potentials of NbO(III)/NbO(II) and NbO(II)/NbO(I) compared to the potentials for the couples Nb(V)/Nb(IV) and Nb(IV)/Nb(III) suggest that NbO(II) is more stable than Nb(IV), and that NbO(I) is more stable than Nb(III) in $AlCl_3$-NaCl (50-50 mole %).

Some vibrational spectroscopic studies of solid Nb_2O_5 and $NiNb_2O_6$ were performed. They indicate that the symmetric stretching frequencies of Nb-O in Nb_2O_5 and $NiNb_2O_6$ are 992 and 882 cm^{-1}, respectively. The higher vibrational frequency of Nb-O in Nb_2O_5 suggests that the Nb-O bond strength in Nb_2O_5 is greater than the Nb-O bond strength in $NiNb_2O_6$.

LIST OF REFERENCES

LIST OF REFERENCES

1. M. Blander, Ed., "Molten Salt Chemistry," Interscience Publishers, New York, N.Y., 1964.

2. B. R. Sundheim, Ed., "Fused Salts," McGraw-Hill, New York, N.Y., 1964.

3. I. R. McDonald and K. Singer, Chem. Brit., 9, 54 (1973).

4. H. Bloom, "The Chemistry of Molten Salts," W. A. Benjamin, New York, N.Y., 1967.

5. G. Mamantov, Ed., "Molten Salts: Characterization and Analysis," Marcel Dekker, New York, N.Y., 1969.

6. J. Braunstein, G. Mamantov, and G. P. Smith, Eds., "Advances in Molten Salt Chemistry," Vol. 1, Plenum Press, New York, N.Y., 1971.

7. S. Petrucci, Ed., "Ionic Interactions," Vol. 1, Academic Press, New York, N.Y., 1971.

8. G. J. Janz, "Molten Salts Handbook," Academic Press, New York, N.Y., 1967.

9. T. Forland, K. Grjotheim, K. Motzfeldt, and S. Urnes, Eds., "Selected Topics in High Temperature Chemistry," Universitetsforlaget, Oslow, 1966.

10. Ann. N.Y. Acad. Sci., 22, 759-1098 (1960).

11. O. J. Kleppa, Ann. Rev. Phys. Chem., 16, 187 (1965).

12. J. Lumsden, "Thermodynamics of Molten Salt Mixtures," Academic Press, New York, N.Y., 1966.

13. D. Inman, A. D. Graves, and R. S. Sethi in "Electrochemistry," Vol. I, A Specialist Periodical Report, The Chemical Society, London, 1970.

14. G. J. Janz and R. D. Reeves in "Advances in Electrochemistry and Electrochemical Engineering," Vol. 5, C. W. Tobias, Ed., Interscience Publishers, New York, N.Y., 1967.

15. S. Petrucci, Ed., "Ionic Interactions," Vol. II, Academic Press, New York, N.Y., 1971.

16. D. M. Gruen, Quart. Rev., 19, 349 (1965).

17. Yu. K. Delimarskii and B. F. Markov, "Electrochemistry of Fused Salts," The Sigma Press, Washington, D.C., 1961.

18. K. W. Fung and G. Mamantov in "Advances in Molten Salt Chemistry," Vol. 2, J. Braunstein, G. Mamantov, and G. P. Smith, Eds., Plenum Press, New York, N.Y., 1973, pp 199-254.

19. A. D. Graves and A. A. Nobile in "Electrochemistry," Vol. 2, A Specialist Periodical Report, The Chemical Society, London, 1972.

20. R. W. Laity in "Reference Electrodes," D. J. G. Ives and G. J. Janz, Eds., Academic Press, New York, N.Y., 1961, pp 524-606.

21. A. F. Alabyshev, M. F. Lantratov, and A. G. Morachevskii, "Reference Electrodes for Fused Salts," English Translation, The Sigma Press, Washington, D.C., 1965.

22. H. Rossotti, Ed., "Chemical Applications of Potentiometry," D. Van Nostrand Co., Ltd., London, 1969, pp 176-194.

23. A. D. Graves, G. J. Hills, and D. Inman in "Advances in Electrochemistry and Electrochemical Engineering," Vol. 5, P. Delahay, Ed., Interscience Publishers, New York, N.Y., 1966, p 117.

24. G. Charlot and B. Tremillon, Translated by P. T. Harrey, "Chemical Reactions in Solvents and Melts, Pergamon Press, 1969.

25. T. B. Reddy, Electrochem. Technol., 1, 325 (1963).

26. J. O'M. Bockris, J. L. White, and J. D. Mackenzie, Eds., "Physicochemical Measurements at High Temperatures," Butterworths, London, 1959.

27. J. D. Corbett and F. R. Duke in "Techniques of Inorganic Chemistry," Vol. 1, H. B. Jonassen and A. Weissberger, Eds., Interscience Publishers, New York, N.Y., 1963, pp 103-156.

28. R. A. Bailey and G. J. Janz in "The Chemistry of Non-Aqueous Solvents," Vol. 1, J. J. Lagowski, Eds., Academic Press, New York, N.Y., 1966, pp 291-371.

29. Y. T. Hsu, R. B. Escue, and T. H. Tidwell, J. Electroanal. Chem., 15, 245 (1967).

30. A. S. Kertes, Actini. Rev., 1, 371 (1971).

31. Nucl. Appl. Tech., 8, 1970, No. 2 issue entirely devoted to molten salt reactor technology.

32. M. W. Rosenthal, P. N. Haubenreich, H. E. McCoy, and L. E. McNeese, Atomic Energy Rev., 9, 601 (1971).

33. A. L. Mathews and C. F. Baes, Jr., Inorg. Chem., 7, 373 (1968).

34. B. F. Hitch and C. F. Baes, Jr., USAEC Report ORNL-4076, 1967, p 19.

35. C. F. Baes, Jr. in "Nuclear Metallurgy," Symposium on the Reprocessing of Nuclear Fuels, 15, 617 (1969).

36. C. E. Bamberger, R. G. Ross and C. F. Baes, Jr., J. Inorg. Nucl. Chem., 33, 767 (1970).

37. C. E. Bamberger and C. F. Baes, Jr., J. Nucl. Mat., 35, 177 (1970).

38. R. G. Ross, C. E. Bamberger, and C. F. Baes, Jr., J. Inorg. Nucl. Chem., 35, 433 (1973).

39. C. E. Bamberger, R. G. Ross, C. F. Baes, Jr., and J. P. Young, J. Inorg. Nucl. Chem., 33, 3591 (1971).

40. J. H. Canterford and R. Colton, "Halides of the Transition Elements Halides of the Second and Third Row Transition Metals," Wiley-Interscience, New York, N.Y., 1968, pp 145-205.

41. F. Fairbrother, "The Chemistry of Niobium and Tantalum," Elsevier Publishing Company, New York, N.Y., 1967.

42. F. Fairbrother in "Halogen Chemistry," Vol. 3, V. Gutmann, Ed., Academic Press, New York, N.Y., 1967, pp 123-178.

43. F. A. Cotton and G. Wilkinson, "Advanced Inorganic Chemistry," 3rd ed., Interscience Publishers, New York, N.Y., 1972, pp 934-944.

44. R. A. Walton in "Progress in Inorganic Chemistry," S. J. Lippard, Ed., Interscience Publishers, New York, N.Y., 1972, pp 1-226.

45. D. L. Kepert, "The Early Transition Metals," Academic Press, New York, N.Y., 1972, pp 142-254.

46. O. Kubaschewski, Atomic Energy Rev., Special Issue No. 2, (1968).

47. W. P. Griffith, Coordin. Chem. Rev., 5, 459 (1970).

48. H. Schäfer and H. G. Schnering, Angew. Chem., 76, 833 (1964).

49. H. Schäfer, R. Gruehn, and F. Schulte, Angew. Chem. Internat. Edit., 5, 40 (1966).

50. P. J. Selbin, Angew. Chem. Internat. Edit., 5, 719 (1966).

51. J. E. Fergusson in "Preparative Inorganic Reactions," Vol. 7, W. L. Jolly, Ed., Wiley-Interscience, New York, N.Y., 1971, pp 93-119.

52. R. Norin and B. Rappinger, Acta Chem. Scand., 25, 18 (1971).

53. R. Bongon and J. Ehretsmann in "Preparative Methods in Solid State Chemistry," P. Hagenmuller, Ed., Academic Press, New York, N.Y., 1972, p 401.

54. A. Reisman and F. Holtzberg in "High Temperature Oxides," Part II, A. M. Alpov, Ed., Academic Press, New York, N.Y., 1970, p 217-255.

55. S. Andersson and A. Astrom, Acta Chem. Scand., 18, 2233 (1964).

56. S. Andersson, Acta Chem. Scand., 18, 2339 (1964); 19, 1401 (1965).

57. A. Astrom, Acta Chem. Scand., 21, 915 (1967).

58. C. F. Weaver and J. S. Gill, USAEC Report ORNL-4717, 1971, p 20.

59. N. Lundberg, Acta Chem. Scand., 25, 3337 (1971).

60. L. A. Bursill, J. Solid State Chem., 6, 195 (1973).

61. G. Pausewang and W. Rüdorff, Z. Anorg. Allg. Chem., 364, 69 (1969).

62. F. Galasso and W. Darby, J. Phys. Chem., 66, 1318 (1962).

63. A. Magneli and S. Nord, Acta Chem. Scand., 19, 1510 (1965).

64. M. Lundberg and S. Andersson, Acta Chem. Scand., 19, 1376 (1965).

65. M. Lundberg, Acta Chem. Scand., 19, 2274 (1965).

66. W. Rüdorff and D. Krug, Z. Anorg. Allgem. Chem., 329, 211 (1964).

67. H. J. Goldschmidt, Metallurgia., 61, 211 (1960).

68. H. J. Goldschmidt, Metallurgia., 61, 241 (1960).

69. F. J. Felten, J. Less Common Metals, 9, 206 (1965).

70. G. Blasse, J. Inorg. Nucl. Chem., 26, 1191 (1964).

71. E. V. Tkachenko, F. Abbattista, and A. Burdeze, Neorgan. Mat., 5, 1671 (1969).

72. F. Abbattista, E. V. Tkatchenko, and C. T. Chiantavetto, Atti. Accad. Sci. Torino., 103, 605 (1969).

73. J. Senegas and J. Galy, J. Solid State Chem., 5, 481 (1972).

74. C. F. Weaver, J. S. Gill, and J. D. Redman, USAEC Report ORNL-4717, 1971, p 20.

75. C. F. Weaver and H. A. Friedman, USAEC Report ORNL-4396, 1969, p 161.

76. L. M. Toth and G. P. Smith, USAEC Report ORNL-4229, 1968, p 64; ORNL-4254, 1968, p 136.

77. G. P. Budova and N. K. Voskresenskaya, Russ. J. Inorg. Chem., 11, 642 (1966).

78. T. S. Fordyce and R. L. Baum, J. Chem. Phys., 44, 1166 (1966).

79. C. F. Weaver and H. A. Friedman, USAEC Report ORNL-4548, 1970, p 123; C. F. Weaver and J. S. Gill, USAEC Report ORNL-4717, 1971, p 31; C. F. Weaver and J. S. Gill, USAEC Report ORNL-4676, 1971, p 85; C. F. Weaver and J. S. Gill, USAEC Report ORNL-4622, 1970, p 71.

80. H. Schäfer, "Chemical Transport Reactions," Academic Press, New York, N.Y., 1964.

81. G. Brauer, "Handbook of Preparative Inorganic Chemistry," Vol. 2, Academic Press, New York, N.Y., 1965, p 1292.

82. O. Kubaschewski, E. L. Evans, and C. B. Alcock, "Metallurgical Thermo-Chemistry," Vol. 1, 4th ed., Pergamon Press, London, 1967.

83. T. Hiraoka, N. Sano, and Y. Matsushita, Trans. Iron Steel Inst. (Japan), 11, 102 (1971).

84. J. F. Elliott and M. Gleiser, "Thermochemistry for Steelmaking, Am. Iron and Steel Inst., Addison-Wesley Publishing Co., New York, N.Y., 1960.

85. J. B. Ainscough and F. W. Trovvse, UKAEA Report IGR-TN/S-717 (1958).

86. J. O. Hill, I. G. Worsley and L. G. Hepler, Chem. Rev., 71, 132 (1971).

87. J. R. Beattie, T. R. Gilson and G. A. Ozin, J. Chem. Soc., (A), 89, 2765 (1968).

88. V. V. Safonov, B. G. Korshunov, and T. N. Zimina, Russ. J. Inorg. Chem., 11, 488 (1966).

89. V. V. Safonov, B. G. Korshunov, and A. A. Yarovoi, Russ. J. Inorg. Chem., 11, 918 (1966).

90. V. V. Safonov, B. G. Korshunov, and T. N. Zimina, Russ. J. Inorg. Chem., 11, 1146 (1966).

91. V. V. Safonov, B. G. Korshunov, and S. N. Steblovskaya, Russ. J. Inorg. Chem., 11, 1148 (1966).

92. B. G. Korshunov and V. V. Safonov, Russ. J. Inorg. Chem., 6, 385 (1961).

93. B. G. Korshunov and V. V. Safonov, Russ. J. Inorg. Chem., 7, 1019 (1962).

94. V. V. Safonov, B. G. Korshunov, and Z. N. Shevtsova, Russ. J. Inorg. Chem., 7, 1021 (1962).

95. G. A. Ozin and D. T. Reynolds, Chem. Cumm., 884 (1969).

96. I. S. Norozov and V. A. Krokhin, Russ. J. Inorg. Chem., 8, 1244 (1963).

97. H. Schäfer, F. E. Wittig, and W. Wilborn, Z. Anorg. Allgem. Chem., 297, 48 (1958).

98. B. G. Korshunov and D. A. Rokblenko, Zh. prikl. Khim., 37, 1941 (1964).

99. J. G. McCullough and L. Meites, J. Electroanal. Chem., 18, 123 (1968).

100. L. R. Sherman and V. S. Archer, Anal. Chem., 42, 1356 (1970).

101. R. Gut, Helv. Chim. Acta, 43, 830 (1960).

102. R. D. Caton and H. Freund, Anal. Chem., 36, 150 (1964).

103. J. Dartnell, K. E. Johnson, and L. L. Shreir, J. Less Common Metals, 6, 85 (1964).

104. M. Sakawa and T. Kuroda, Denki Kagaku., 36, 653 (1968); 37, 99 (1969).

105. L. Yang, R. G. Hudson, and C. Y. Chien, "Physical Chemistry of Process Metallurgy," Part 2, Metallurgical Society Conference, Vol. 8, Interscience, New York, N.Y., 1959, p 925.

106. Y. Saeki and T. Suzuki, J. Less Common Metals, 9, 362 (1965).

107. T. Suzuki, Electrochim. Acta, 15, 127 (1970).

108. V. F. Pimenov, Izv. Vyssh. Ucheh. Zaved., Tsvet. Met., 11, 64 (1968).

109. L. E. Ivanovskii and M. T. Krasilnikov, Electrochem. Molten and Solid Electrolytes., 7, 48 (1969).

110. V. F. Pimenov and Yu. V. Baimakov, Soviet Electrochem., 4, 1220 (1968).

111. D. Inman, R. S. Sethi, and K. Spencer, J. Electroanal. Chem., 29, 137 (1971).

112. S. Senderoff and G. M. Mellors, J. Electrochem. Soc., 113, 66 (1966).

113. F. R. Clayton, Jr., Ph.D. Dissertation, University of Tennessee, Knoxville, Tennessee, 1971, pp 121-123.

114. H. Lux, Z. Electrochem., 45, 303 (1939).

115. H. Flood and T. Forland, Acta Chem. Scand., 1, 592 (1947).

116. B. Tremillon and G. Letisse, J. Electroanal. Chem., 17, 371 (1968).

117. C. R. Boston in "Advances in Molten Salt Chemistry," Vol. 1, J. Braunstein, G. Mamantov, and G. P. Smith, Eds., Plenum Press, New York, N.Y., 1971, pp 129-155.

118. L. G. Boxall, H. L. Jones, and R. A. Osteryoung, J. Electrochem. Soc., 120, 223 (1973).

119. T. Kraal and H. A. Øye, Acta Chem. Scand., 26, 1647 (1972).

120. E. Rytter, H. A. Øye, S. J. Cyvin, B. N. Cyvin, and P. K. Aeboe, J. Inorg. Nucl. Chem., 35, 1185 (1973).

121. G. Torsi and G. Mamantov, Inorg. Chem., 10, 1900 (1971).

122. G. Torsi and G. Mamantov, Inorg. Chem., 11, 1439 (1972).

123. A. A. Fannin, Jr., L. A. King, and D. W. Seegmiller, J. Electrochem. Soc., 119, 801 (1972).

124. R. A. Potts, R. D. Barnes, and J. D. Corbett, Inorg. Chem., 7, 2258 (1968).

125. N. J. Bjerrum, C. R. Boston, and G. P. Smith, Inorg. Chem., 6, 1162 (1967).

126. N. J. Bjerrum and G. P. Smith, Inorg. Chem., 6, 1968 (1967).

127. G. Torsi, K. W. Fung, G. M. Begun, and G. Mamantov, Inorg. Chem., 10, 2285 (1971).

128. N. J. Bjerrum, Inorg. Chem., 9, 1965 (1970).

129. N. J. Bjerrum, Inorg. Chem., 11, 2648 (1972).

130. H. A. Øye, Acta Chem. Scand., 26, 1640 (1972).

131. D. W. Sundermeyer, Angew. Chem. Internat. Edit., 4, 222 (1965).

132. P. Delahay, "New Instrumental Methods in Electrochemistry," Interscience Publishers, New York, N.Y., 1954, pp 17,119,124,184,412.

133. H. W. Jenkins, G. Mamantov, and D. L. Manning, J. Electrochem. Soc., 117, 183 (1970).

134. H. C. Gaur and H. L. Jindal, Electrochim. Acta, 15, 1113 (1970).

135. J. A. Plambeck, J. Chem. Eng. Data, 12, 77 (1967).

136. J. Braunstein and H. Braunstein in "Experimental Thermodynamics," Vol. 2, I.U.P.A.C., B. Vodor and B. Le Neindve, Eds., to be published.

137. K. W. Fung and G. Mamantov in "Comprehensive Analytical Chemistry," Wilson and Wilson, Eds., Elsevier Publishing Co., to be published.

138. M. Pourbaix, "Atlas Electrochemical Equilibria in Aqueous Solutions," Pergamon Press, London, 1966.

139. A. Conte and M. P. Ingram, Electrochim. Acta, 13, 1551 (1968).

140. R. Littlewood, J. Electrochem. Soc., 109, 525 (1962).

141. C. Edeleanu and R. Littlewood, Electrochim. Acta, 3, 195 (1960).

142. D. Lewis, J. Inorg. Nucl. Chem., 33, 2121 (1971).

143. S. L. Marchiano and A. T. Arvia, Electrochim. Acta, 17, 861 (1972).

144. S. L. Marchiano and A. J. Arvia, Electrochim. Acta, 17, 25 (1972).

145. R. S. Nicholson and I. Shain, Anal. Chem., 36, 706 (1964).

146. G. Mamantov, D. L. Manning, and J. M. Dale, J. Electroanal. Chem., 9, 253 (1965).

147. H. Matsuda and Y. Ayabe, Z. Electrochem., 59, 494 (1955).

148. R. S. Nicholson, Anal. Chem., 37, 1351 (1965).

149. R. S. Nicholson and I. Shain, Anal. Chem., 37, 178 (1965).

150. M. Mastragostino, L. Nadjo, and J. M. Saveant, Electrochim. Acta, 13, 721 (1968).

151. C. P. Andrieux, L. Nadjo, and J. M. Saveant, J. Electroanal. Chem. 26, 147 (1970).

152. M. S. Shuman, Anal. Chem., 42, 521 (1960).

153. J. M. Saveant and E. Vianello, Compt. Rend., 256, 2597 (1963).

154. J. M. Saveant and E. Vianello, Electrochim. Acta, 10, 905 (1965).

155. J. M. Saveant and E. Vianello, Electrochim. Acta, 12, 1545 (1967).

156. M. S. Shuman, Anal. Chem., 41, 142 (1969).

157. R. S. Nicholson, Anal. Chem., 37, 667 (1965).

158. M. L. Olmstead, R. C. Hamilton and R. S. Nicholson, Anal. Chem., 41, 260 (1969).

159. D. S. Polcyn and I. Shain, Anal. Chem., 38, 370 (1966).

160. D. S. Polcyn and I. Shain, Anal. Chem., 38, 376 (1966).

161. E. R. Brown and R. F. Large, S. Piekarski, and R. N. Adams in "Techniques of Chemistry," Vol. I, Part IIA, A. Weissberger and B. W. Rossiter, Eds., Wiley-Interscience, New York, N.Y., 1971, pp 425-530 and pp 531-589.

162. G. J. Hills, J. E. Oxley, and D. W. Turner, Silicates Ind., 26, 559 (1961).

163. M. Paunovic, J. Electroanal. Chem., 14, 447 (1967).

164. D. G. Davis in "Electroanalytical Chemistry," Vol. 1, A. J. Bard, Ed., Marcel Dekker, New York, N.Y., 1966, pp 157-196.

165. P. T. Lingane, Critical Rev. Anal. Chem., 1, 587 (1971).

166. R. N. Adams, "Electrochemistry at Solid Electrodes," Marcel Dekker, New York, N.Y., 1969 , pp 165,249.

167. W. H. Reinmuth, Anal. Chem., 32, 1514 (1960).

168. W. H. Reinmuth, Anal. Chem., 33, 322 (1961).

169. A. C. Testa and W. H. Reinmuth, Anal. Chem., 33, 1320 (1961).

170. A. J. Bard, Anal. Chem., 35, 340 (1963).

171. H. A. Laitinen and W. S. Ferguson, Anal. Chem., 29, 4 (1957).

172. H. A. Laitinen and H. C. Gaur, Anal. Chim. Acta, 18, 1 (1958).

173. G. Mamantov, P. Papoff, and P. Delahay, J. Amer. Chem. Soc., 79, 4034 (1957).

174. H. A. Laitinen, Pure Appl. Chem., 15, 227 (1967).

175. G. C. Barker and A. W. Gardner, AERE-C/R-2297 (1958).

176. E. P. Parry and R. A. Osteryoung, Anal. Chem., 37, 1634 (1965).

177. R. H. Wopschall and I. Shain, Anal. Chem., 39, 1514 (1967).

178. M. H. Hulbert and I. Shain, Anal. Chem., 42, 162 (1970).

179. R. H. Wopschall and I. Shain, Anal. Chem., 39, 1535 (1967).

180. R. H. Wopschall and I. Shain, Anal. Chem., 39, 1527 (1967).

181. S. V. Tatwawadi and A. T. Bard, Anal. Chem., 36, 2 (1964).

182. H. A. Laitinen and L. M. Chambers, Anal. Chem., 36, 5 (1964).

183. P. T. Lingane, Anal. Chem., 39, 485 (1967).

184. G. S. Savchenko and I. V. Tananaev, USAEC Report AEC-tr-6069, 1963.

185. K. W. Fung and G. Mamantov, Inorg. Nucl. Chem. Lett., 8, 219 (1972).

186. C. J. Barton, M. A. Bredig, L. O. Gilpatrick, and J. A. Fredericksen, Inorg. Chem., 9, 307 (1970).

187. C. R. Bamberger in "Advances in Molten Salt Chemistry, J. Braunstein, G. Mamantov, and G. P. Smith, Eds., Vol. 3, Plenum Press, New York, N.Y., to be published.

188. G. Mamantov and D. L. Manning, Anal. Chem., 38, 1494 (1966).

189. T. R. Mueller and H. C. Jones, Chem. Instrum., 2, 65 (1969).

190. H. R. Bronstein and D. L. Manning, J. Electrochem. Soc., 119, 125 (1972).

191. T. H. Shaffer, USAEC Report ORNL-4616 (1971).

192. K. W. Fung and G. Mamantov, J. Electroanal. Chem., 35, 27 (1972).

193. C. R. Boston, J. Chem. Eng. Data, 11, 262 (1966).

194. R. E. Thoma, USAEC Report ORNL-4658, 1971, pp 94-99.

195. B. F. Hitch and C. F. Baes, Jr., Inorg. Chem., 8, 201 (1969).

196. P. H. Tsui, V. I. Konstantinov, and N. P. Luzhnaya, Russ. J. Inorg. Chem., 8, 204 (1963).

197. A. S. Quist, J. B. Bates, and G. E. Boyd, J. Phys. Chem., 76, 78 (1972).

198. O. L. Keller, Jr., Inorg. Chem., 2, 783 (1963).

199. K. Schwitzgebel, P. S. Lowell, T. B. Parsons, and K. T. Sladek, J. Chem. Eng. Data, 16, 418 (1971).

200. C. F. Bell and K. A. K. Lott,"Modern Approach to Inorganic Chemistry," 2nd ed., D. Van Nostrand Company, Inc., London, 1966, p 52.

201. N. N. Greenwood, "Ionic Crystals Lattice Defects and Nonstoicheiometry," Butterworths, London, 1968.

202. M. Fredericks and R. B. Temple, Inorg. Chem., 11, 968 (1972).

203. W. H. Reinmuth, Anal. Chem., 33, 485 (1961).

204. A. Broll, H. G. Von Schnering, and H. Schäfer, J. Less Common. Metals, 22, 243 (1970).

205. E. T. Maas and R. E. McCarley, Inorg. Chem., 12, 1096 (1973).

206. R. S. Nicholson, Anal. Chem., 38, 1406 (1966).

207. J. M. Saveant, C. P. Andrieux, and L. Nadjo, J. Electroanal. Chem., 41, 137 (1973).

208. R. M. De Fremont, R. Rosset, and M. Levoy, Bull. Soc. Chim., France, 706 (1964).

209. The Sandler Standard, Inorganic, Vol. 2, Y380K, 1965.

VITA

Gann Ting was born in Chu-Cheng, Shantung Province, China, on March 4, 1940. He graduated from Taiwan Miao-Li High School in 1959. He received his B.E. degree in Chemical Engineering from the Chung-Cheng Institute of Technology in 1964. He was appointed a teaching assistant at the Chemical Engineering Department, Chung-Cheng Institute of Technology from 1964 to 1966.

He entered the graduate school of National Tsing Hua University in the fall of 1966 and graduated with an M.S. in Radiochemistry in July, 1968. He joined the Nuclear Chemistry Division, Institute of Nuclear Energy Research as an assistant chemist from August 1968 to August 1970. He received a research fellowship from the Chinese Atomic Energy Council to come to the United States of America to do research at the Oak Ridge National Laboratory from September 1970 to September 1973. In September 1970 he also entered the Graduate School of the University of Tennessee.